JAERI-M
91-001

STUDY ON ECC INJECTION MODES IN REFLOOD TESTS WITH SCTF CORE II

— COMPARISON BETWEEN GRAVITY AND FORCED FEEDS —

February 1991

Akira OHNUKI, Makoto SOBAJIMA, Takamichi IWAMURA
Hiromichi ADACHI*, Tsutomu OKUBO, Yutaka ABE and Yoshio MURAO

日本原子力研究所
Japan Atomic Energy Research Institute

JAERI-Mレポートは，日本原子力研究所が不定期に公刊している研究報告書です。
入手の問合わせは，日本原子力研究所技術情報部情報資料課（〒319-11茨城県那珂郡東海村）あて，お申しこしください。なお，このほかに財団法人原子力弘済会資料センター（〒319-11 茨城県那珂郡東海村日本原子力研究所内）で複写による実費頒布をおこなっております。

JAERI-M reports are issued irregularly.
Inquiries about availability of the reports should be addressed to Information Division, Department of Technical Information, Japan Atomic Energy Research Institute, Tokai-mura, Naka-gun, Ibaraki-ken 319-11, Japan.

編集兼発行　日本原子力研究所
印　　刷　㈱原子力資料サービス

JAERI-M 91-001

Study on ECC Injection Modes in Reflood Tests with SCTF Core II
- Comparison between Gravity and Forced Feeds -

Akira OHNUKI, Makoto SOBAJIMA[+], Takamichi IWAMURA
Hiromichi ADACHI[*], Tsutomu OKUBO, Yutaka ABE
and Yoshio MURAO

Department of Reactor Engineering
Tokai Research Establishment
Japan Atomic Energy Research Institute
Tokai-mura, Naka-gun, Ibaraki-ken

(Received January 5, 1991)

In Slab Core Test Facility (SCTF) tests, a forced feed reflooding mode is adopted as ECC water injection method to investigate parameter effects in detail on thermal-hydraulic behaviors in pressure vessel under the same boundary conditions at core inlet. This is because a gravity feed mode with cold leg injection, which is considered to be better simulation for PWR, has an uncertainty against the boundary conditions of core due to the parameter change. However, it is necessary to justify the validity of forced feed mode because the solid system of that mode might change two-dimensional thermal-hydraulic behaviors in pressure vessel to be investigated in SCTF.

This report makes clear the effects of difference in ECC water injection mode (Gravity Feed/Forced Feed) on the thermal-hydraulic behaviors in the pressure vessel using the comparison between the data in the gravity feed test and in the forced feed one and the comparison between the data and the predictions with REFLA code. Major conclusion is that the difference in feed mode does not affect the thermal-hydraulic behaviors in the pressure vessel including the two-dimensional behaviors as far as the boundary conditions of the core are similar.

+ Department of Fuel Safety Research
* Yamagata University

Keywords: Reactor Safety, PWR-LOCA, Two-Phase Flow, ECCS, Reflood, SCTF, Two-Dimensional Thermal-Hydraulics, Heat Transfer, Quench, Void Fraction

JAERI－M 91－001

平板第２次炉心再冠水試験における ＥＣＣ注入モードに関する研究 ―重力冠水及び強制冠水の比較―

日本原子力研究所東海研究所原子炉工学部
大貫　晃・傍島　真[+]・岩村　公道・安達　公道[*]
大久保　努・阿部　豊・村尾　良夫

（1991年１月５日受理）

平板炉心（ＳＣＴＦ）試験では，同一の炉心入口条件のもとで圧力容器内熱水力学的挙動に及ぼすパラメータ効果を詳細に調べる際，ＥＣＣ水注入方法として強制冠水モードを採用している。これは，ＰＷＲに対しより良い模擬と考えられるコールドレグ注入の重力冠水モードではパラメータの変化により炉心境界条件が変化するためである。しかしながら，強制冠水モードのかたいシステムはＳＣＴＦにおいて調べる圧力容器内の２次元熱水力学的挙動に影響を及ぼすことが考えられるため，強制冠水モードの妥当性を確かめる必要がある。

本報告書では，ＥＣＣ水注入モードの違い（重力冠水／強制冠水）が圧力容器内の熱水力学的挙動に及ぼす効果を，重力冠水試験及び強制冠水試験のデータの比較及びデータとＲＥＦＬＡコードによる予測結果との比較により明らかにする。主な結論として，炉心境界条件が両注入モードで同等であれば，モードの違いは２次元挙動を含む圧力容器内の熱水力学的挙動に影響しないことがわかった。

東海研究所：〒319－11 茨城県那珂郡東海村白方字白根２－４
＋ 燃料安全工学部
＊ 山形大学

Contents

目　　次

1. Introduction

The Slab Core Test Facility (SCTF) test program is a part of the large scale reflood test program under a contract with the Atomic Energy Bureau of Science and Technology Agency of Japan together with the Cylindrical Core Test Facility (CCTF) test program. Major objective of the CCTF test program is to investigate system characteristics during the reflood phase of a loss-of-coolant accident (LOCA) of a pressurized water reactor (PWR) [1]-[3]. On the other hand, major objective of the SCTF test program is to investigate two-dimensional thermal-hydraulic behaviors in pressure vessel during the reflood phase of a PWR-LOCA [4]-[7]. In order to meet this objective, SCTF simulates a full radius slab section of a PWR with 8 bundles arranged in a row and the heating power for each bundle can be independently controlled.

In the SCTF tests, the following two test modes were adopted: (1) Mode of gravity feed with ECC injection into cold leg and (2) Mode of forced feed with ECC injection into lower plenum by closing the bottom of downcomer. Although the first mode is considered to be better simulation for an actual reactor, the boundary conditions at the core inlet (mass flow rate and subcooling) are affected due to the parameter change (for example, change of system pressure and of core heating power, etc.). Therefore, in the case investigating the effect of the parameter change on the two-dimensional thermal-hydraulic behaviors in the pressure vessel, the forced feed test mode was adopted in order to obtain accurate boundary conditions at the core inlet. However, it is necessary to justify the validity of the forced feed mode because the solid system of that mode might change the thermal-hydraulic behaviors in the pressure vessel including the two-dimensional behaviors.

In this report, the effect of difference between the gravity feed and the forced feed modes is evaluated on the thermal-hydraulic behaviors in the pressure vessel including the two-dimensional behaviors by comparing the data under the gravity feed and the forced feed modes in the SCTF Core-II tests. In order to make clear whether the difference between the data is caused by the difference in the boundary conditions or by that in the feed mode, sensitivity studies on the boundary conditions are performed with REFLA-1D code[8][9].

2. Test Description

2.1 Test Facility

A schematic diagram of SCTF is shown in Fig. 2.1. The primary coolant loop consists of a hot leg equivalent to four actual hot legs, a steam/water separator in place of four actual steam generators, an intact cold leg equivalent to three intact cold legs, a broken cold leg on the pressure vessel side, and a broken cold leg on the steam/water separator side. These two broken cold legs are connected to two containment tanks as shown in Fig. 2.1.

The SCTF pressure vessel simulates a full radius slab section of a 1,100 MWe PWR. The scaling ratio of flow area is 1/21 of the referred PWR, whereas the height of each component is preserved.

The emergency core cooling system (ECCS) consists of an Acc system and a LPCI system. The injection ports for the Acc and LPCI systems are the lower plenum and the intact cold leg, respectively.

Figure 2.2 shows a vertical cross section of the pressure vessel. The pressure vessel includes a simulated core, an upper plenum with internals, a lower plenum, a core baffle and a downcomer.

The simulated core consists of 8 bundles arranged in a row with full radial width. Each bundle consists of 234 heater rods and 22 non-heated rods arranged in 16 x 16 array. The outer diameter and the heated length of the heater rod are 10.7 mm and 3660 mm, respectively. The dimension and arrangement pitch of the rods are based on those for a 15 x 15 fuel rod bundle of a Westinghouse type PWR.

The core and the upper plenum are enveloped by honeycomb thermal insulators with wall plates to minimize the wall thermal effects.

Brief descriptions of the SCTF Core-Ⅱ facility and instruments are presented in Appendix A.

2.2 Test Procedure

The test procedure was as follows: After setting initial conditions, core heating was initiated. When four cladding temperature signals exceeded a specified value, the Acc injection was initiated into the lower plenum and the core heating power was kept constant. After a few seconds of the power keeping, the core heating power was decreased along a specified decay curve.

After a period of Acc injection, the ECC injection was switched from Acc to LPCI and the injection location was also switched from the lower plenum to the intact cold leg only in the gravity feed tests. The tests were terminated at 900 seconds after the initiation of LPCI.

2.3 Test Conditions and Achieved Boundary Conditions

The tests referred to in this report are Tests S2-SH1, S2-AC1, S2-SH2, S2-06, S2-10, S2-11, S2-17 and S2-16. These eight tests are classified into the four couples, as shown in Table 2.1, with the parameters of the radial core power distribution and the injection flow rate and duration time of Acc. Major measured test conditions for these eight tests are listed in Table 2.2. Since the radial core power distribution is a dominant parameter for the characteristics of two-dimensional thermal-hydraulic behaviors in the core[5)-7)], three groups with different radial core power distribution were examined. In Base Case group in Table 2.2, the radial core power distribution was set to that predicted for a 1,100 MWe Westinghouse initial core. On the other hand, in Flat Q and T group and Steep Q and T group, both the radial core power and temperature distributions were flat and steep, respectively. The initial total stored energy in the core as well as the total core heating power were set to be the same for these six tests.

The ECC injection flow rate was determined in order to give the same flow rate at the core inlet between the gravity feed and the forced feed modes in each group in Table 2.2. The bottom of downcomer was closed in the forced feed mode by a blocking plate and the ECC water was injected only into the lower plenum. The ECC water temperature in the forced feed mode was higher than that in the gravity feed mode because the condensation effect in the intact cold leg is not included in the forced feed mode. Some selected test data obtained in Tests S2-10, S2-11, S2-16 and S2-17 are presented in Appendices B through E. Selected data obtained in Tests S2-SH1, S2-AC1, S2-SH2 and S2-06 are presented in references (5) and (10).

The achieved boundary conditions such as the core inlet ECC water flow rate, integrated ECC water mass into the core and the core inlet subcooling are compared in Figs. 2.3(1) through 2.3(4) in each group. The achieved conditions of the pressure at core center and at containment tank and the supplied core power are compared in Figs. 2.4 and 2.5, respectively. These values are plotted with the time after reflood initiation in each test. The

core inlet flow rate was estimated by a mass balance method described in Ref.(5).

Although these boundary conditions were intended to be the same between the gravity feed and the forced feed modes, some differences are observed except for the supplied core power because of the difficulty of control for the ECC injection flow rate, the ECC water temperature and the constant pressure regulation at containment tank.

The core inlet flow rate is higher in the forced feed mode than that in the gravity feed mode for all groups. The core inlet flow rate in the Acc injection period is higher in the group of High and Short Acc group and the flow rate in the LPCI period is higher in other groups.

The core inlet subcooling is higher in the forced feed mode than that in the gravity feed mode in the period after about 200-300 seconds after reflood initiation for all groups. Before the period, the subcooling is almost the same between the modes although the subcooling in the gravity feed mode is higher in the group of Flat Q and T than that in the forced feed mode.

The pressure at the core center is higher in the forced feed mode in the period of 100-200 seconds after reflood initiation for all groups. After the period, the pressure is almost the same except for the group of Base Case in which the pressure becomes lower in the forced feed mode than that in the gravity feed mode.

3. Test Results and Discussion

3.1 Effect of Difference in Feed Mode on Overall Thermal-Hydraulic Behaviors

Figures 3.1(1) through 3.1(4) show the comparison of transients of core full height differential pressure in bundle 4, sectional void fraction in bundle 4 (highest power bundle) and de-entrained water mass in the upper plenum in each group. For all groups, the amount of water accumulation in the core and in the upper plenum is larger in the forced feed test than that in the gravity feed test. Since the higher core inlet flow rate and core inlet subcooling give the larger water accumulation in the core and in the upper plenum[2][11][12], the results mentioned above are consistent with the difference of boundary conditions shown in Figs. 2.3(1) through 2.3(4). For example, the core full height differential pressure and the de-entrained water mass in the upper plenum are almost the same between gravity feed and forced feed tests until about 200 seconds in Base Case group (Fig. 3.1(1)) because the integrated water mass into the core and the core inlet subcooling are almost the same between the tests in the period as shown in Fig. 2.3(1). After the period, the core full height differential pressure and the de-entrained water mass in the upper plenum became larger in the forced feed test than those in the gravity feed test because the core inlet flow rate and subcooling in the forced feed test became higher than those in the gravity feed test.

Figures 3.2(1) through 3.2(4) show the comparison of clad surface temperature at a specified elevation measured from the bottom of heated part in Bundle 4 in each group. The clad surface temperature at each location was obtained by averaging data of several thermocouples at a elevation in a bundle. These figures show better heat transfer in the forced feed tests than that in the gravity feed tests especially in the middle part and the upper part of core. This characteristic of better core cooling in the forced feed tests is consistent with the larger water accumulation in the core due to the mismatching of the boundary conditions discussed above. It will be examined in the next section using REFLA-1D code whether the differences of core thermal-hydraulics between the gravity feed and the forced feed tests can be explained by the differences of boundary conditions quantitatively or not.

3.2 Sensitivity Study on Boundary Conditions with REFLA Code

In order to investigate the sensitivity of difference of boundary conditions for the core thermal-hydraulics quantitatively, the test data in the gravity feed and the forced feed modes are analyzed using REFLA-1D code[8][9] with the modification for effect of liquid flow rate on film boiling heat transfer by Ohnuki, et al.[13]. The accuracy of correlations in the code and of the code prediction has been verified with several small scale test data and also with the CCTF and the SCTF test data[13][14][15]. In the case of SCTF analyses, there has been reported to be some uncertainties for the input of core flow area[15] because the SCTF has some additional flow area and fluid volume around the core such as core baffle region and the gap between core barrel and pressure vessel wall as shown in Table A-1 in Appendix A. It is not clear how the additional flow area and fluid volume affect effective flooding velocity, steam velocity and liquid velocity in the core. Since the change of the core flow area has been reported to give a relatively large sensitivity for the predictions of void fraction and clad temperature[15], the effect of the difference of core flow area is also examined in this section.

The test groups of Base Case and Flat Q and T were analyzed with the REFLA code as typical cases. In the Base Case group, the core inlet flow rate and subcooling were higher in the forced feed test than those in the gravity feed test and, in Flat Q and T group, the core inlet subcooling was higher until about 300 seconds in the gravity feed test though the core inlet flow rate was higher in the forced feed test as shown in Figs 2.3(1) and 2.3(3), respectively.

Figures 3.3(1) and 3.3(2) show the comparison between the data and the predictions with the REFLA code on the core full height differential pressure in bundle 4. The difference between the forced feed and the gravity feed tests for the measured differential pressure and for the predicted one is also plotted in the lower figure. The core flow area adopted in each calculation except for Case 1 did not include the additional flow area mentioned above (Base calculations). In the Case 1 calculations, flooding velocity was estimated with the flow area including the gap between core barrel and pressure vessel wall.

The REFLA code predicts the tendency of higher differential pressure in the forced feed tests. The amount of difference between the gravity feed

and the forced feed tests is predicted well by the Base calculations until about 200 seconds and after the period the Case 1 calculations become to predict well the data. These results indicate that the difference between the gravity feed and the forced feed modes on the hydraulic behavior can be explained by the difference of the boundary conditions with taking into account the uncertain band for the effective flooding velocity depending on the selection of core flow area.

Figures 3.4(1) and 3.4(2) show the comparison of the clad surface temperature in bundle 4 between the data averaged at an elevation and the predictions with the REFLA code. The difference of the temperature at 1.905m elevation between the forced feed and the gravity feed tests is shown in Fig. 3.5. Measured difference is represented by the data band using maximum and minimum differences among several thermocouples data at the elevation in the bundle.

The REFLA code predicts the tendency of higher heat transfer at each elevation in the forced feed tests. This tendency of better core cooling is consistent with the larger water accumulation in the core in the forced feed tests discussed above. The difference between the gravity feed and the forced feed modes in the Base and the Case 1 calculations is included within the data band although the difference in Base calculations is smaller than that in the tests after about 100 seconds. These results indicate that the difference between the gravity feed and the forced feed modes on the thermal behavior can be also explained by the difference of the boundary conditions with taking into account the uncertain band for the effective flooding velocity.

3.3 Effect of Difference in Feed Mode on Two-Dimensional Thermal-Hydraulic Behaviors in Pressure Vessel

In this section, the effect of difference in feed mode on the two-dimensional thermal-hydraulic behaviors in the pressure vessel is examined using the data of test groups which were obtained with a radial power distribution, i.e., Base Case, High and Short Acc and Steep Q and T groups.

Figures 3.6(1) through 3.6(3) show the comparison of two-dimensional distribution of the core full-height differential pressure in bundles 2, 4 and 8. The comparison of the maximum difference of the differential pressure among the bundles is shown in the lower figure. In each group, the

maximum difference becomes larger with time and however the amount of the difference is almost the same between the gravity feed and the forced feed tests.

Figures 3.7(1) and 3.7(2) show the comparisons of two-dimensional distribution of sectional void fraction in Base Case and in Steep Q and T groups. Non-uniform distribution is observed in the upper region of the core in the Base Case group and in the middle and the upper regions in the Steep Q and T group. This non-uniform distribution has been clarified in Ref. (5) by the effects of radial distribution of the core power and of radial distribution of the upper plenum water accumulation. However, the difference between gravity and forced feed tests is not recognized on the amount of the radial difference of sectional void fraction.

Figure 3.8 shows the comparisons of transient of horizontal differential pressure at middle (1905 m) and upper (3.235 m) elevations from bundles 1 to 4 and from bundles 4 to 8. There is no significant difference on the readings of horizontal differential pressure from bundles 1 to 4 at each elevation between gravity feed and forced feed tests as shown in the upper two figures. And there is also no significant difference on that from bundles 4 to 8 between the two feed mode tests as shown in the lower two figures except for the later period at 1.905 m elevation.

In the later period at 1.905 m elevation, the sign of differential pressure varies from plus to minus earlier in the forced feed test than in the gravity feed test. Since the timing is correspond to that of passing the quench front at that elevation as discussed in Ref. (5), the difference in the timing is considered to be caused by the faster quench propagation in the forced feed test shown in Fig. 3.2 due to the slight difference in boundary conditions.

Figures 3.9(1) through 3.9(4) show the comparison of radial distribution of collapsed liquid level in the upper plenum and the comparison of the difference of liquid levels between above bundle 8 and above bundle 1. It can be observed irrespective of the differences of the feed mode and the group that the liquid level above bundle 8 becomes higher than that above bundle 1 with time. There is no significant difference between the gravity feed and the forced feed tests on the degree of non-uniformity for the liquid level distribution in the upper plenum.

It can be summarized from the results on the two-dimensional hydraulic behaviors described above that the difference in feed mode does not affect

the two-dimensional hydraulic behaviors in the pressure vessel.

In order to investigate the effect of the difference in feed mode on two-dimensional thermal behaviors in the core, heat transfer coefficients are plotted against the distance from quench front, since the plots are reported to be not so sensitive to the propagation velocity of the quench front. Figures 3.10(1) through 3.10(3) show the relation in bundles 2, 4, 6 and 8 at three axial elevations. Since the heat transfer coefficient was calculated based on the average value of several thermocouples at each elevation of each bundle, some spikes of heat transfer coefficient were caused by the partial quenching of some thermocouples at the upper elevation. Therefore the spikes do not indicate the real increase of the heat transfer coefficient above the quench front.

The heat transfer enhancement in the higher power bundle (bundle 4) and the heat transfer degradation in the lower power bundle (bundle 8) are observed at each elevation. The radial distribution of the heat transfer has been reported as the effect of radial core power distribution in Refs. (5) through (7). It is found that the difference between the heat transfer coefficients in the higher power bundle and those in the lower one at a distance from quench front are larger with the increase of the degree of steepness of radial core power distribution. There is no significant difference between the tendency in the gravity feed and in the forced feed tests in each group against the degree of the difference of heat transfer coefficient at the same distance from quench front between in the higher power bundle and in the lower one. This result indicates that the difference in feed mode does not affect the two-dimensional thermal behaviors in the core.

4. Conclusion

The effect of the difference between the gravity feed and the forced feed modes on the thermal-hydraulic behaviors including the two-dimensional behaviors in the pressure vessel was examined using the comparison of the data in the SCTF Core-Ⅱ tests and the comparison between the data and the predictions with the REFLA code. The objective was to clarify whether the forced feed mode was able to be used as the test method similarly as in the gravity feed mode or not because the solid system of the forced feed mode might change the thermal-hydraulic behaviors in comparison with the gravity feed mode which is considered to be better simulation for the soft system of PWR. The following concluding remarks were obtained from this study:

(1) Although the amount of water accumulation in the core was larger, the heat transfer was higher and the de-entrained water mass in the upper plenum was larger in the forced feed tests than those in the gravity feed tests, those differences were able to be explained qualitatively by the difference in the core inlet boundary conditions such as the core inlet flow rate and the core inlet subcooling.

(2) The sensitivity study with the REFLA code revealed quantitatively that the difference on the overall thermal-hydraulic behaviors mentioned in the above (1) was caused by the difference in the boundary conditions taking into account the uncertain band for the effective flooding velocity depending on the selection of the core flow area.

(3) The difference in the feed mode did not affect the two-dimensional thermal-hydraulic behaviors in the pressure vessel such as the radial distribution of sectional void fraction in the core, the horizontal differential pressure in the core, the radial distribution of collapsed liquid level in the upper plenum and the radial distribution of heat transfer coefficient in the core.

These remarks indicate that the test method of forced feed mode is equivalent to that of gravity feed mode as far as the boundary conditions of the core are similar.

Acknowledgment

The authors would like to express their appreciation to Mr. T. Iguchi, Drs. J. Sugimoto and H. Akimoto of Japan Atomic Energy Research Institute for their useful discussions.

References

(1) Y. Murao, et al. : Evaluation Report on CCTF Core-Ⅰ Reflood Test C1-19(Run 38) - Experimental Assessment of the Evaluation Model for the Safety Analysis on the Reflood Phase of a PWR-LOCA -, JAERI-M 83-029, (1983).

(2) T. Okubo, et al. : Experimental Study of Ecc Water Injection Rate Effects on Reflood Phase of PWR-LOCA, J. Nucl. Sci. Tech., 22[2], 93-108, (1985).

(3) H. Akimoto, et al. : Core Radial Power Profile Effect on System and Core Cooling Behavior during Reflood Phase of PWR-LOCA with CCTF Data, J. Nucl. Sci. Tech., 22[7], 538-550, (1985).

(4) H. Adachi, et al. : Design of Slab Core Test Facility (SCTF) in Large Scale Reflood Test Program, Part Ⅱ: CORE-Ⅱ, JAERI-M report, to be published.

(5) T. Iwamura, et al. : Two-Dimensional Thermal-Hydraulic Behavior in Core in SCTF Core Ⅱ Cold Leg Injection Tests (Radial Power profile Test Results), JAERI-M 85-106, (1985).

(6) T. Iwamura, et al. : Effects of Radial Core Power Profile on Core Thermo-Hydraulic Behavior during Reflood Phase in PWR-LOCA, J. Nucl. Sci. Tech., 20[9], 743-751, (1983).

(7) T. Iwamura, et al. : Two-Dimensional Thermal-Hydraulic Behavior in Core in SCTF Core-Ⅱ Forced Feed Reflood Tests (Effects of Radial Power and Temperature Distributions), JAERI-M 86-195, (1987).

(8) Y. Murao, et al. : REFLA-1D/MODE3 : A Computer Code for Reflood Thermo-Hydrodynamic Analysis during PWR-LOCA -User's Manual-, JAERI-M 84-243, (1985).

(9) T. Hojo, et al. : User's Manual of the REFLA-1D/MODE4 Reflood Thermo-Hydrodynamic Analysis Code, JAERI-M 85-210, (1986) in Japanese.

(10) H. Adachi, et al. : Development of SCTF Cold Leg Injection Test Method for Eliminating U-Tube Oscillation during the Initial Period, JAERI-M

Acknowledgment

The authors would like to express their appreciation to Mr. T. Iguchi, Drs. J. Sugimoto and H. Akimoto of Japan Atomic Energy Research Institute for their useful discussions.

References

(1) Y. Murao, et al. : Evaluation Report on CCTF Core-Ⅰ Reflood Test C1-19(Run 38) - Experimental Assessment of the Evaluation Model for the Safety Analysis on the Reflood Phase of a PWR-LOCA -, JAERI-M 83-029, (1983).

(2) T. Okubo, et al. : Experimental Study of Ecc Water Injection Rate Effects on Reflood Phase of PWR-LOCA, J. Nucl. Sci. Tech., 22[2], 93-108, (1985).

(3) H. Akimoto, et al. : Core Radial Power Profile Effect on System and Core Cooling Behavior during Reflood Phase of PWR-LOCA with CCTF Data, J. Nucl. Sci. Tech., 22[7], 538-550, (1985).

(4) H. Adachi, et al. : Design of Slab Core Test Facility (SCTF) in Large Scale Reflood Test Program, Part Ⅱ: CORE-Ⅱ, JAERI-M report, to be published.

(5) T. Iwamura, et al. : Two-Dimensional Thermal-Hydraulic Behavior in Core in SCTF Core Ⅱ Cold Leg Injection Tests (Radial Power profile Test Results), JAERI-M 85-106, (1985).

(6) T. Iwamura, et al. : Effects of Radial Core Power Profile on Core Thermo-Hydraulic Behavior during Reflood Phase in PWR-LOCA, J. Nucl. Sci. Tech., 20[9], 743-751, (1983).

(7) T. Iwamura, et al. : Two-Dimensional Thermal-Hydraulic Behavior in Core in SCTF Core-Ⅱ Forced Feed Reflood Tests (Effects of Radial Power and Temperature Distributions), JAERI-M 86-195, (1987).

(8) Y. Murao, et al. : REFLA-1D/MODE3 : A Computer Code for Reflood Thermo-Hydrodynamic Analysis during PWR-LOCA -User's Manual-, JAERI-M 84-243, (1985).

(9) T. Hojo, et al. : User's Manual of the REFLA-1D/MODE4 Reflood Thermo-Hydrodynamic Analysis Code, JAERI-M 85-210, (1986) in Japanese.

(10) H. Adachi, et al. : Development of SCTF Cold Leg Injection Test Method for Eliminating U-Tube Oscillation during the Initial Period, JAERI-M

90-107, (1990).

(11) A. Ohnuki, et al. : Effect of Core Inlet Water Mass Flow Rate on Reflooding Phenomena in the Forced Feed SCTF Core-Ⅰ Tests, JAERI-M 88-166, (1988).

(12) T. Iwamura, et al. : Effects of Core Inlet Water Subcooling on Reflooding Phenomena -SCTF Core-Ⅰ Forced Feed Flooding Test-, JAERI-M 83-122, (1983).

(13) A. Ohnuki, et al. : Effect of Liquid Flow Rate on Film Boiling Heat Transfer during Reflood in Rod Bundle, J. Nucl. Sci. Tech., 27[6], 535-546, (1990).

(14) T. Okubo and Y. Murao : Assessment of Core Thermo-Hydrodynamic Models of REFLA-1D with CCTF Data, JAERI-M 83-103, (1983).

(15) T. Iguchi and Y. Murao : Predictability of REFLA Core Model for SCTF data, JAERI-M 87-163, (1987) in Japanese.

Table 2.1 List of test number and main parameter

Test number	gravity feed	S2-SH1	S2-AC1	S2-SH2	S2-06
	forced feed	S2-10	S2-11	S2-17	S2-16
Core heating power distribution		Standard	Standard	Flat	Steep
Acc injection flow rate		Low	High	Low	Low
Duration time of Acc		Long	Short	Long	Long

Table 2.2 List of major measured test condition

Group	Base Case		High and Short Acc		Flat Q and T		Steep Q and T	
Feed Mode	Gravity Feed	Forced Feed	Gravity Feed	Forced Feed	Gravity Feed	Forced Feed	Gravity Feed	Forced Feed
Test No.	Test S2-SH1	Test S2-10	Test S2-AC1	Test S2-11	Test S2-SH2	Test S2-17	Test S2-06	Test S2-16
ECC Injection Port	Lower Plenum (Acc) Intact Cold Leg (LPCI)	Lower Plenum	Lower Plenum (Acc) Intact Cold Leg (LPCI)	Lower Plenum	Lower Plenum(Acc) Intact Cold Leg (LPCI)	Lower Plenum	Lower Plenum (Acc) Intact Cold Leg (LPCI)	Lower Plenum
Initial System Pressure (MPa)	0.2	0.2	0.2	0.2	0.2	0.2	0.2	0.2
Max. Core Temp. at BOCREC* (K)	1076	1078	1077	1072	1040	1033	1163	1158
Max. ECC Inj. Mass Flow Rate (kg/s)	18.9 (in Acc period)	19.6	78.3 (in Acc)	61.3	19.3 (in Acc)	12.5	19.1 (in Acc)	19.3
ECC Inj. Mass Flow Rate in LPCI Period (kg/s)	5.41	5.2	4.15	4.9	5.41	5.4	5.41	5.0
ECC Water Temp. (K)	363 (Acc) 350 (LPCI)	377 → 392	365 (Acc) 351 (LPCI)	359 → 384	364 (Acc) 350 (LPCI)	360 → 391	362 (Acc) 350 (LPCI)	362 → 393
Initial Supplied Total Power (MW)	7.12	7.12	7.09	7.09	7.12	7.12	7.12	7.12
Supplied Power Ratio Bundles 1&2:3&4: 5&6:7&8	1.001:1.065:1.015: 0.919	1.001:1.065:1.015: 0.919	1.001:1.063 1.016:0.921	1.001:1.063 1.016:0.921	1.0:1.0:1.0:1.0	1.0:1.0:1.0:1.0	1.0:1.2:1.0:0.8	1.0:1.2:1.0:0.8
Power Decay Curve	(ANS+Actinides) x 1.02 from 40s after scram	(ANS+Actinides) x 1.02 from 40s after scram	(ANS+Actinides) x 1.02 from 20s after scram	(ANS+Actinides) x 1.02 from 20s after scram	(ANS+Actinides) x 1.02 from 40s after scram	(ANS+Actinides) x1.02 from 40s after scram	(ANS+Actinides) x 1.02 from 40s after scram	(ANS+Actinides) x 1.02 from 40s after scram

* - Bottom of Core Recovery (= Reflood Initiation Time)

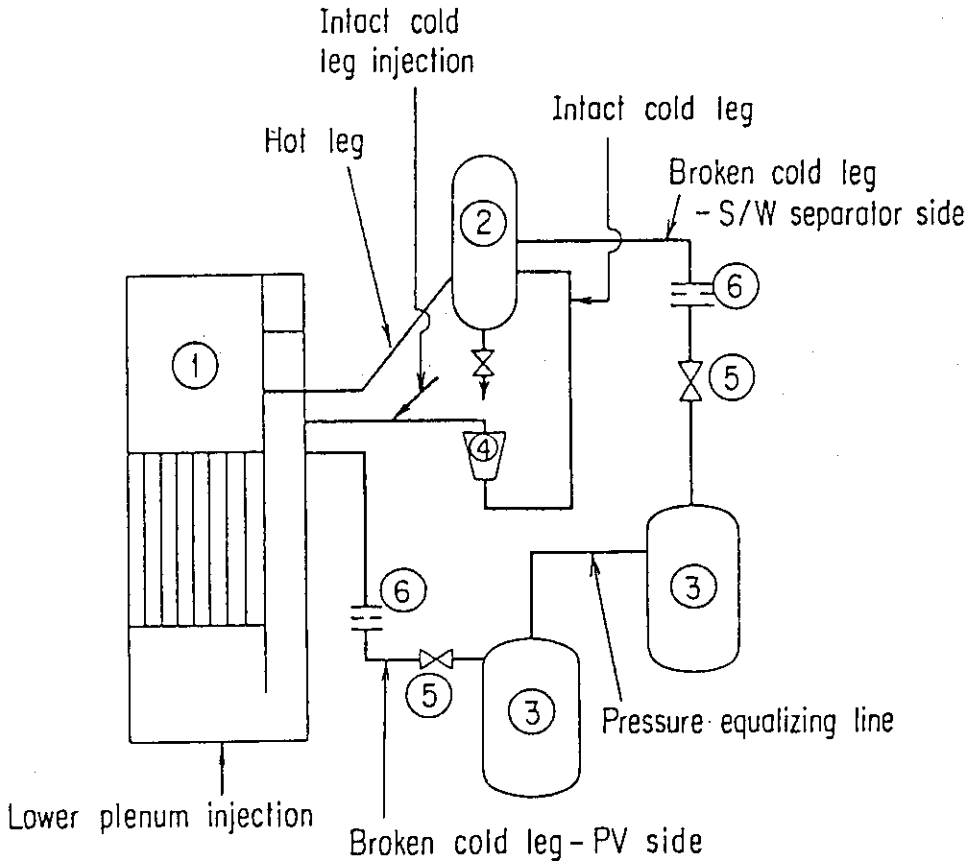

Fig.2.1 Schematic diagram of SCTF

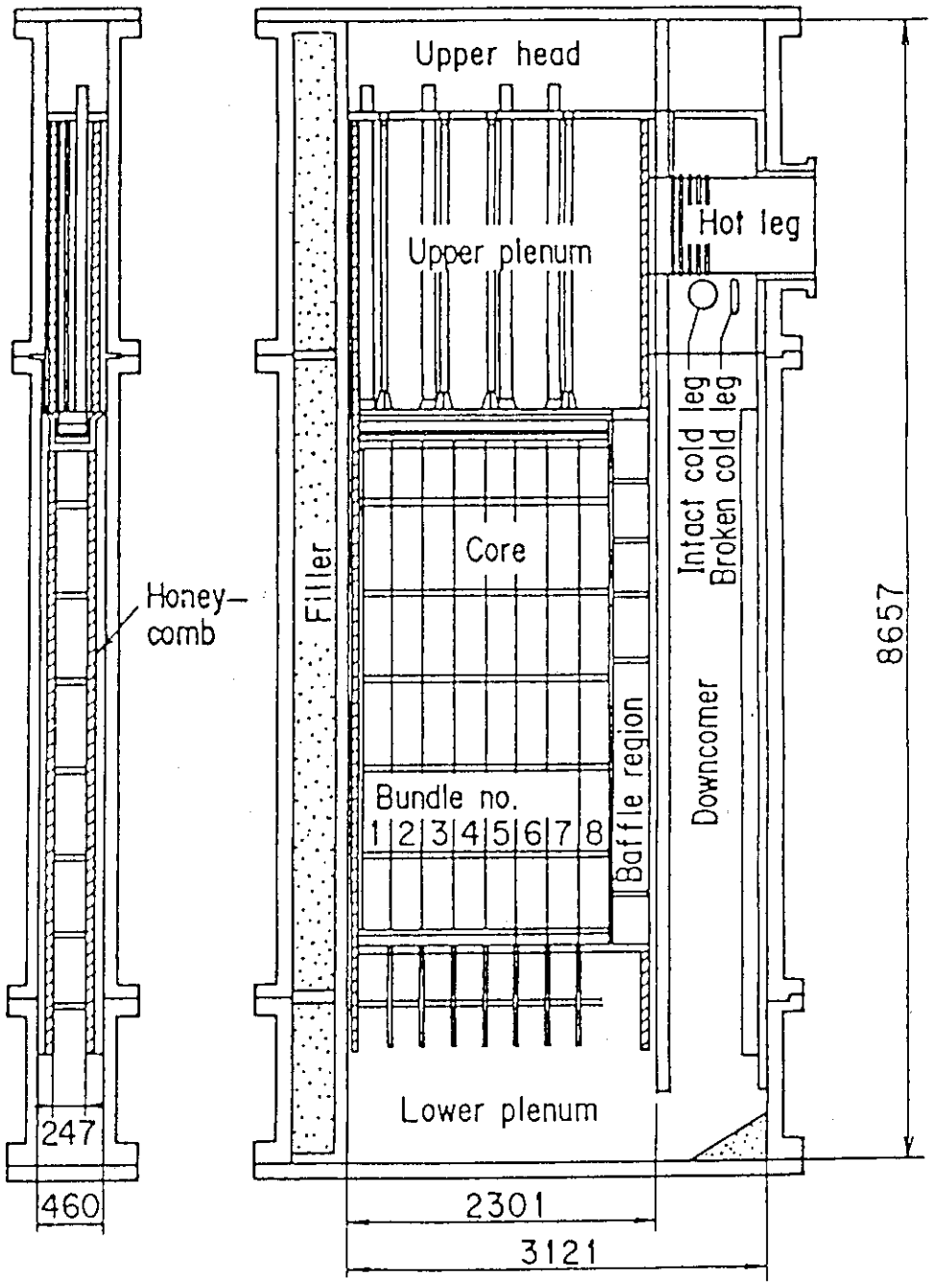

Fig.2.2 Vertical cross section of pressure vessel

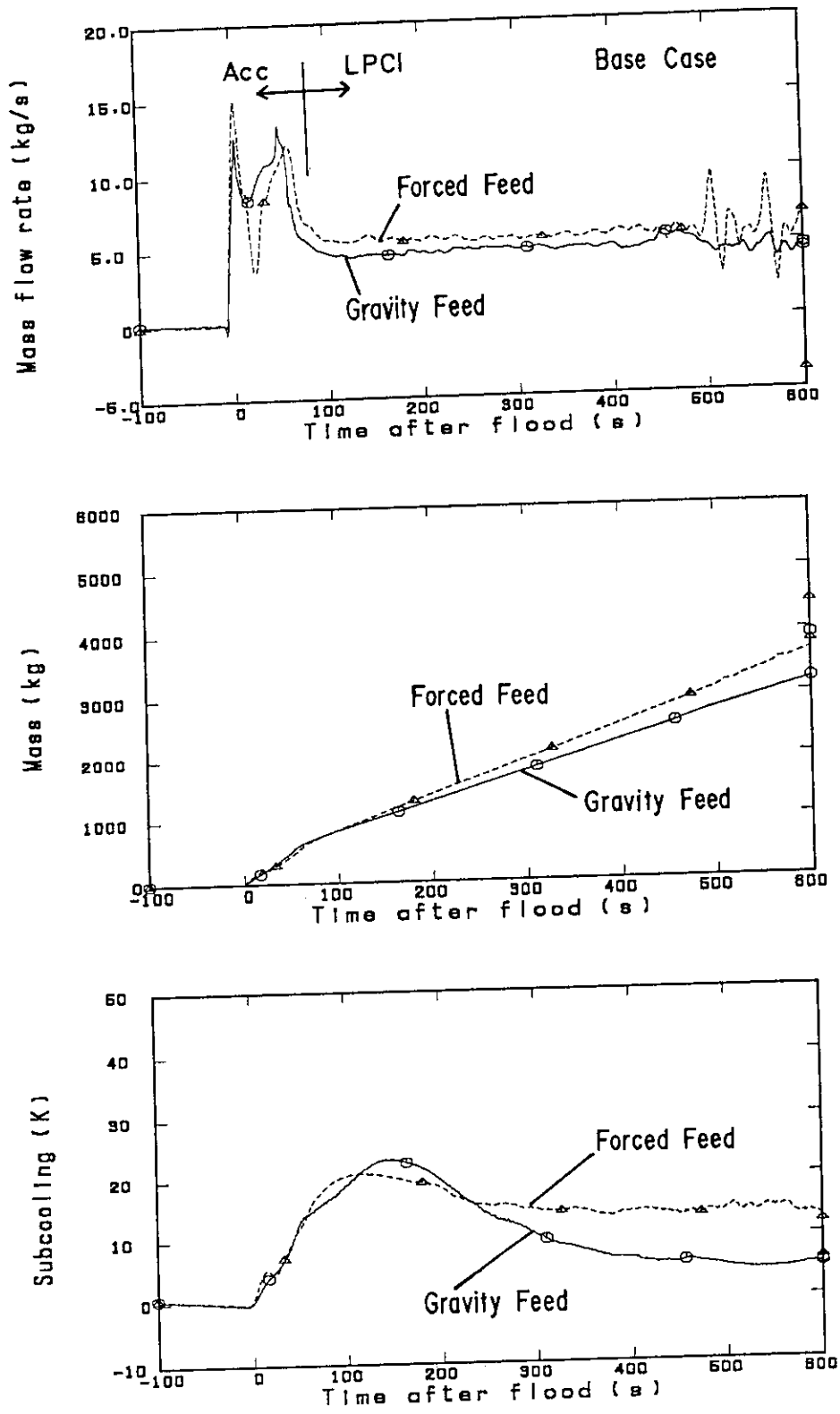

Fig.2.3(1) Comparison of core inlet boundary conditions in Base Case tests (Upper figure - core inlet mass flow rate, Middle - integrated core inlet mass and Lower - core inlet subcooling)

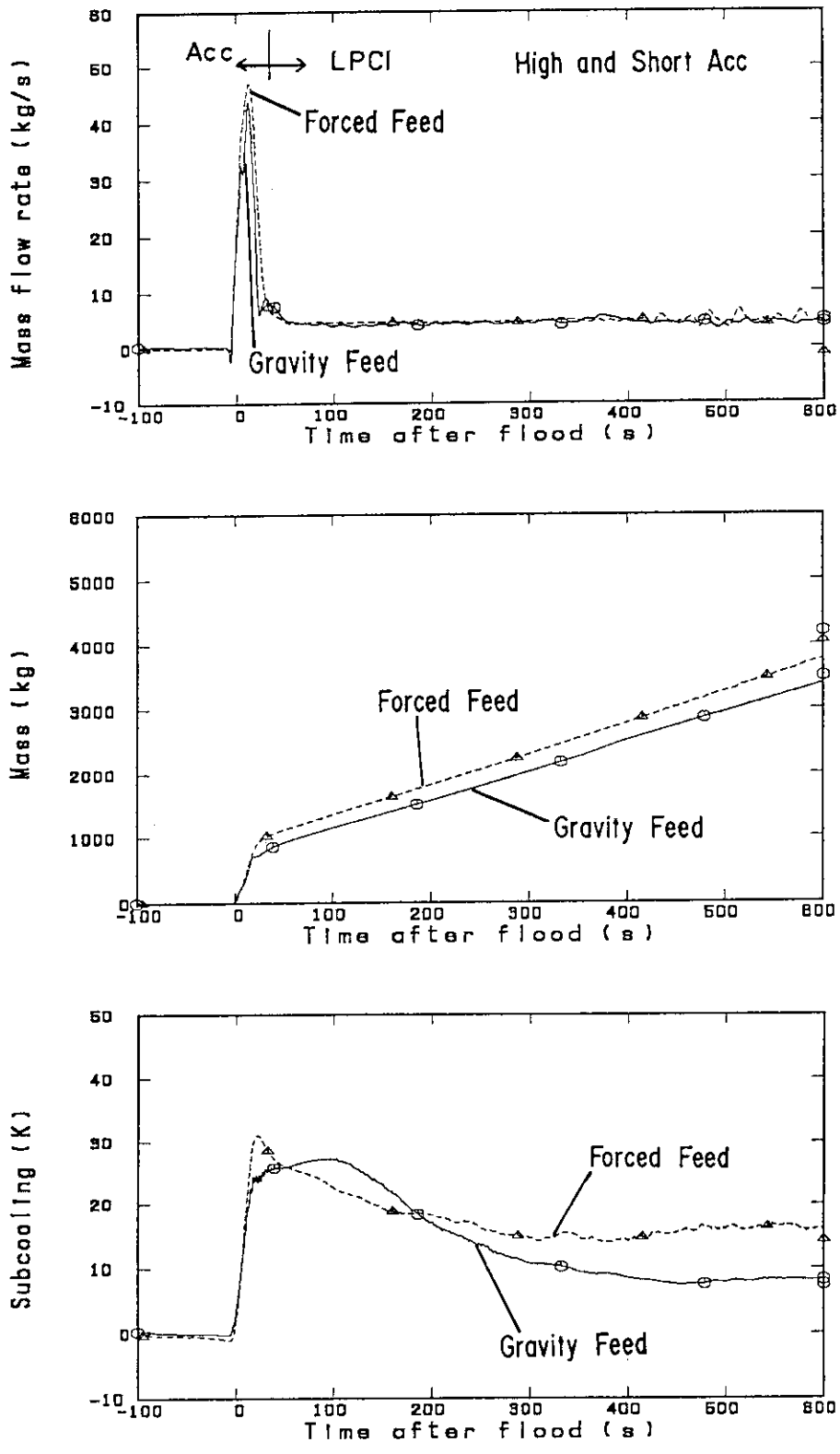

Fig.2.3(2) Comparison of core inlet boundary conditions in High and Short Acc tests (Upper figure - core inlet mass flow rate, Middle - integrated core inlet mass and Lower - core inlet subcooling)

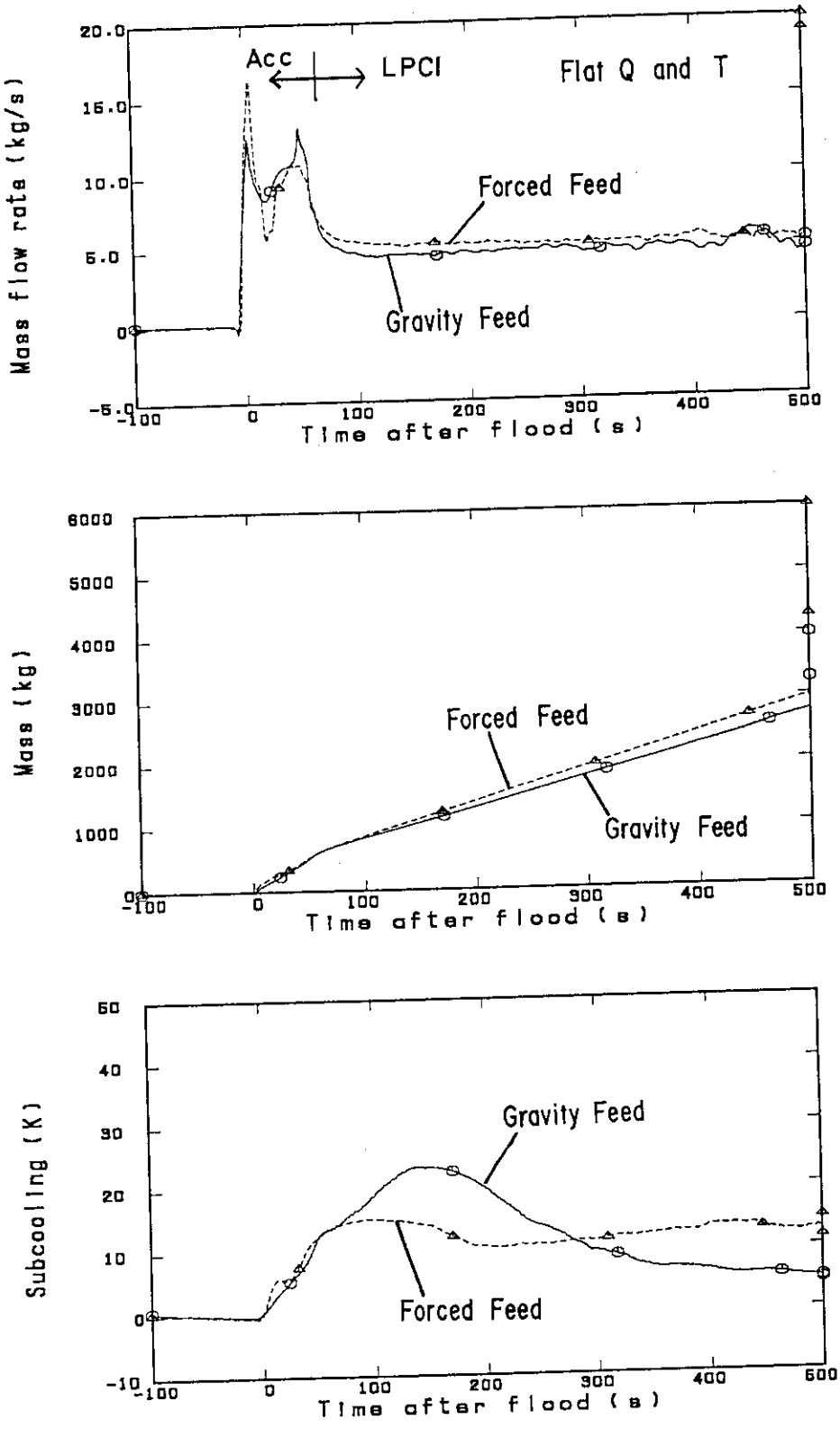

Fig.2.3(3) Comparison of core inlet boundary conditions in Flat Q and T tests (Upper figure - core inlet mass flow rate, Middle - integrated core inlet mass and Lower - core inlet subcooling)

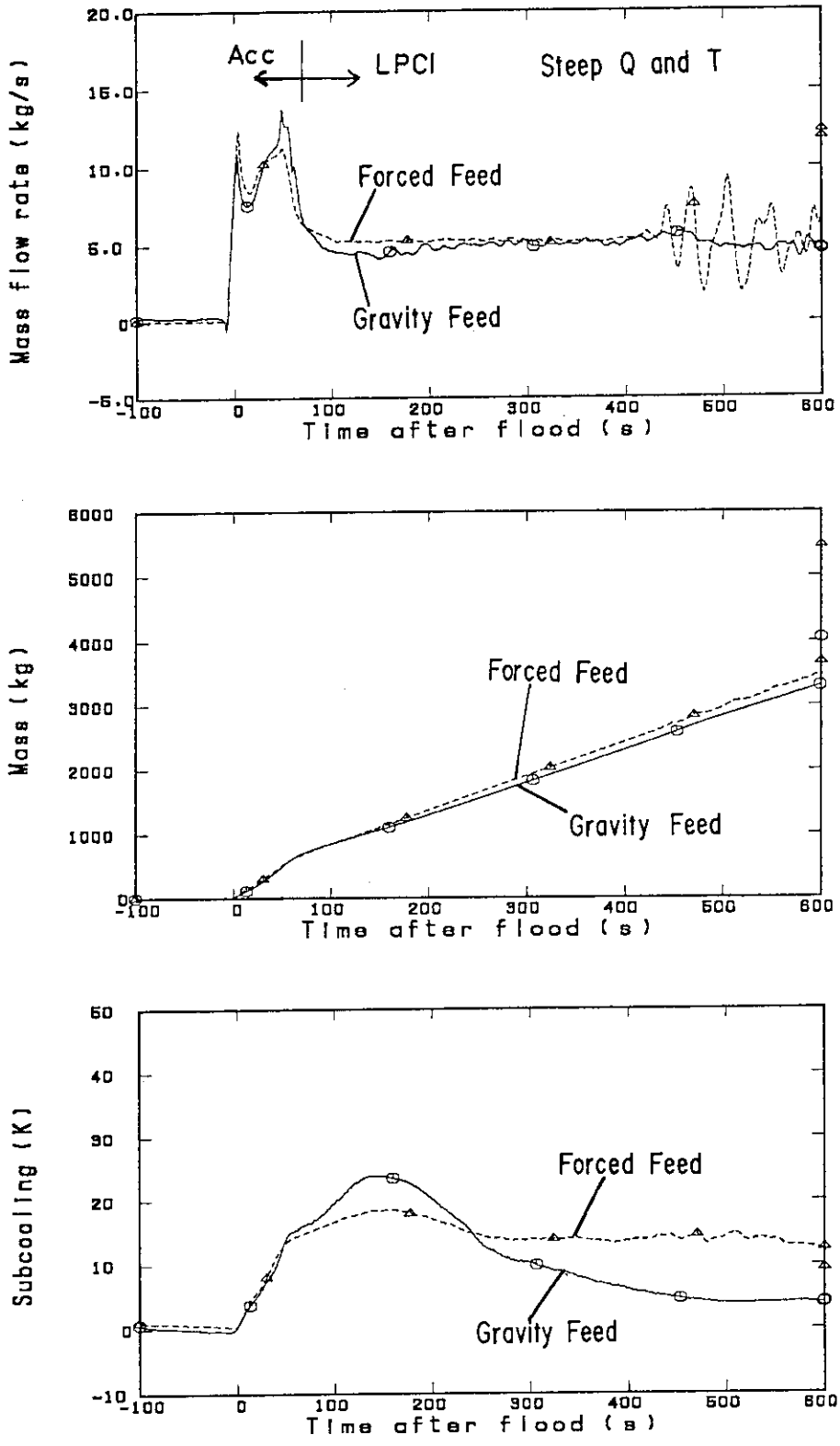

Fig.2.3(4) Comparison of core inlet boundary conditions in Steep Q and T tests (Upper figure - core inlet mass flow rate, Middle - integrated core inlet mass and Lower - core inlet subcooling)

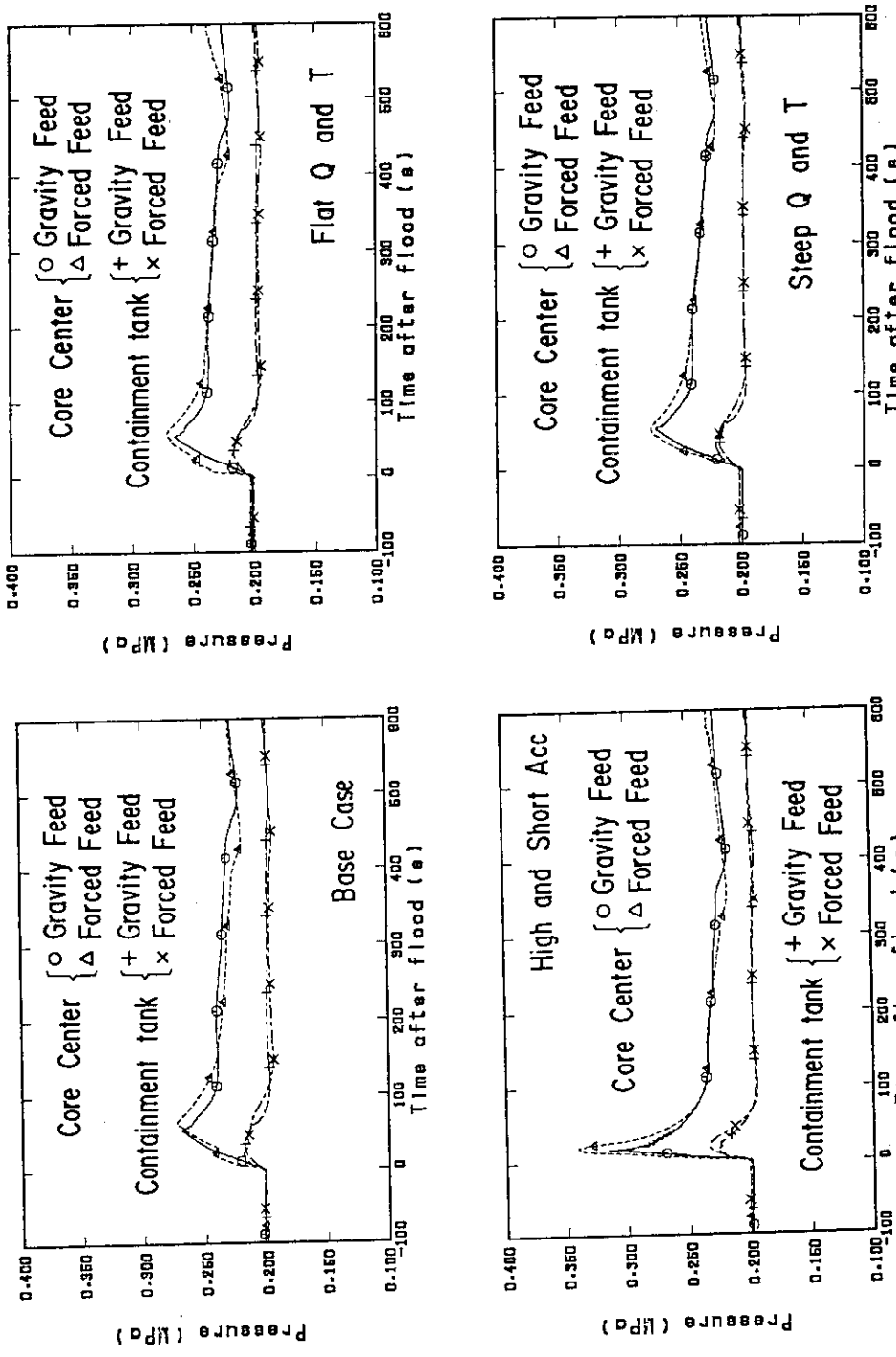

Fig.2.4 Comparison of pressure at core center and at containment tank

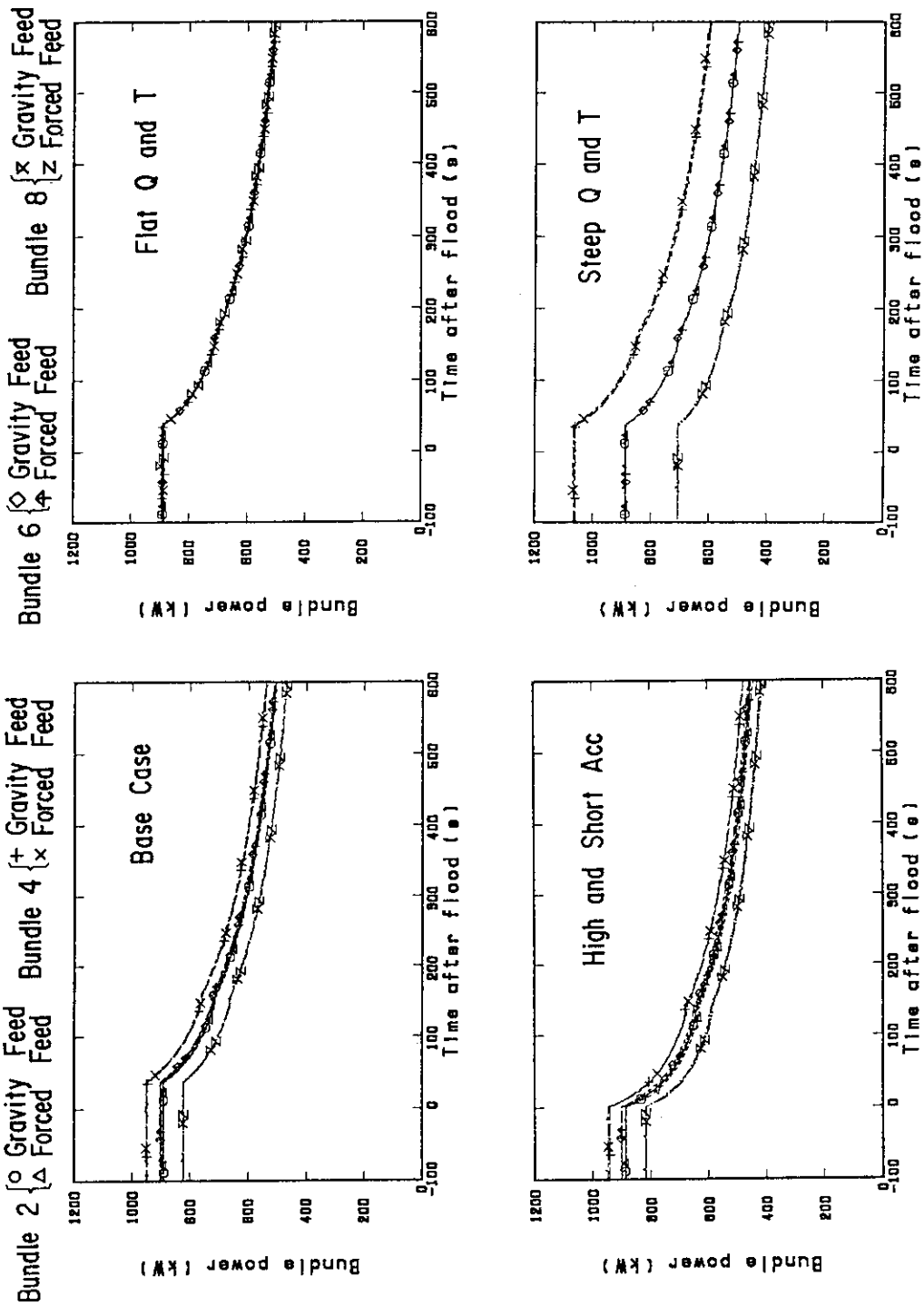

Fig.2.5 Comparison of core supplied power in bundles 2, 4, 6 and 8

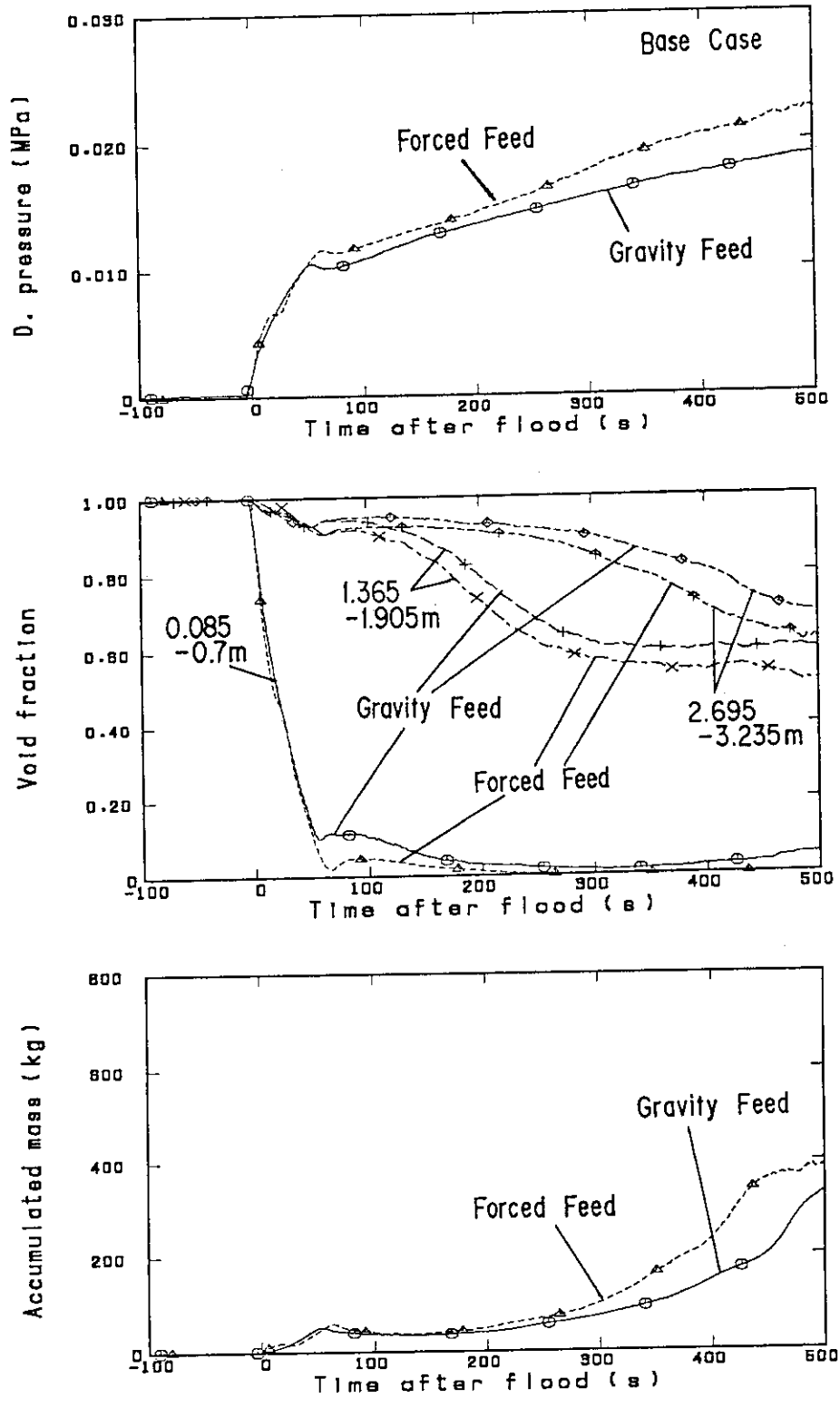

Fig.3.1(1) Comparison of overall hydraulic behaviors in pressure vessel in Base Case tests (Upper figure - core full height differential pressure in bundle 4, Middle - sectional void fraction in bundle 4 and Lower - de-entrained water mass accumulated in upper plenum)

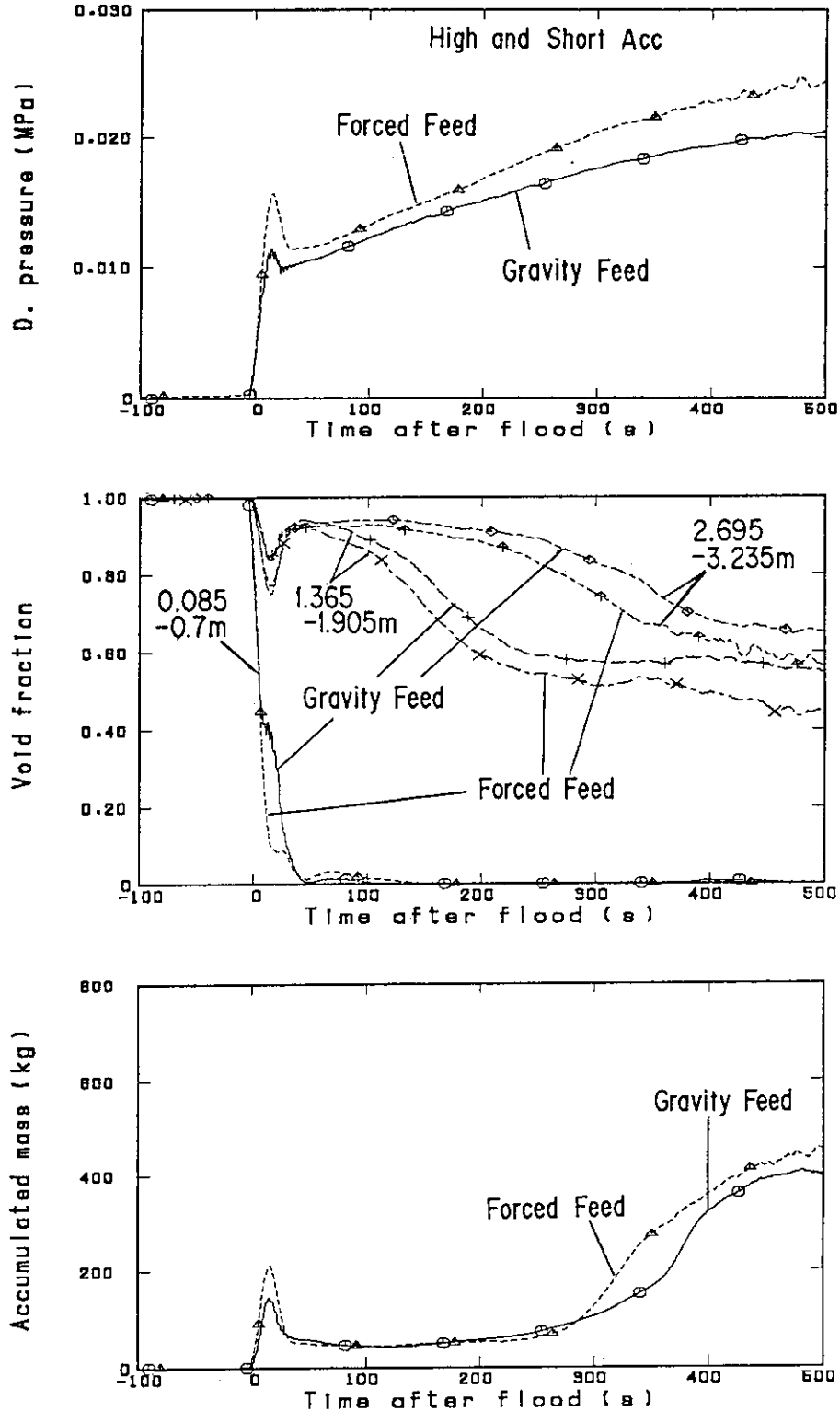

Fig.3.1(2) Comparison of overall hydraulic behaviors in pressure vessel in High and Short Acc tests (Upper figure - core full height differential pressure in bundle 4, Middle - sectional void fraction in bundle 4 and Lower - de-entrained water mass accumulated in upper plenum)

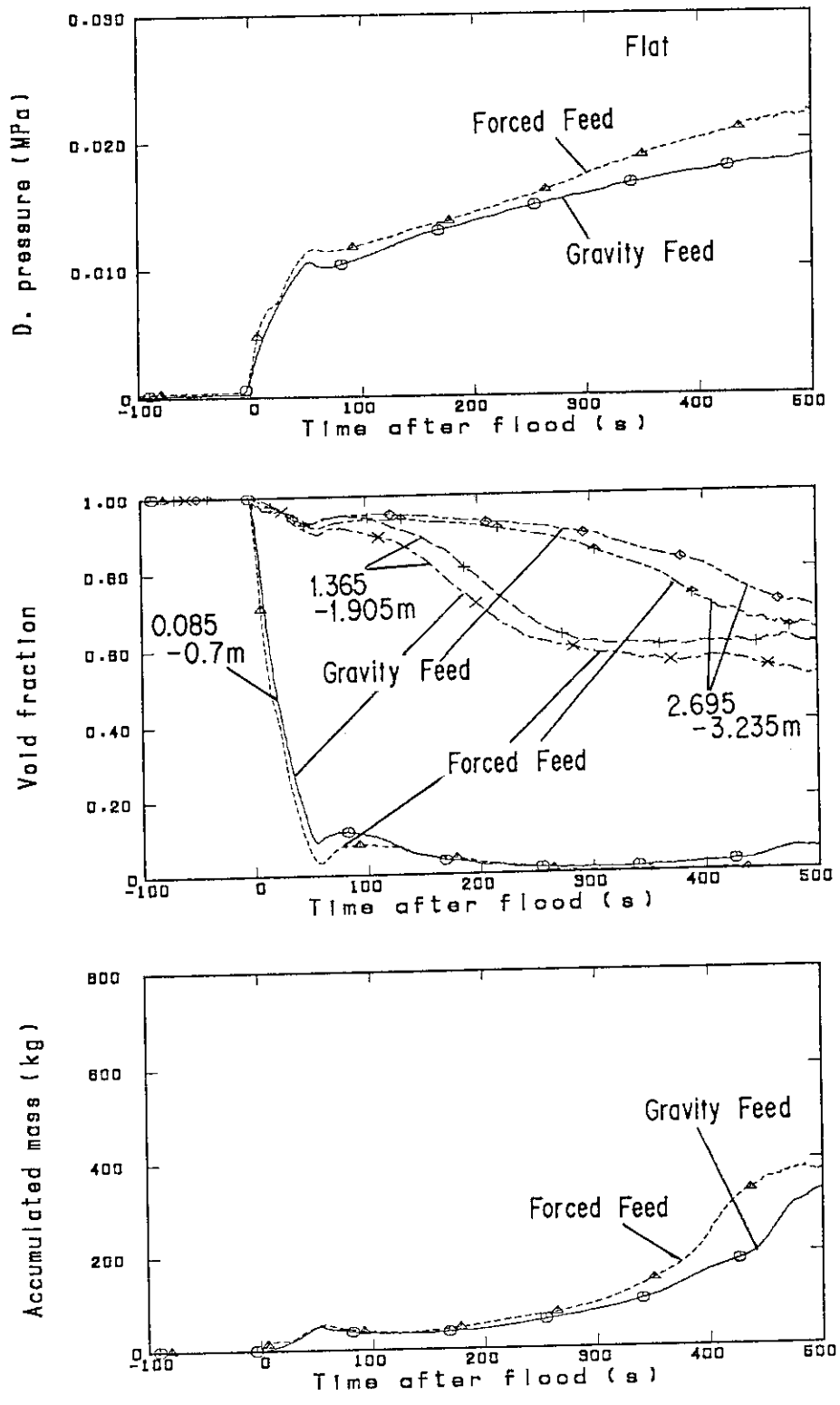

Fig.3.1(3) Comparison of overall hydraulic behaviors in pressure vessel in Flat Q and T tests (Upper figure - core full height differential pressure in bundle 4, Middle - sectional void fraction in bundle 4 and Lower - de-entrained water mass accumulated in upper plenum)

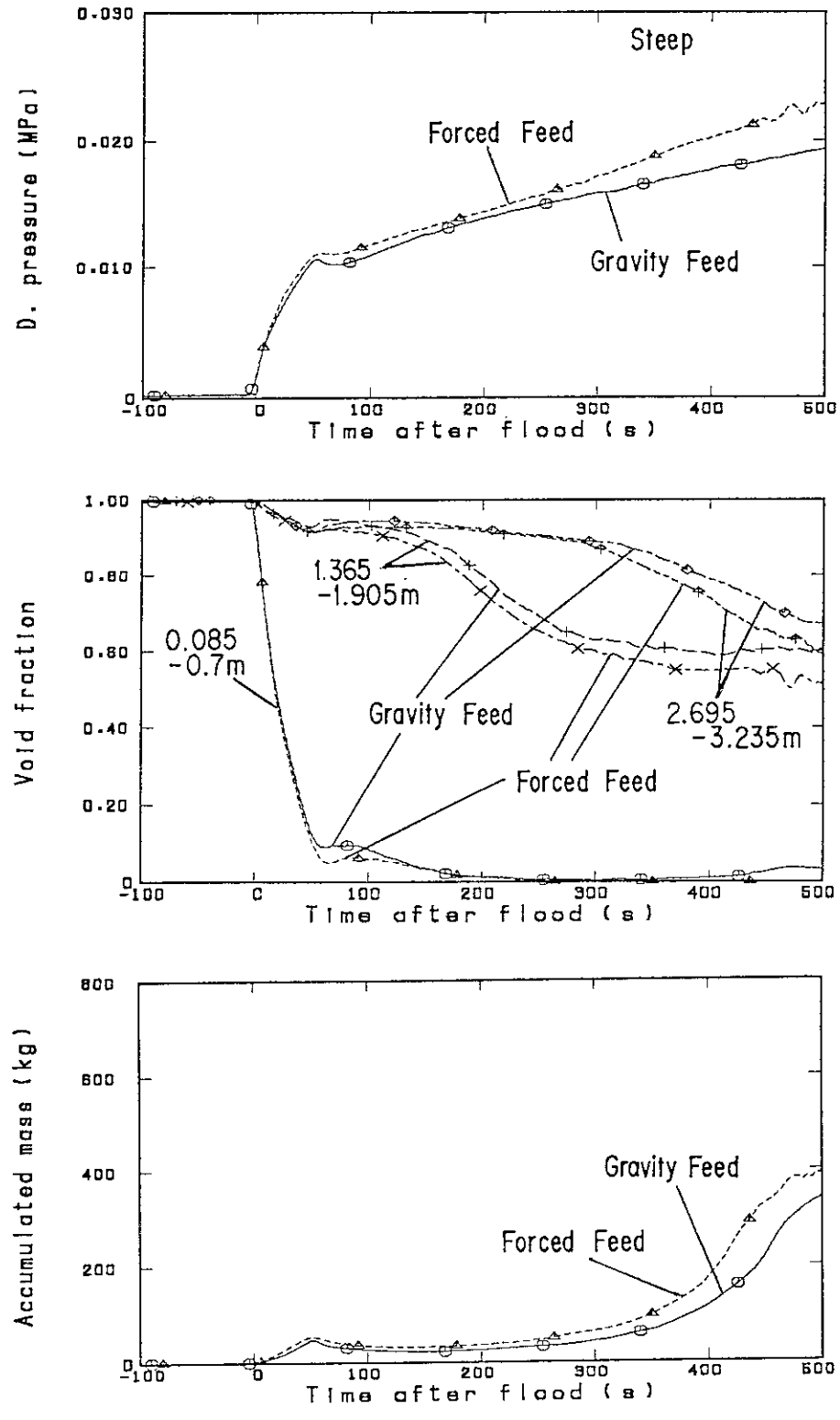

Fig.3.1(4) Comparison of overall hydraulic behaviors in pressure vessel in Steep Q and T tests (Upper figure - core full height differential pressure in bundle 4, Middle - sectional void fraction in bundle 4 and Lower - de-entrained water mass accumulated in upper plenum)

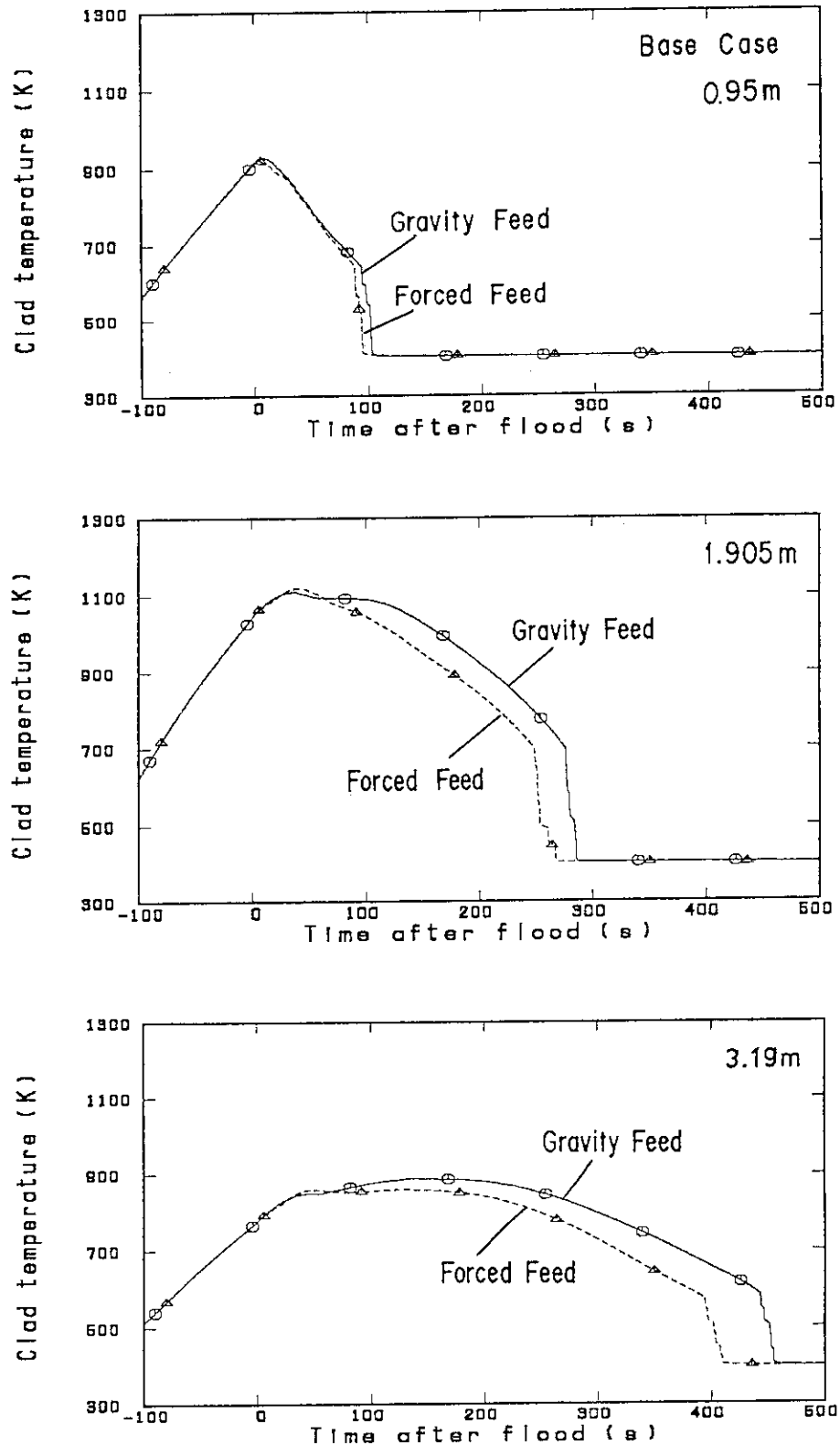

Fig.3.2(1) Comparison of clad surface temperature averaged at a specified elevation in bundle 4 in Base Case tests

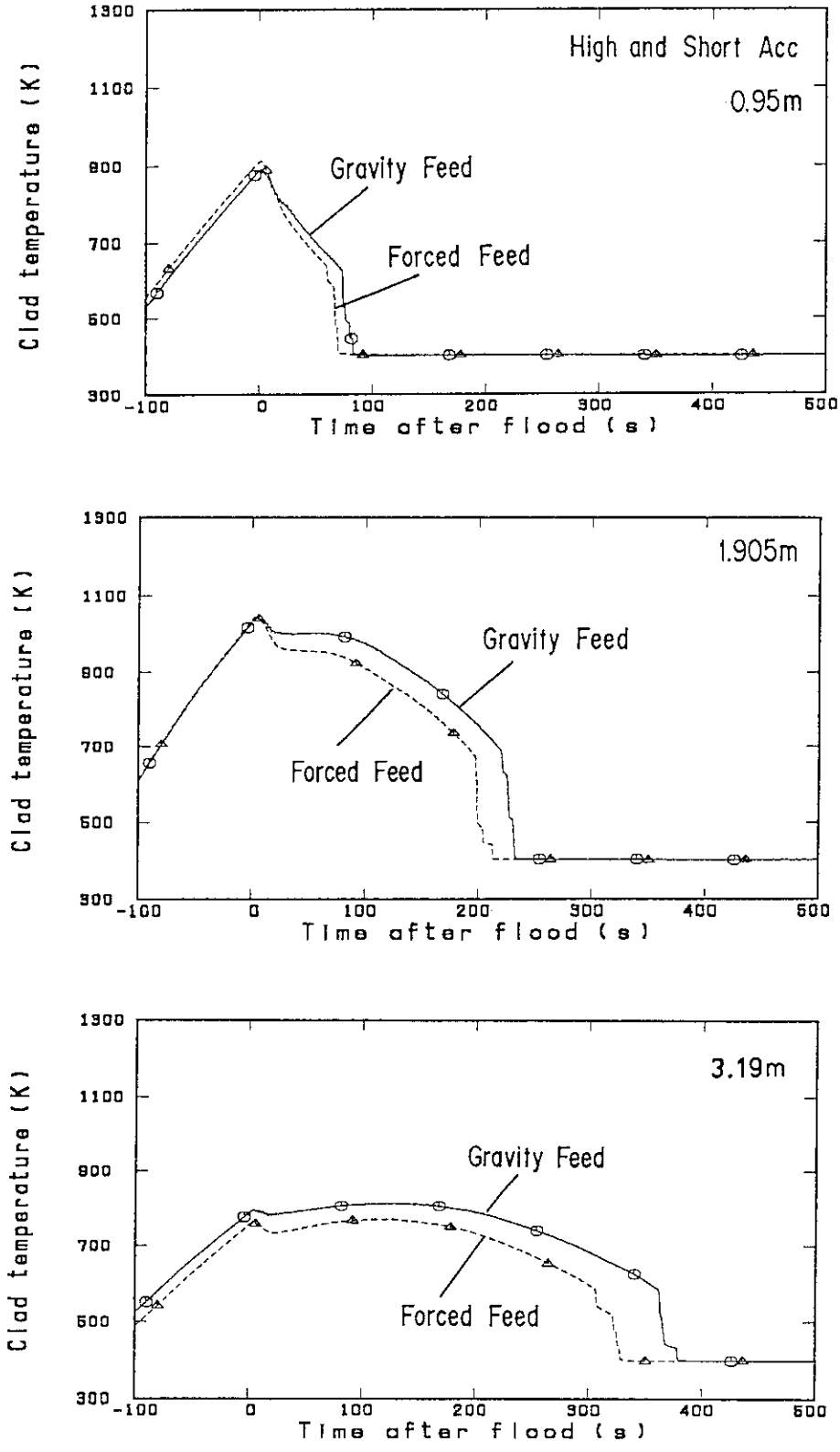

Fig.3.2(2) Comparison of clad surface temperature averaged at a specified elevation in bundle 4 in High and Short Acc tests

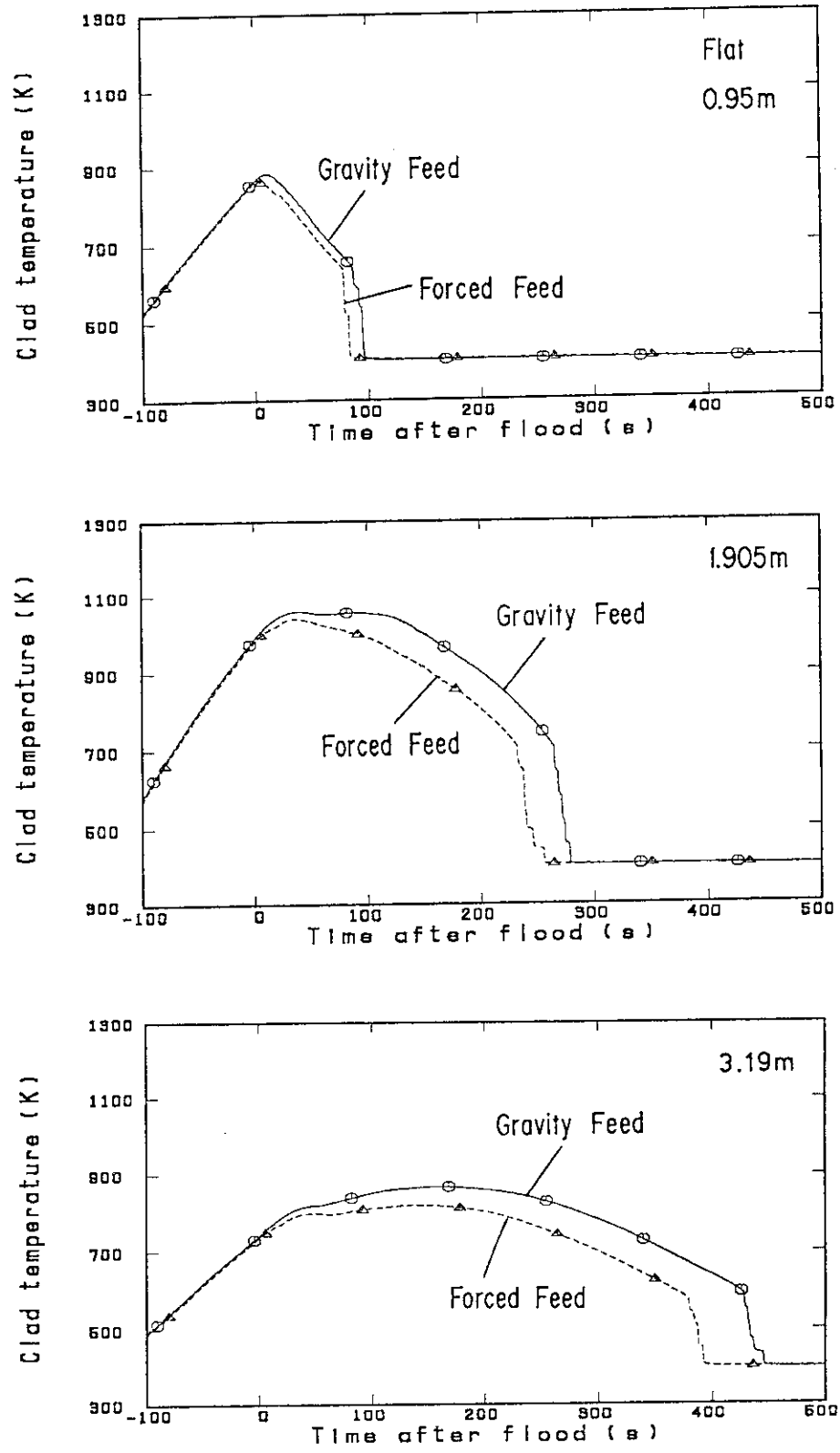

Fig.3.2(3) Comparison of clad surface temperature averaged at a specified elevation in bundle 4 in Flat Q and T tests

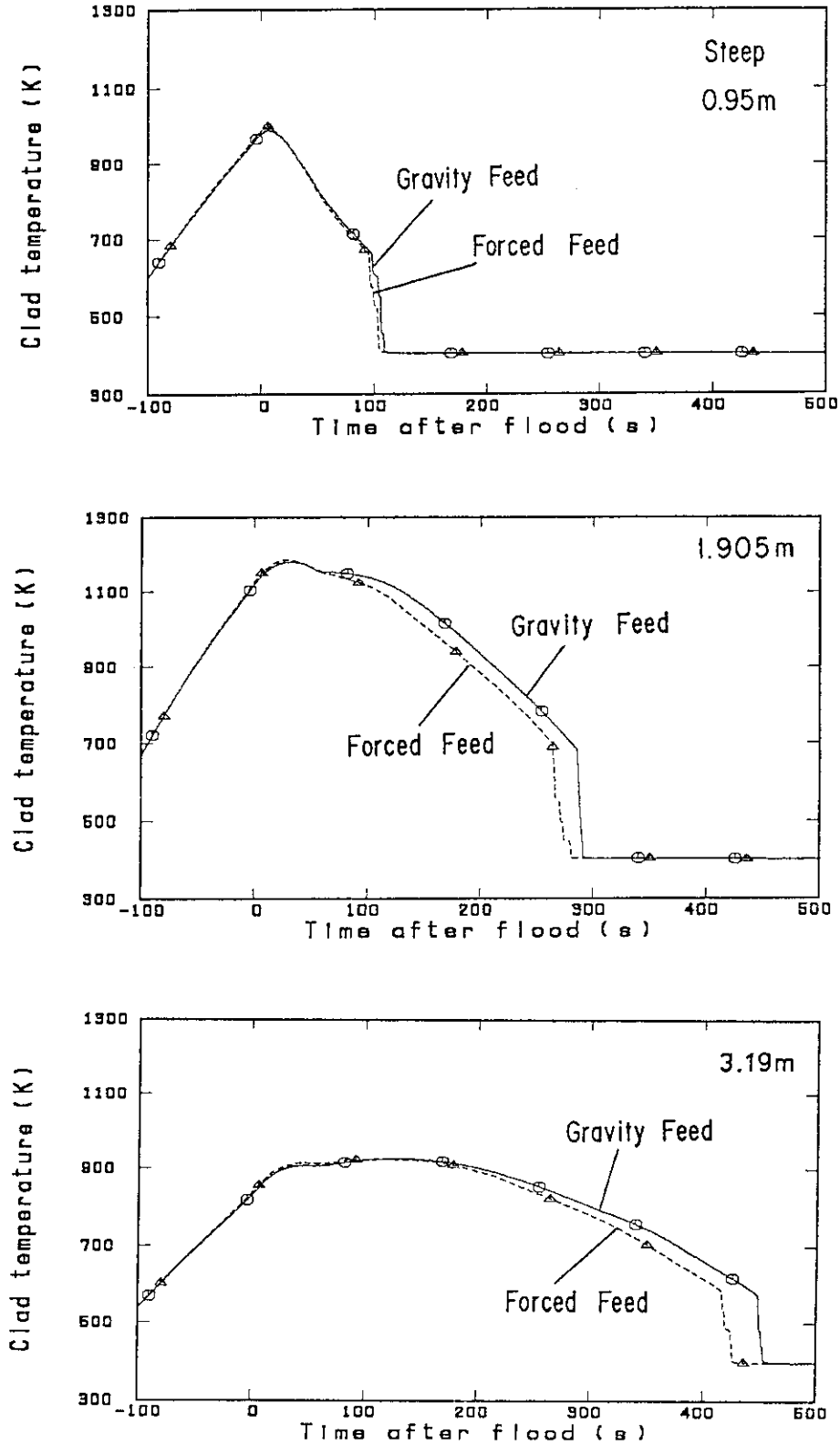

Fig.3.2(4) Comparison of clad surface temperature averaged at a specified elevation in bundle 4 in Steep Q and T tests

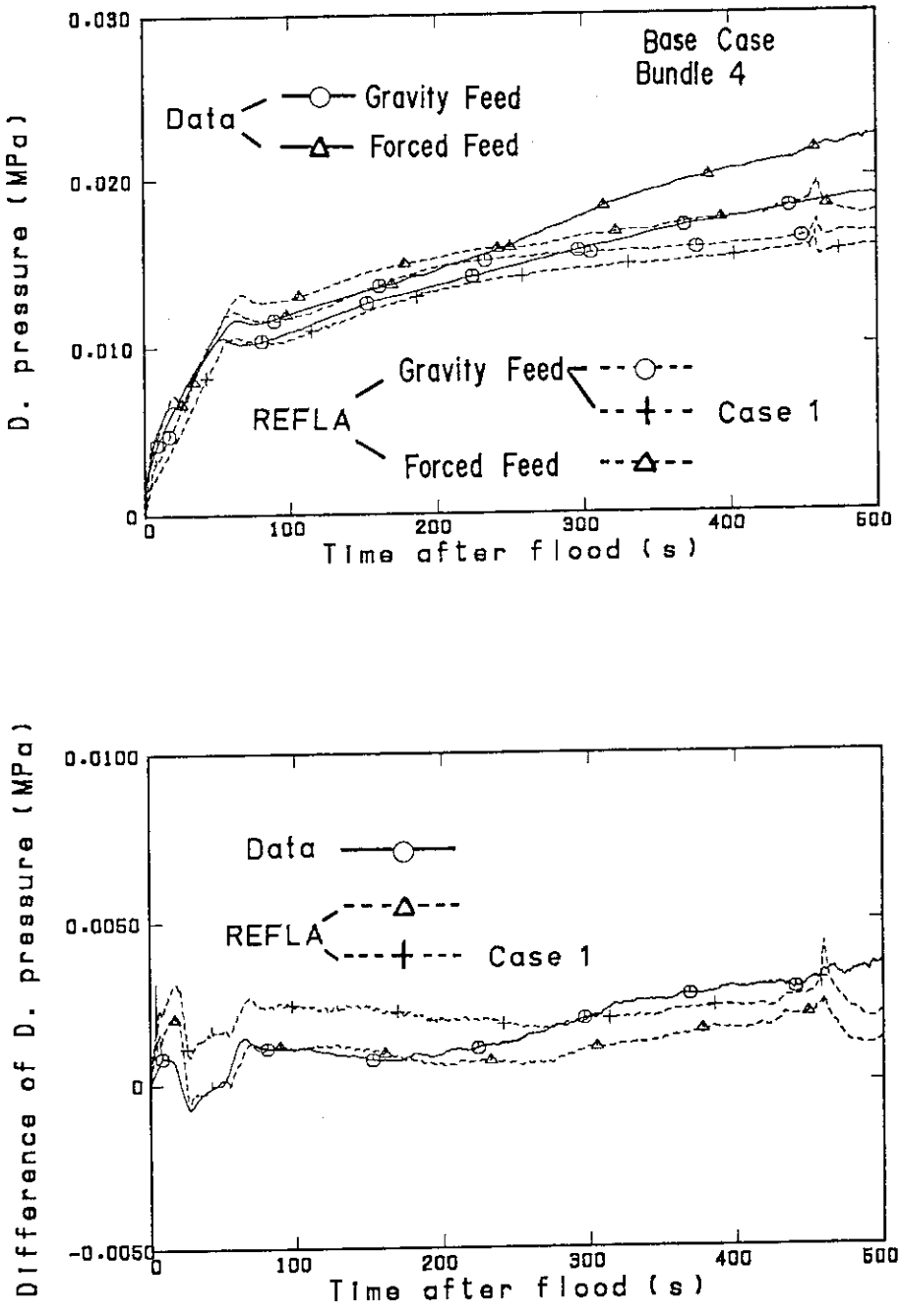

Fig.3.3(1) Comparison between data and predictions with REFLA code on core full height differential pressure in Base Case tests

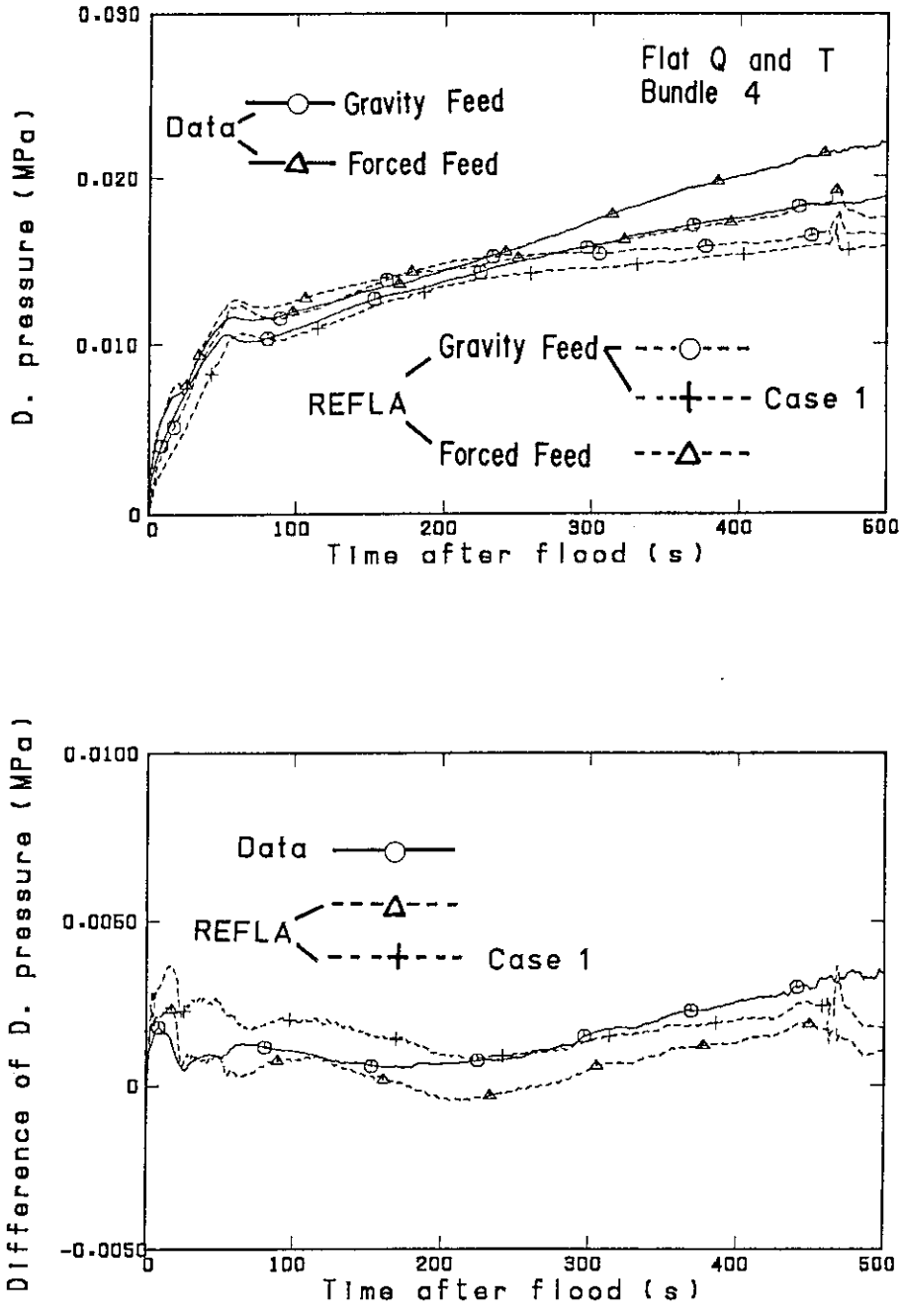

Fig.3.3(2) Comparison between data and predictions with REFLA code on core full height differential pressure in Flat Q and T tests

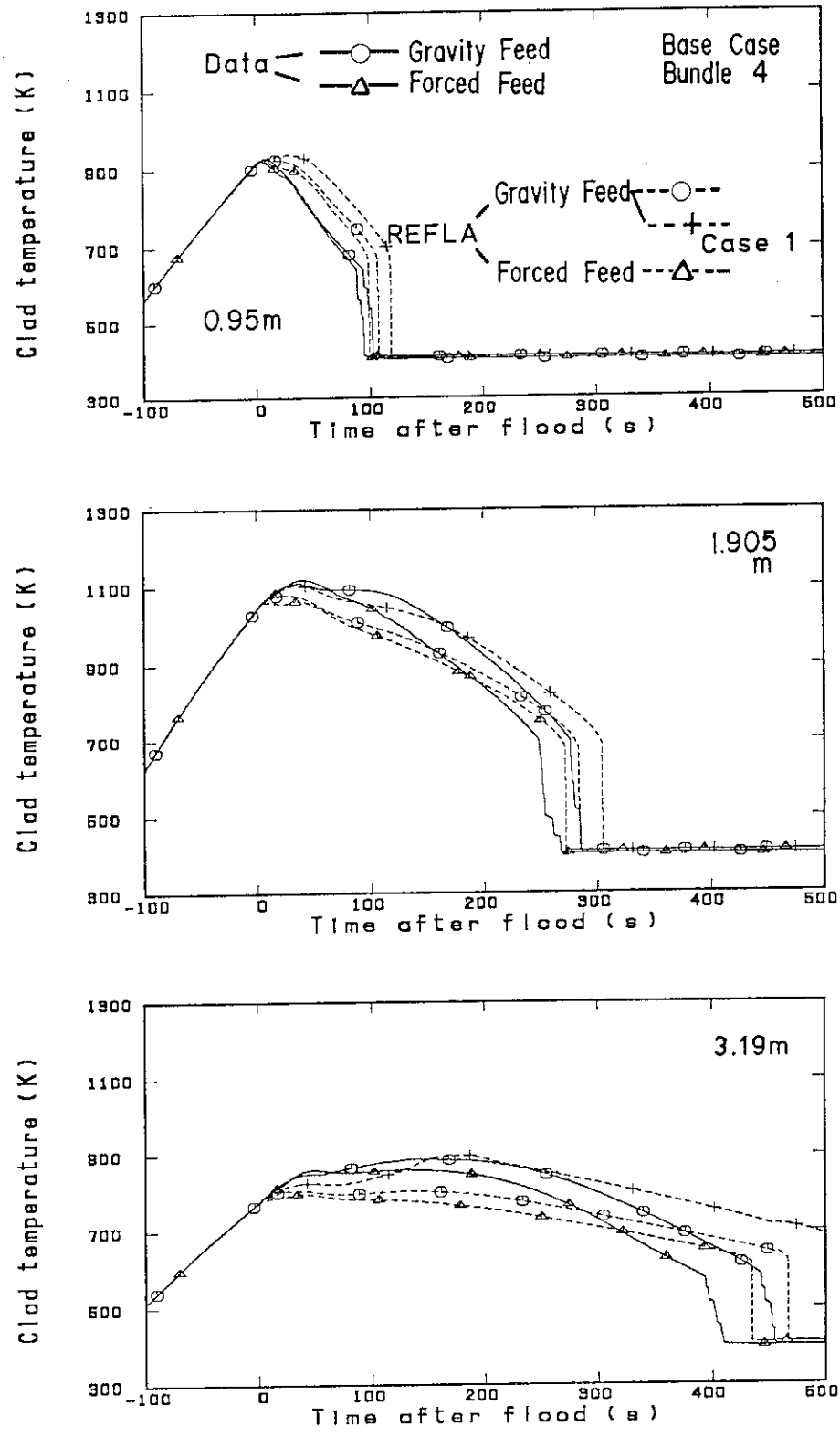

Fig.3.4(1) Comparison between data and predictions with REFLA code on clad surface temperature at a specified elevation in bundle 4 in Base Case tests

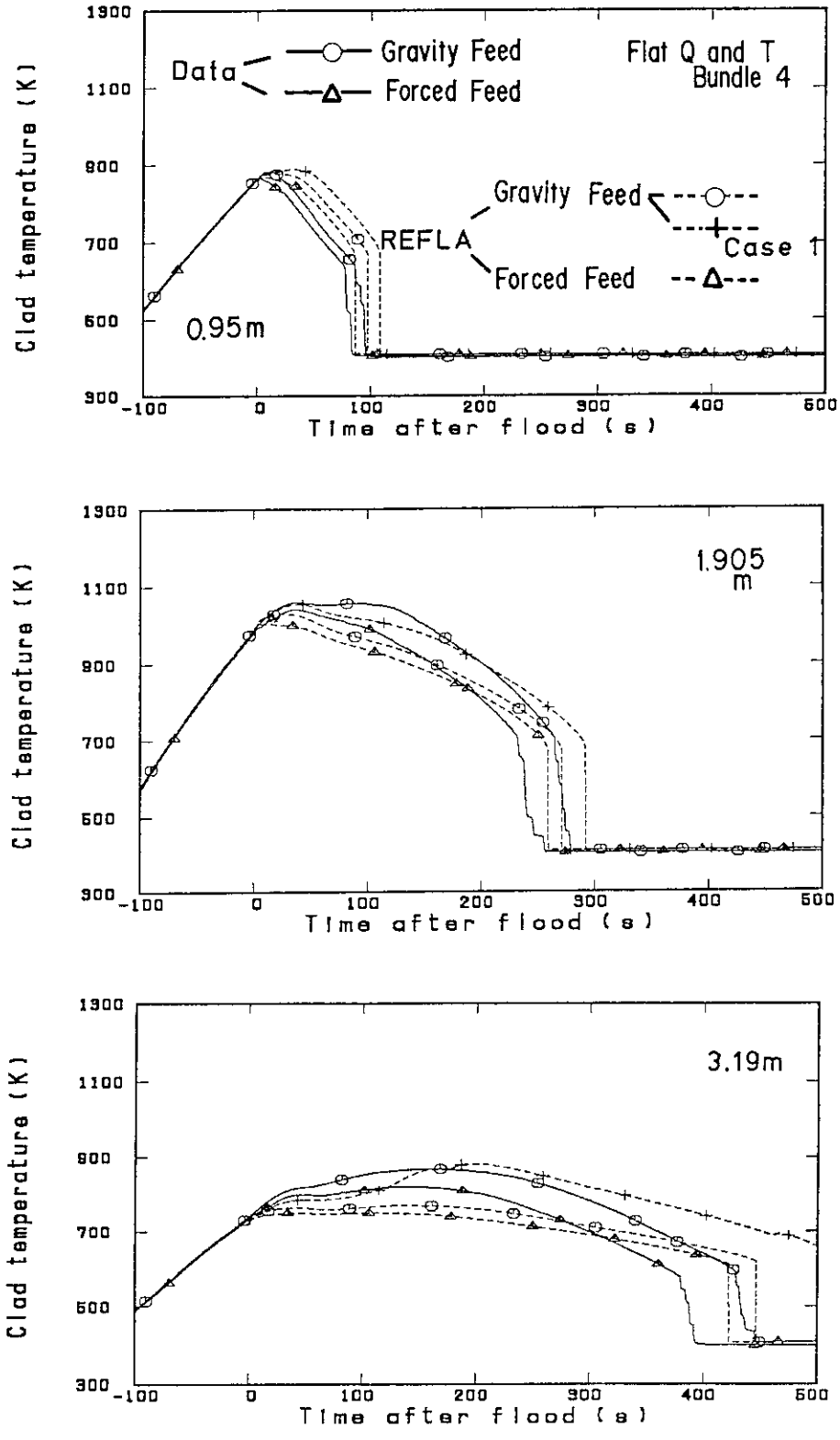

Fig.3.4(2) Comparison between data and predictions with REFLA code on clad surface temperature at a specified elevation in bundle 4 in Flat Q and T tests

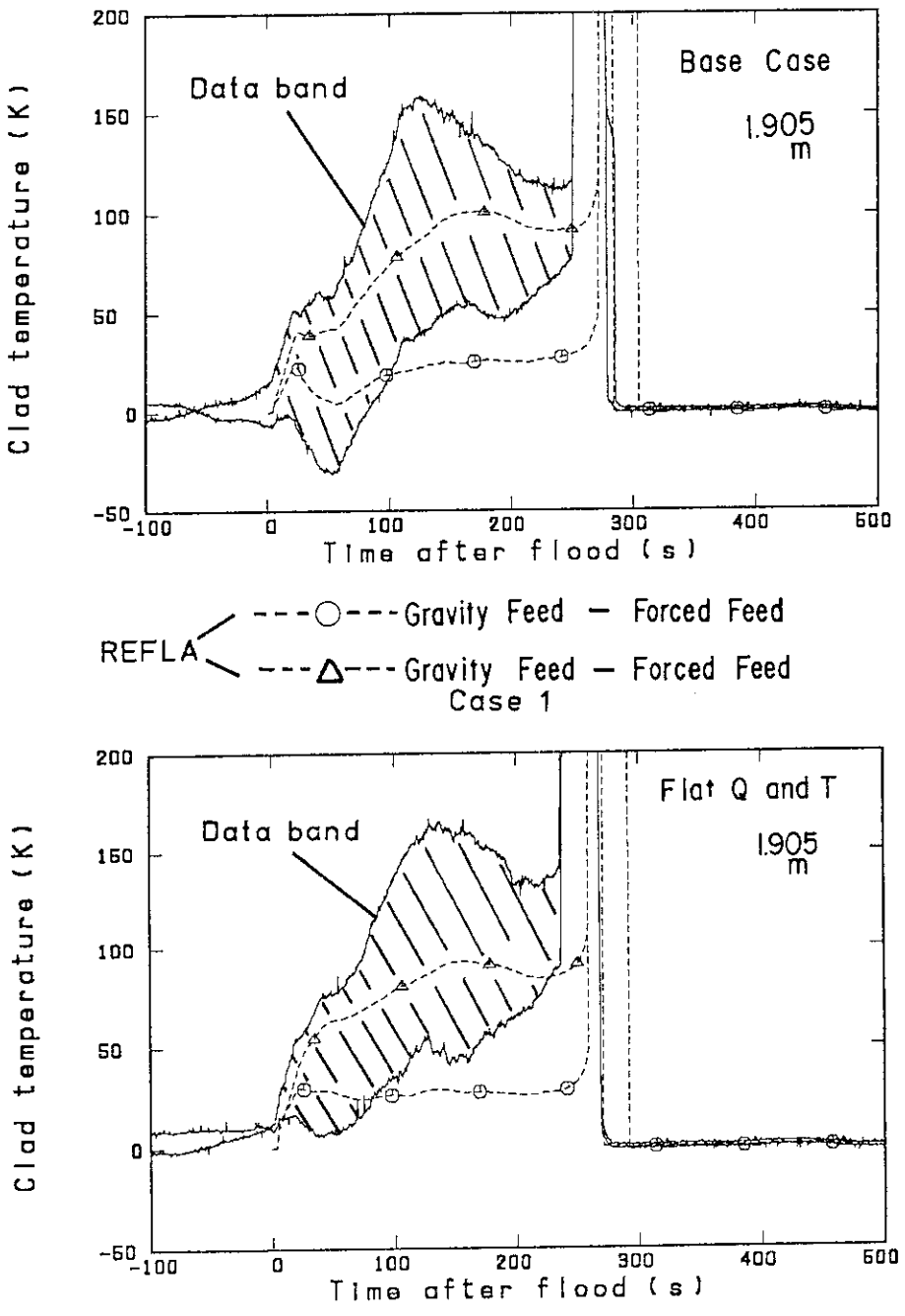

Fig.3.5 Comparison of differences of clad surface temperature between gravity and forced feeds in tests and between those in predictions

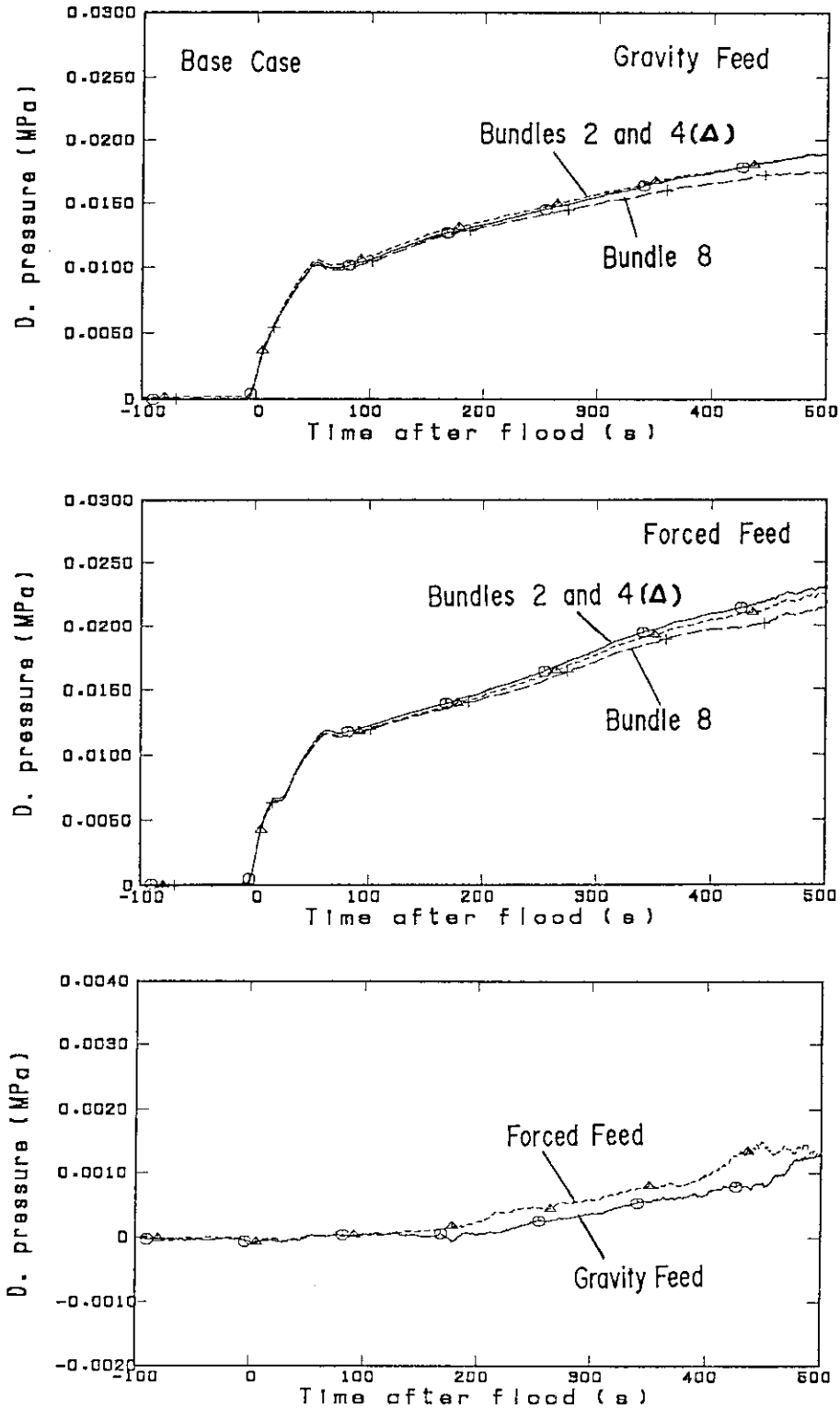

Fig.3.6(1) Comparison of radial distribution on core full height differential pressure in Base Case tests (Upper figure - gravity feed test, Middle - forced feed test and Lower - difference between the maximum differential pressure and the minimum one)

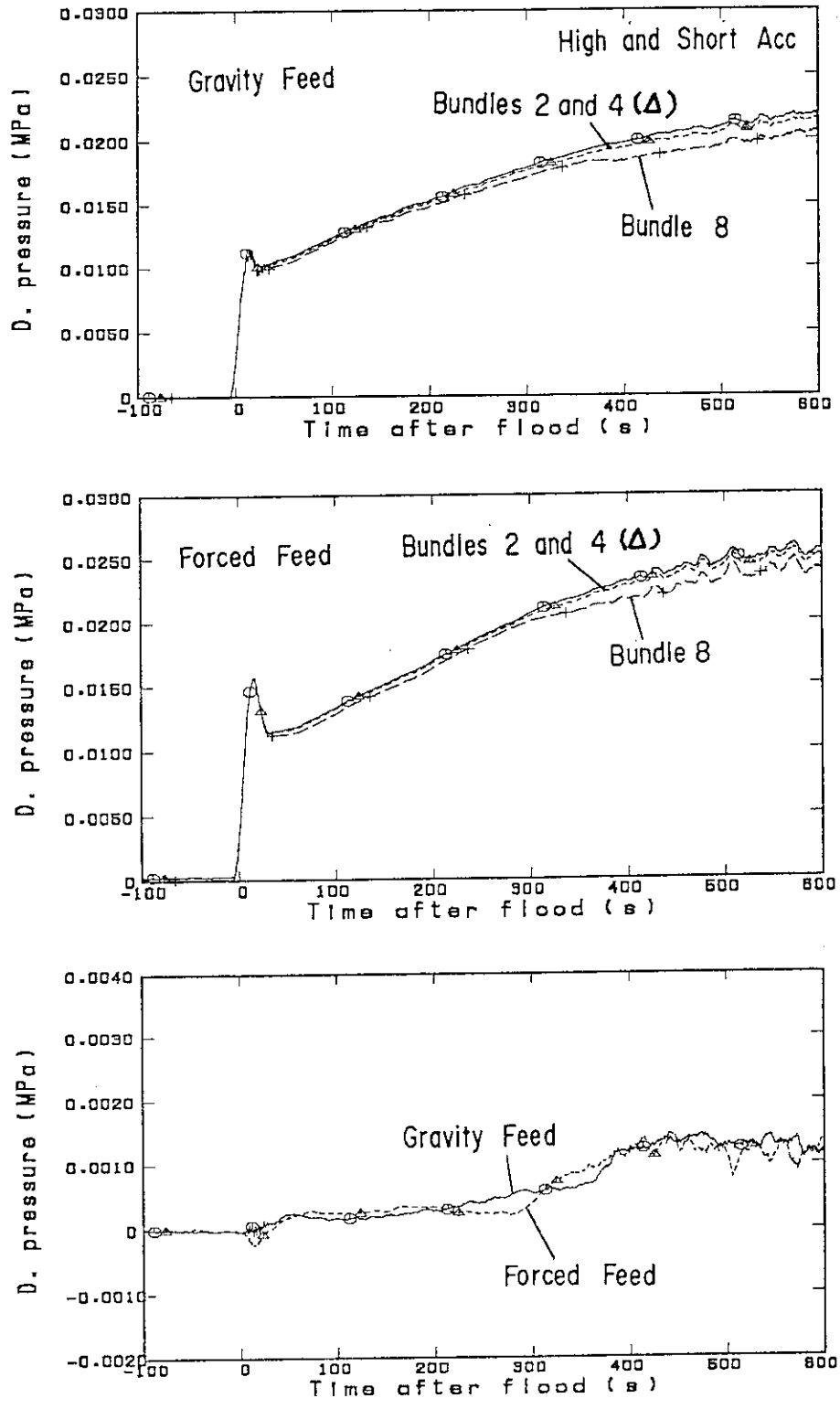

Fig.3.6(2) Comparison of radial distribution on core full height differential pressure in High and Short Acc tests (Upper figure - gravity feed test, Middle - forced feed test and Lower - difference between the maximum differential pressure and the minimum one)

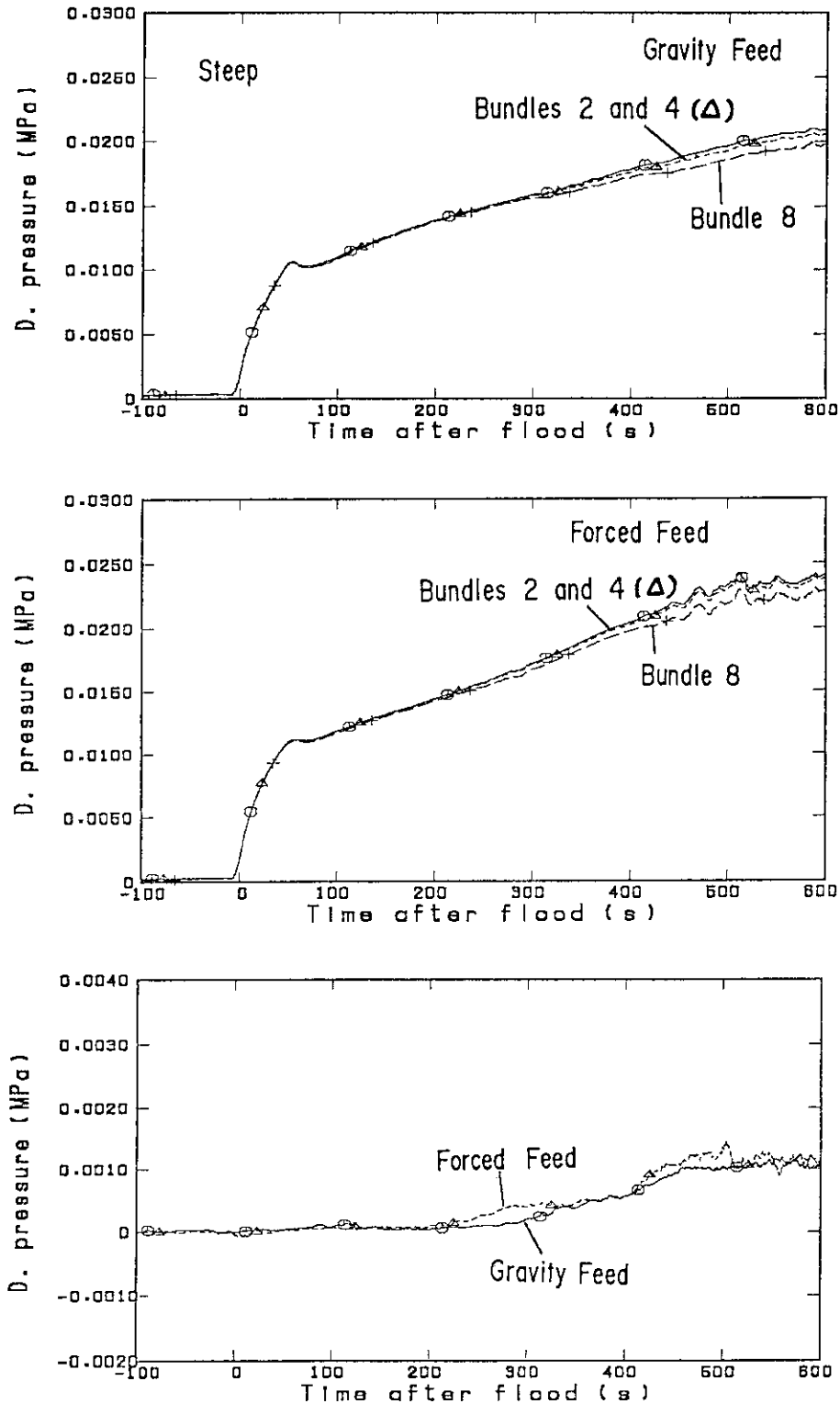

Fig.3.6(3) Comparison of radial distribution on core full height differential pressure in Steep Q and T tests (Upper figure - gravity feed test, Middle - forced feed test and Lower - difference between the maximum differential pressure and the minimum one)

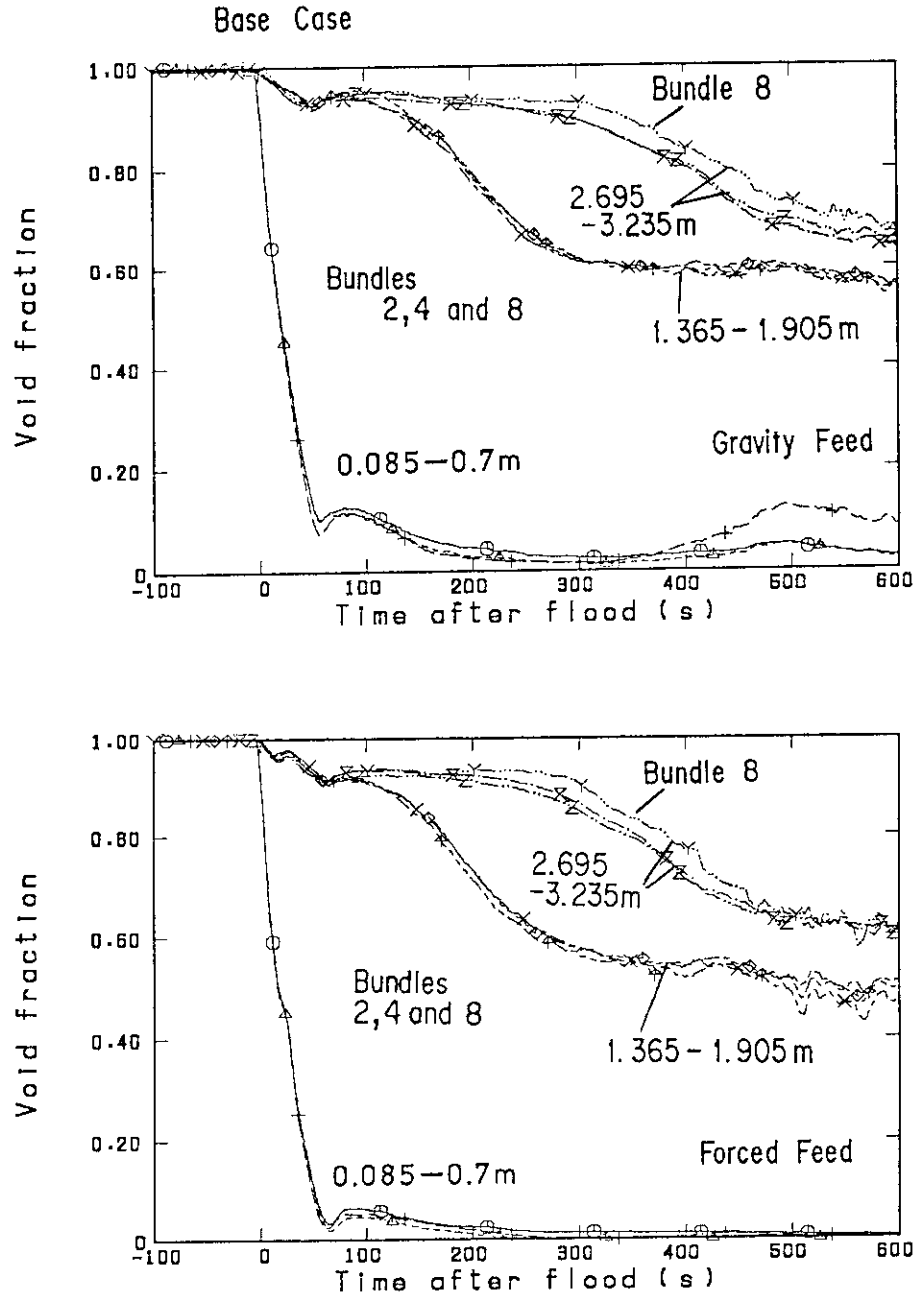

Fig.3.7(1) Comparison of radial distribution on sectional void fraction in Base Case tests (Upper figure - gravity feed test and Lower - forced feed test)

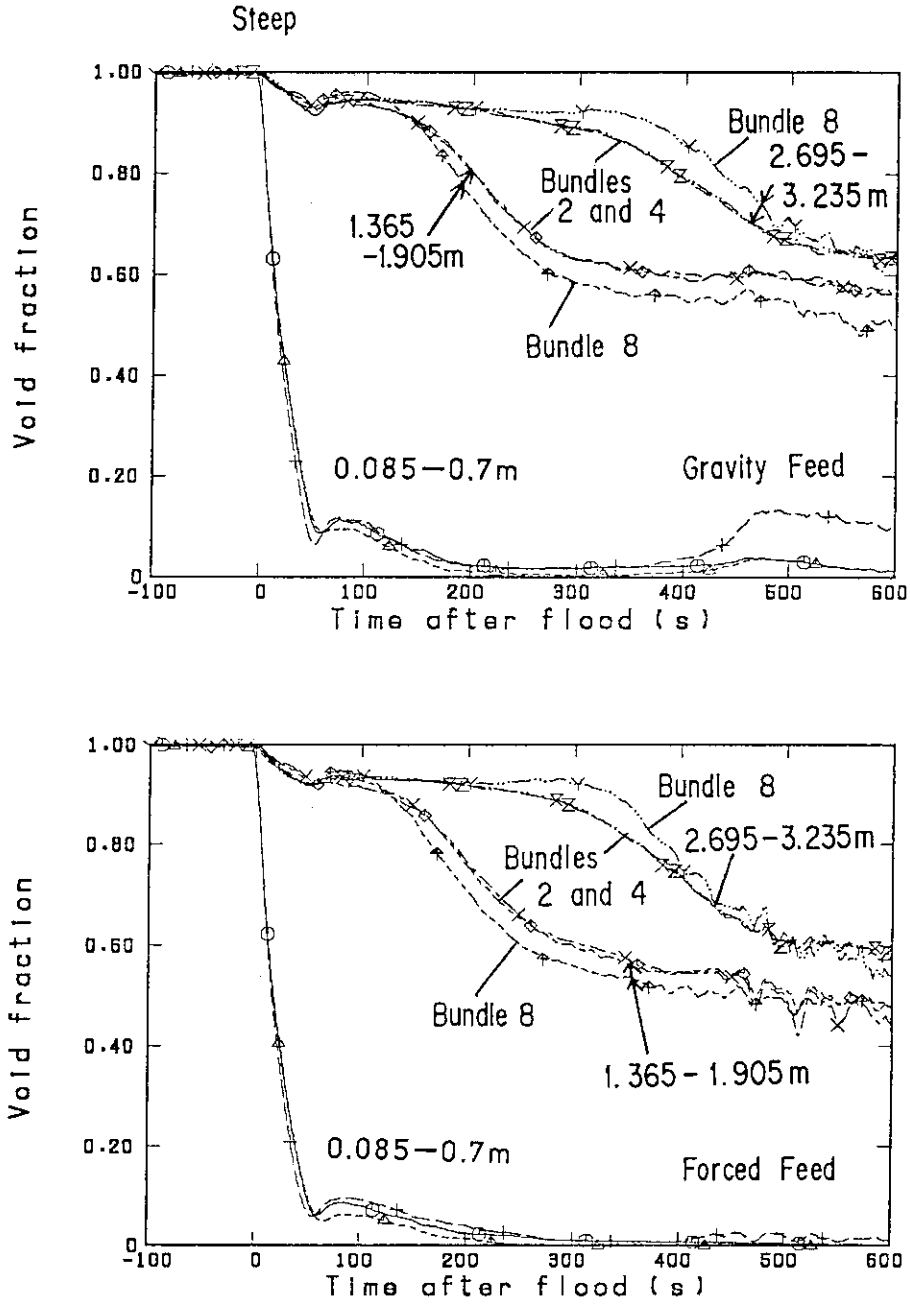

Fig.3.7(2) Comparison of radial distribution on sectional void fraction in Steep Q and T tests (Upper figure - gravity feed test and Lower - forced feed test)

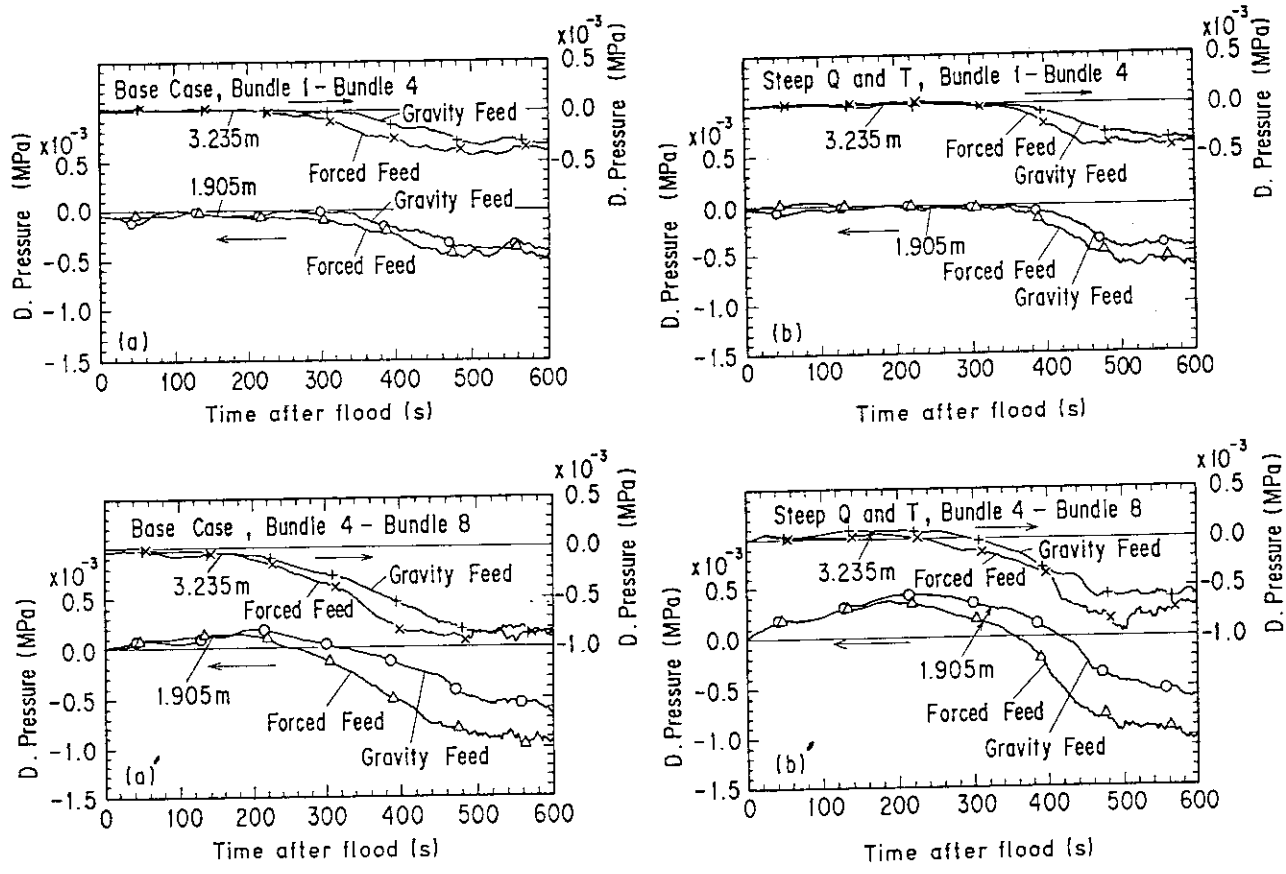

Fig.3.8 Comparison of horizontal differential pressure at 1.905m and 3.235m elevations ((a) and (a)' - Base Case tests, (b) and (b)' - Steep Q and T tests, Upper position - differential pressure between bundles 1 and 4 and Lower position - differential pressure between bundles 4 and 8)

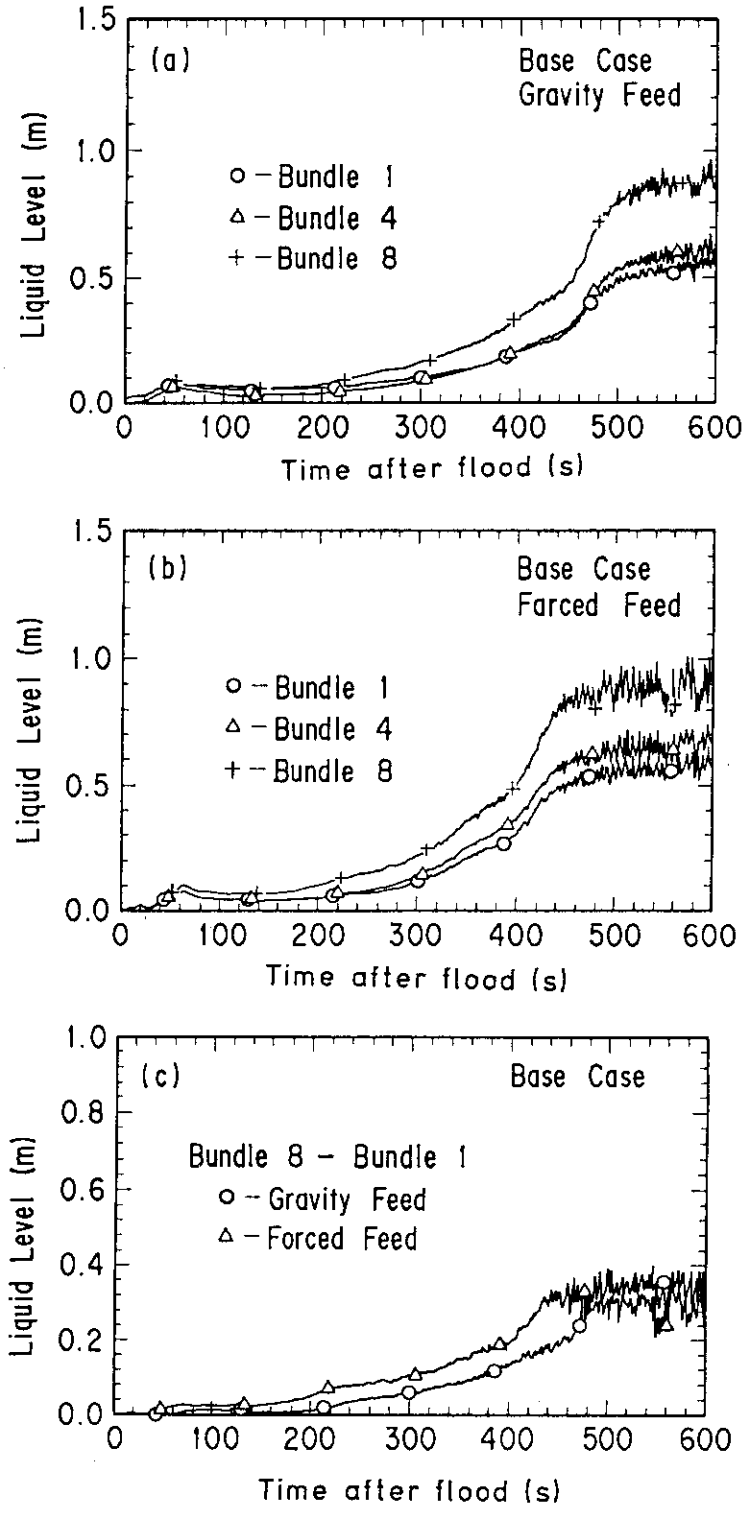

Fig.3.9(1) Comparison of radial distribution on collapsed liquid level in upper plenum in Base Case tests (Upper figure - gravity feed test, Middle - forced feed test and Lower - difference between the liquid level above bundles 1 and 8)

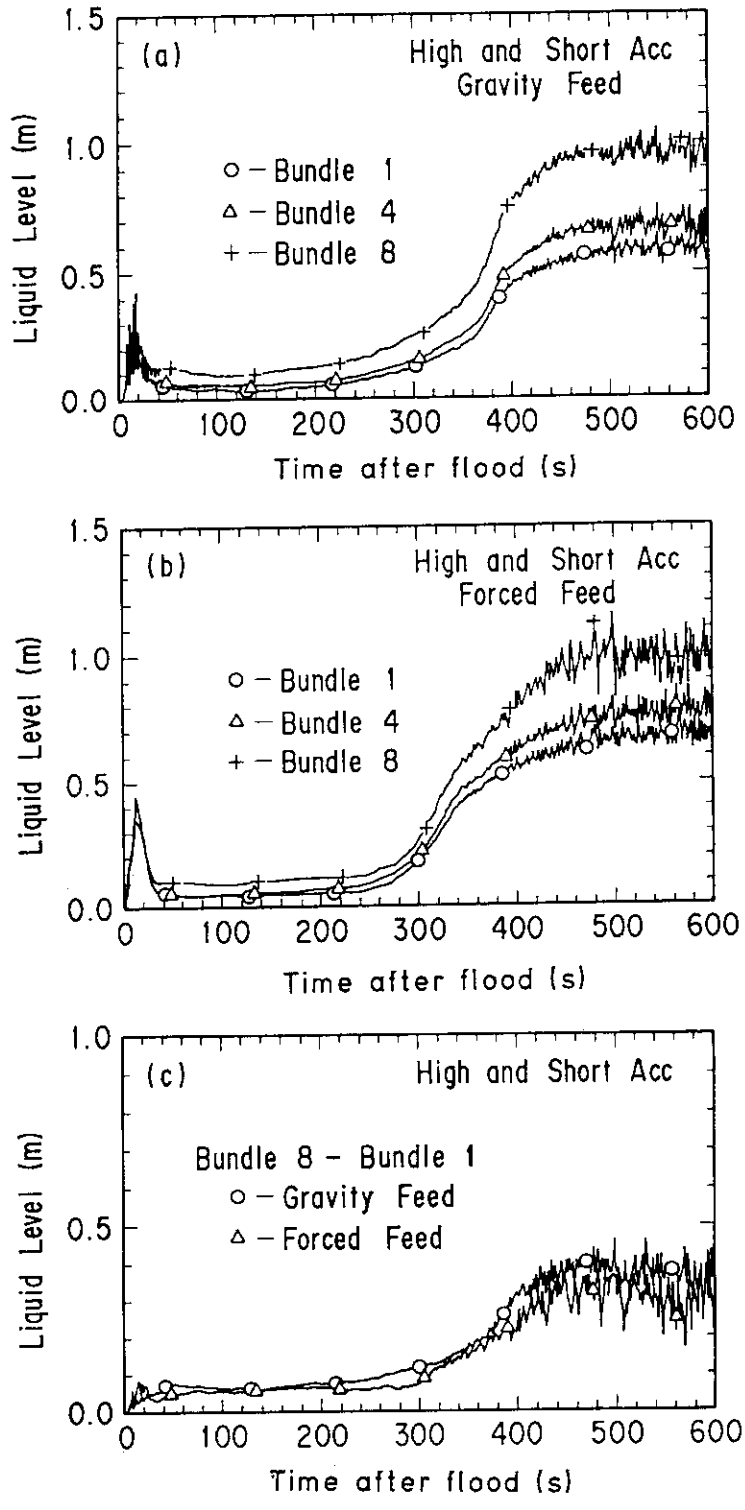

Fig.3.9(2) Comparison of radial distribution on collapsed liquid level in upper plenum in High and Short Acc tests (Upper figure - gravity feed test, Middle - forced feed test and Lower - difference between the liquid level above bundles 1 and 8)

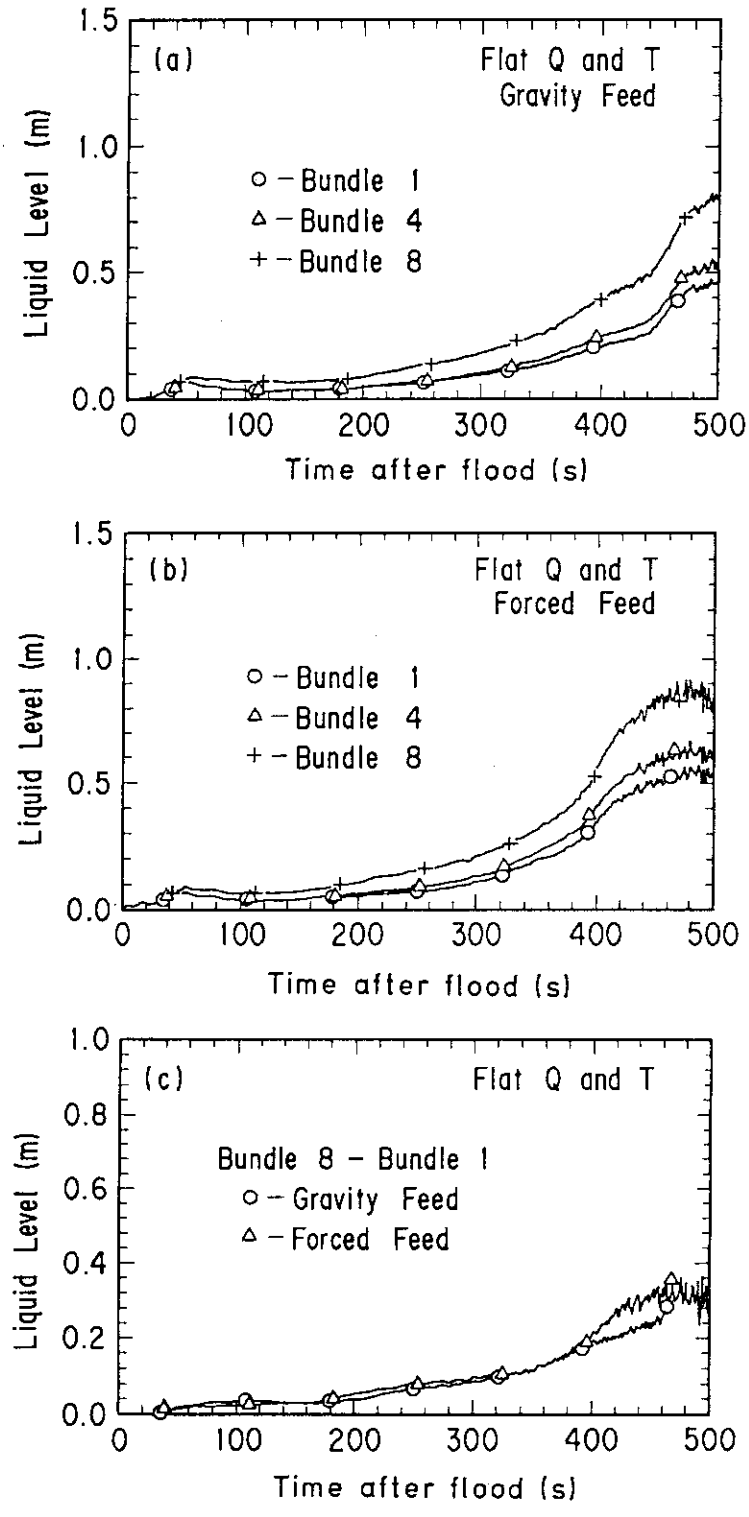

Fig.3.9(3) Comparison of radial distribution on collapsed liquid level in upper plenum in Flat Q and T tests (Upper figure - gravity feed test, Middle - forced feed test and Lower - difference between the liquid level above bundles 1 and 8)

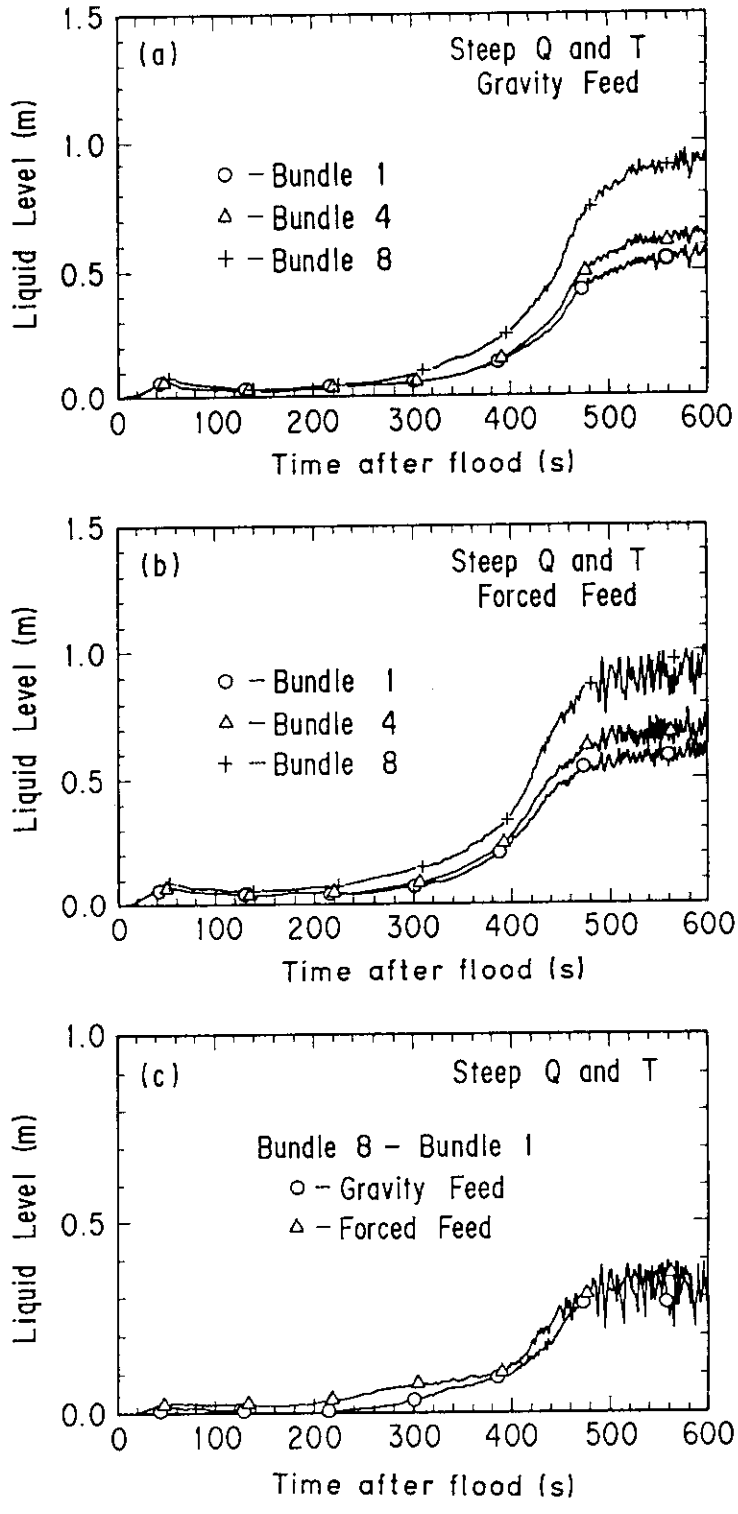

Fig.3.9(4) Comparison of radial distribution on collapsed liquid level in upper plenum in Steep Q and T tests (Upper figure - gravity feed test, Middle - forced feed test and Lower - difference between the liquid level above bundles 1 and 8)

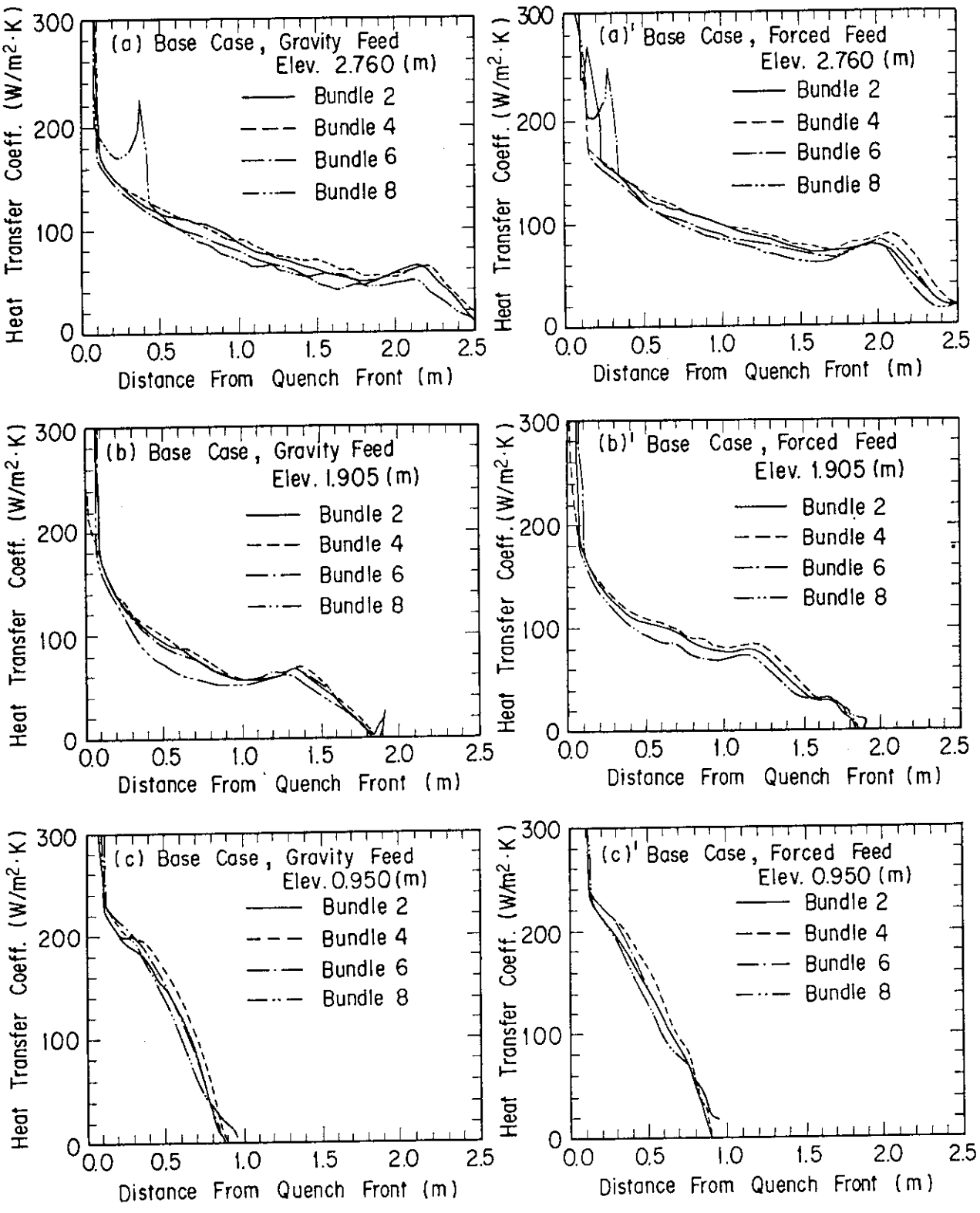

Fig.3.10(1) Comparison of radial distribution on heat transfer coefficient in Base Case tests (Right hand side - forced feed tests and Left one - gravity feed tests)

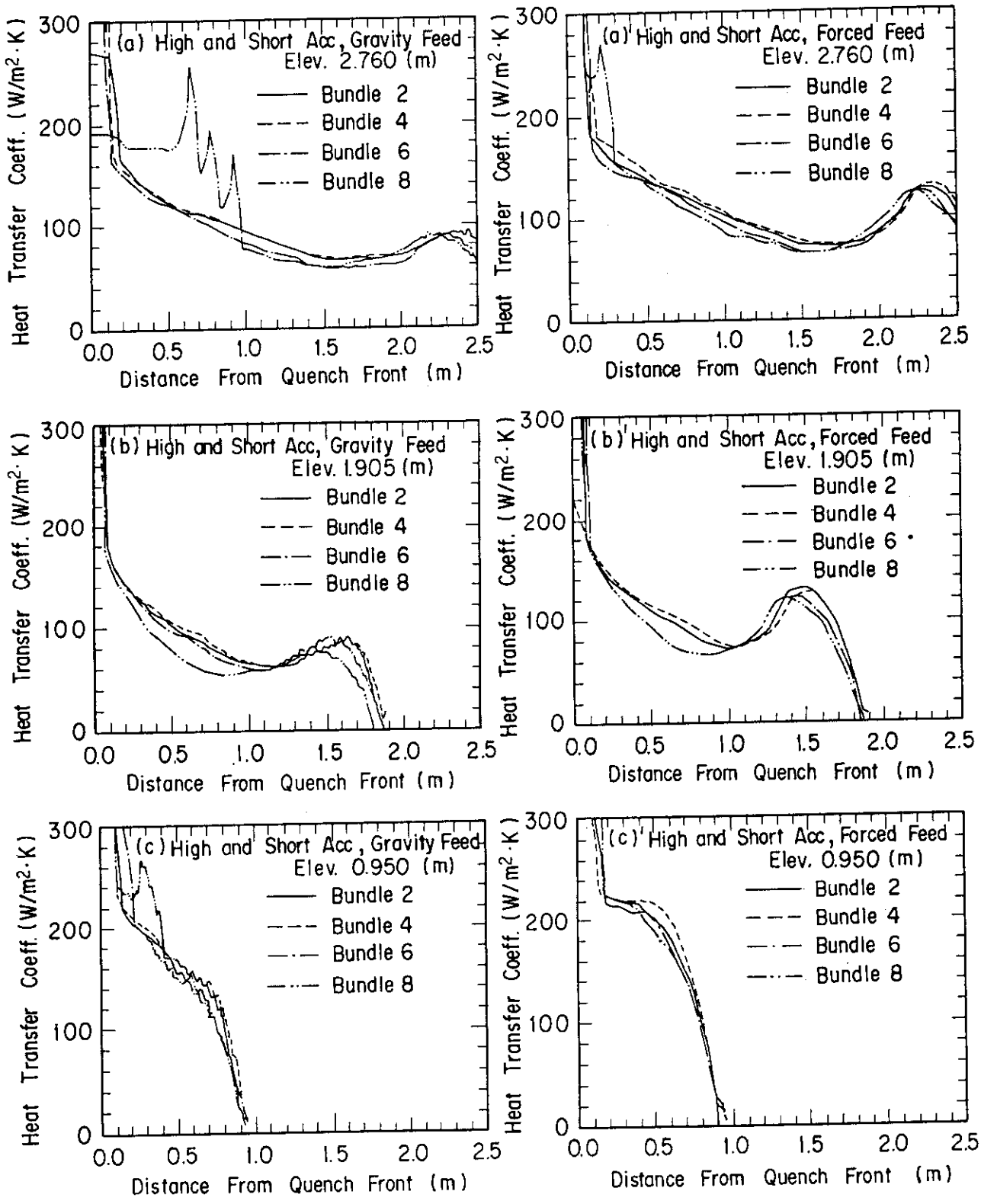

Fig.3.10(2) Comparison of radial distribution on heat transfer coefficient in High and Short Acc tests (Right hand side - forced feed tests and Left one - gravity feed tests)

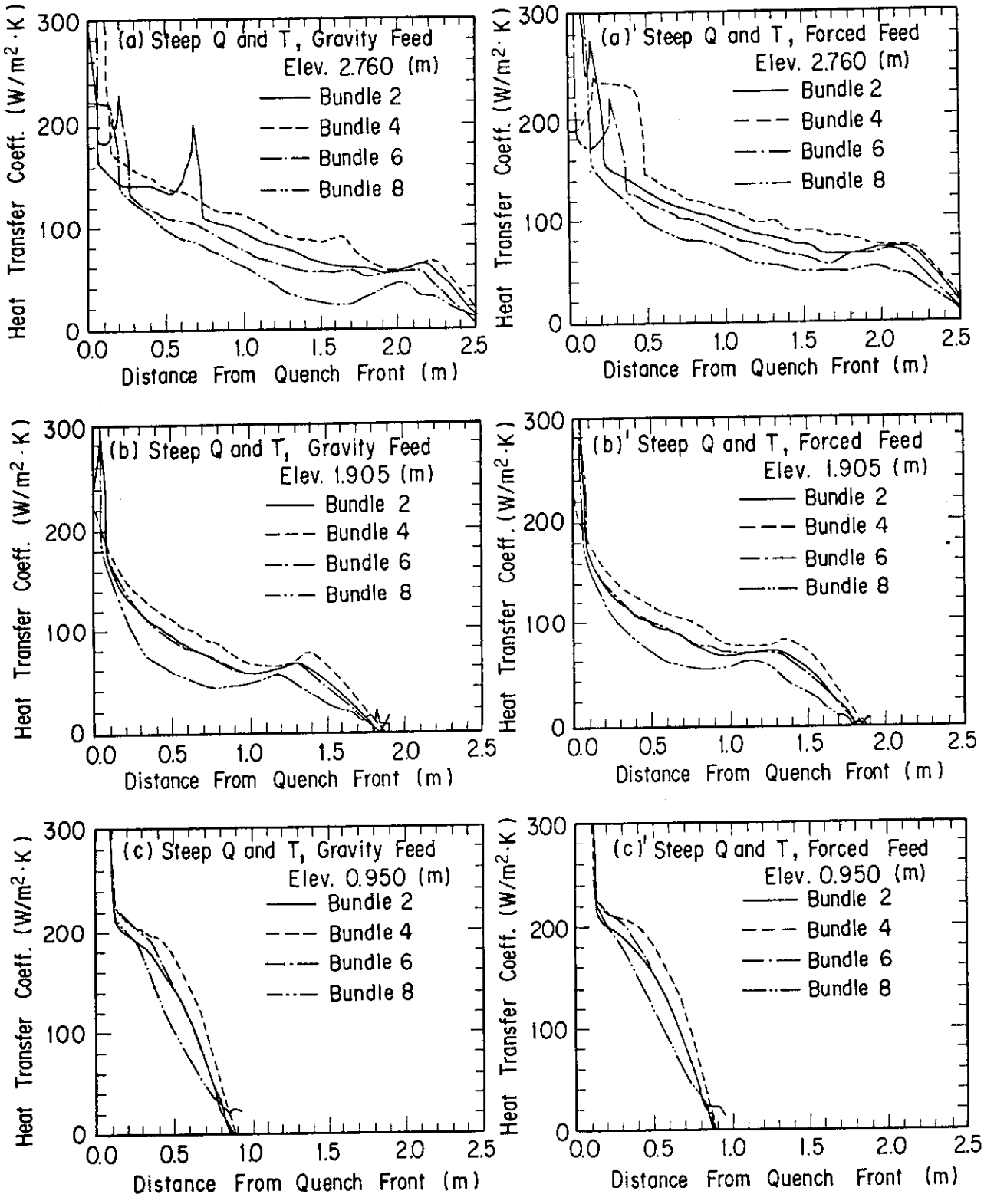

Fig.3.10(3) Comparison of radial distribution on heat transfer coefficient in Steep Q and T tests (Right hand side - forced feed tests and Left one - gravity feed tests)

Appendix A Slab Core Test Facility (SCTF) Core-II

A.1 Test Facility

The Slab Core Test Facility is designed under the following design philosophy and design criteria:

a. Design Philosophy

(1) The facility should provide the capability to study the two-dimensional thermohydraulic behavior in a reactor pressure vessel especially due to the radial power distribution during the end of blowdown, refill and reflood phases of a postulated LOCA in a PWR.

(2) To properly simulate the core heat transfer and hydrodynamics, a special emphasis is put on the proper simulation of the components in the pressure vessel. Provided as the components in the pressure vessel are the simulated core, downcomer, core baffle region, lower plenum, upper plenum and upper head. On the other hand, simplified primary coolant loops are also provided. Provided as the primary coolant loop components are a hot leg, an intact cold leg, broken cold legs and a steam/water separator which is to simulate single steam phase flow downstream of a steam generator and to measure the flow rate of carryover water coming from the upper plenum.

b. Design Criteria

(1) The reference reactor to be simulated in SCTF is the Trojan reactor in the United States which is a four-loop 3300 MWt PWR. The Ooi reactor etc. in Japan are also referred which are of the similar type to the Trojan reactor except the provision of UHI system.

(2) A full scale radial and axial section of core with single bundle width of the pressurized water reactor is provided as the simulated core of SCTF.

(3) The simulated core consists of 8 bundles arranged in a row. Each bundle has electrically heated rods simulating fuel rods and non-heated rods with 16×16 array, with the diameter and the pitch for Trojan which has 15×15 rod array.

(4) The flow area and fluid volume of components are scaled down based on the nominal core flow area scaling, 1/21.

(5) To properly simulate the flow behavior of carryover water or entrainment, the elevations of hot leg and cold legs are designed to be the same as the PWR as much as possible.

(6) A honeycomb structure is used for side walls with surface plates which accomodates the slab core, the upper plenum and the upper part of lower plenum, so as to minimize the effect of walls on the core heat transfer and hydrodynamics.

(7) To investigate the effect of flow resistance in the primary loop are provided the orifices of which dimension is changeable.

(8) The maximum allowable temperature of the simulated fuel rods is 900°C (1173 K) and the maximum allowable pressure of the facility is 0.6 MPa.

(9) The facility is equipped with the hot leg equivalent to four hot legs connecting the upper plenum and the steam/water separator, the intact cold leg equivalent to three intact cold legs connecting the steam/water separator and the downcomer and the two broken cold legs, one is for the steam/water separator side and another for the pressure vessel side.

(10) The ECCS consists of an accumulator (Acc), a low pressure coolant injection (LPCI) system and a combined injection system.

(11) ECC water injection ports are at the cold leg, the hot leg, the upper plenum, the downcomer, the lower plenum and above the upper core support plate. These ports are to be chosen according to the objective of the test.

(12) For better simulation of lower plenum flow resistance, simulated fuel rods do not penetrate through the bottom plate of the lower plenum but terminate at below the bottom of the core.

(13) For measurements in the pressure vessel including core, the feature of the slab geometry of the pressure vessel is utilized as much as possible. Design and arrangement of the instruments are done so as to be able to carry out installation, calibration and removal of the instruments.

(14) View windows are provided where flow pattern recognition is important. Their locations are the interface between the core and the upper plenum, the hot leg, the pressure vessel side broken cold leg and the downcomer.

(15) Blocked bundle test is carried out in Core-I in order to investigate the effect of ballooned fuel rods and unblocked normal bundle

test follows in the Core-II and -III.

(16) Types of break simulated are cold leg break and hot leg break.

(17) The components and systems such as the containment tanks and ECC water supply system in CCTF are shared with SCTF to the maximum extent.

The overall schematic diagram of SCTF is shown in Fig. A-1. The principal dimensions of the facility is shown in Table A-1, and the comparison of dimensions between SCTF and the reference PWR is shown in Fig. A-2.

A.1.1 Pressure Vessel and Internals

The pressure vessel is of slab geometry as shown in Fig. A-3. The height of the components in the pressure vessel is almost the same as the reference reactor's, and the flow area and the fluid volume of each component are scaled down based on the nominal core flow area scaling, 1/21.

The core consists of 8 bundles arranged in a row and each bundle includes heater rods and non-heated rods with 16 × 16 array. The core is enveloped by the honeycomb thermal insulator which is attached on the back surface of core wall plate.

The downcomer is located at one end of the pressure vessel which corresponds to the periphery of the actual reactor pressure vessel. The core baffle region located between the core and the downcomer is basically isolated for Core-II to minimize uncertainty in actual core flow. However, some leak holes are still existing. For better understanding, the cross section of the pressure vessel at the elevation of midplane of the core is shown in Fig. A-4.

The design of upper plenum internals is based on that for the new Westinghouse 17 × 17 array fuel assemblies. The internals consist of control rod guide tubes, support columns and orifice plates which are attached to the upper core support plate (UCSP). The UCSP has some open holes without internals. Those arrangement is shown in Fig. A-5. The radius of each internal is scaled down based on the factor of 8/15 of an actual reactor. Baffle plates are inserted in the guide tubes. The elevation and the configuration of baffle plates are shown in Figs. A-6 and A-7.

The heights of the hot leg and cold legs are designed as close to

the reference PWR as possible. However, in order to avoid the interference of the nozzles in the downcomer, the heights of nozzles for the broken cold leg and the intact cold leg are shifted down compared to that of the hot leg as shown in Fig. A-3.

A.1.2 Simulated Core

The simulated core for the SCTF Core-II consists of 8 heater rod bundles arranged in a row. Each bundle has 234 electrically heated rods and 22 non-heated rods. The dimensions of the heater rods are based on 15 × 15 fuel rods bundle for a PWR and the heated length and the outer diameter of each heater rod are 3.66 m and 10.7 mm, respectively. A heater rod consists of a nichrome heater element, boron nitride (BN) or magnesium oxide (MgO) depending on elevation in the heated zone and Nichrofer 7216 (equivalent to Inconel 600) sheath. The sheath thickness is about 1.0 mm and is thicker than the actual fuel cladding because of the requirements for thermocouple installation. The heater element is a helical coil and has a 17 step chopped cosine axial power profile as shown in Fig. A-8. The peaking factor is 1.4.

Non-heated rods are either pipes or solid rods of stainless steel with 13.8 mm O.D. The heater rods and non-heated rods are fixed at the top of the core allowing downward expansion. In Fig. A-9, relative elevation of rods and spacers is shown.

For better simulation of flow resistance in the lower plenum the simulated fuel rods end in the lower plenum and do not penetrate through the bottom plate of the lower plenum as shown in Fig. A-9.

A.1.3 Primary Loops and ECCS

Primary loops consist of a hot leg equivalent to four hot legs in area, a steam/water separator for simulating single steam phase flow downstream of the steam generator and for measuring flow rate of carry-over water, an intact cold leg equivalent to three intact loops, a broken cold leg on the pressure vessel side and a broken cold leg on the steam/water separator side. These two broken cold legs are connected to two containment tanks through break valves, respectively. The arrangement of the primary loops is shown in Fig. A-10. The flow area of each loop is scaled down based on the core flow area scaling, 1/21.

It should be emphasized that the cross section of the hot leg is an elongated circle with an actual height to realize proper flow pattern in the hot leg. The steam/water separator has a steam generator inlet plenum simulator to correctly simulate the flow characteristics of carryover water into the U-tubes. The cross section of the hot leg and the configuration of the steam generator inlet plenum simulator are shown in Fig. A-11.

A pump simulator and a loop seal part are provided for the intact cold leg. The arrangement of the intact cold leg is shown in Fig. A-12. The pump simulator consists of the casing and duct simulators and an orifice plate as shown in Fig. A-13. The loop resistance is adjusted with the orifice plates attached to the intact cold leg, the steam/water separator side and pressure vessel side broken cold legs and the pump simulator.

ECCS consists of the Acc and an LPCI systems. Injection ports are located as already described in the design criteria section. Besides, the UCSP water extraction system and the UCSP water injection system are provided for combined injection tests.

A.1.4 Containment Tanks and Auxiliary System

Two containment tanks are provided to SCTF. The containment tank-I is connected with the downcomer through the pressure vessel side broken cold leg and the containment tank-II is connected with the steam/water separator through the steam/water separator side broken cold leg. Especially in the containment tank-I, carryover water from the downcomer is measured by the differentiation of the liquid level. These containment tanks and auxiliary system such as a pressurizer for injecting water from the Acc tanks, etc. are shared with CCTF.

A.2 Instrumentation

The instrumentation in SCTF has been provided both by JAERI and USNRC. The JAERI-provided instrumentation includes the measurement of temperatures, pressures, differential pressures, liquid levels, flow velocities, and heating powers. USNRC has provided film probes, impedance probes, string probes, liquid level detectors (LLDs), fluid

distribution grids (FDGs), turbine meters, drag disks, densitometers, spool pieces and video optical probes. Locations of major instruments are shown in Figs. A-14 through A-21.

Table A-1 Principal dimensions of test facility

1.	Core Dimension	
(1)	Quantity of Bundle	8 Bundles
(2)	Bundle Array	1×8
(3)	Bundle Pitch	230 mm
(4)	Rod Array in a Bundle	16×16
(5)	Rod Pitch in a Bundle	14.3 mm
(6)	Quantity of Heater Rod in a Bundle	234 rods
(7)	Quantity of Non-Heated Rod in a Bundle	22 rods
(8)	Total Quantity of Heater Rods	234×8 = 1872 rods
(9)	Total Quantity of Non-Heated Rods	22×8 = 176 rods
(10)	Effective Heated Length of Heater Rod	3660 mm
(11)	Diameter of Heater Rod	10.7 mm
(12)	Diameter of Non-Heated Rod	13.8 mm
2.	Flow Area & Fluid Volume	
(1)	Core Flow Area (Nominal)	0.227 m^2
(2)	Core Fluid Volume	0.92 m^3
(3)	Baffle Region Flow Area	0.10 m^2
(4)	Baffle Region Fluid Volume (Nominal)	0.36 m^3
(5)	Effective Core Flow Area Based on the Measured Level-Volume Relationship Including Gap between Core Barrel and Pressure Vessel Wall and Various Penetration Holes	0.35 m^2
(6)	Downcomer Flow Area	0.121 m^2
(7)	Upper Annulus Flow Area	0.158 m^2
(8)	Upper Plenum Horizontal Flow Area	0.525 m^2
(9)	Upper Plenum Fluid Volume	1.16 m^3
(10)	Upper Head Fluid Volume	0.86 m^3
(11)	Lower Plenum Fluid Volume	1.38 m^3
(12)	Steam Generator Inlet Plenum Simulator Flow Area	0.626 m^2
(13)	Steam Generator Inlet Plenum Simulator Fluid Volume	0.931 m^3
(14)	Steam Water Separator Fluid Volume	5.3 m^3
(15)	Flow Area at the Top Plate of Steam Generator Inlet Plenum Simulator	0.195 m^2
(16)	Hot Leg Flow Area	0.0826m^2
(17)	Intact Cold Leg Flow Area (Diameter = 297.9 mm)	0.9697m^2
(18)	Broken Cold Leg Flow Area (Diameter = 151.0 mm)	0.0179m^2

Table A-1 (Continued)

(19)	Containment Tank-I Fluid Volume	30	m^3
(20)	Containment Tank-II Fluid Volume	50	m^3
(21)	Flow Area of Exhausted Steam Line from Containment Tank-II to the Atmosphere	see Ref. (4)	

3. Elevation & Height

(1)	Top Surface of Upper Core Support Plate (UCSP)	0	mm
(2)	Bottom Surface of UCSP	- 76	mm
(3)	Top of the Effective Heated Length of Heater Rod	- 393	mm
(4)	Bottom of the Skirt in the Lower Plenum	-5270	mm
(5)	Bottom of Intact Cold Leg	+ 724	mm
(6)	Bottom of Hot Leg	+1050	mm
(7)	Top of Upper Plenum	+2200	mm
(8)	Bottom of Steam Generator Inlet Plenum Simulator	+1933	mm
(9)	Centerline of Loop Seal Bottom	-2281	mm
(10)	Bottom Surface of End Box	- 185.1	mm
(11)	Top of the Upper Annulus of Downcomer	+2234	mm
(12)	Height of Steam Generator Inlet Plenum Plenum Simulator	1595	mm
(13)	Height of Loop Seal	3140	mm
(14)	Inner Height of Hot Leg Pipe	737	mm
(15)	Bottom of Lower Plenum	-5770	mm
(16)	Top of Upper Head	+2887	mm

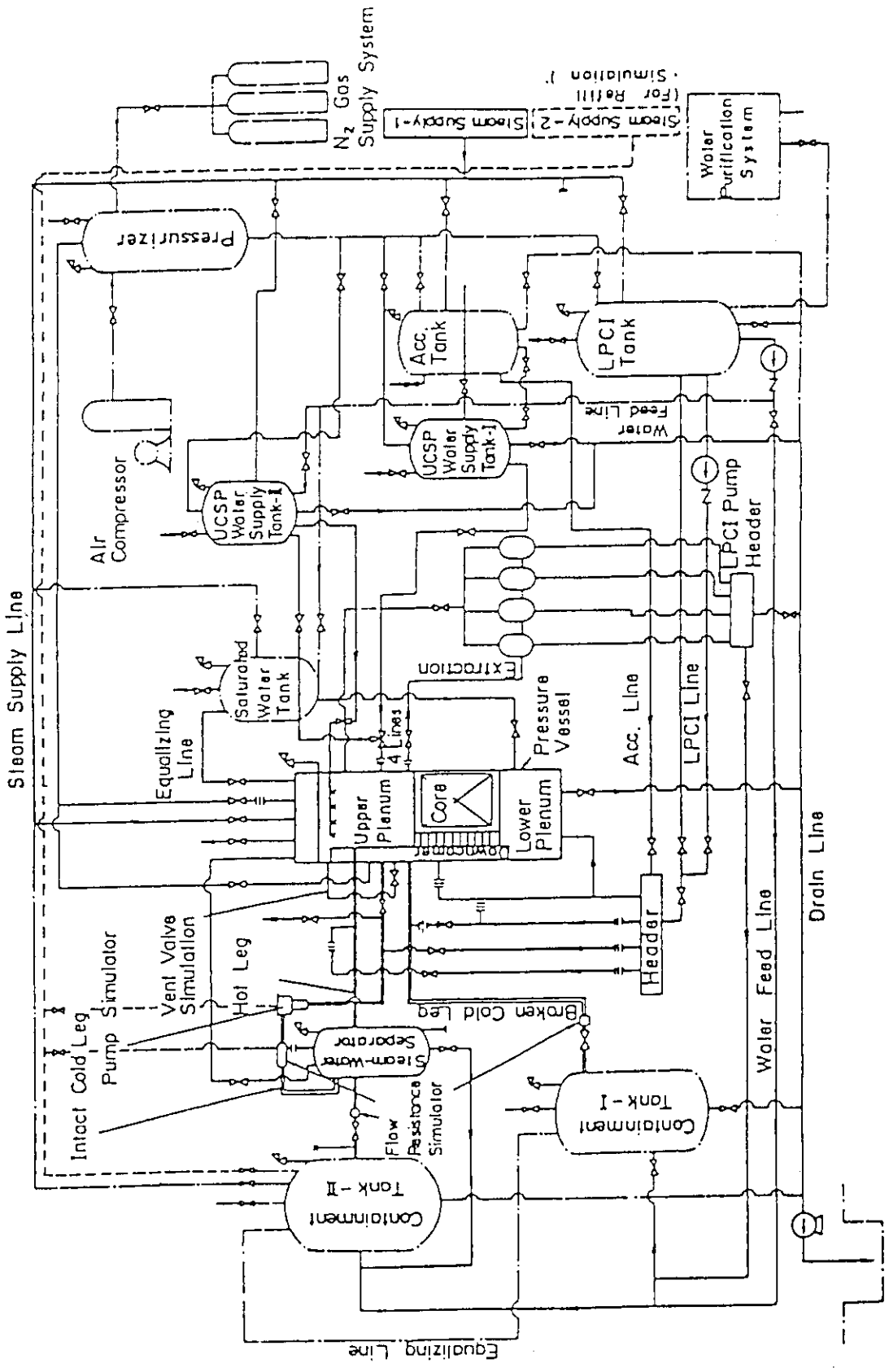

Fig.A-1 Schematic diagram of slab core test facility

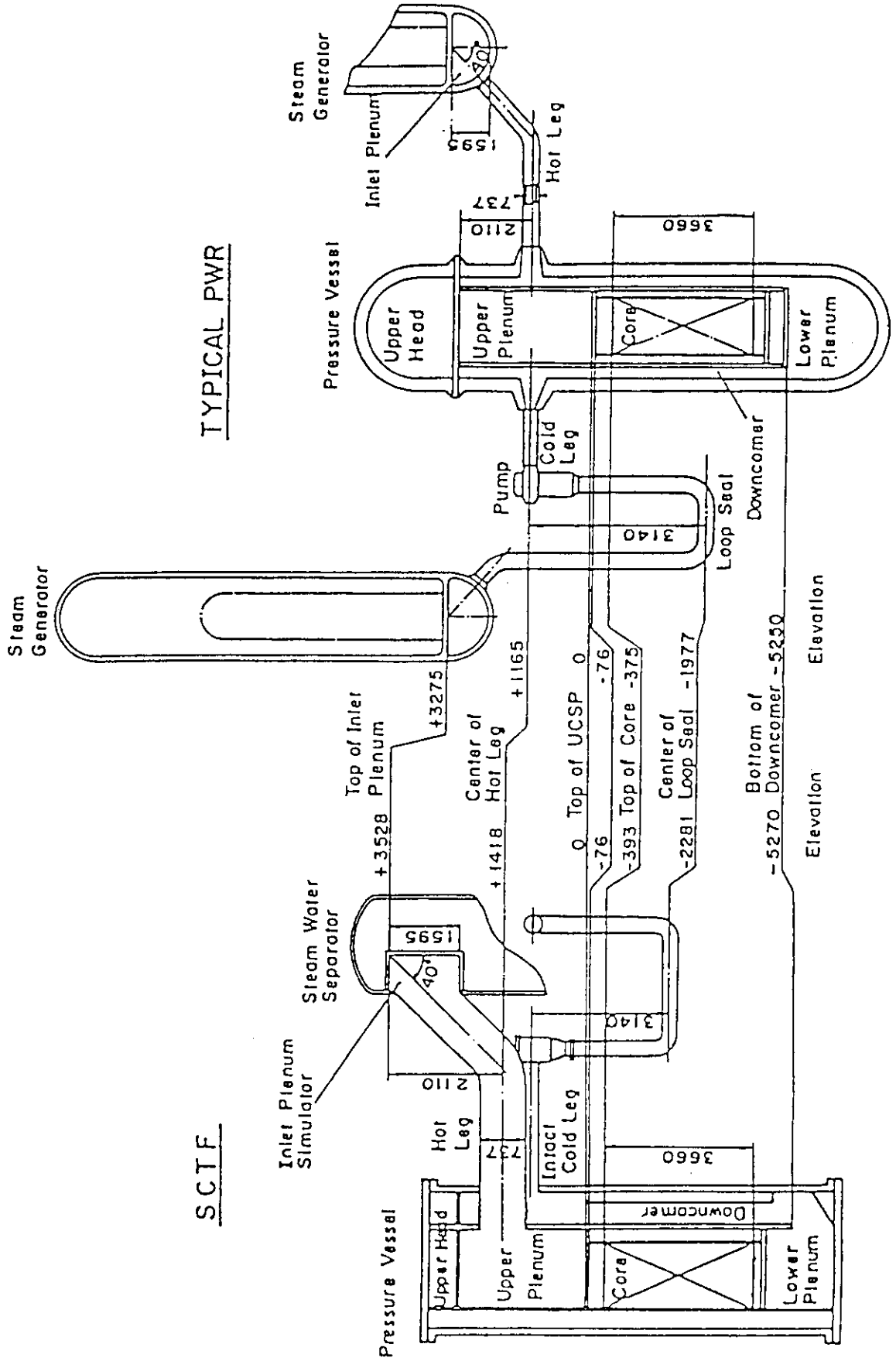

Fig.A-2 Comparison of dimensions between SCTF and a reference PWR

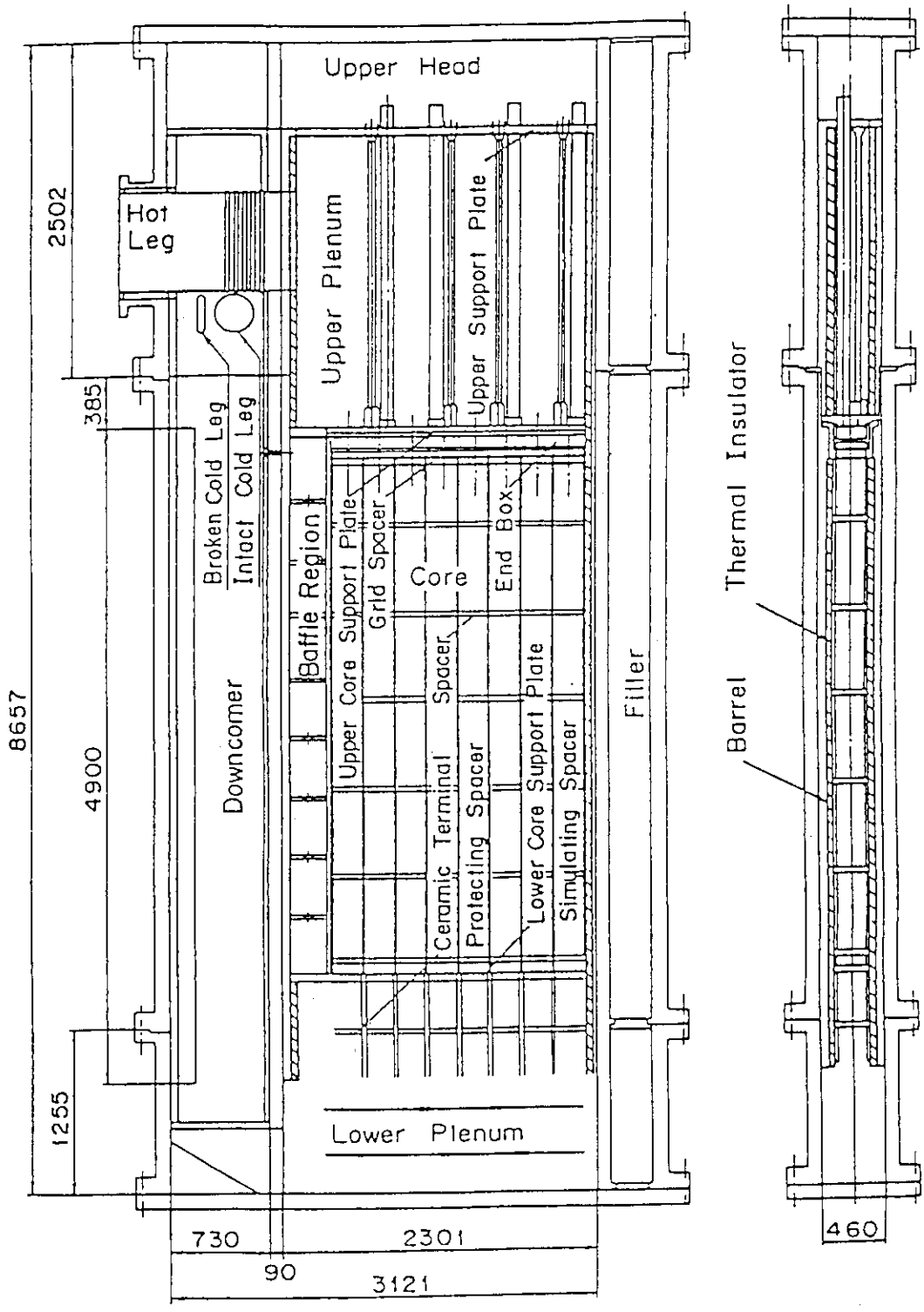

Fig.A-3 Vertical cross section of the pressure vessel

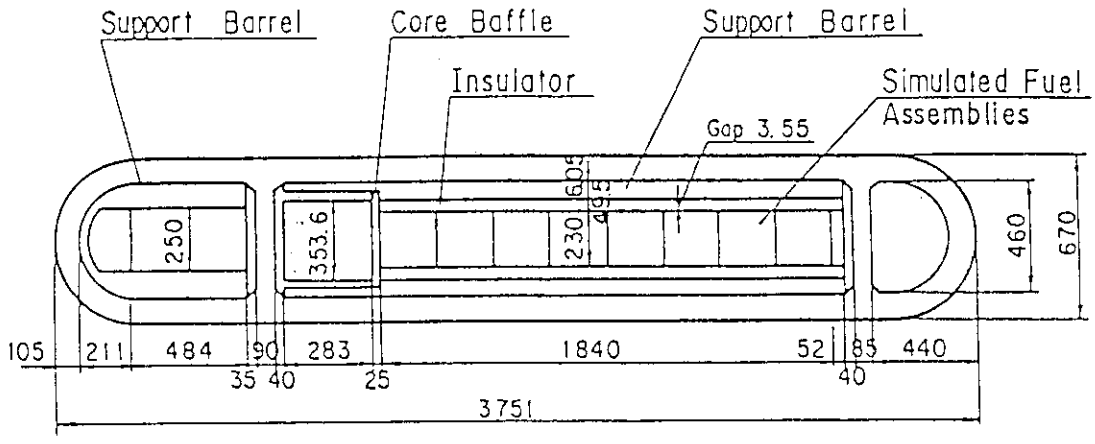

Fig.A-4 Horizontal cross section of the pressure vessel (1)

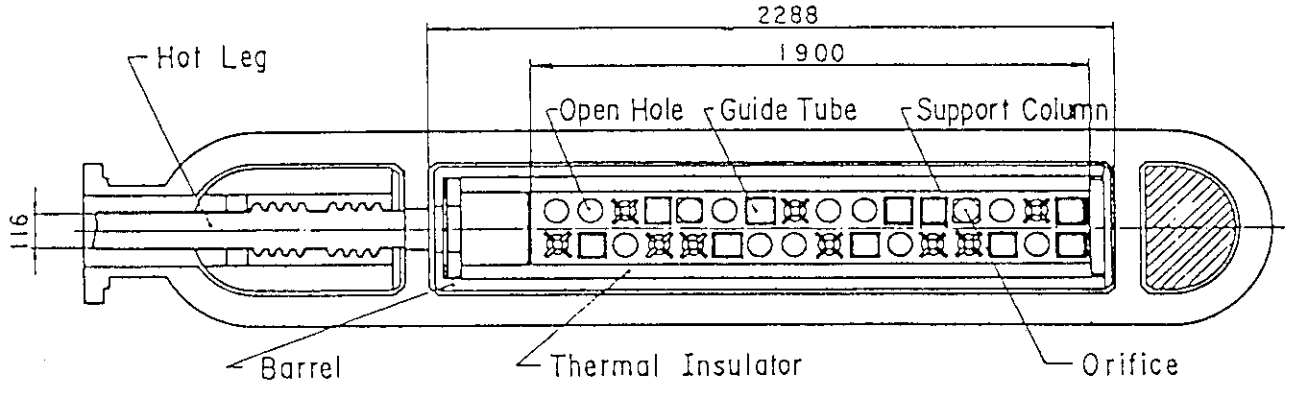

Fig.A-5 Horizontal cross section of the pressure vessel (2)

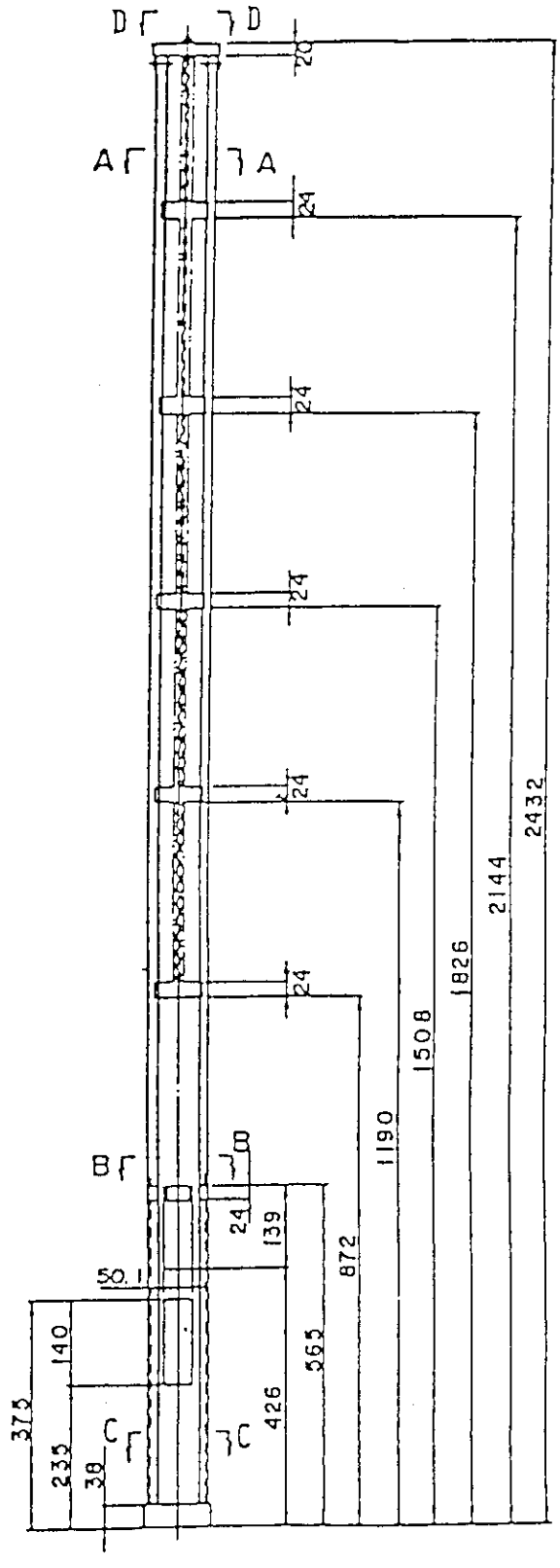

Fig.A-6 Dimension of guide tube (1)

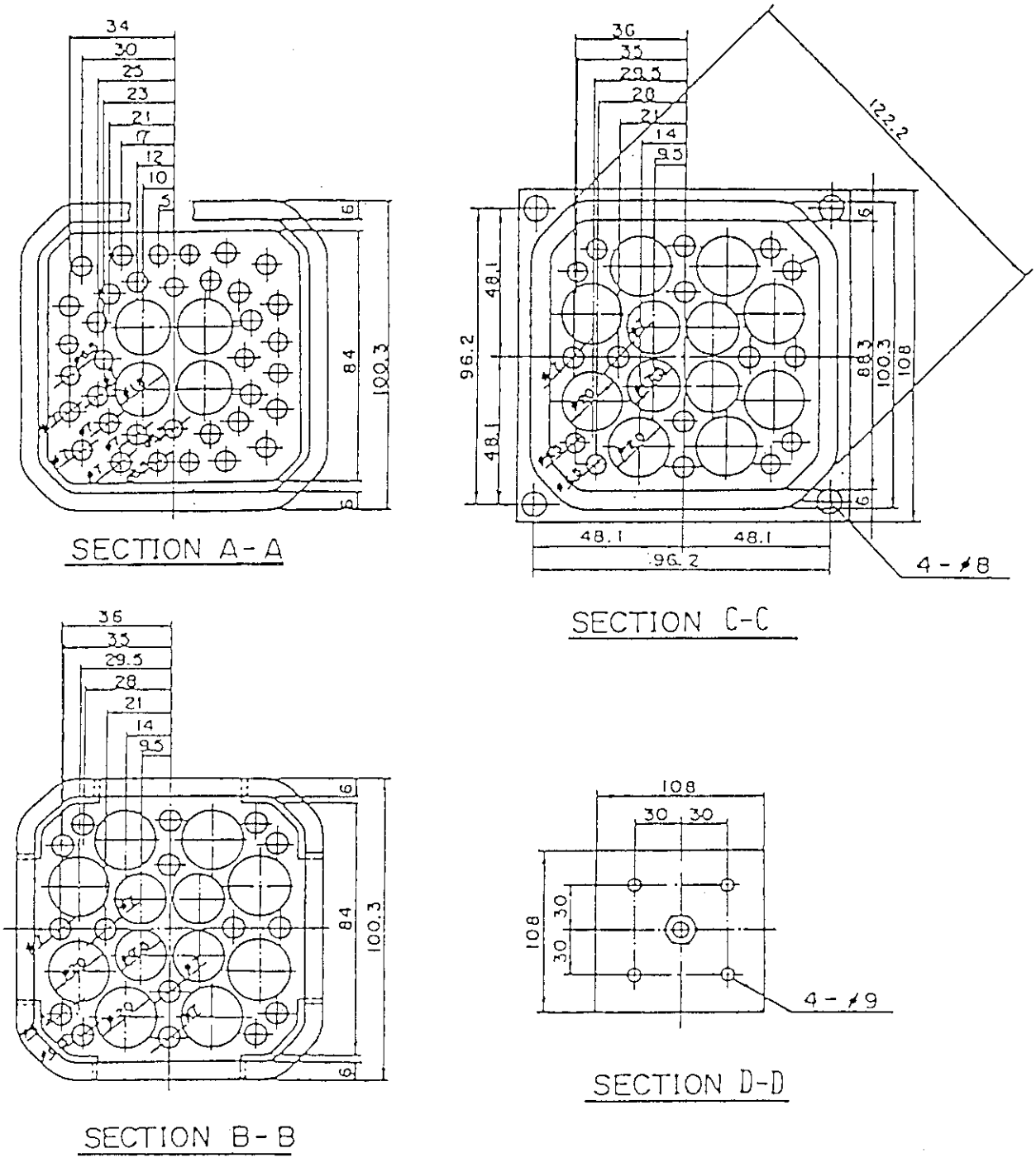

Fig.A-7 Dimension of guide tube (2)

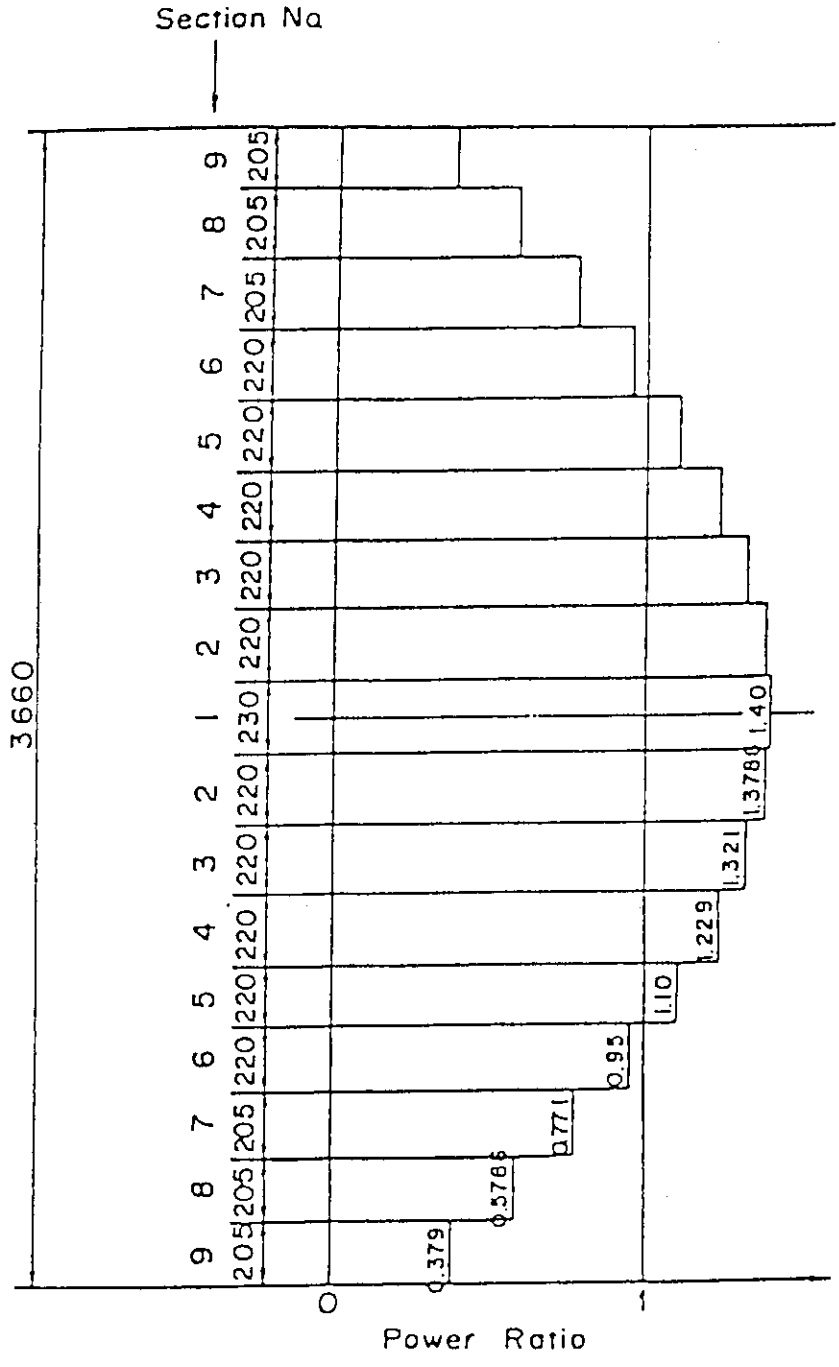

Fig.A-8 Axial power distribution of heater rod

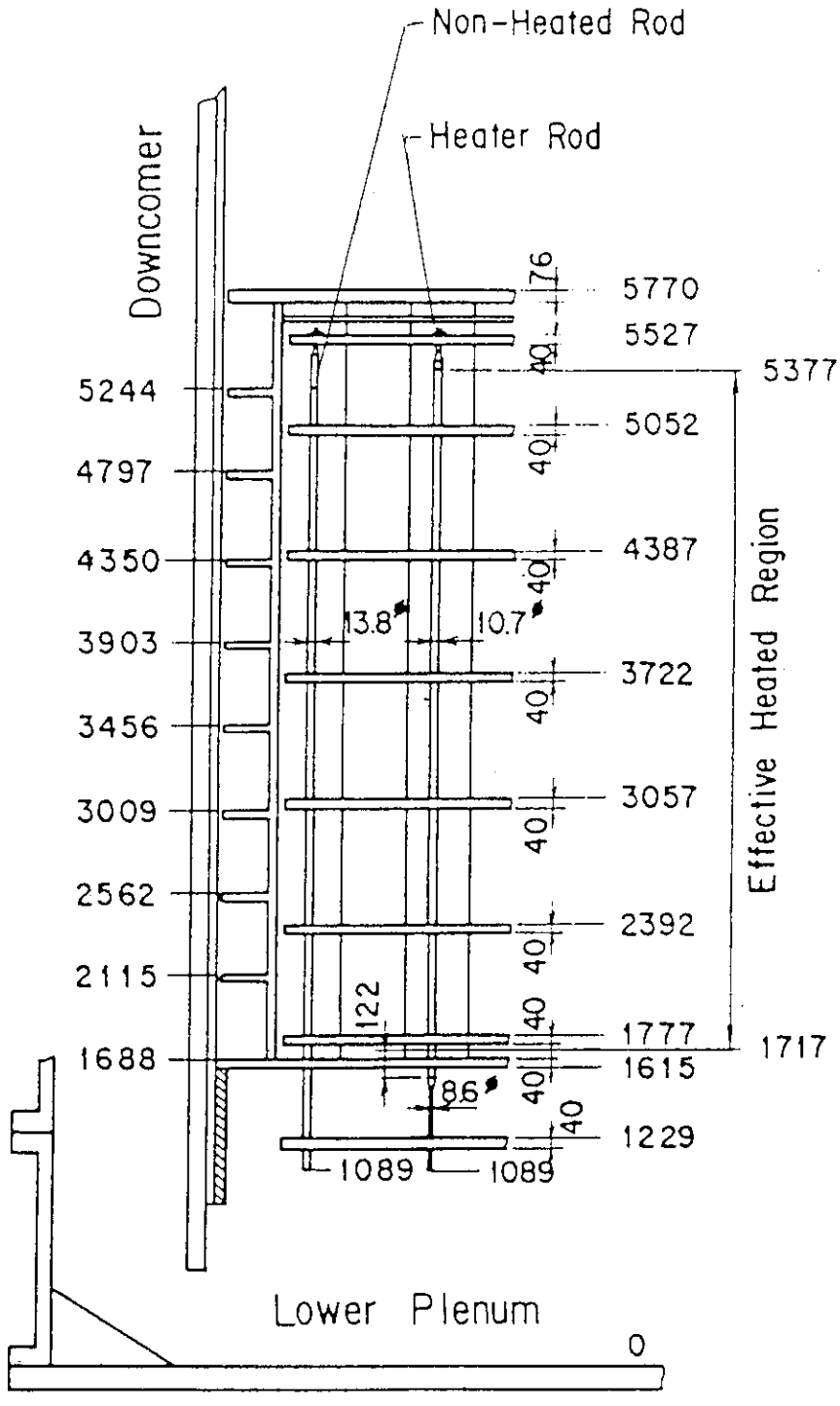

Fig.A-9 Relative elevation and dimension of the core in SCTF

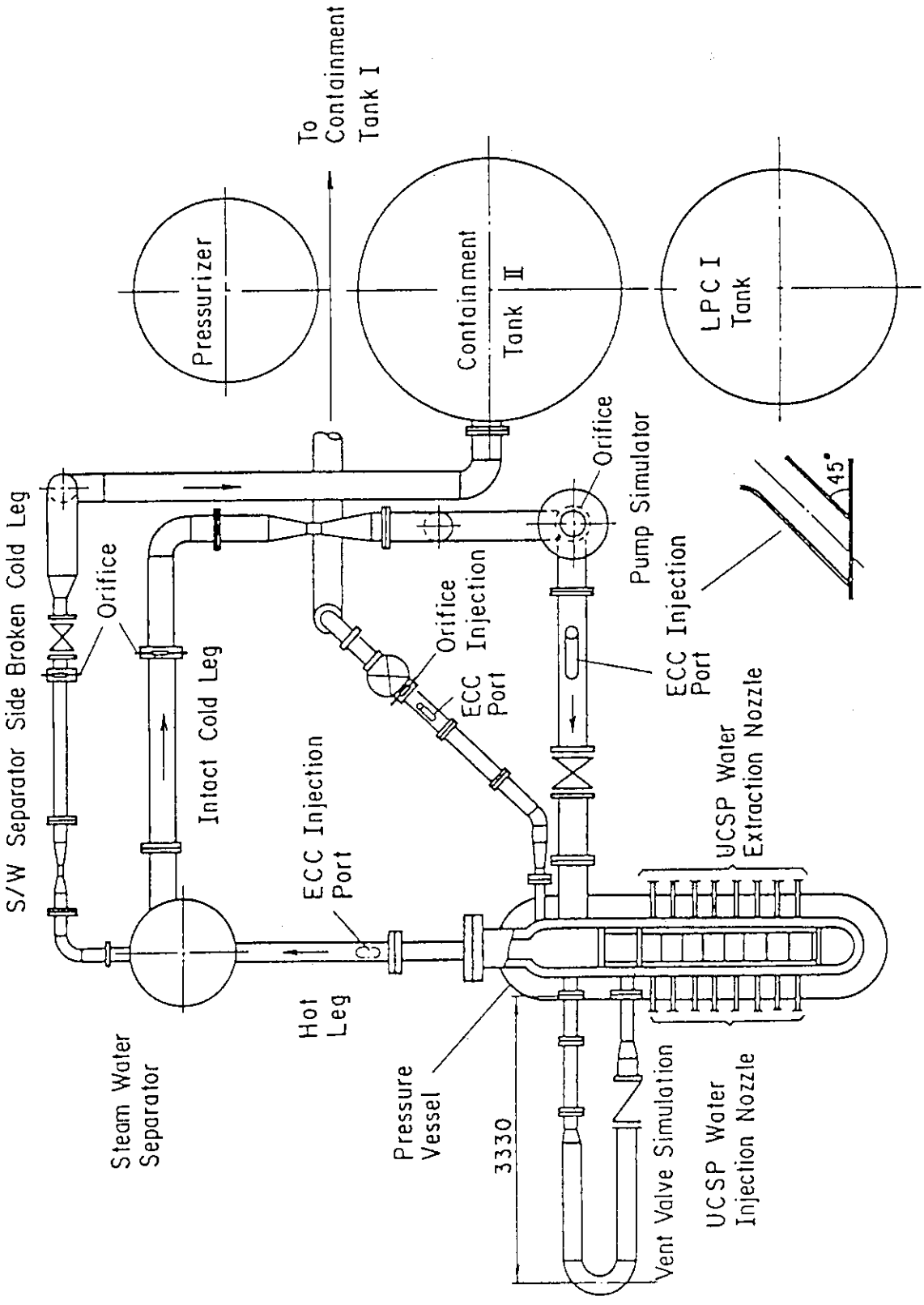

Fig.A-10 Overview of the arrangement of the SCTF

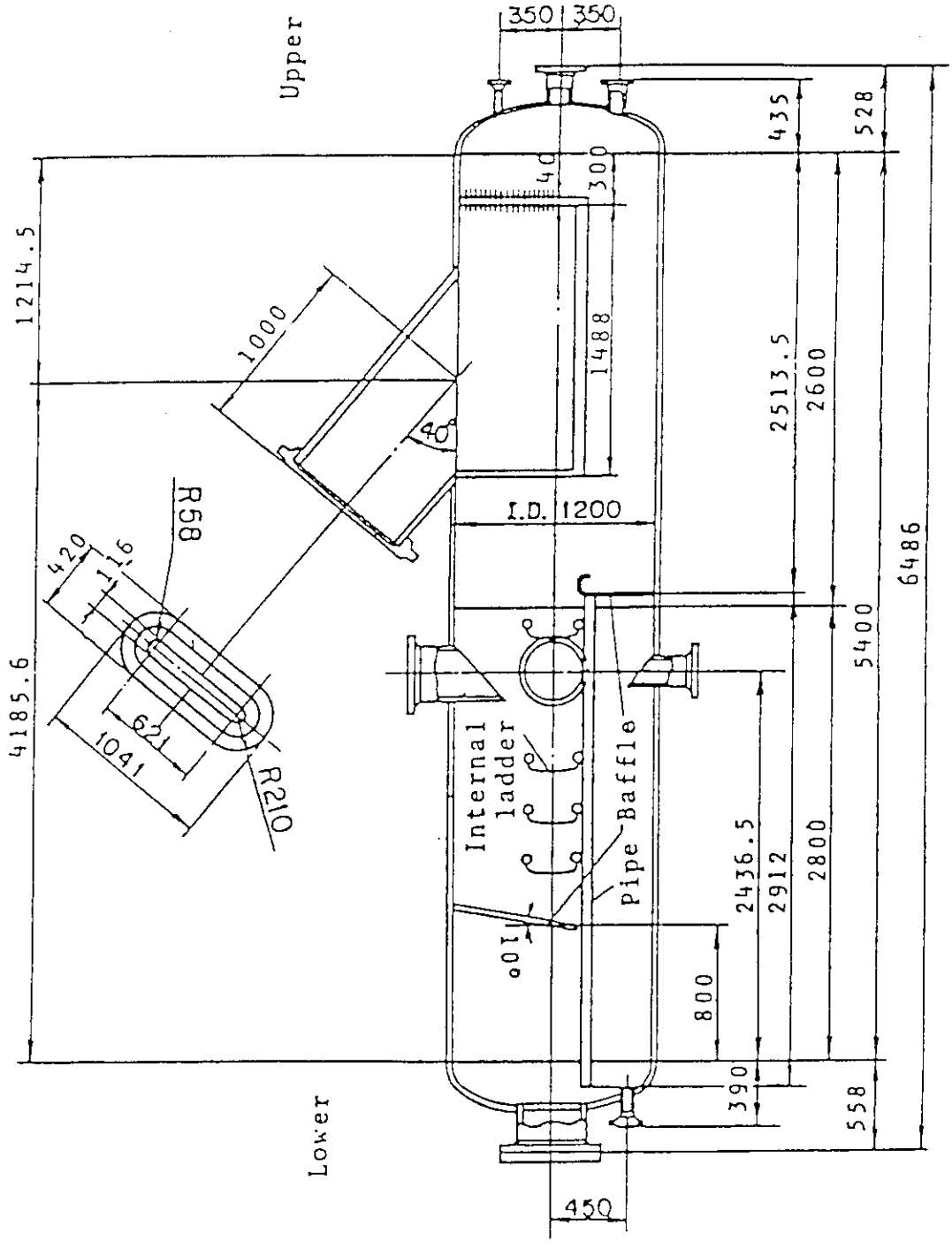

Fig.A-11 Steam-water separator

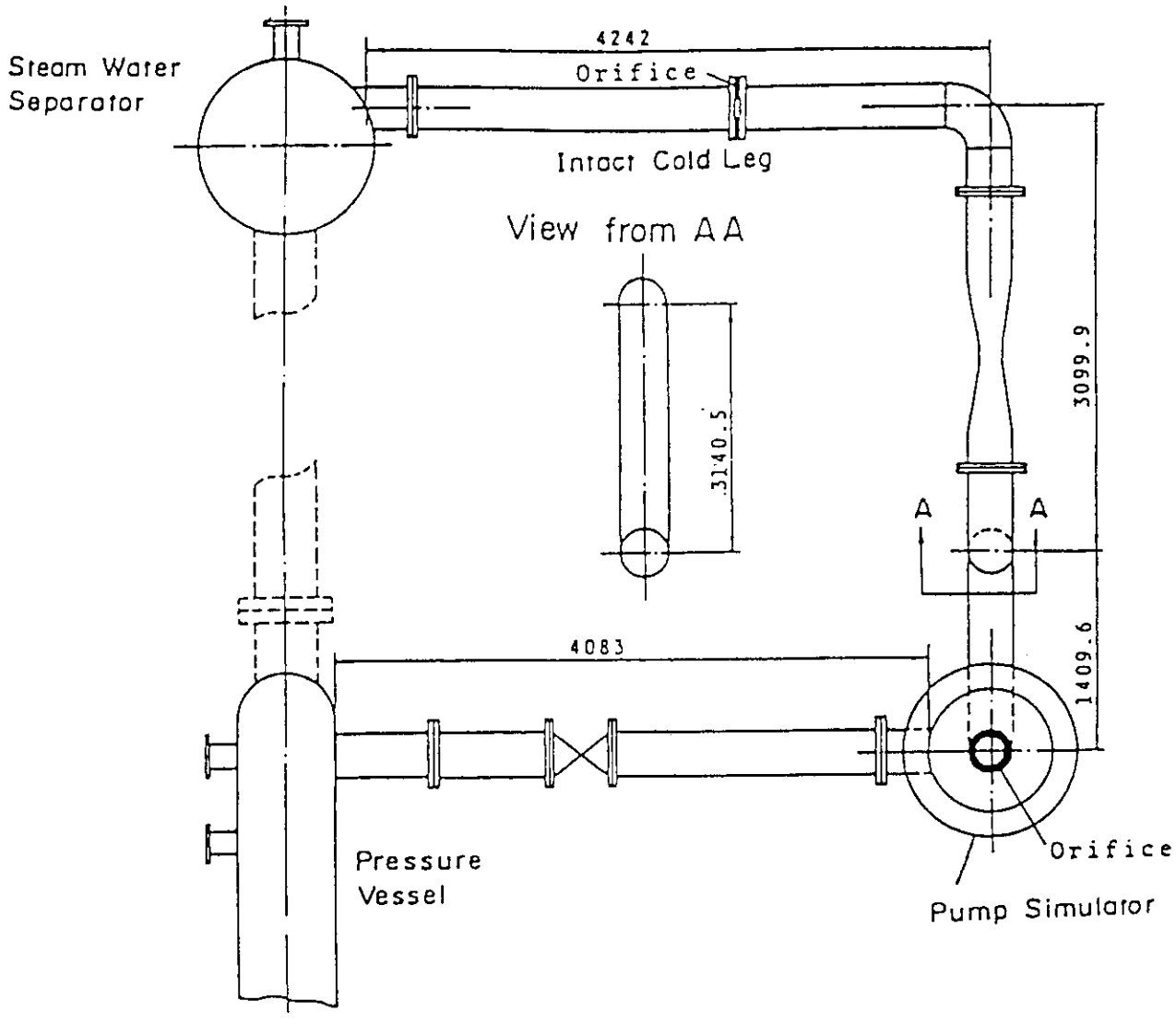

Fig.A-12 Arrangement of intact cold leg

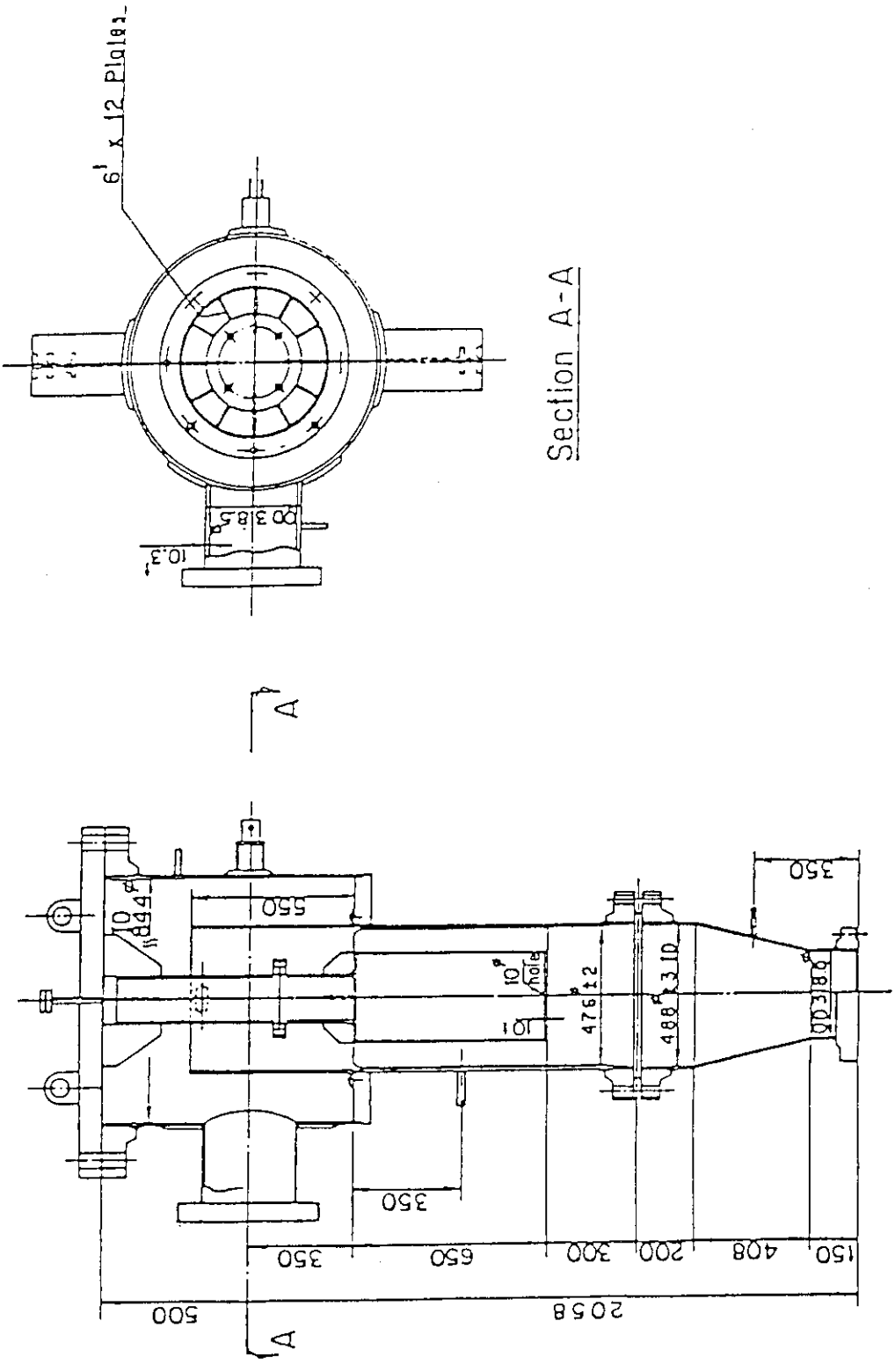

Fig.A-13 Configuration and dimension of pump simulator

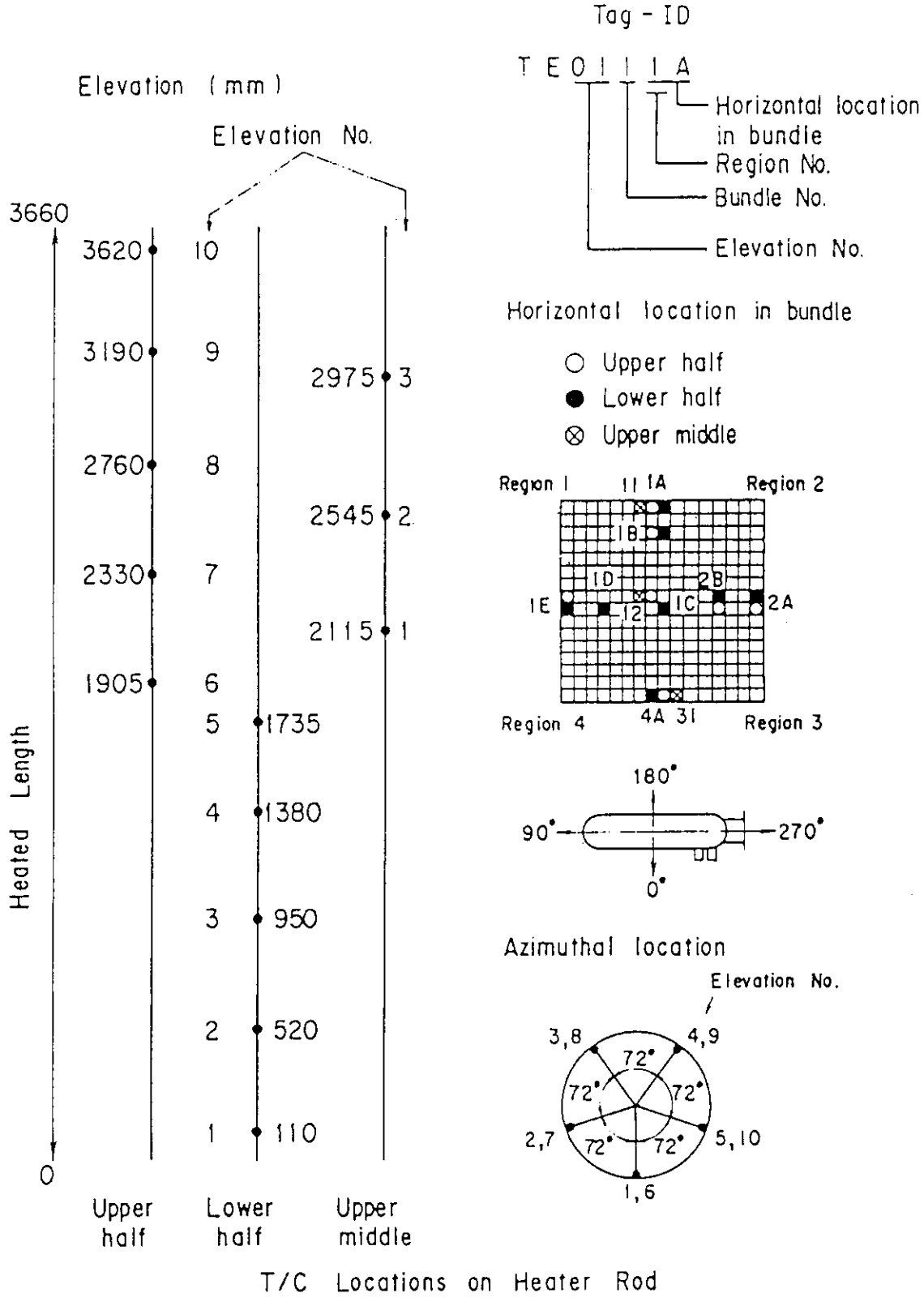

T/C Locations on Heater Rod

Fig.A-14 Thermocouple locations of heater rod surface temperature measurement

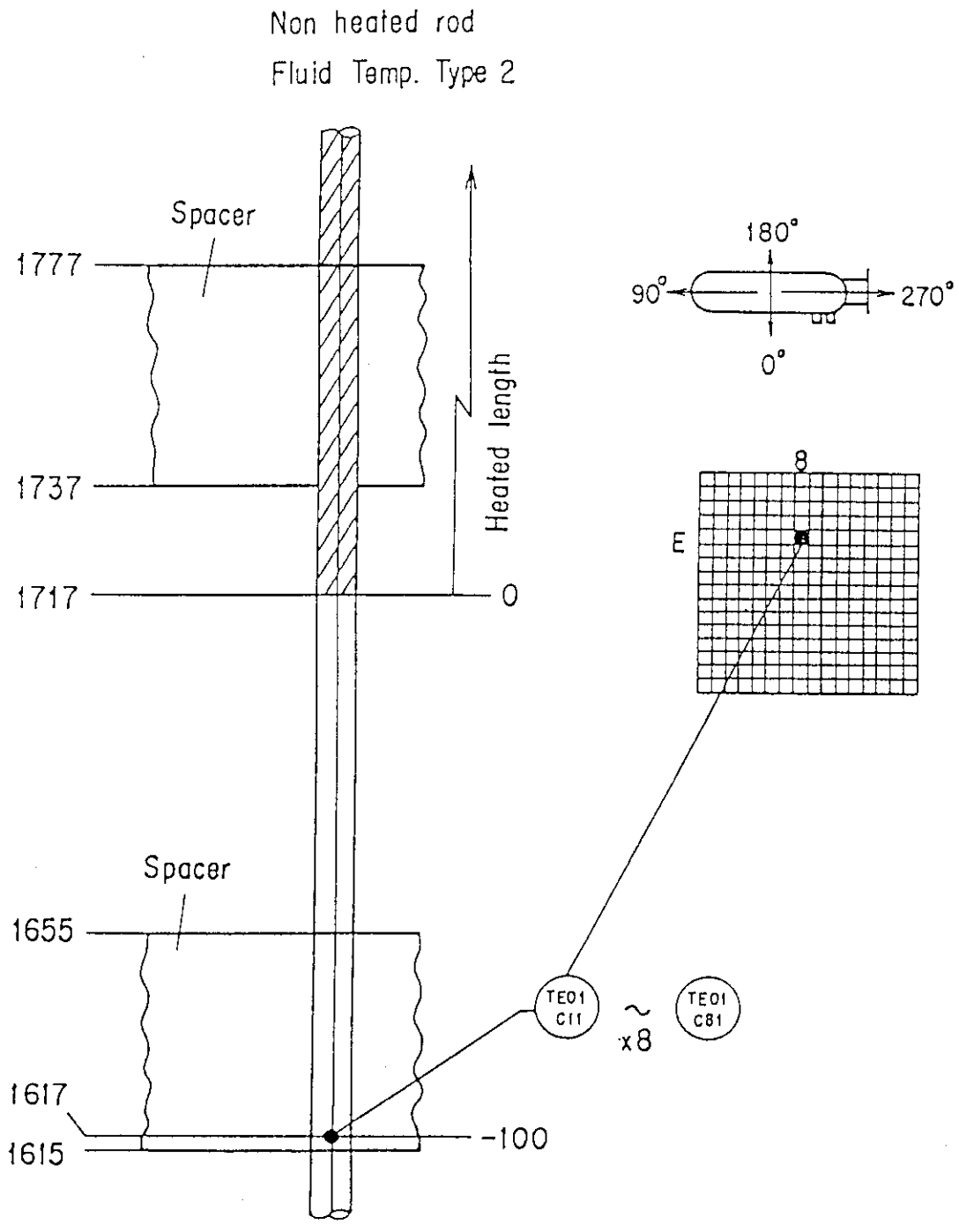

Fig.A-15 Thermocouple locations of fluid temperature measurement at core inlet

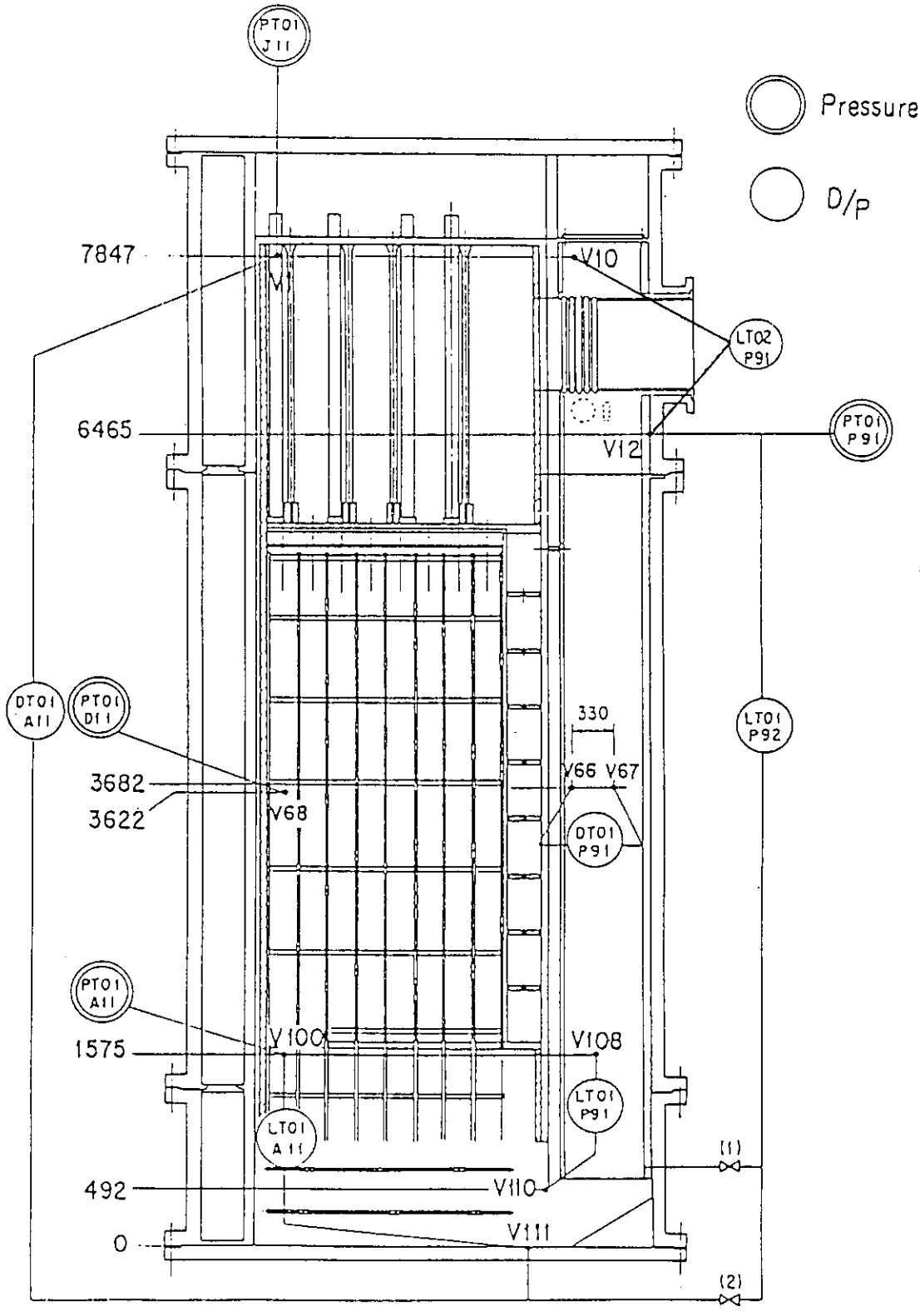

Fig.A-16 Locations of pressure measurement in pressure vessel, differential pressure measurement between upper and lower plenum and liquid level measurement in downcomer and lower plenum

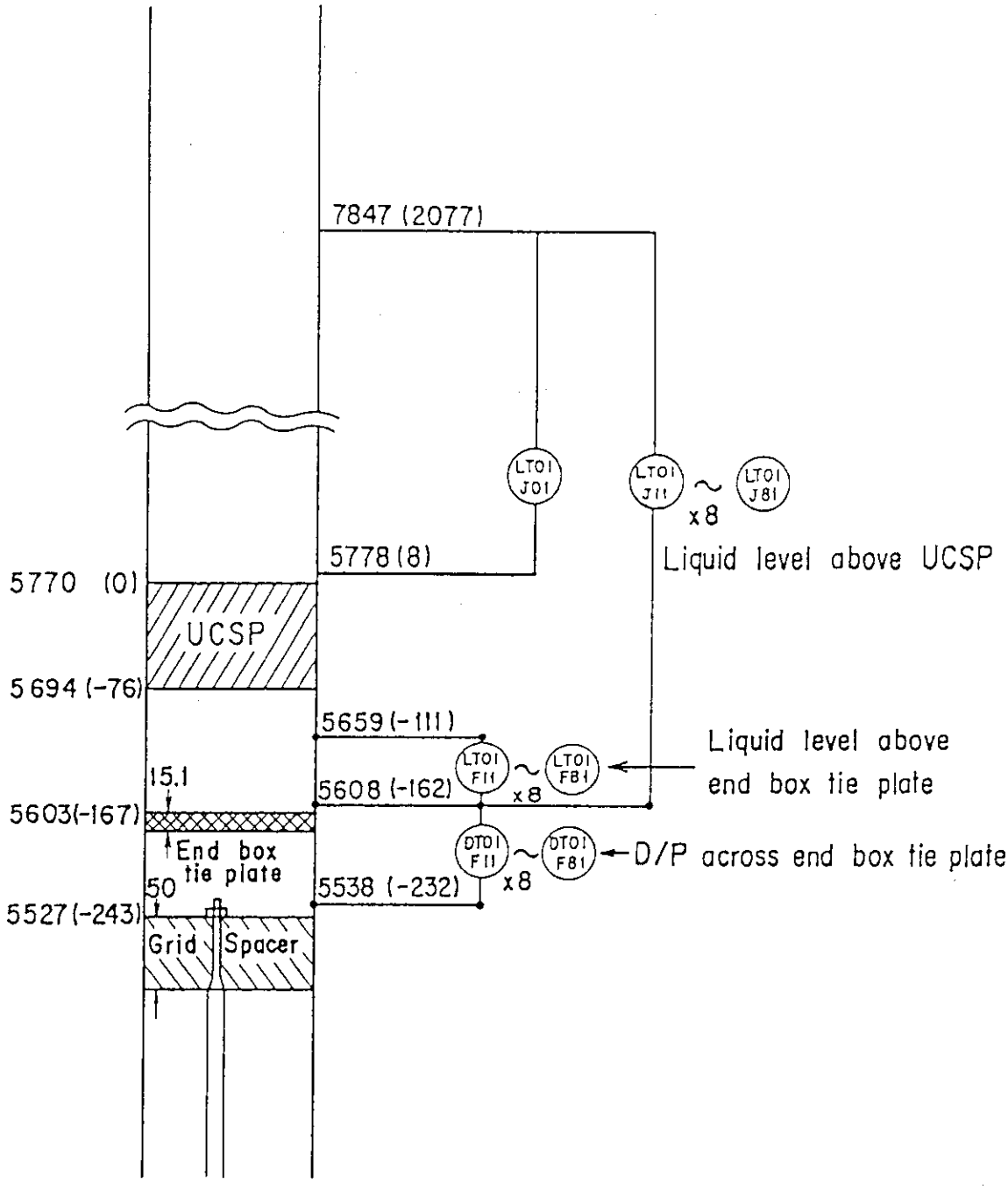

Fig.A-17 Locations of differential pressure measurement across end box tie plate and liquid level measurement above UCSP and end box tie plate

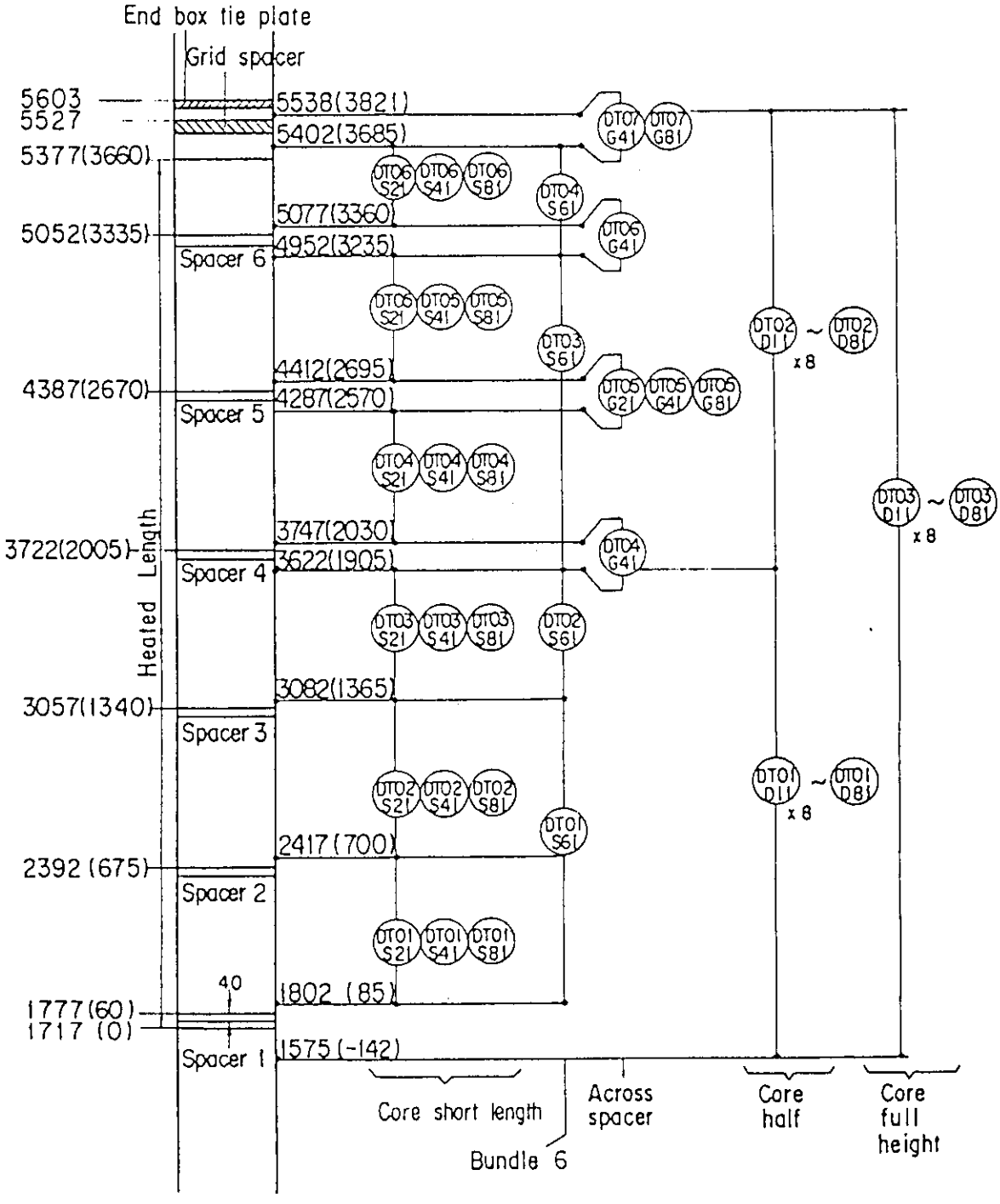

Fig.A-18 Locations of vertical differential pressure measurement in core

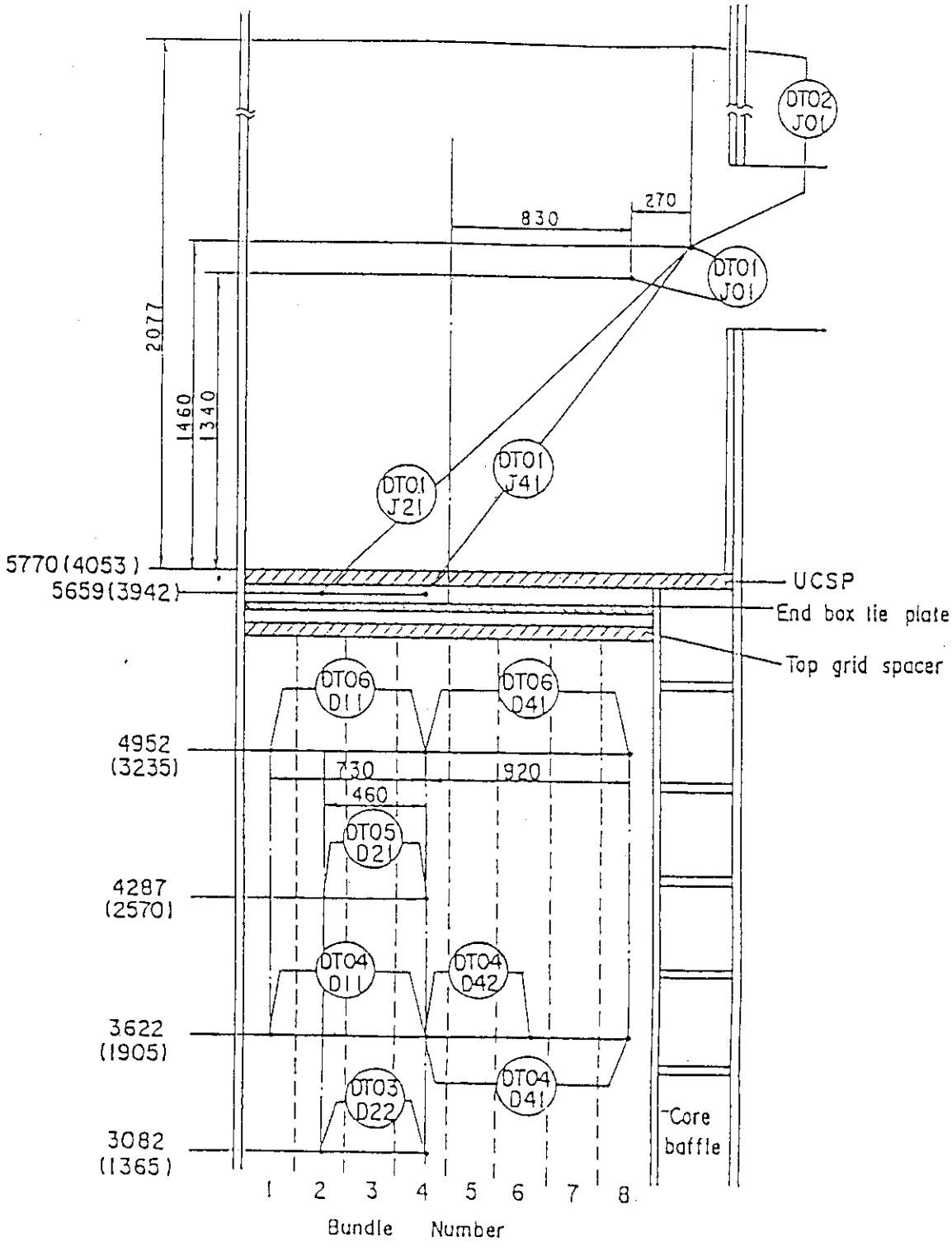

Fig.A-19 Locations of horizontal differential pressure measurement in core and differential pressure measurement between end box and inlet of hot leg

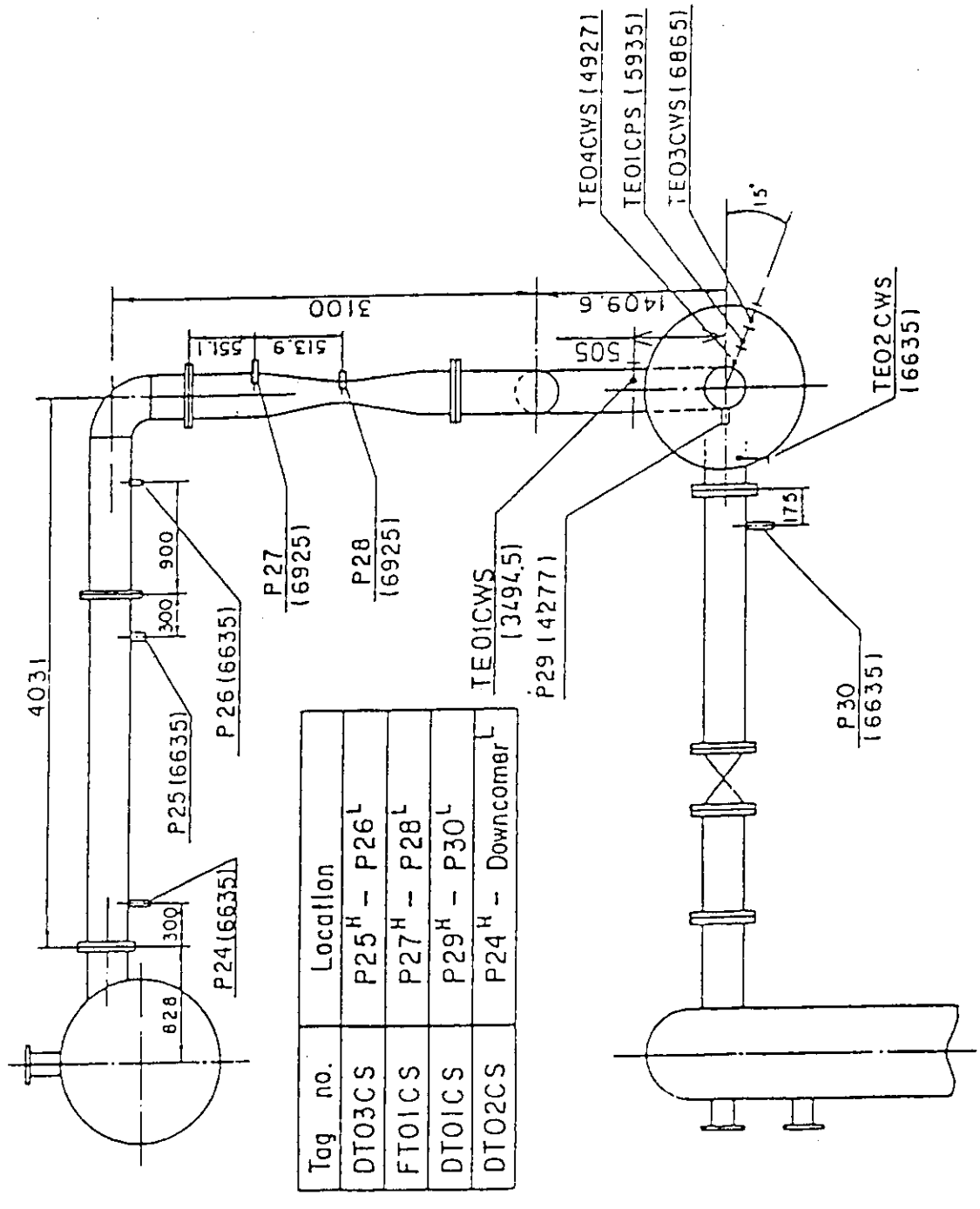

Fig.A-20 Locations of intact cold leg instrumentation

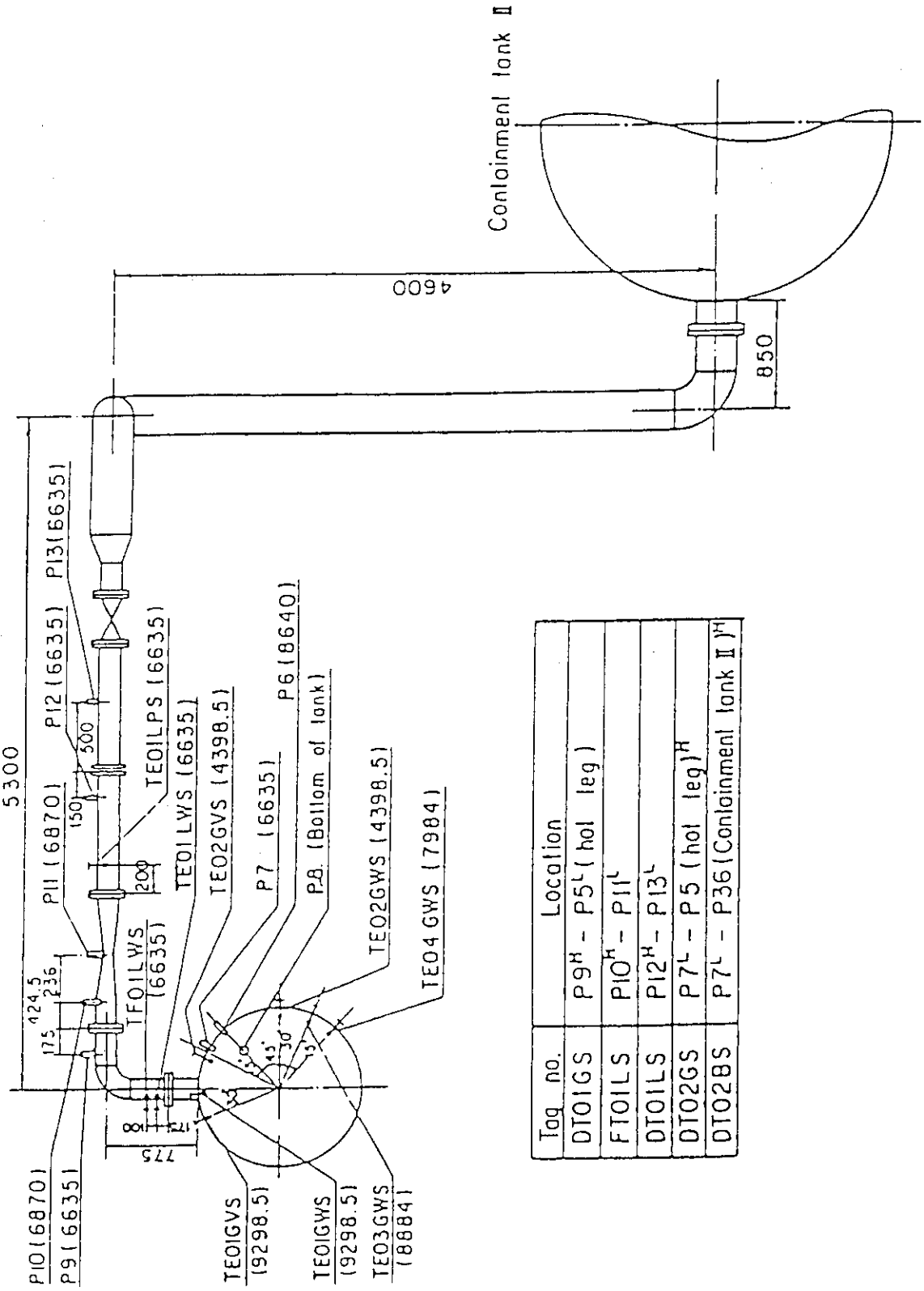

Tag no.	Location
DT01GS	$P9^H - P5^L$ (hot leg)
FT01LS	$P10^H - P11^L$
DT01LS	$P12^H - P13^L$
DT02GS	$P7^L - P5$ (hot leg)^H
DT02BS	$P7^L - P36$ (Containment tank Ⅱ)^H

Fig.A-21 Locations of steam-water separator side broken cold leg instrumentation

Appendix B Selected Data of Test S2-10

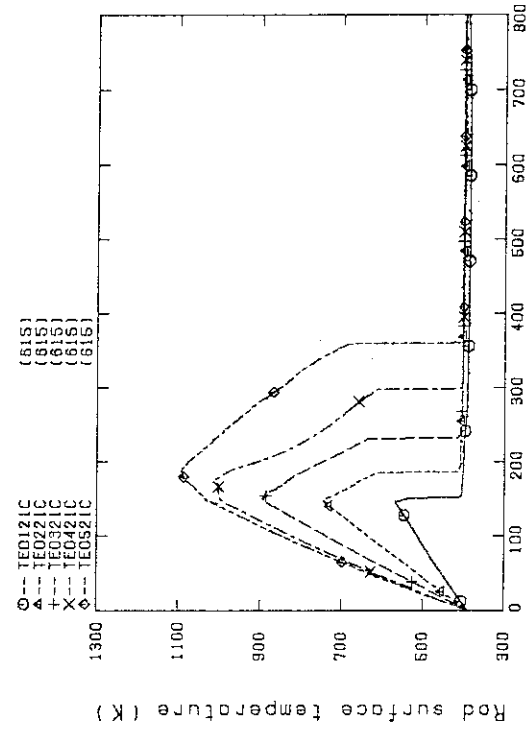

Fig.B-3 Heater rod temperature
(Bundle 2-1C, Lower half)

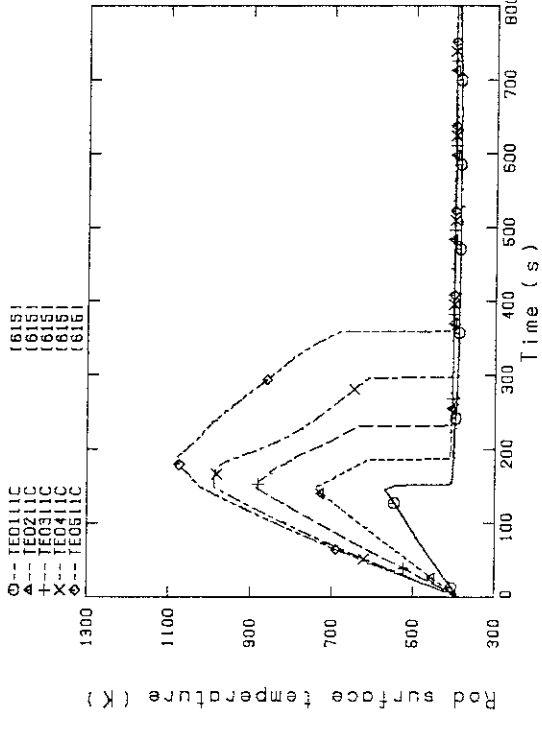

Fig.B-1 Heater rod temperature
(Bundle 1-1C, Lower half)

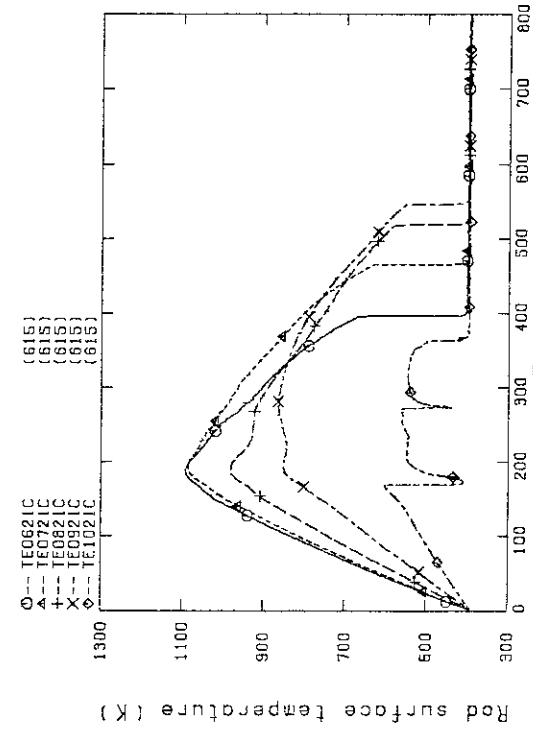

Fig.B-4 Heater rod temperature
(Bundle 2-1C, Upper half)

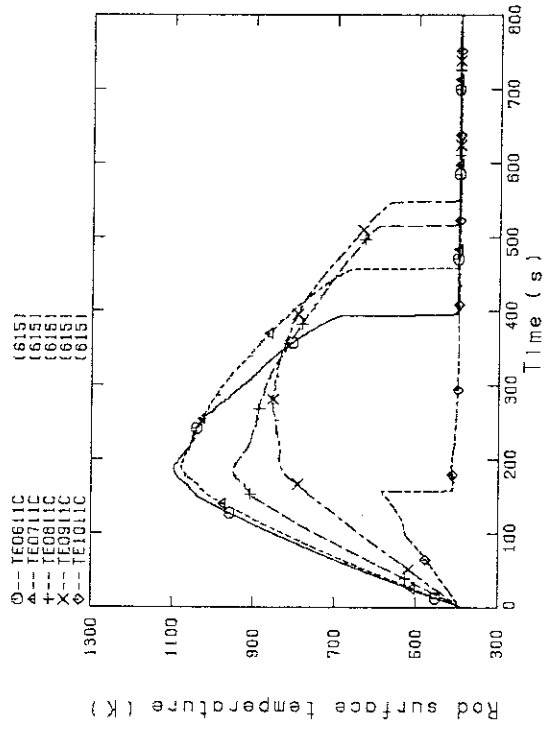

Fig.B-2 Heater rod temperature
(Bundle 1-1C, Upper half)

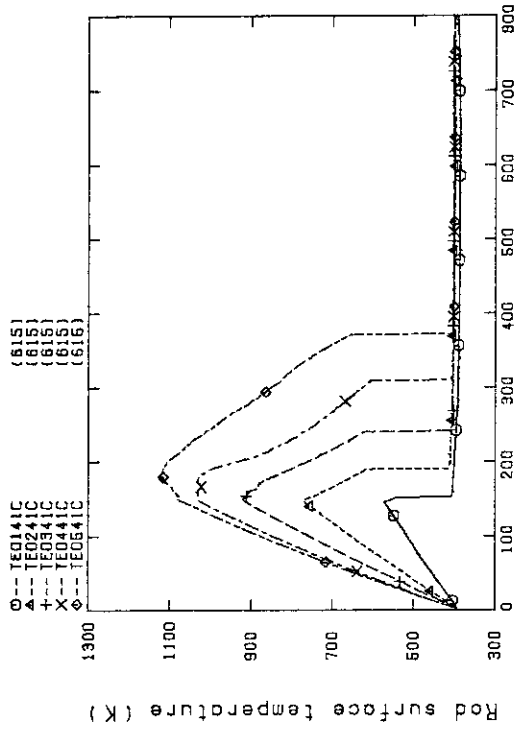

Fig.B-7 Heater rod temperature (Bundle 4-1C, Lower half)

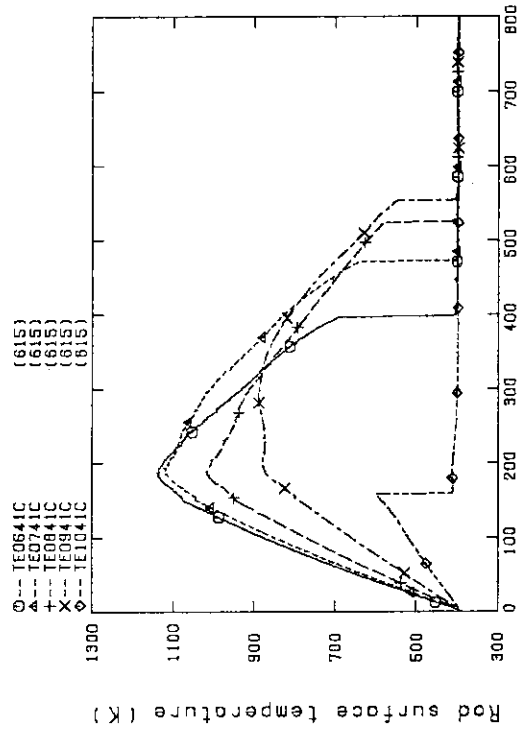

Fig.B-8 Heater rod temperature (Bundle 4-1C, Upper half)

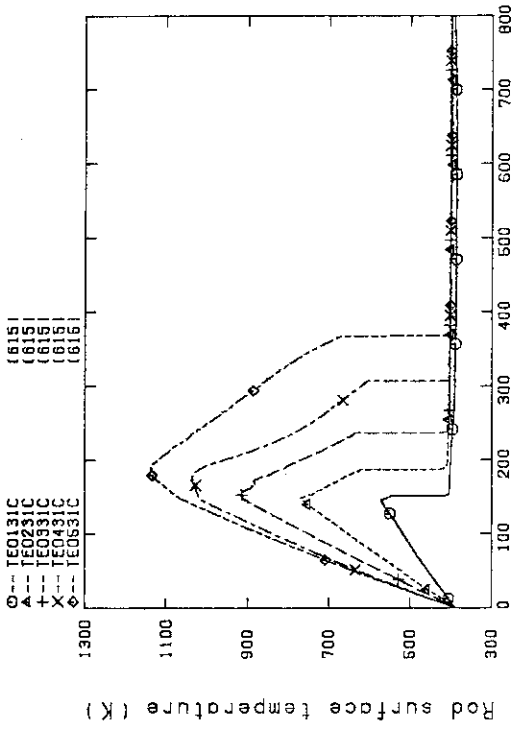

Fig.B-5 Heater rod temperature (Bundle 3-1C, Lower half)

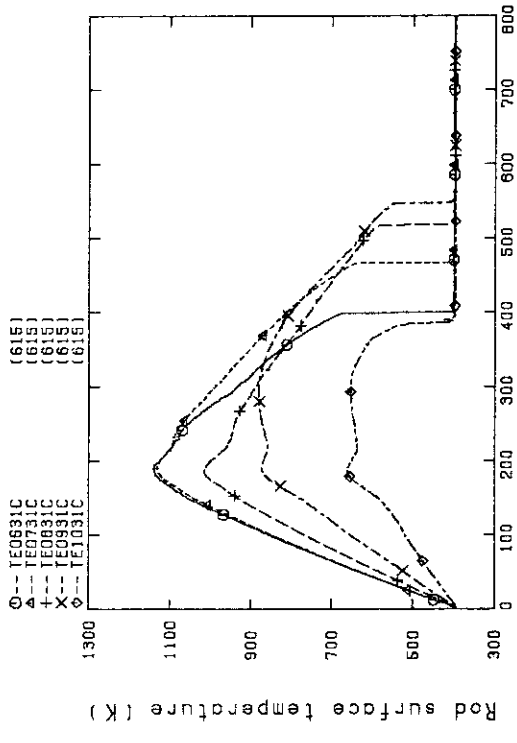

Fig.B-6 Heater rod temperature (Bundle 3-1C, Upper half)

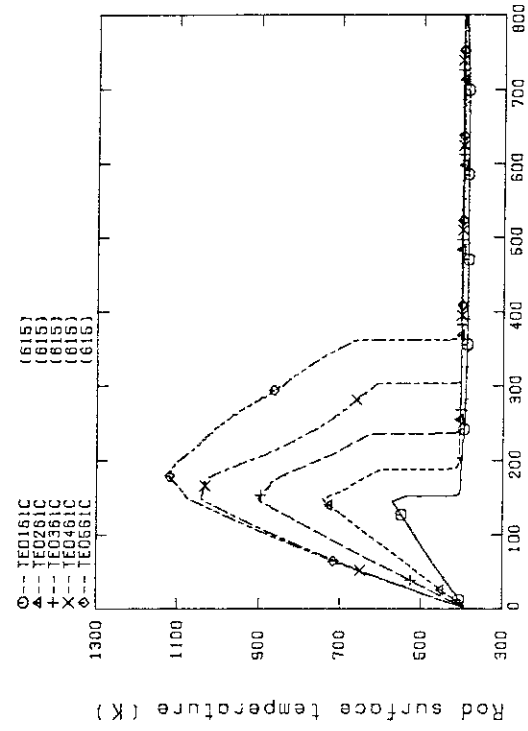

Fig.B-9 Heater rod temperature (Bundle 5-1C, Lower half)

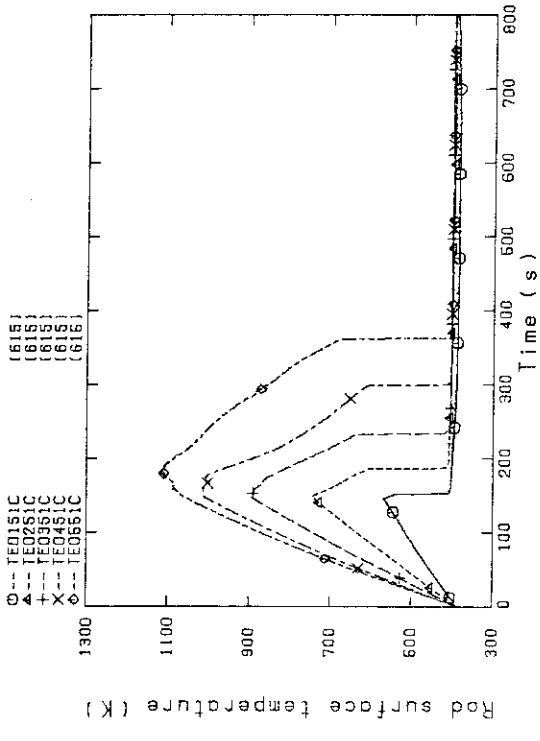

Fig.B-11 Heater rod temperature (Bundle 6-1C, Lower half)

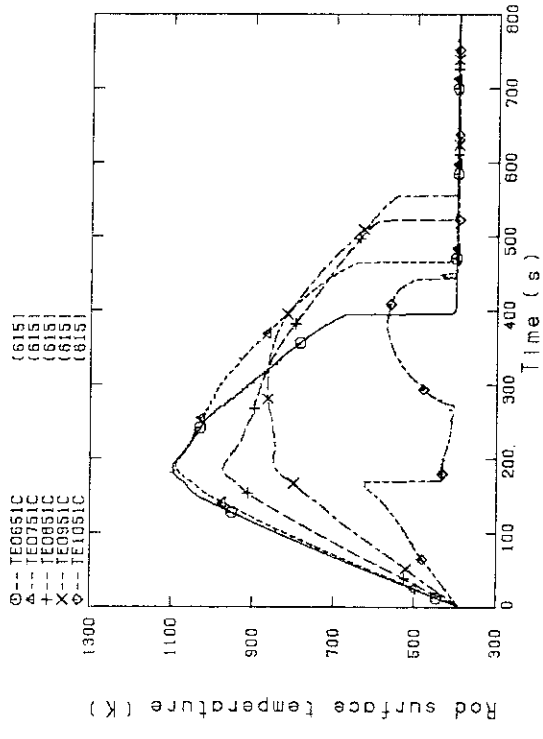

Fig.B-10 Heater rod temperature (Bundle 5-1C, Upper half)

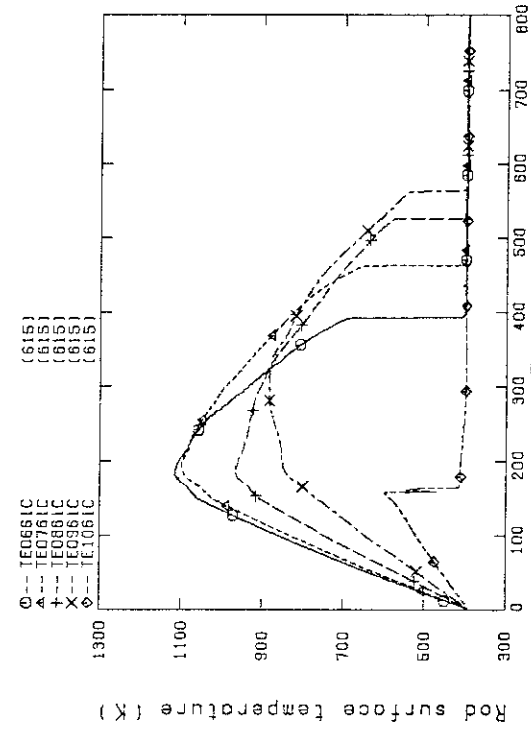

Fig.B-12 Heater rod temperature (Bundle 6-1C, Upper half)

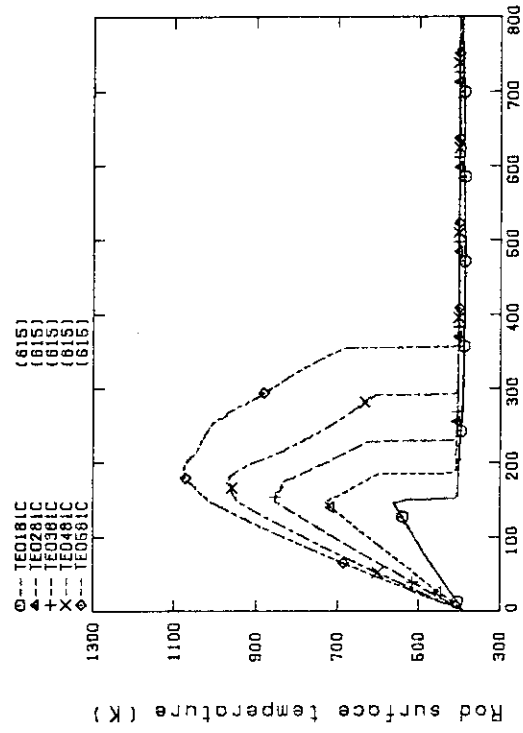

Fig.B-15 Heater rod temperature (Bundle 8-1C, Lower half)

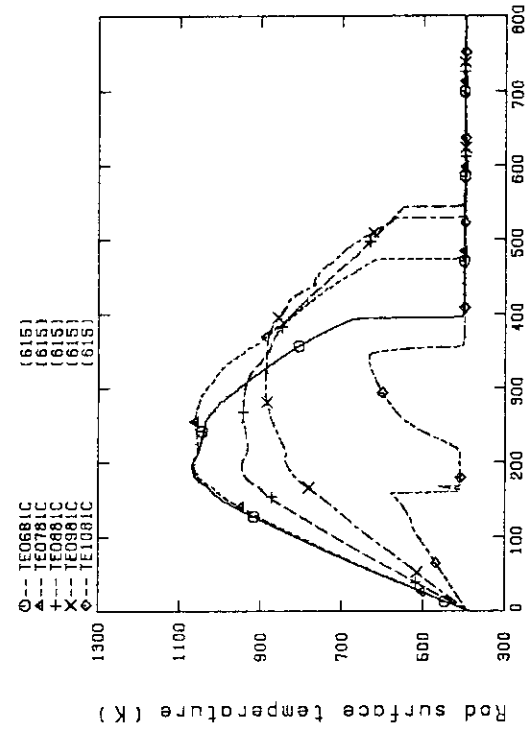

Fig.B-16 Heater rod temperature (Bundle 8-1C, Upper half)

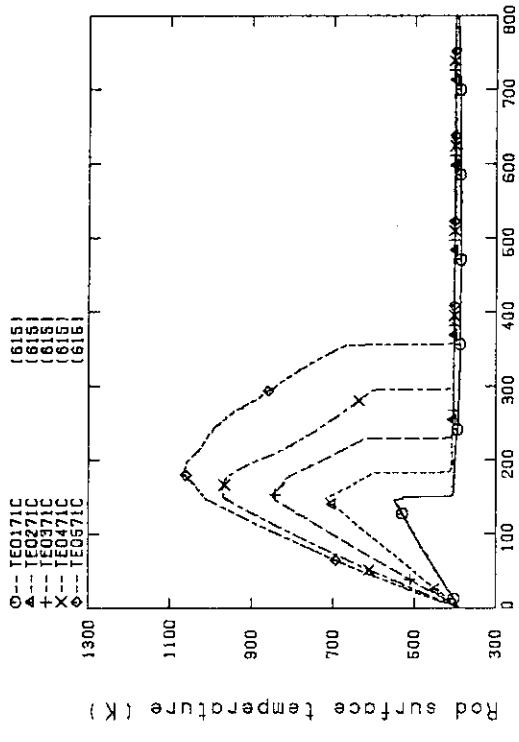

Fig.B-13 Heater rod temperature (Bundle 7-1C, Lower half)

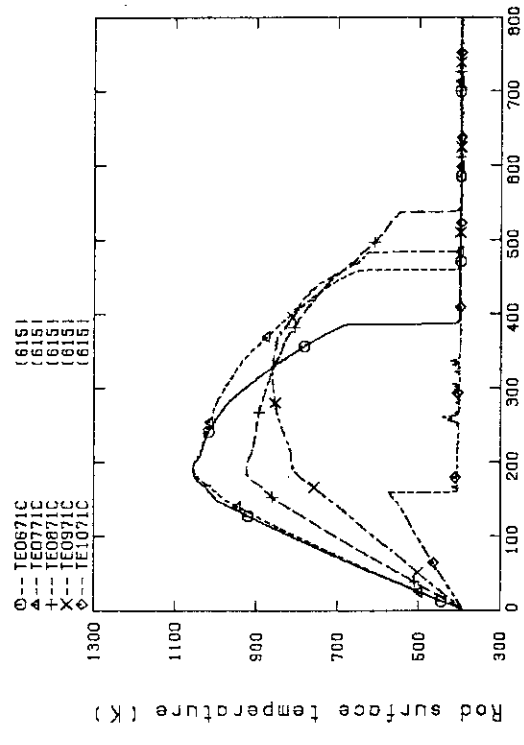

Fig.B-14 Heater rod temperature (Bundle 7-1C, Upper half)

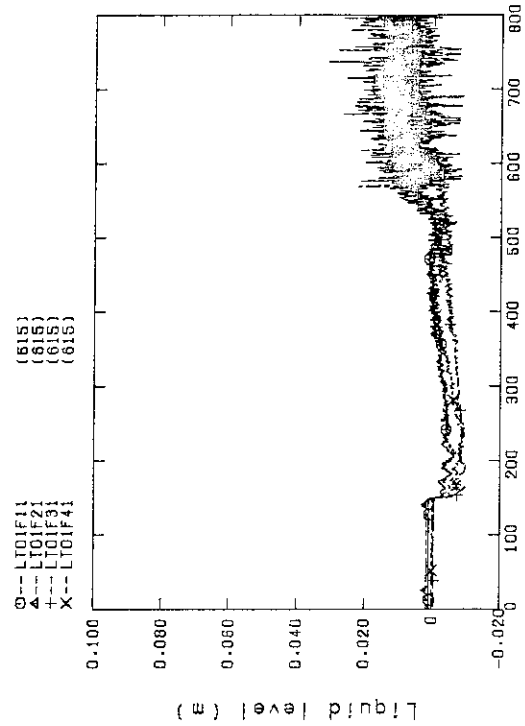

Fig.B-19 Liquid level above end box tie plate (Bundle 1,2,3,4)

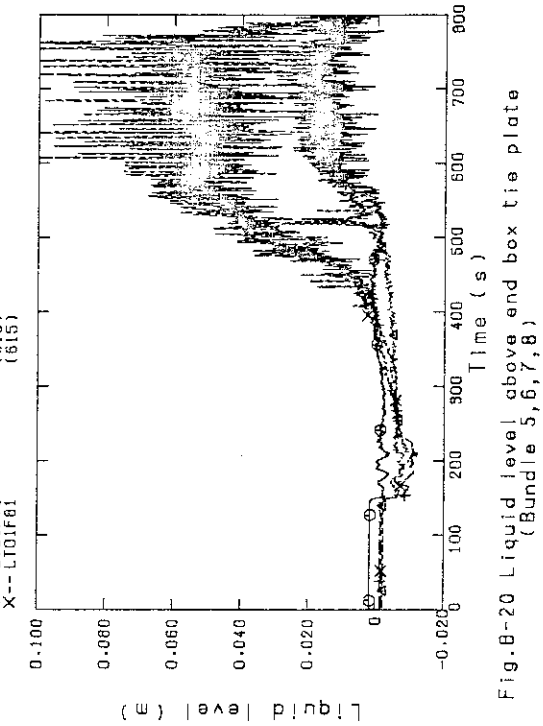

Fig.B-20 Liquid level above end box tie plate (Bundle 5,6,7,8)

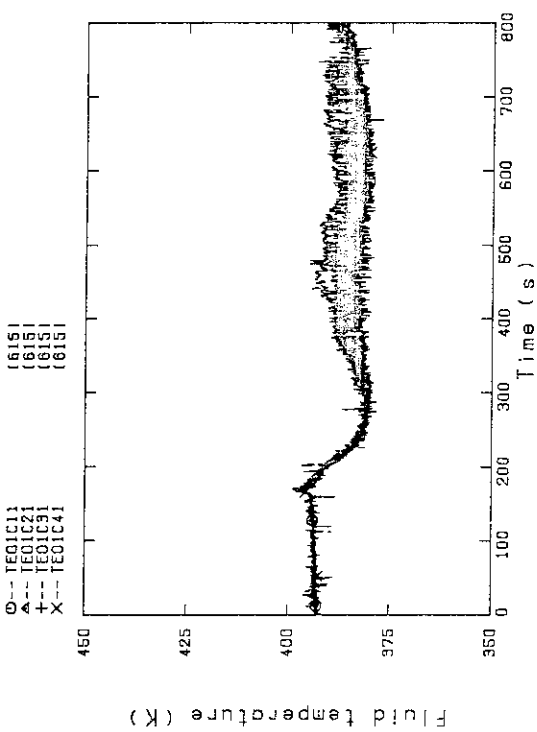

Fig.B-17 Fluid temperature at core inlet (Bundle 1,2,3,4, 100mm below heated part)

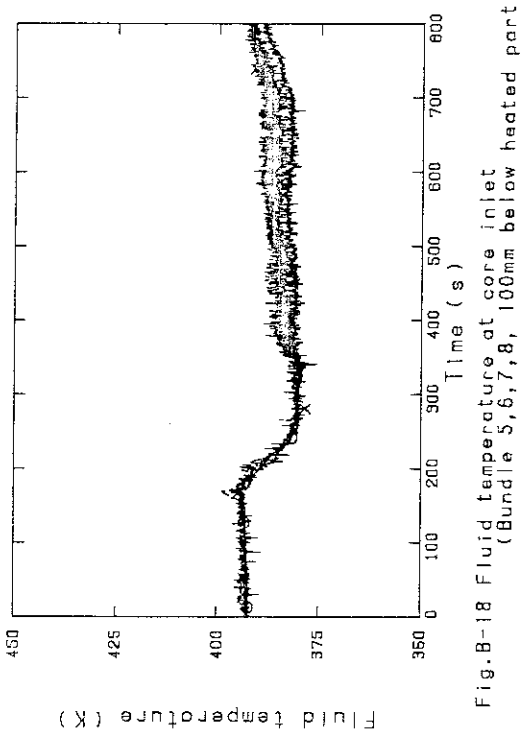

Fig.B-18 Fluid temperature at core inlet (Bundle 5,6,7,8, 100mm below heated part)

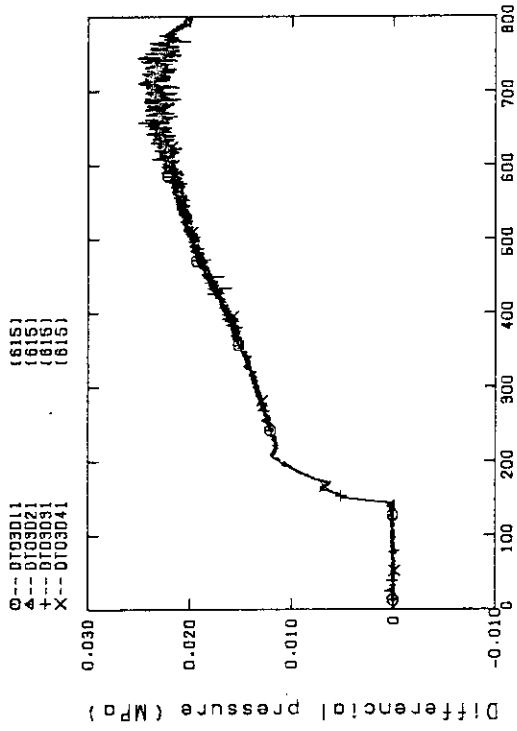

Fig.B-23 Differencial pressure of core full height (Bundle 1,2,3,4)

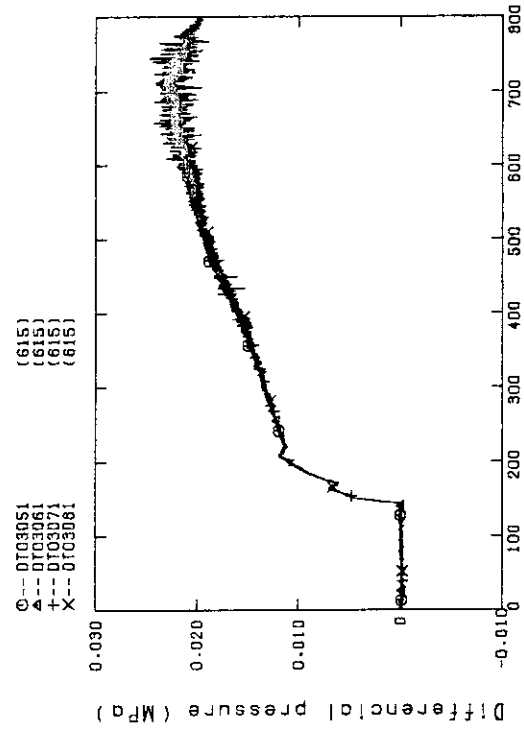

Fig.B-24 Differencial pressure of core full height (Bundle 5,6,7,8)

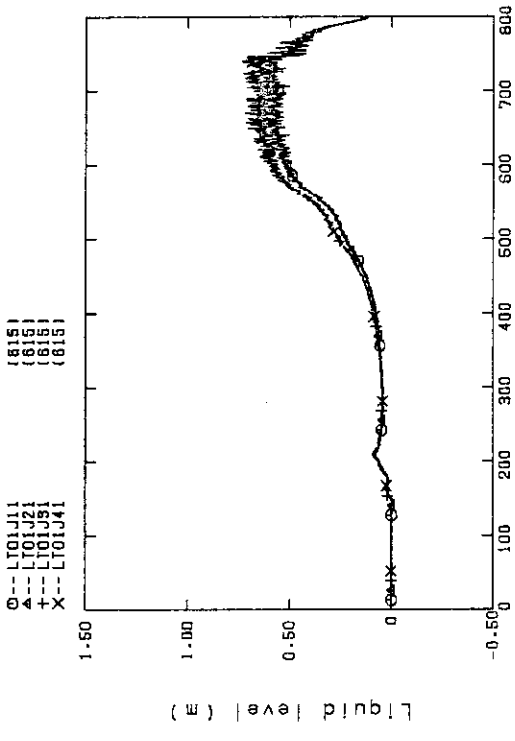

Fig.B-21 Liquid level above UCSP (Bundle 1,2,3,4)

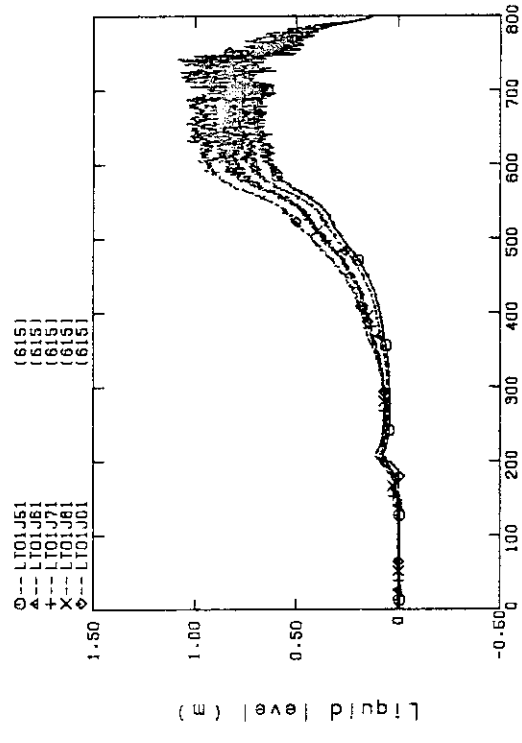

Fig.B-22 Liquid level above UCSP (Bundle 5,6,7,8 and core baffle)

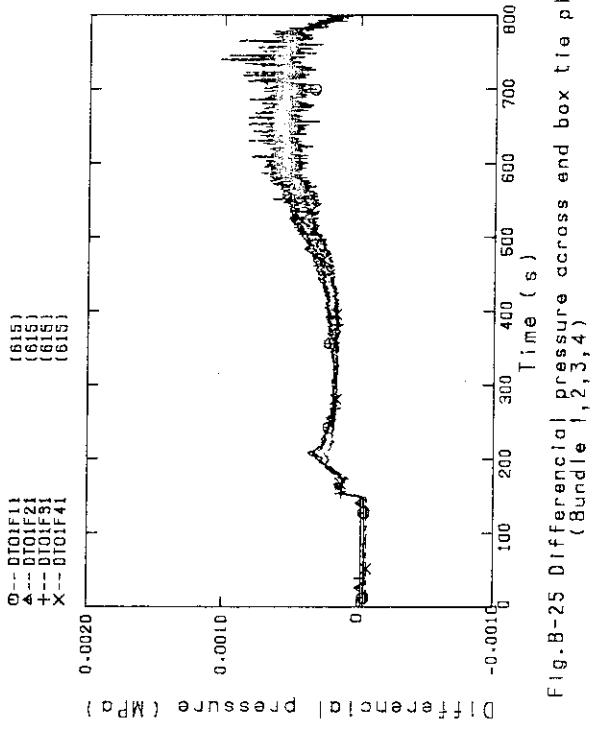

Fig.B-25 Differencial pressure across end box tie plate (Bundle 1,2,3,4)

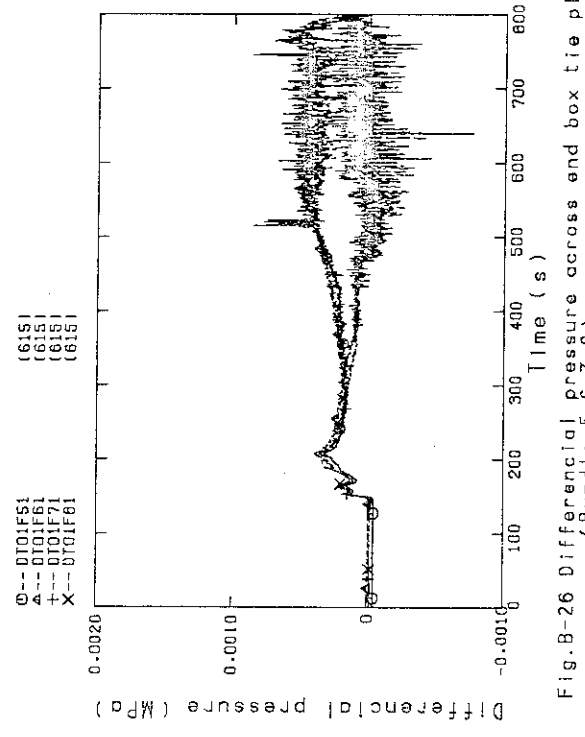

Fig.B-26 Differencial pressure across end box tie plate (Bundle 5,6,7,8)

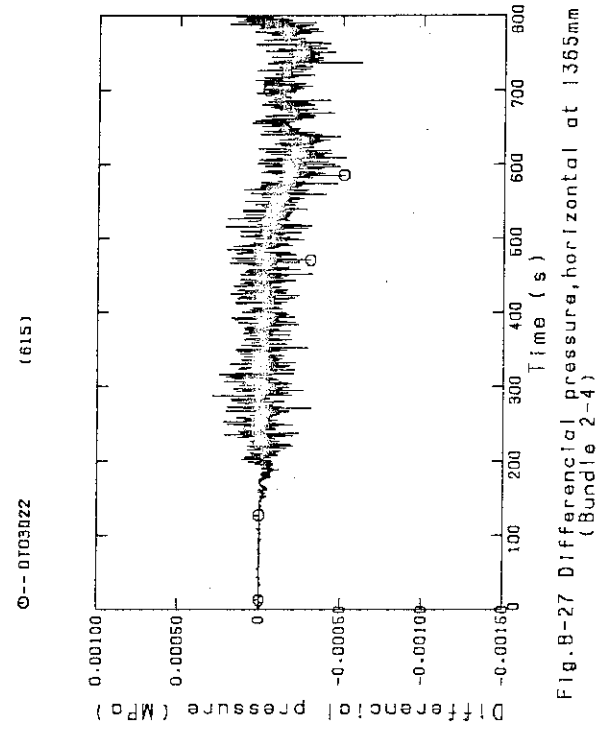

Fig.B-27 Differencial pressure,horizontal at 1365mm (Bundle 2-4)

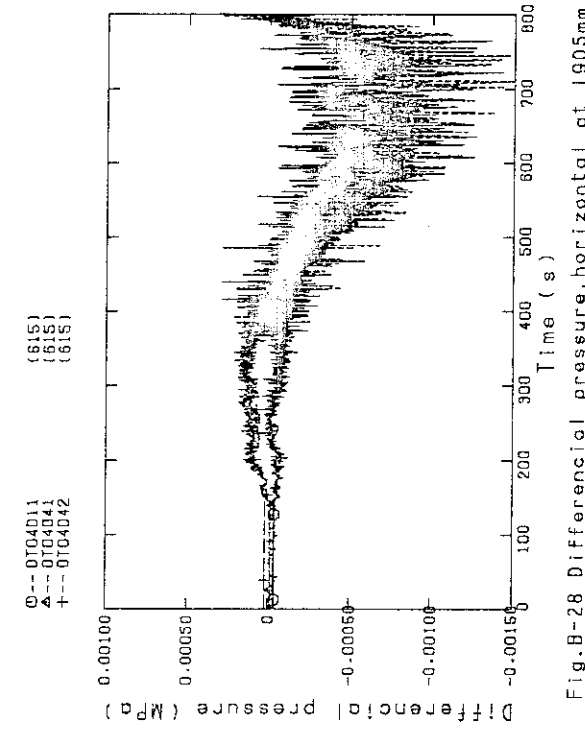

Fig.B-28 Differencial pressure horizontal at 1905mm (11-Bundle 1-4,41-Bundle 4-8,42-Bundle4-6)

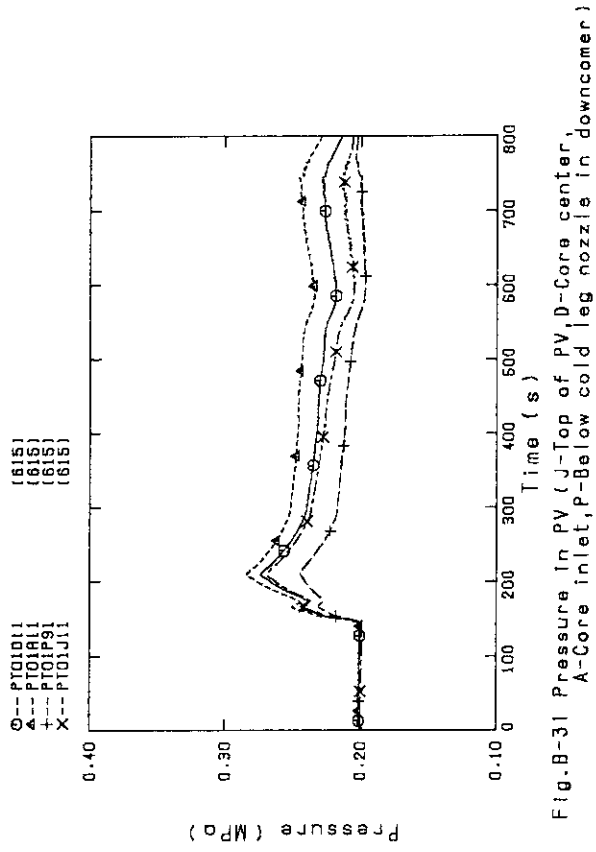

Fig.B-31 Pressure in PV (J-Top of PV, D-Core center, A-Core inlet, P-Below cold leg nozzle in downcomer)

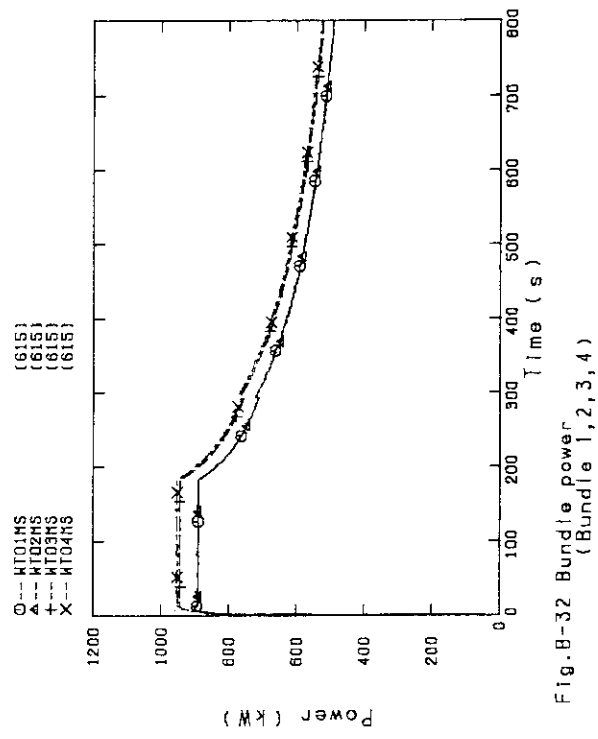

Fig.B-32 Bundle power (Bundle 1,2,3,4)

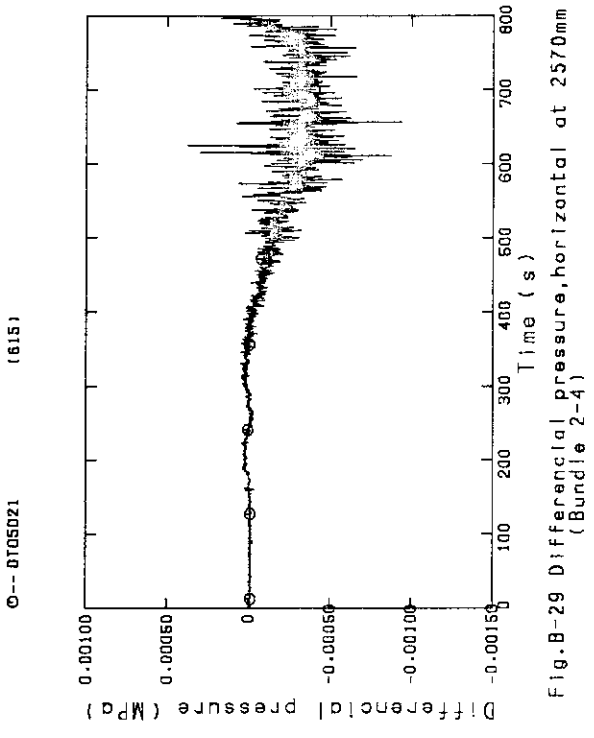

Fig.B-29 Differencial pressure,horizontal at 2570mm (Bundle 2-4)

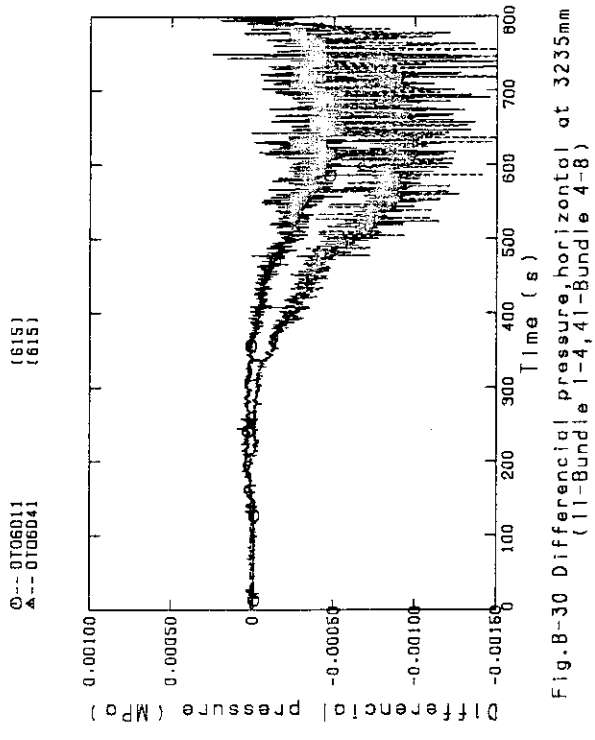

Fig.B-30 Differencial pressure,horizontal at 3235mm (11-Bundle 1-4,41-Bundle 4-8)

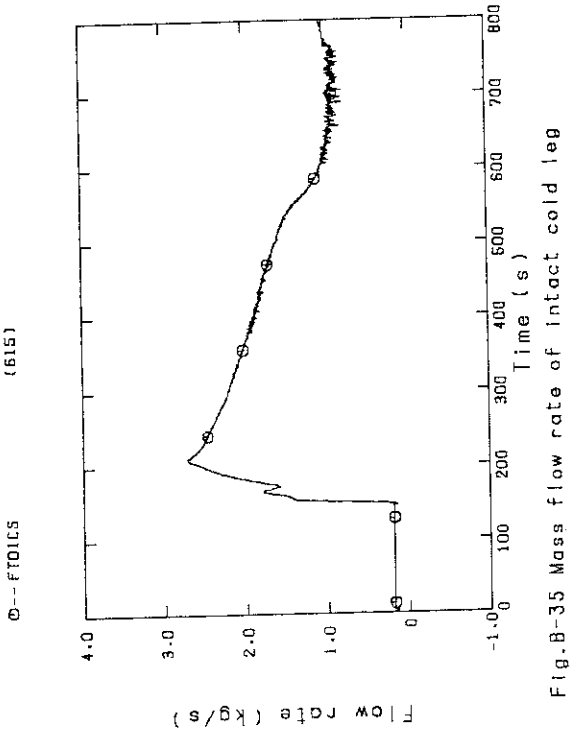

Fig.B-35 Mass flow rate of intact cold leg

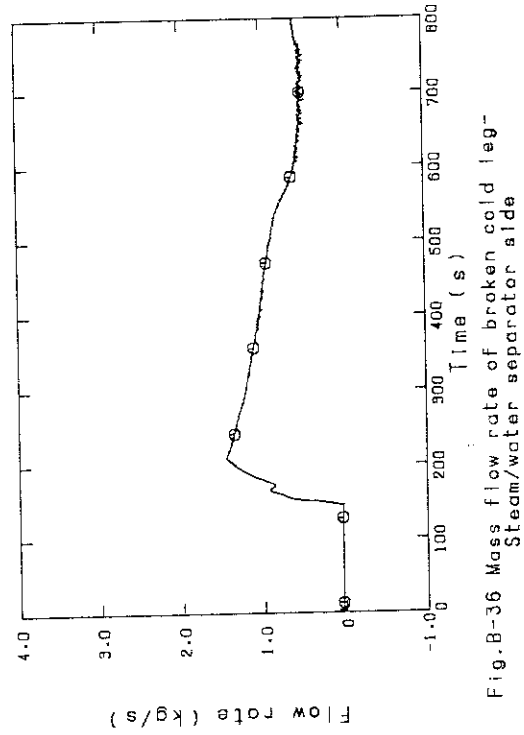

Fig.B-36 Mass flow rate of broken cold leg-Steam/water separator side

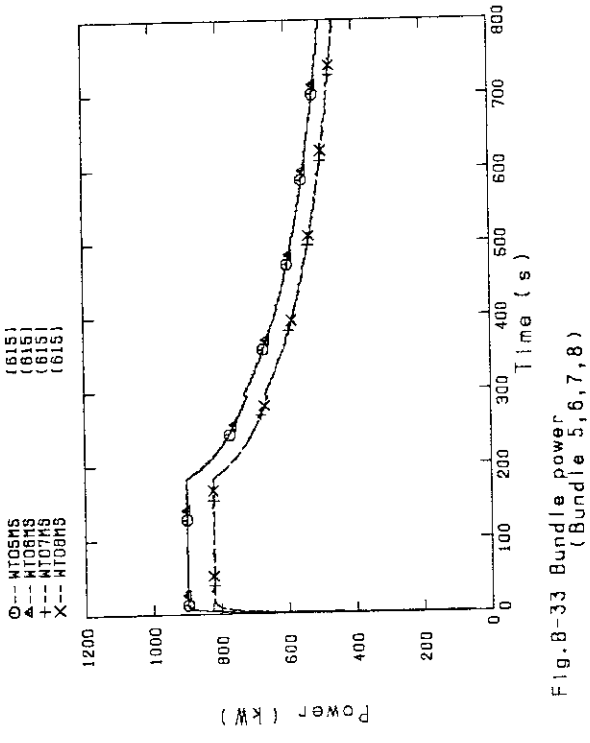

Fig.B-33 Bundle power (Bundle 5,6,7,8)

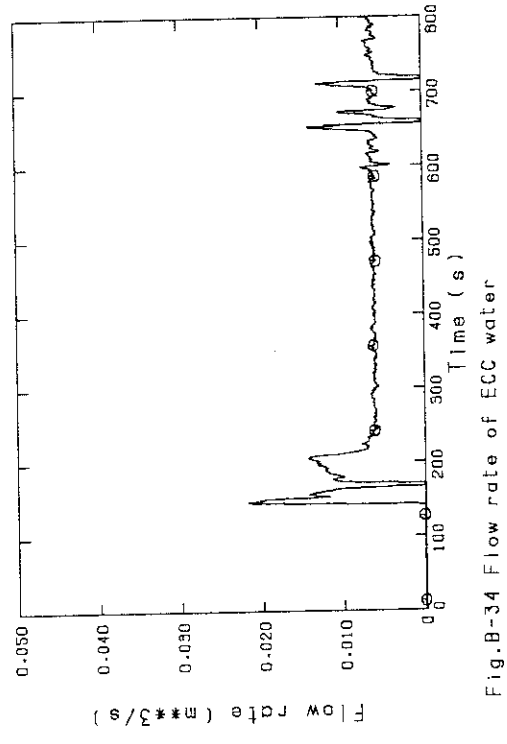

Fig.B-34 Flow rate of ECC water

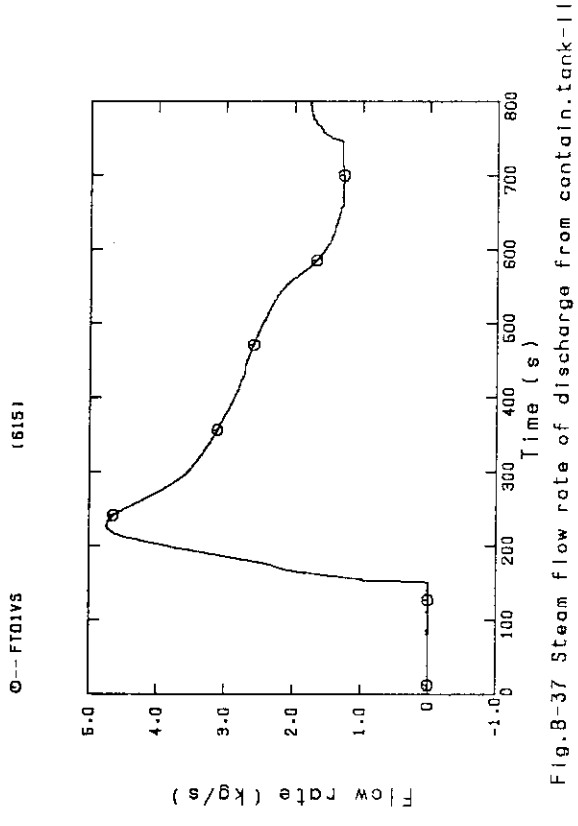

Fig.B-37 Steam flow rate of discharge from contain.tank-11

Appendix C Selected Data of Test S2-11

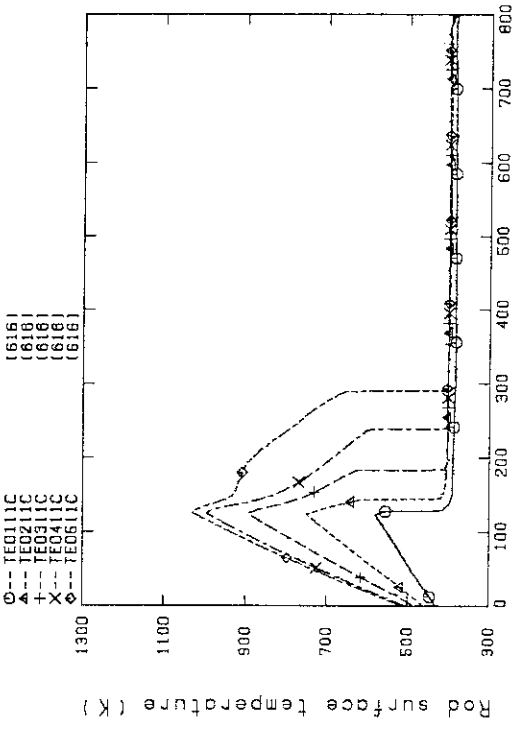

Fig.C-1 Heater rod temperature (Bundle 1-1C, Lower half)

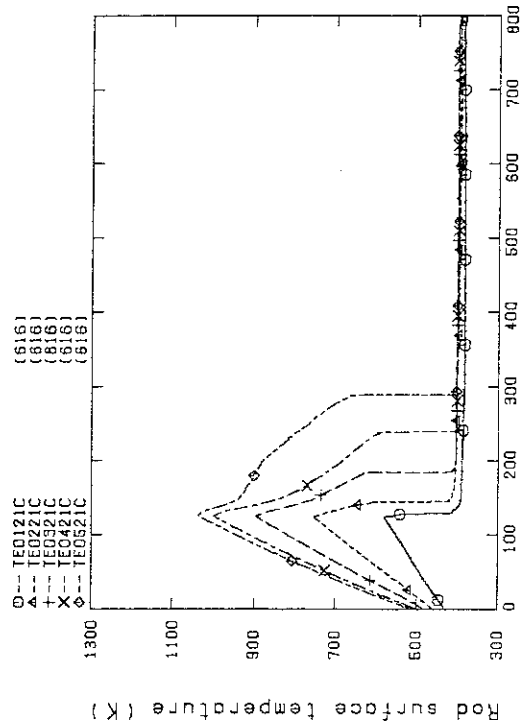

Fig.C-3 Heater rod temperature (Bundle 2-1C, Lower half)

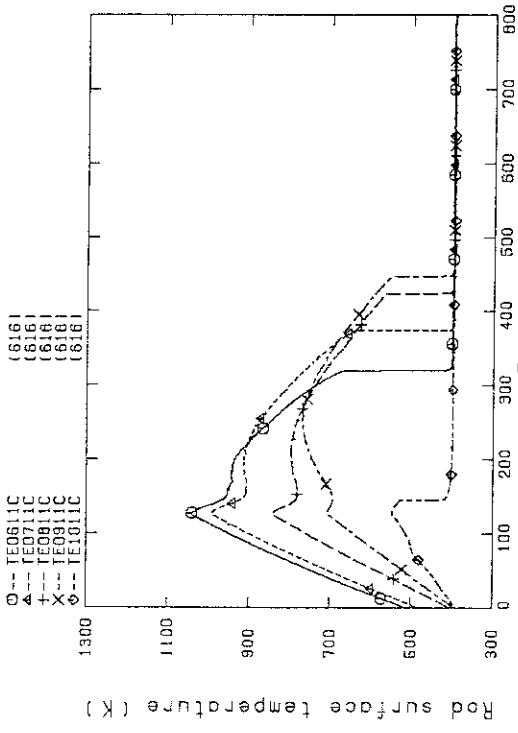

Fig.C-2 Heater rod temperature (Bundle 1-1C, Upper half)

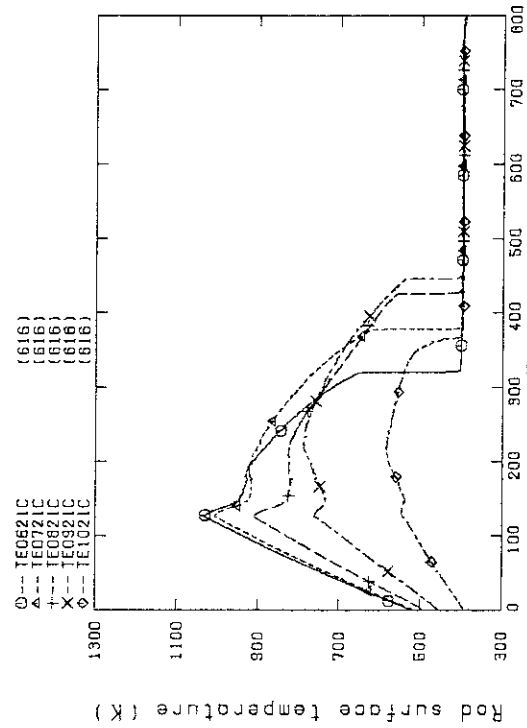

Fig.C-4 Heater rod temperature (Bundle 2-1C, Upper half)

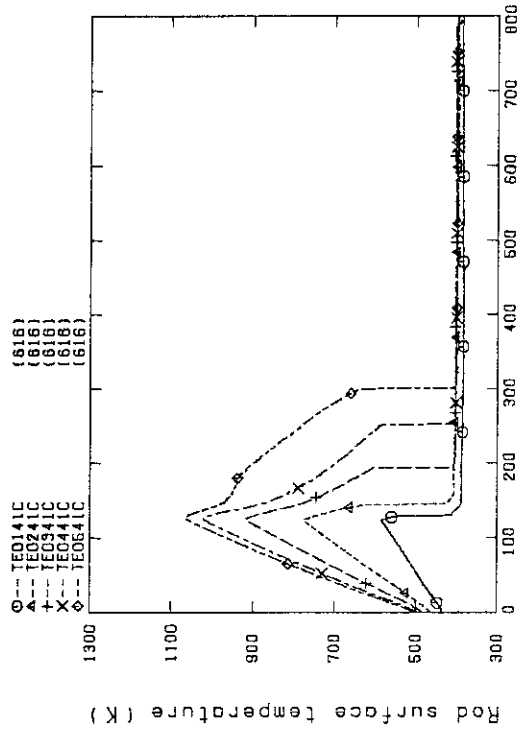

Fig.C-5 Heater rod temperature (Bundle 3-1C, Lower half)

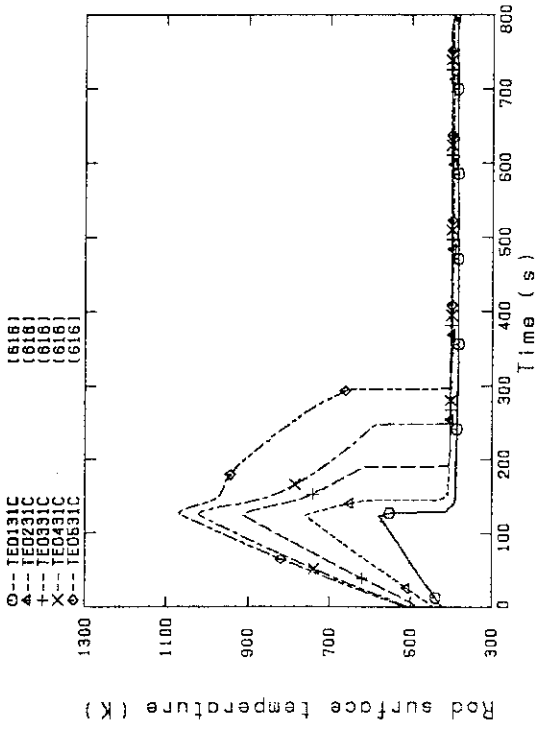

Fig.C-7 Heater rod temperature (Bundle 4-1C, Lower half)

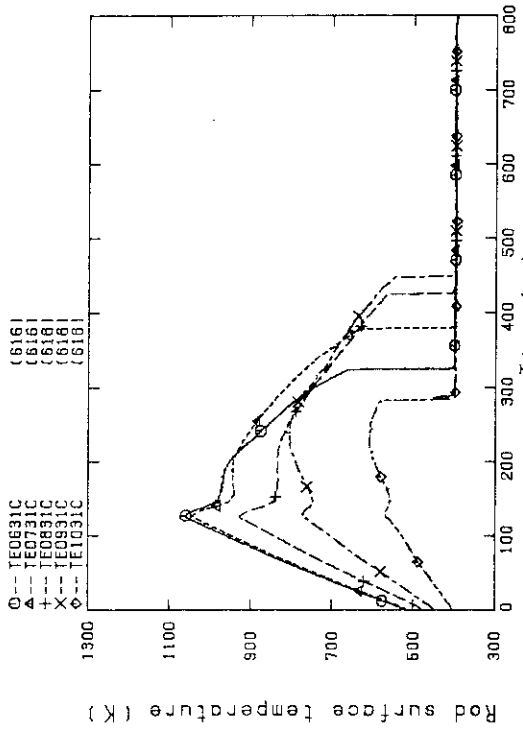

Fig.C-6 Heater rod temperature (Bundle 3-1C, Upper half)

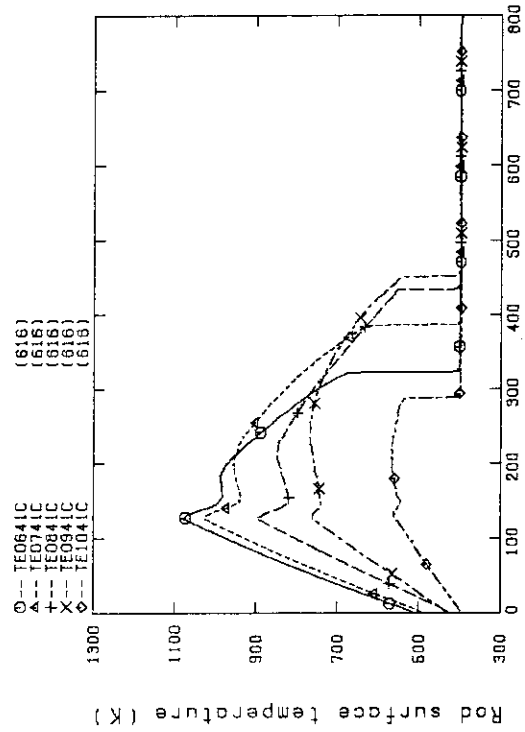

Fig.C-8 Heater rod temperature (Bundle 4-1C, Upper half)

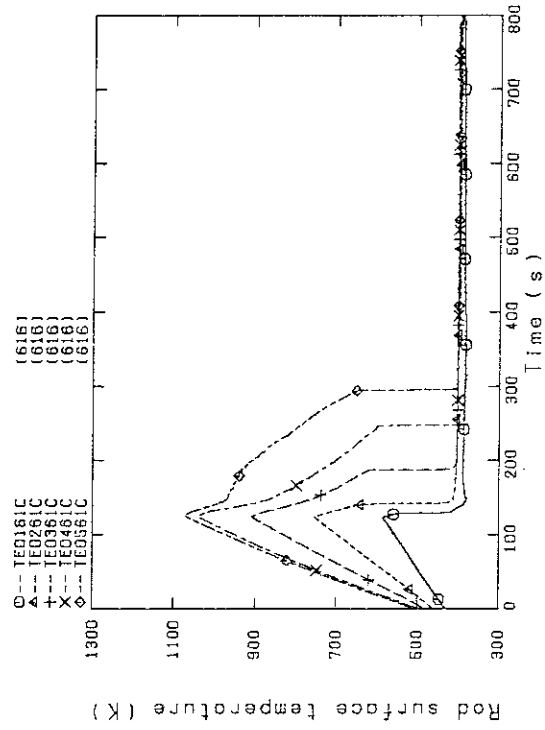

Fig.C-11 Heater rod temperature
(Bundle 6-1C, Lower half)

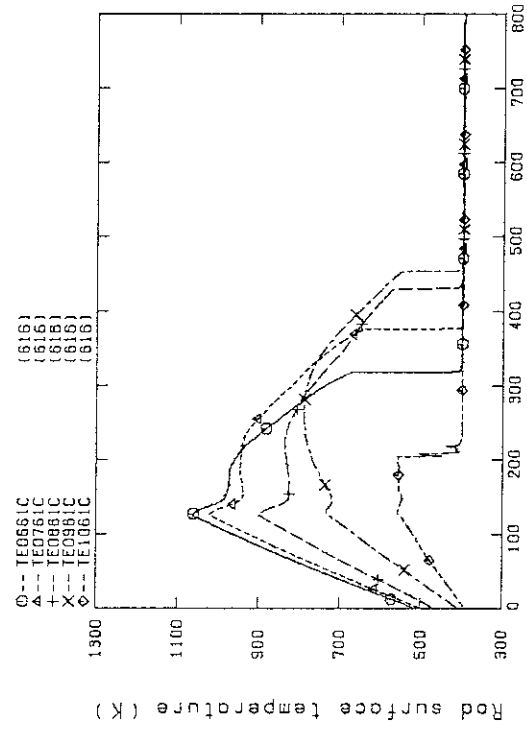

Fig.C-12 Heater rod temperature
(Bundle 6-1C, Upper half)

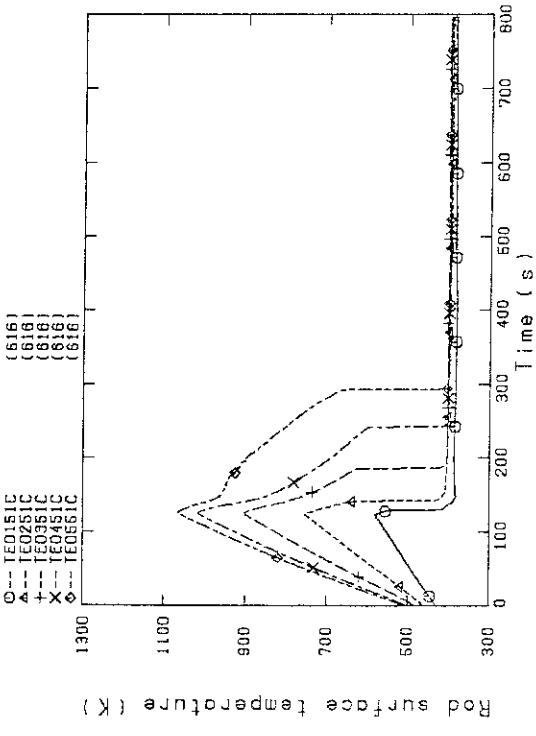

Fig.C-9 Heater rod temperature
(Bundle 5-1C, Lower half)

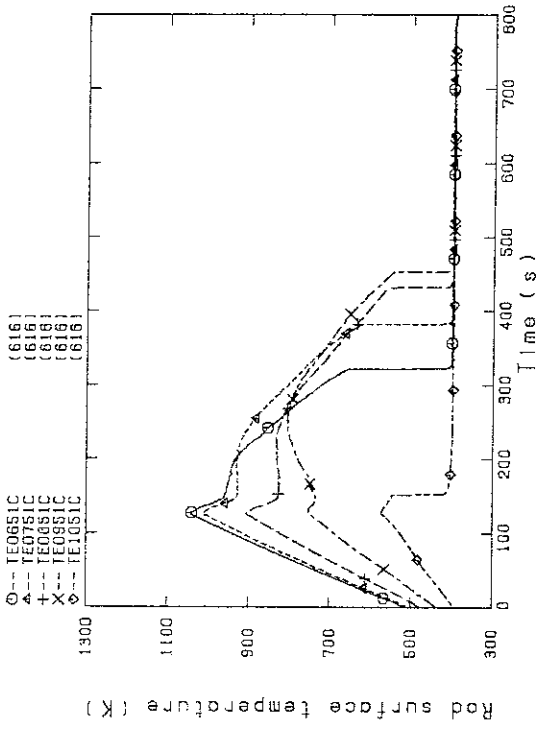

Fig.C-10 Heater rod temperature
(Bundle 5-1C, Upper half)

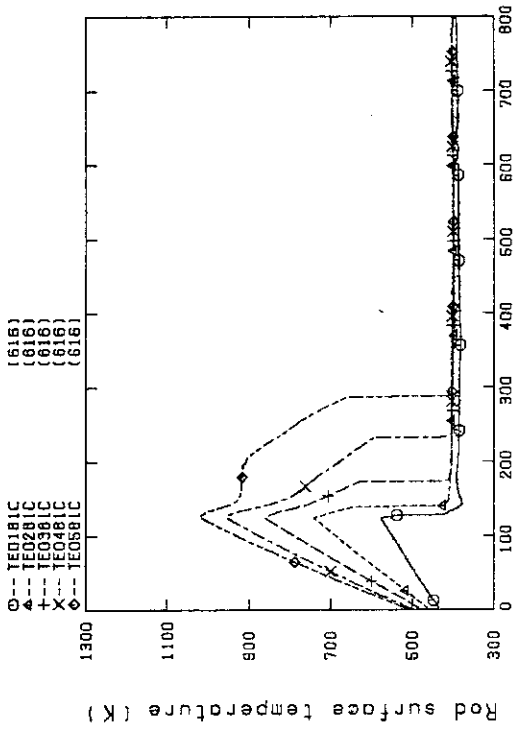

Fig.C-15 Heater rod temperature (Bundle 8-1C, Lower half)

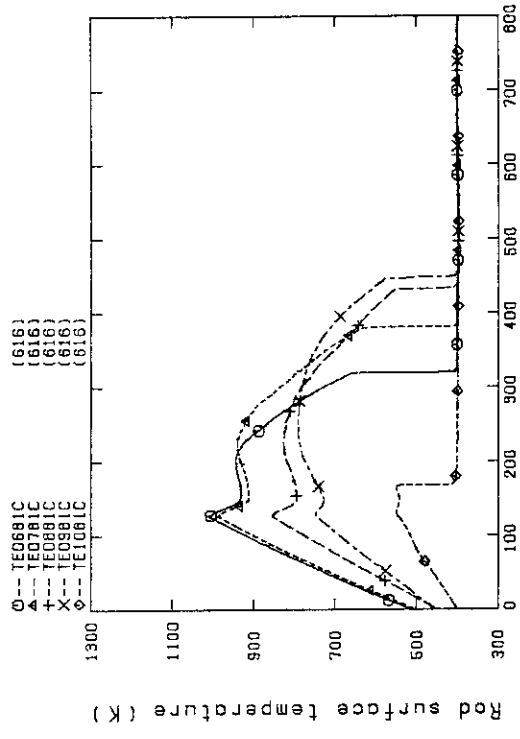

Fig.C-16 Heater rod temperature (Bundle 8-1C, Upper half)

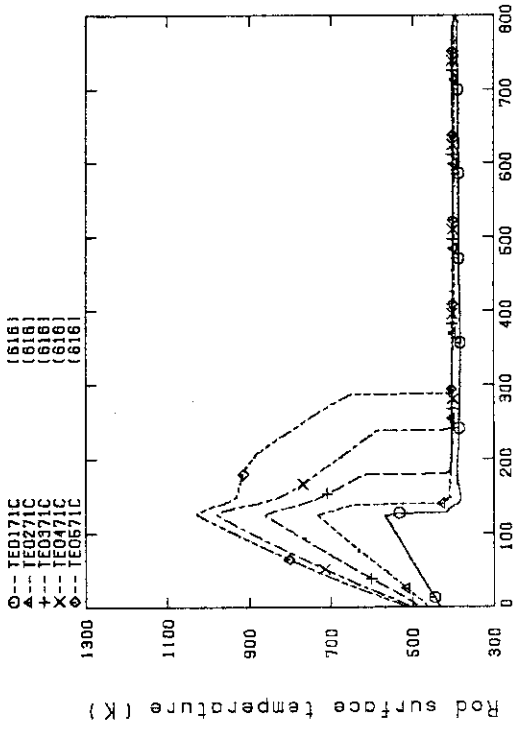

Fig.C-13 Heater rod temperature (Bundle 7-1C, Lower half)

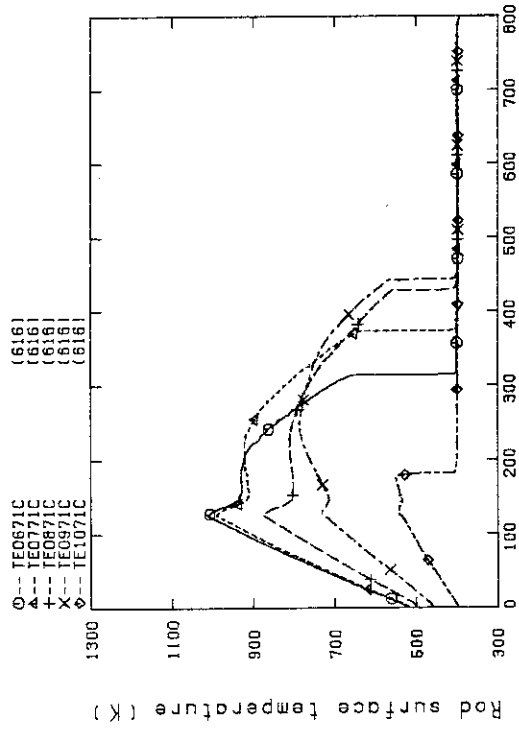

Fig.C-14 Heater rod temperature (Bundle 7-1C, Upper half)

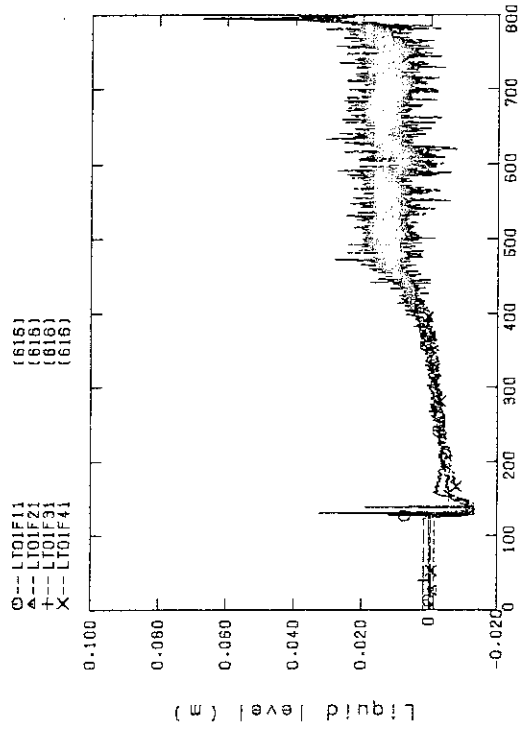

Fig.C-19 Liquid level above end box tie plate (Bundle 1,2,3,4)

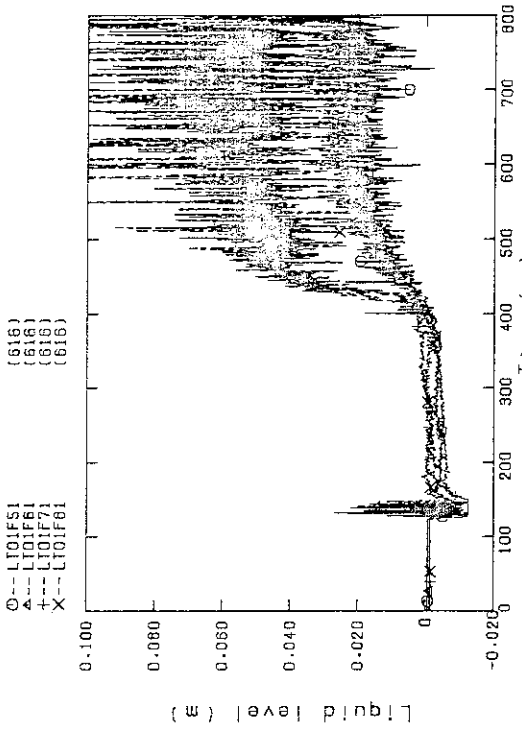

Fig.C-20 Liquid level above end box tie plate (Bundle 5,6,7,8)

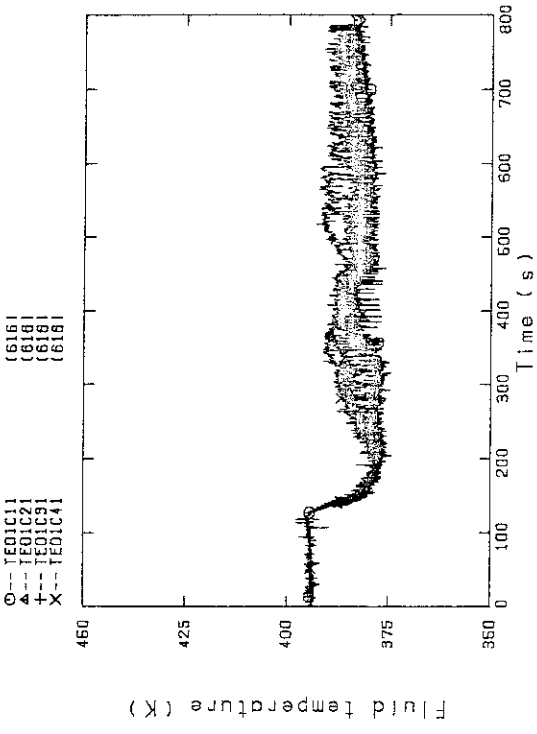

Fig.C-17 Fluid temperature at core inlet (Bundle 1,2,3,4, 100mm below heated part)

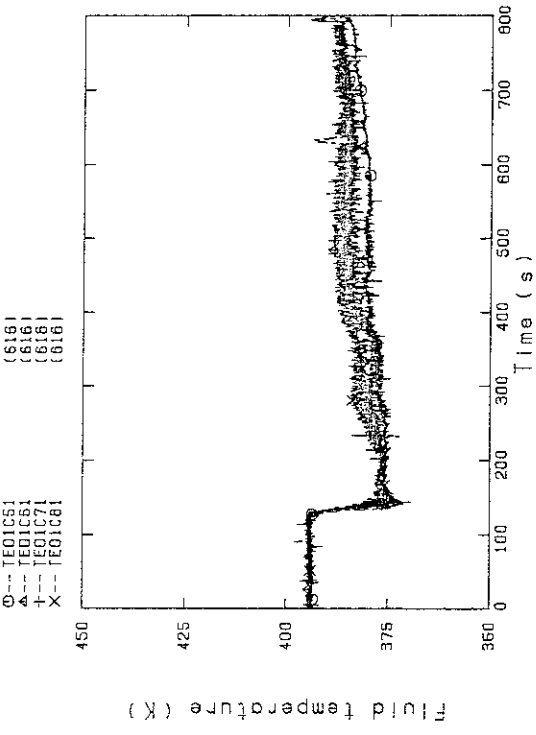

Fig.C-18 Fluid temperature at core inlet (Bundle 5,6,7,8, 100mm below heated part)

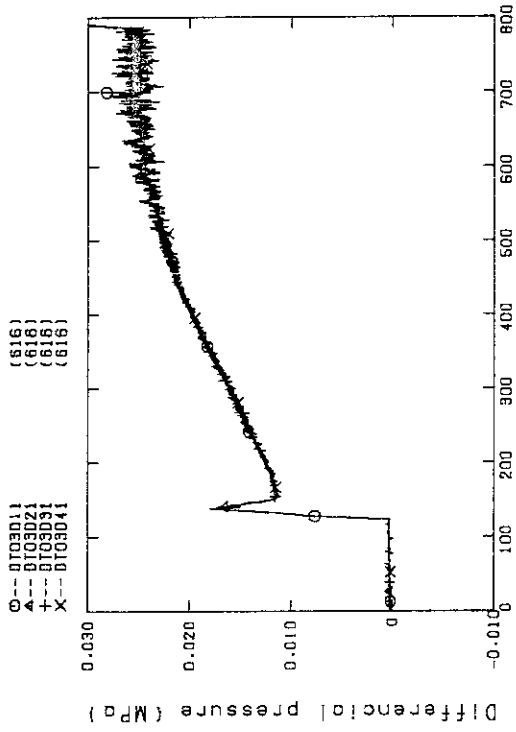

Fig.C-23 Differencial pressure of core full height (Bundle 1,2,3,4)

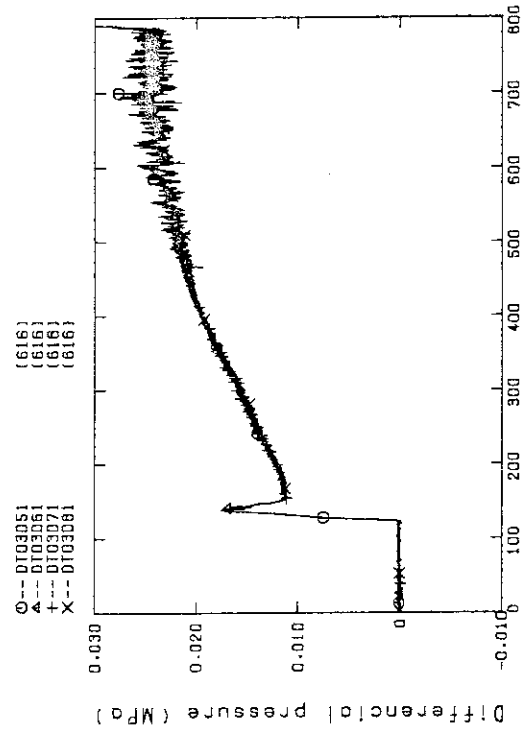

Fig.C-24 Differencial pressure of core full height (Bundle 5,6,7,8)

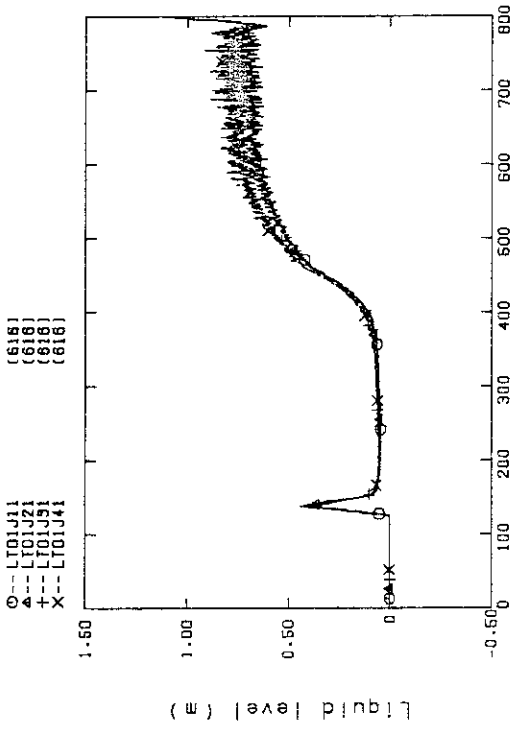

Fig.C-21 Liquid level above UCSP (Bundle 1,2,3,4)

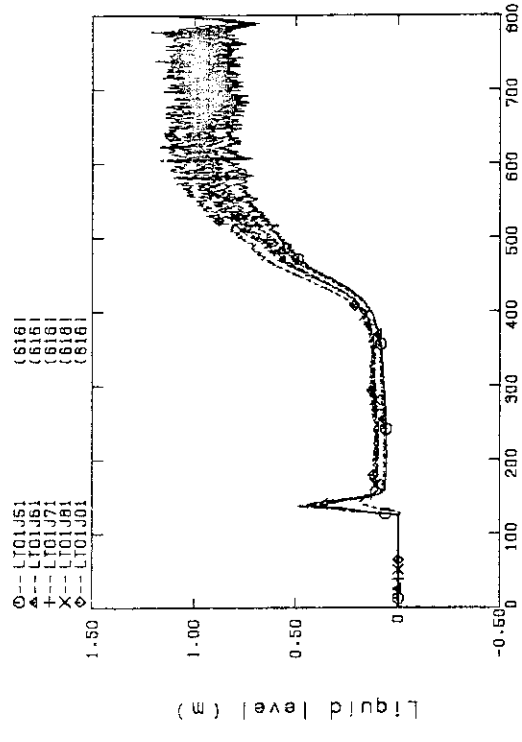

Fig.C-22 Liquid level above UCSP (Bundle 5,6,7,8 and core baffle)

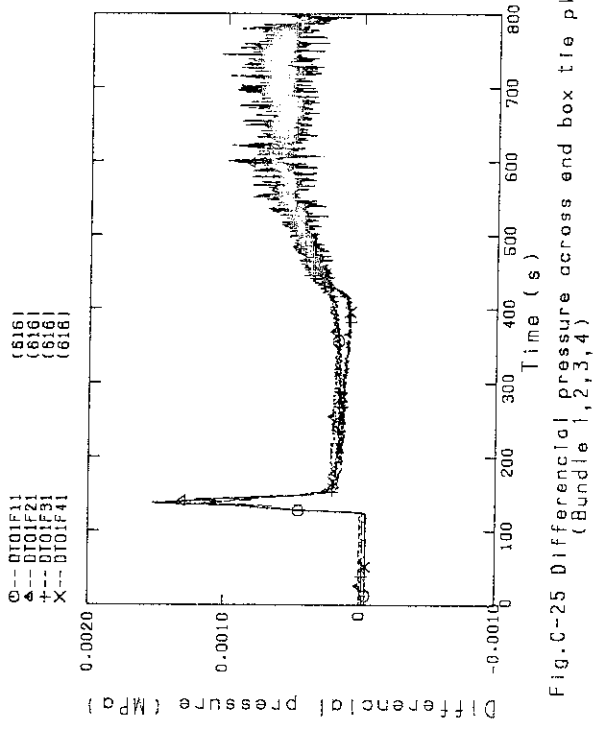

Fig.C-25 Differencial pressure across end box tie plate
(Bundle 1,2,3,4)

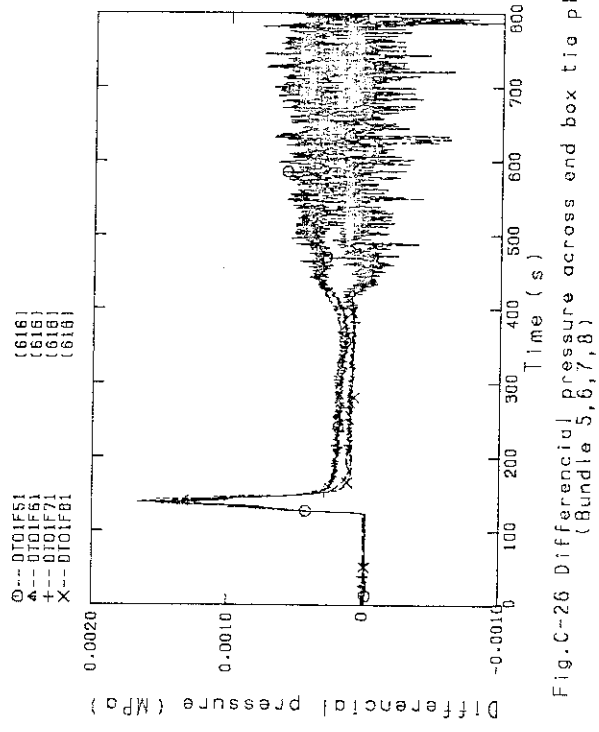

Fig.C-26 Differencial pressure across end box tie plate
(Bundle 5,6,7,8)

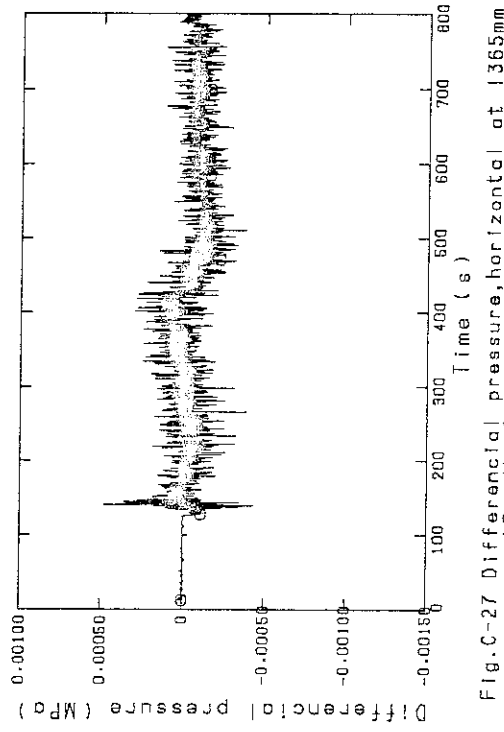

Fig.C-27 Differencial pressure,horizontal at 1365mm
(Bundle 2-4)

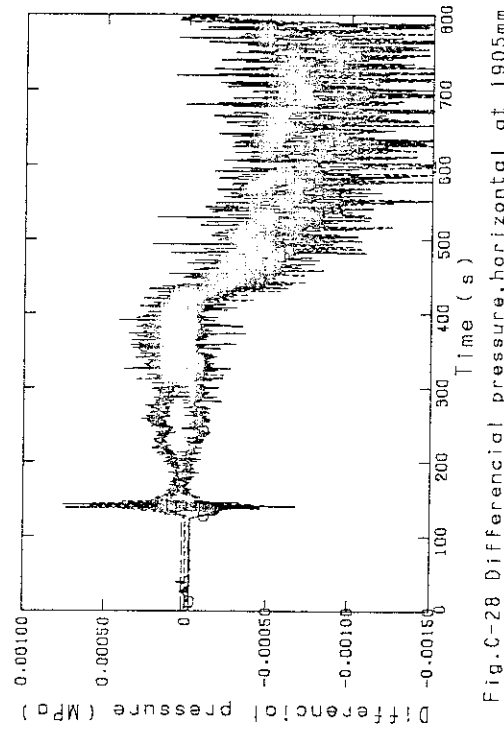

Fig.C-28 Differencial pressure,horizontal at 1905mm
(11-Bundle 1-4,41-Bundle 4-8,42-Bundle4-6)

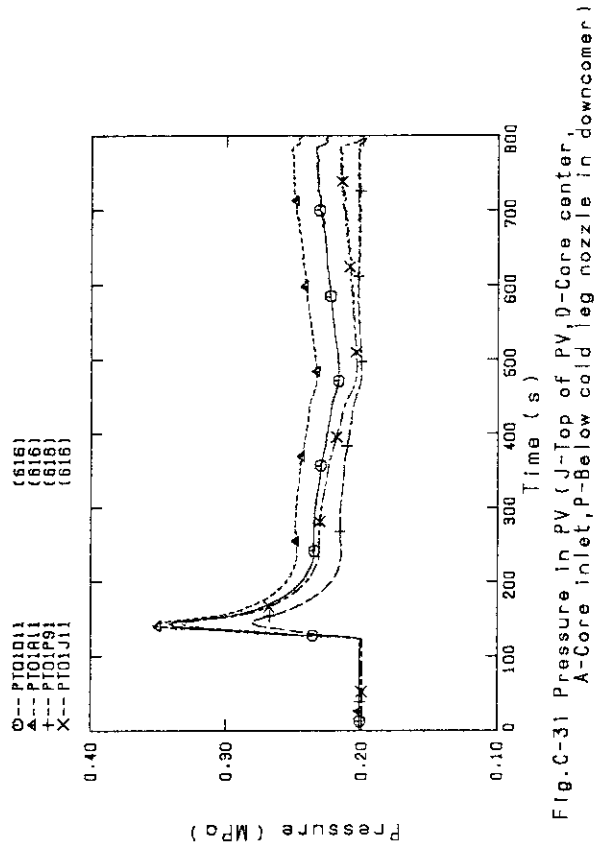

Fig.C-31 Pressure in PV (J-Top of PV,D-Core center, A-Core inlet,P-Below cold leg nozzle in downcomer)

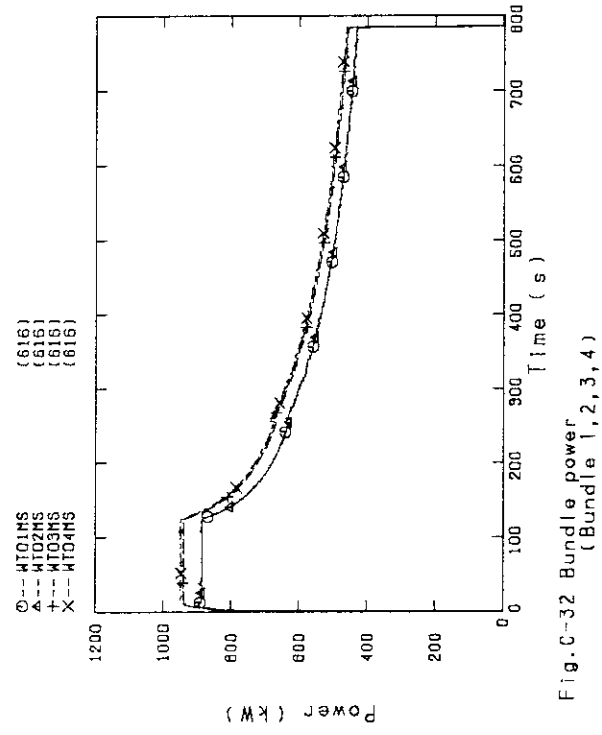

Fig.C-32 Bundle power (Bundle 1,2,3,4)

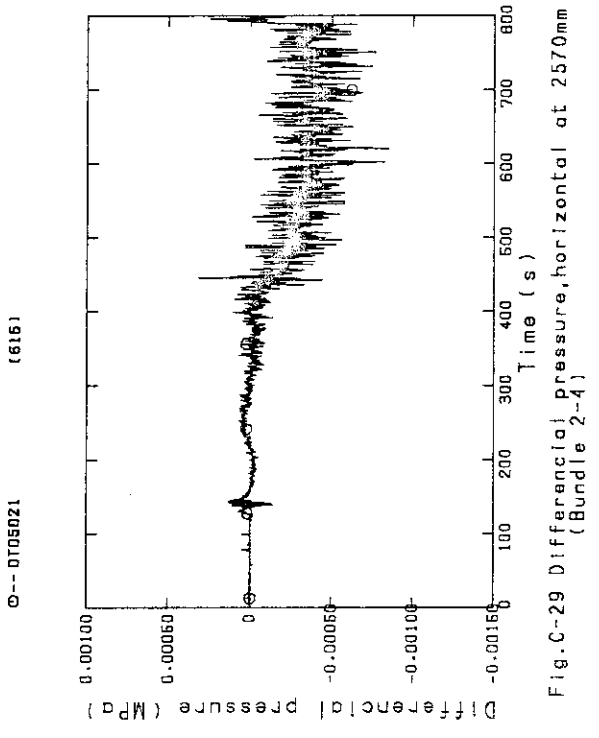

Fig.C-29 Differencial pressure,horizontal at 2570mm (Bundle 2-4)

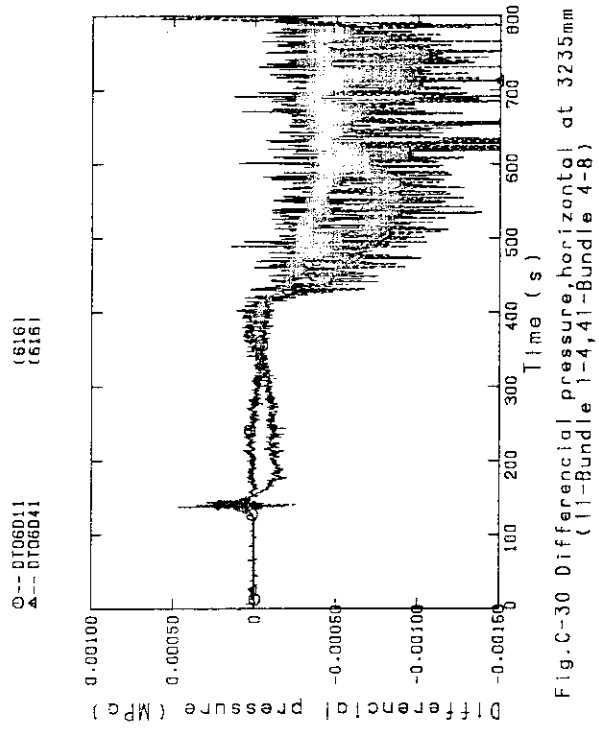

Fig.C-30 Differencial pressure,horizontal at 3235mm (11-Bundle 1-4,41-Bundle 4-8)

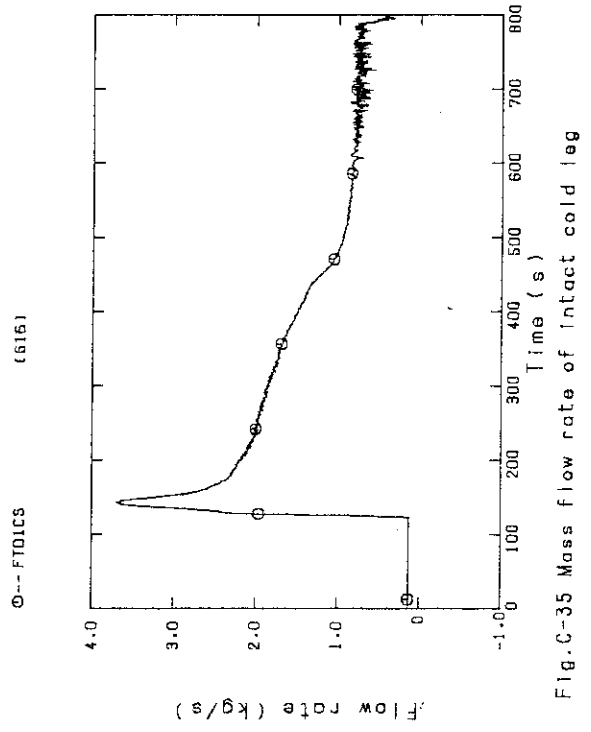

Fig.C-35 Mass flow rate of intact cold leg

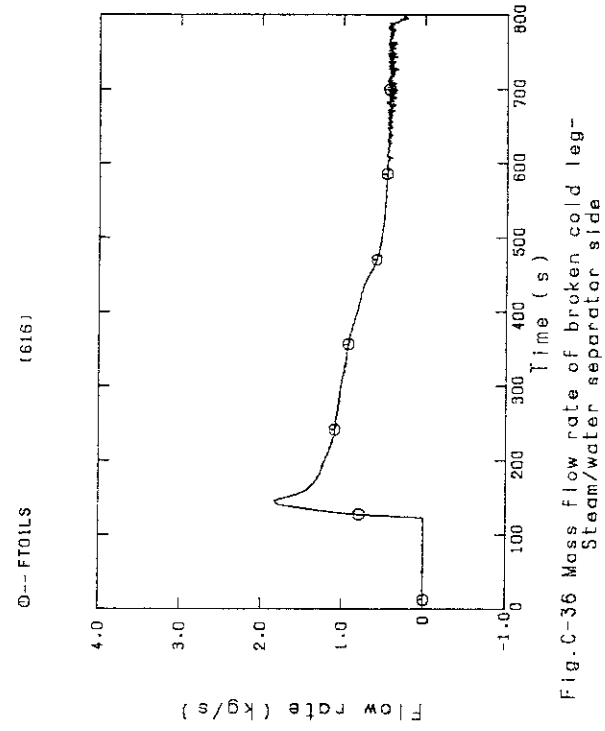

Fig.C-36 Mass flow rate of broken cold leg-Steam/water separator side

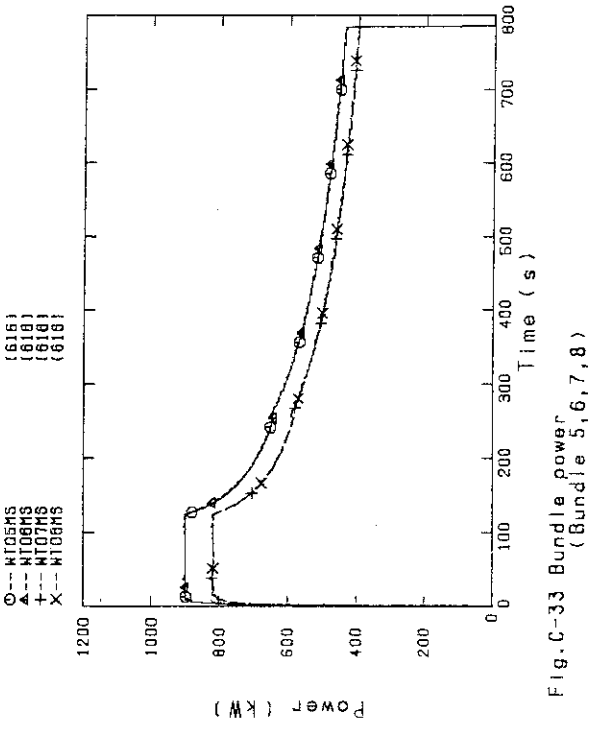

Fig.C-33 Bundle power (Bundle 5,6,7,8)

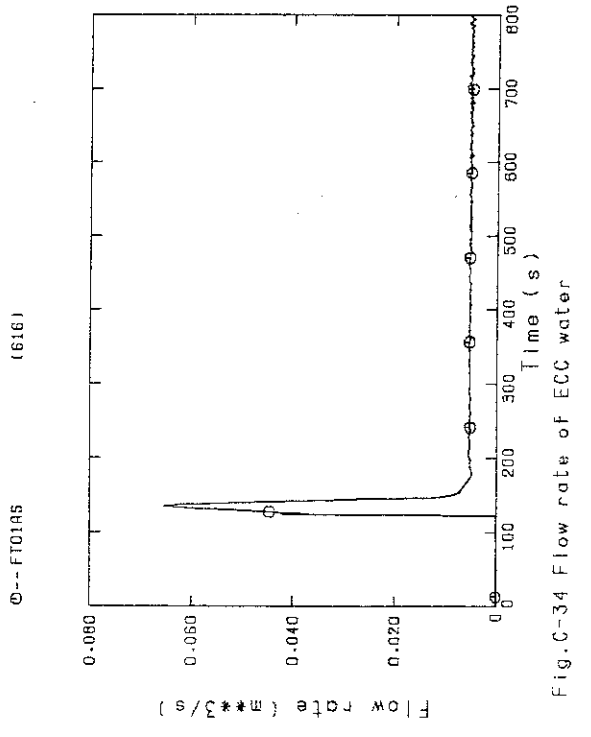

Fig.C-34 Flow rate of ECC water

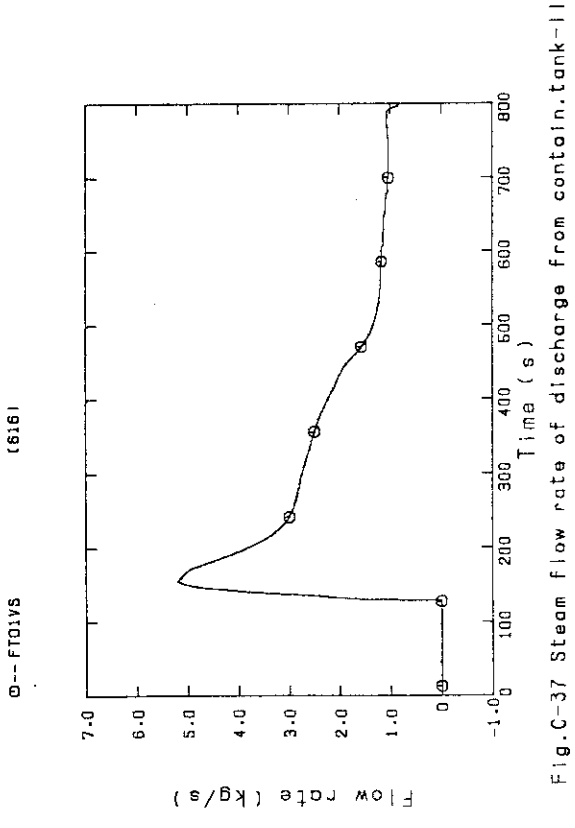

Fig.C-37 Steam flow rate of discharge from contain.tank-II

Appendix D Selected Data of Test S2-16

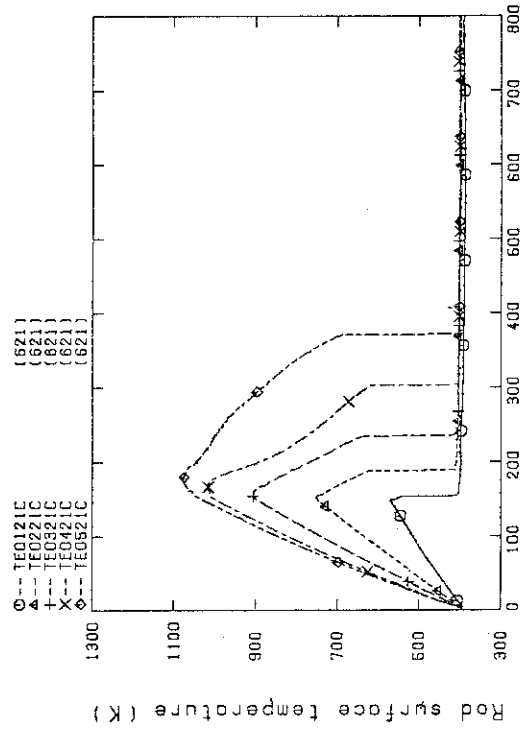

Fig.D-1 Heater rod temperature (Bundle 1-1C, Lower half)

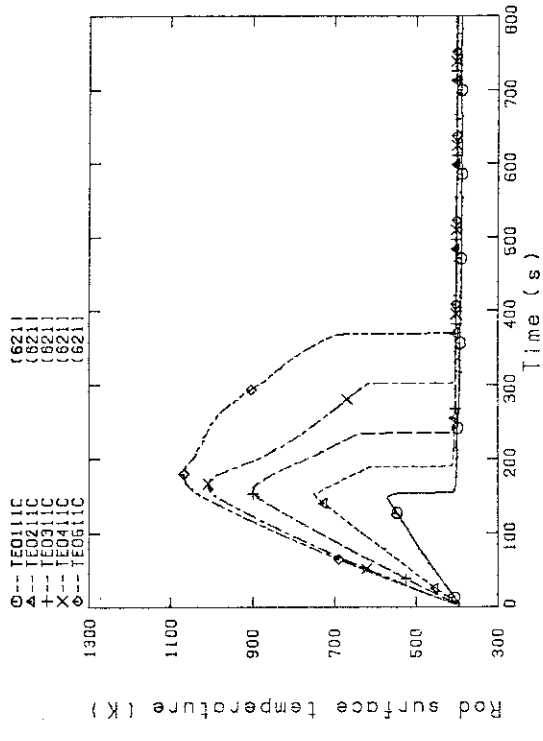

Fig.D-3 Heater rod temperature (Bundle 2-1C, Lower half)

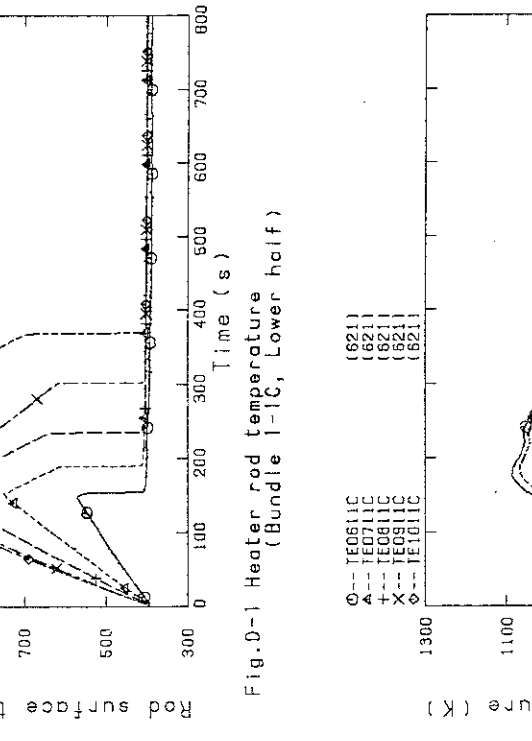

Fig.D-2 Heater rod temperature (Bundle 1-1C, Upper half)

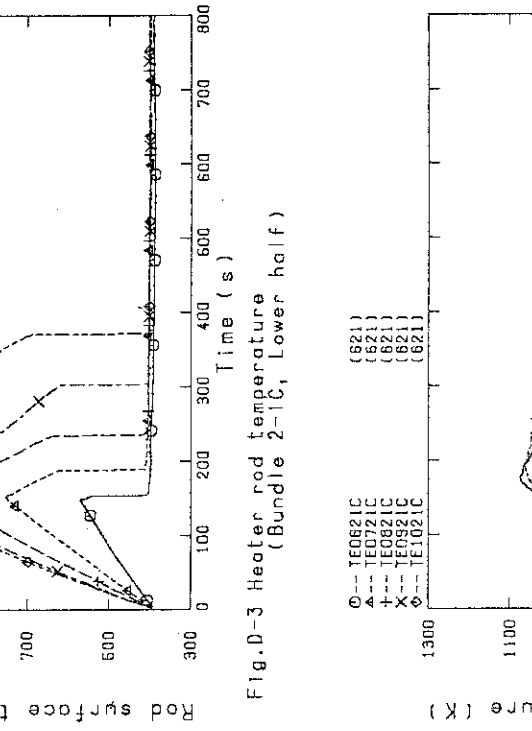

Fig.D-4 Heater rod temperature (Bundle 2-1C, Upper half)

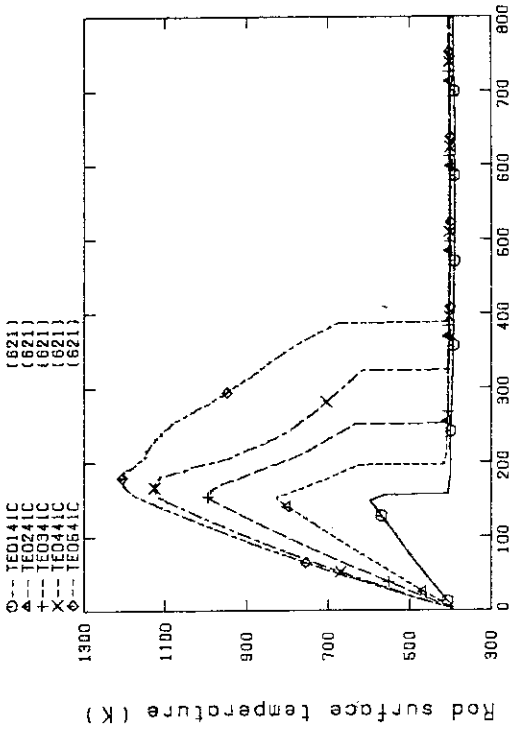

Fig.D-5 Heater rod temperature
(Bundle 3-1C, Lower half)

Fig.D-7 Heater rod temperature
(Bundle 4-1C, Lower half)

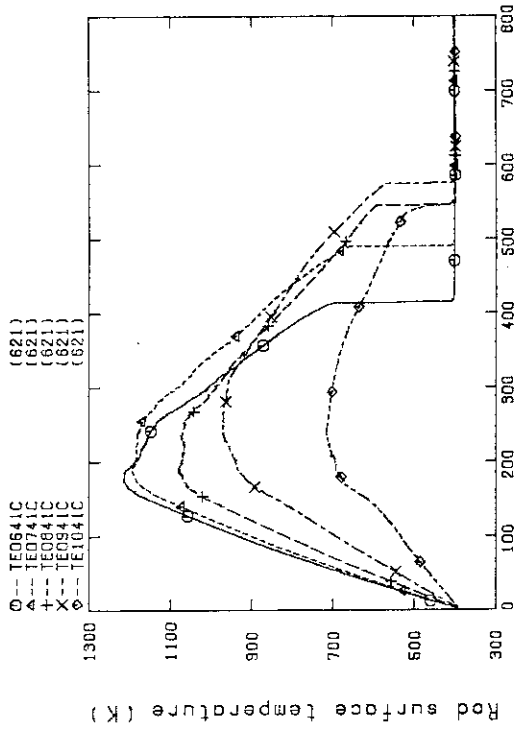

Fig.D-6 Heater rod temperature
(Bundle 3-1C, Upper half)

Fig.D-8 Heater rod temperature
(Bundle 4-1C, Upper half)

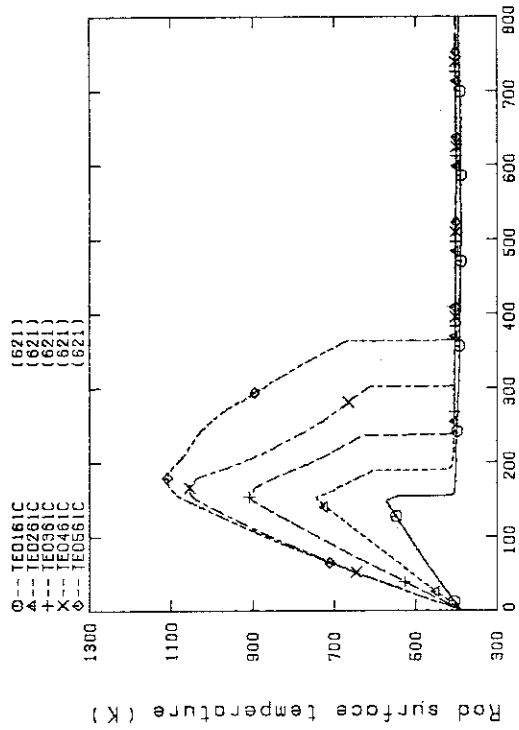

Fig.D-9 Heater rod temperature
(Bundle 5-1C, Lower half)

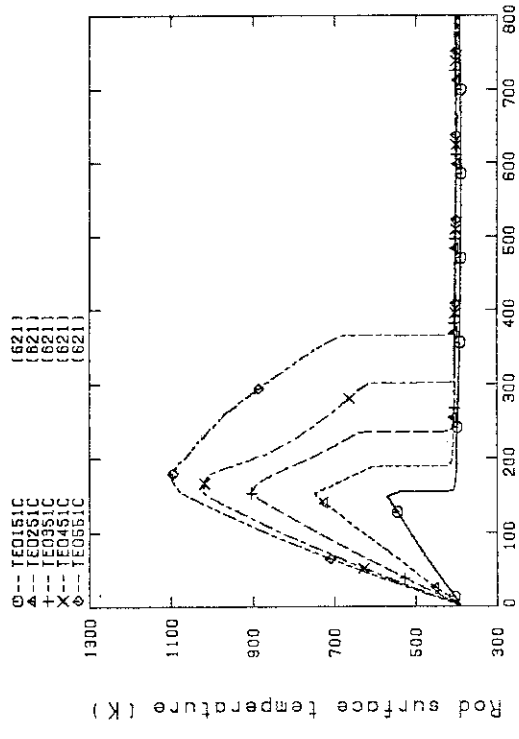

Fig.D-11 Heater rod temperature
(Bundle 6-1C, Lower half)

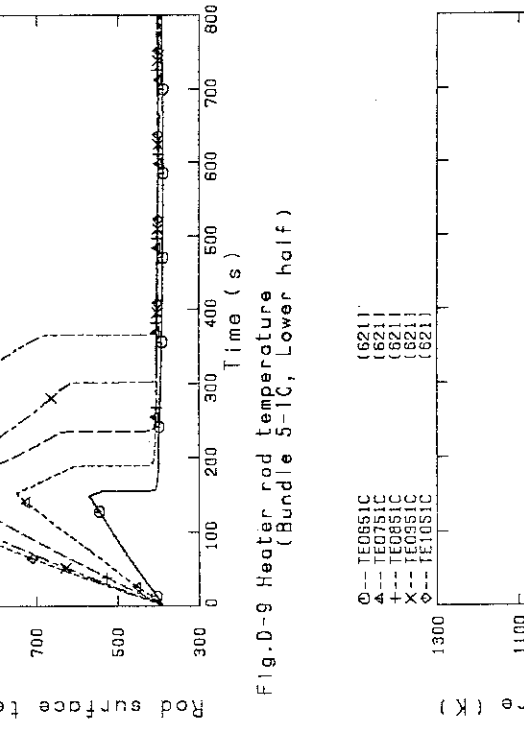

Fig.D-10 Heater rod temperature
(Bundle 5-1C, Upper half)

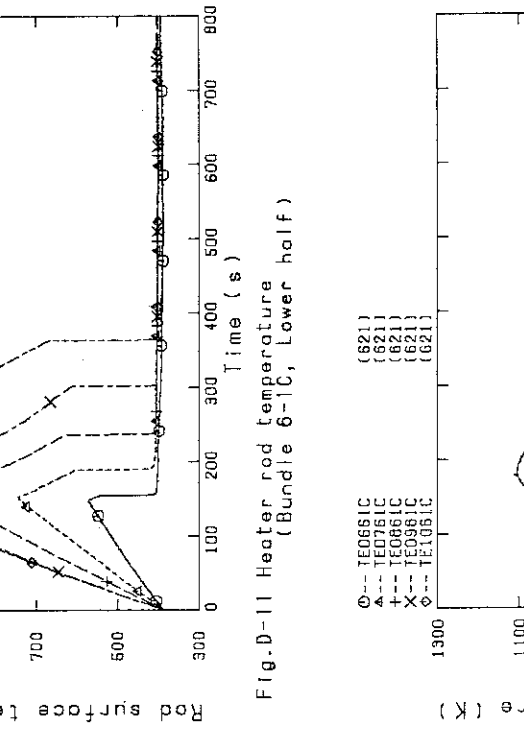

Fig.D-12 Heater rod temperature
(Bundle 6-1C, Upper half)

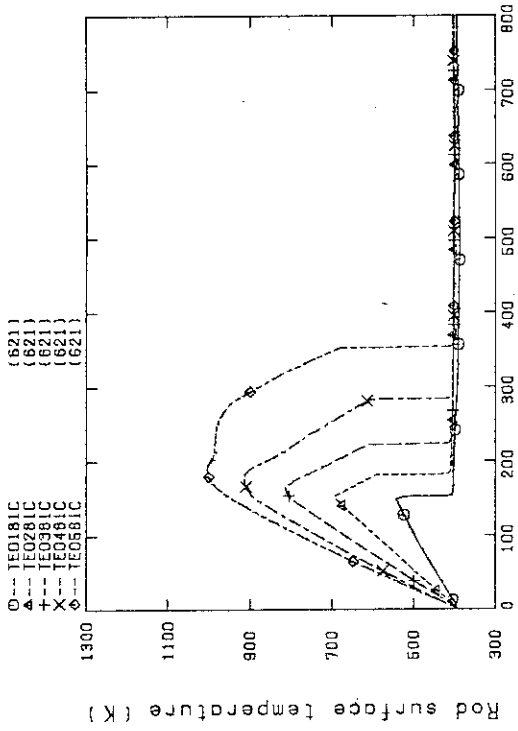

Fig.D-15 Heater rod temperature (Bundle 8-1C, Lower half)

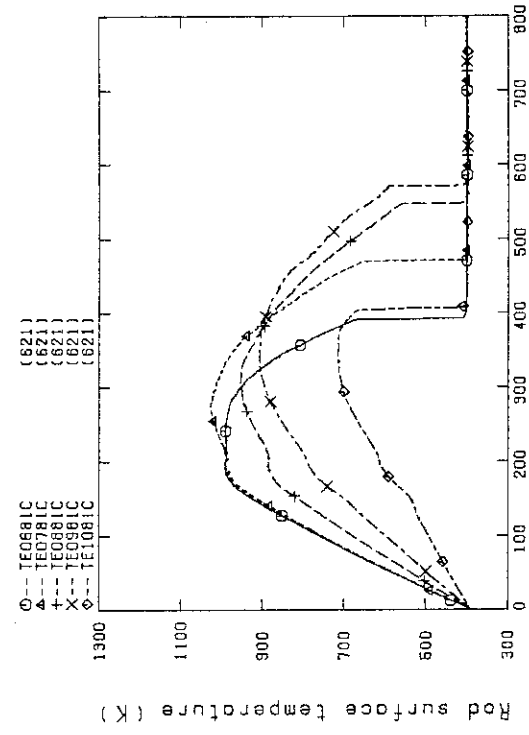

Fig.D-16 Heater rod temperature (Bundle 8-1C, Upper half)

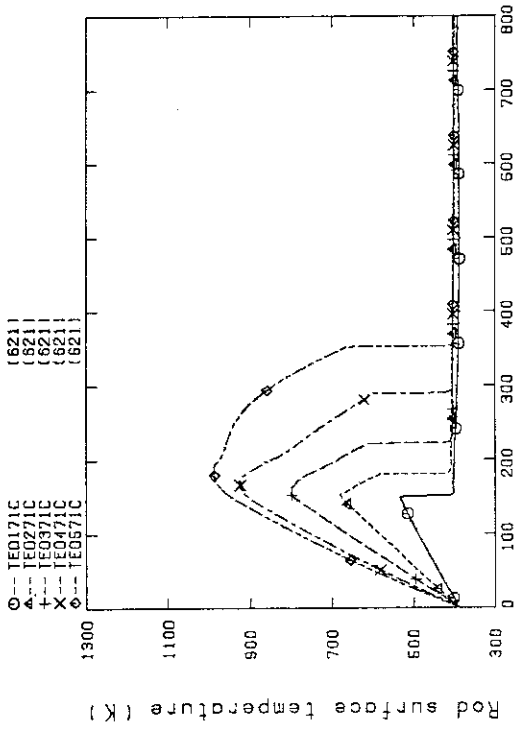

Fig.D-13 Heater rod temperature (Bundle 7-1C, Lower half)

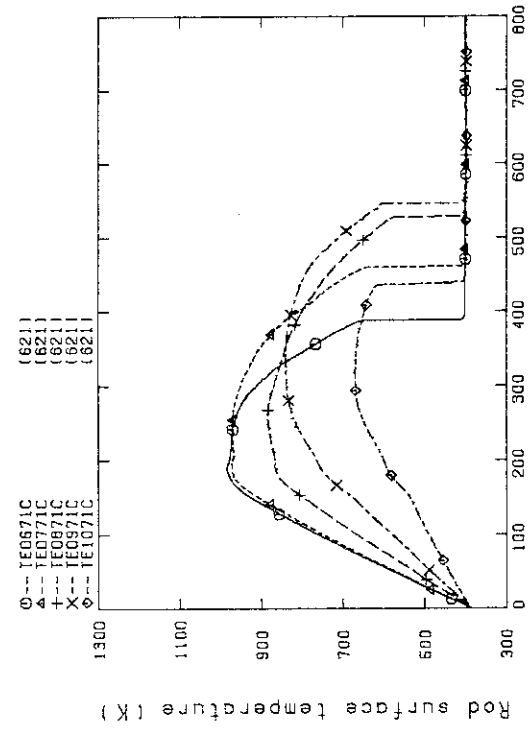

Fig.D-14 Heater rod temperature (Bundle 7-1C, Upper half)

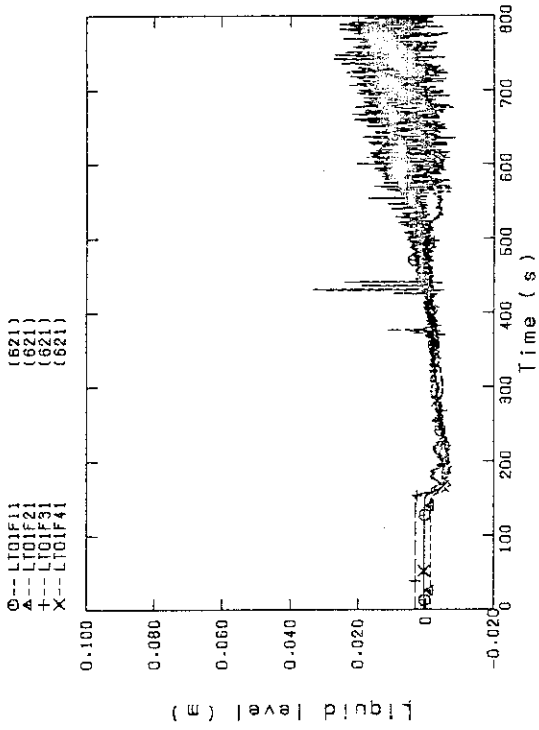

Fig.D-19 Liquid level above end box tie plate
(Bundle 1,2,3,4)

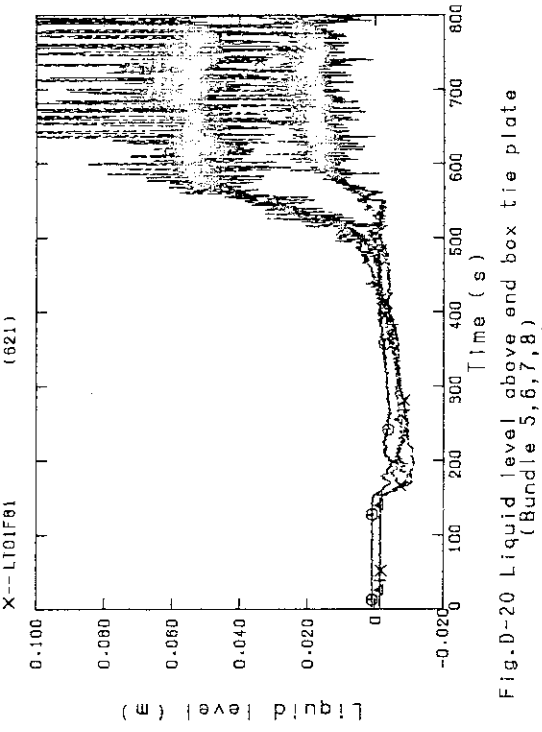

Fig.D-20 Liquid level above end box tie plate
(Bundle 5,6,7,8)

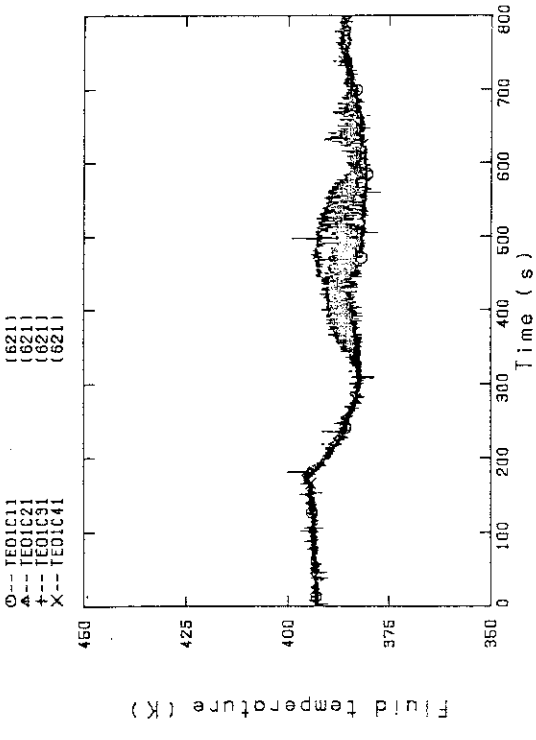

Fig.D-17 Fluid temperature at core inlet
(Bundle 1,2,3,4, 100mm below heated part)

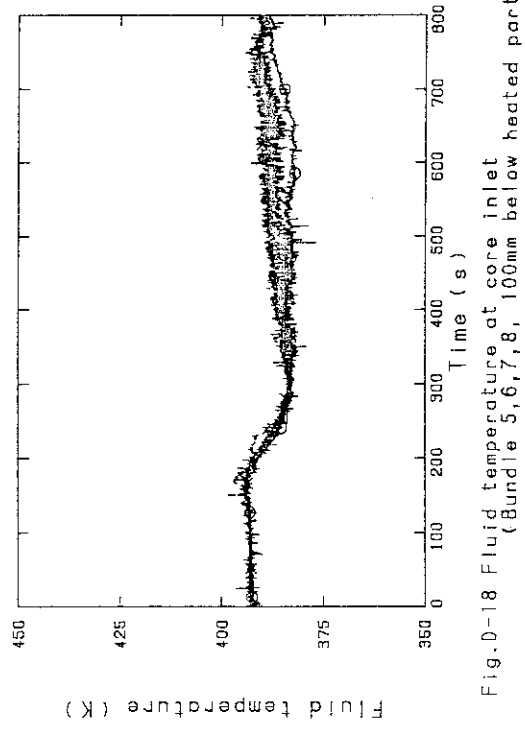

Fig.D-18 Fluid temperature at core inlet
(Bundle 5,6,7,8, 100mm below heated part)

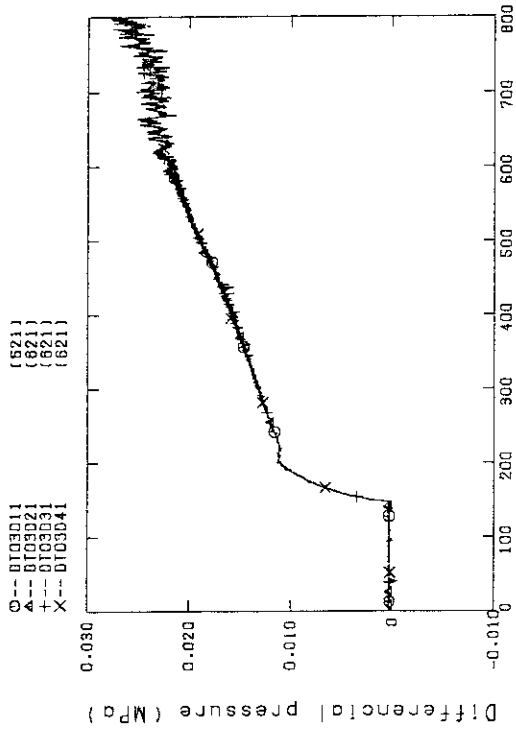

Fig.D-23 Differencial pressure of core full height (Bundle 1,2,3,4)

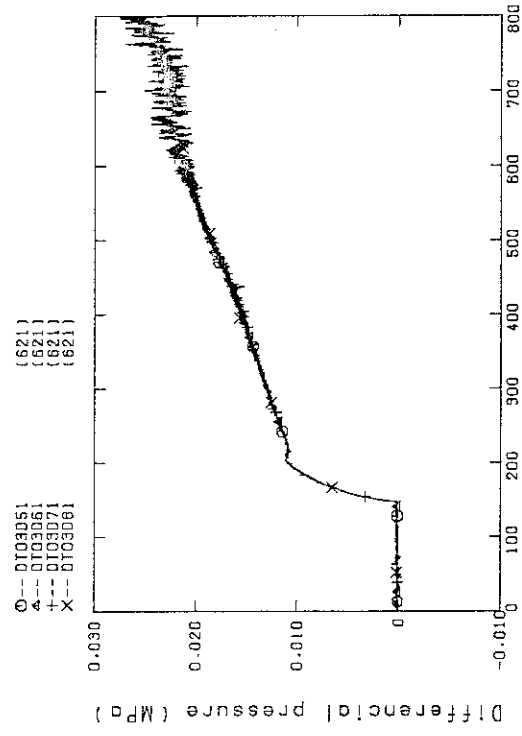

Fig.D-24 Differencial pressure of core full height (Bundle 5,6,7,8)

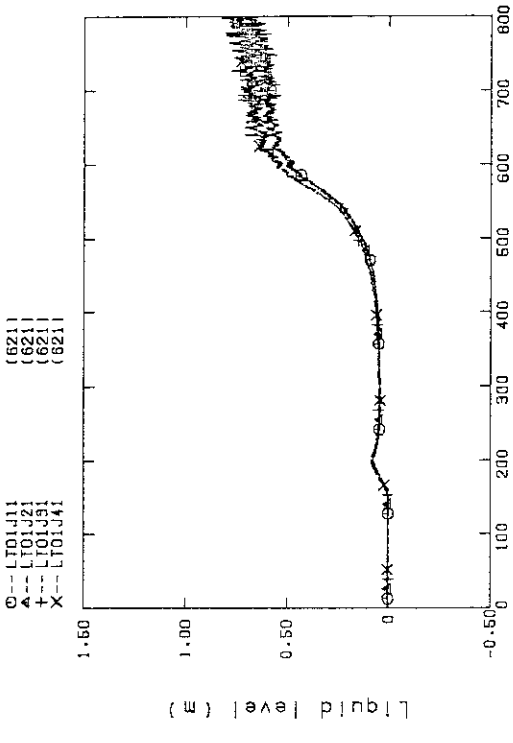

Fig.D-21 Liquid level above UCSP (Bundle 1,2,3,4)

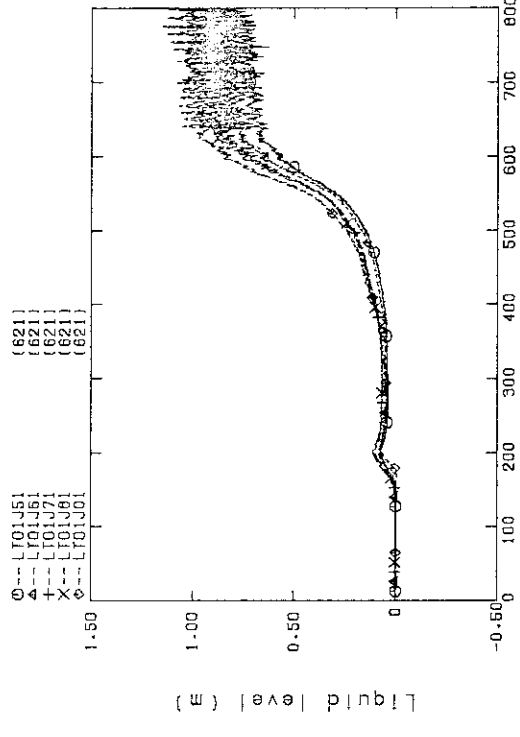

Fig.D-22 Liquid level above UCSP (Bundle 5,6,7,8 and core baffle)

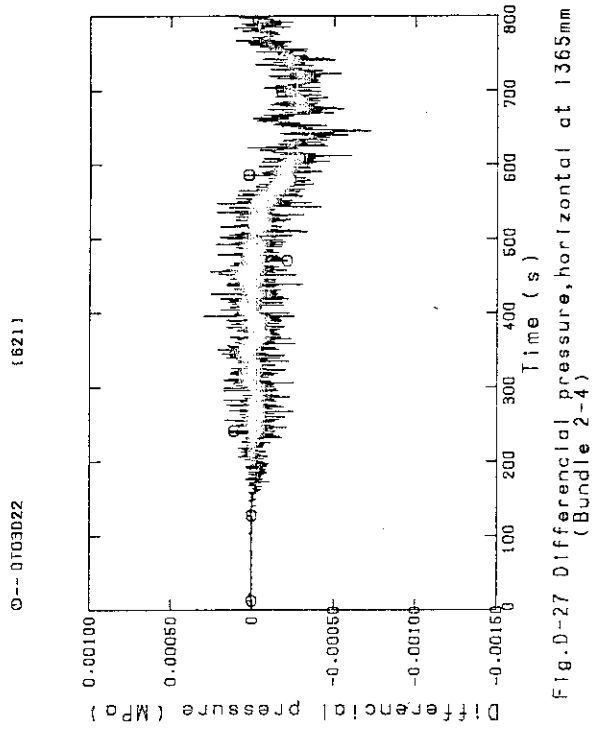

Fig.D-27 Differencial pressure,horizontal at 1365mm (Bundle 2-4)

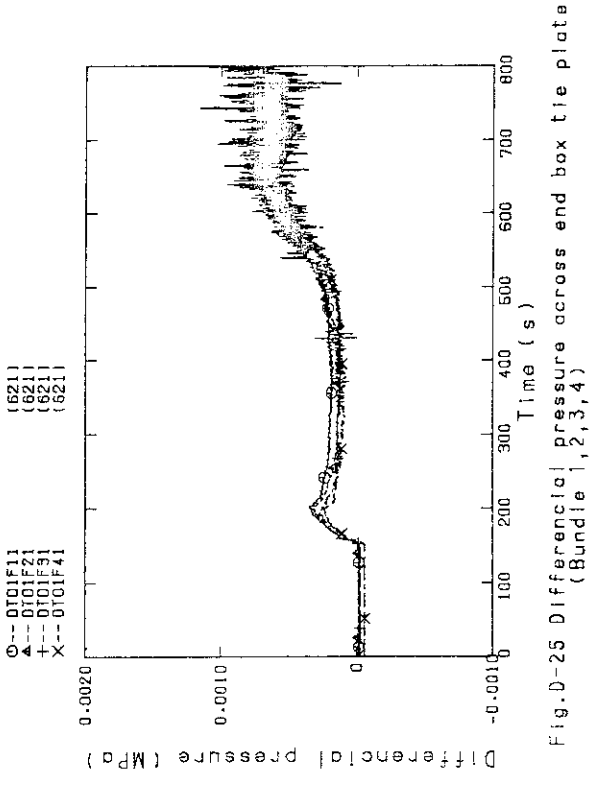

Fig.D-25 Differencial pressure across end box tie plate (Bundle 1,2,3,4)

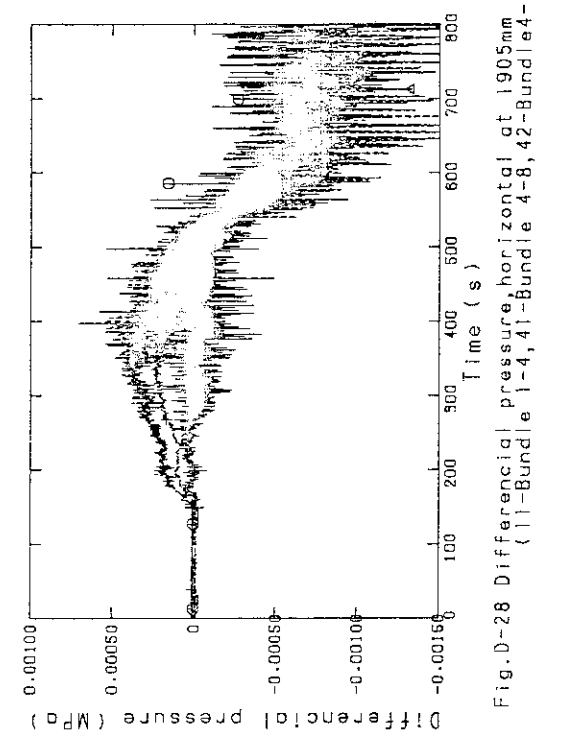

Fig.D-28 Differencial pressure,horizontal at 1905mm (11-Bundle 1-4,41-Bundle 4-8,42-Bundle4-6)

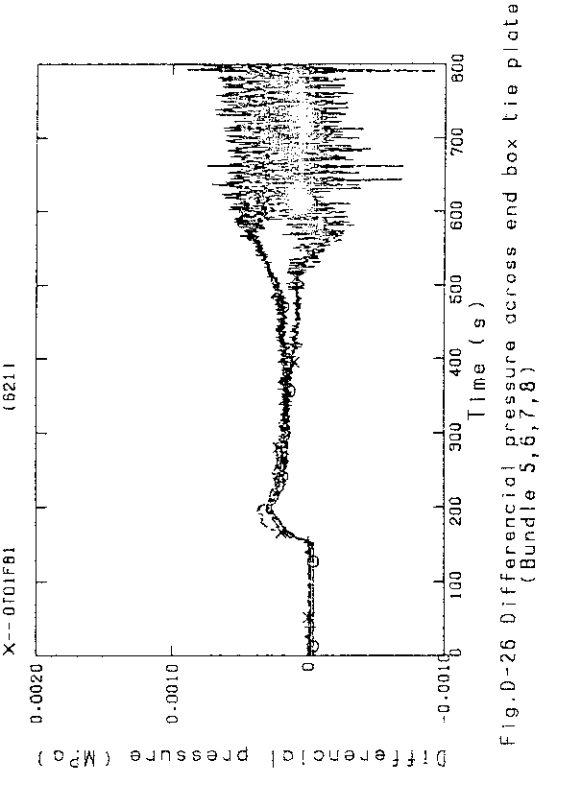

Fig.D-26 Differencial pressure across end box tie plate (Bundle 5,6,7,8)

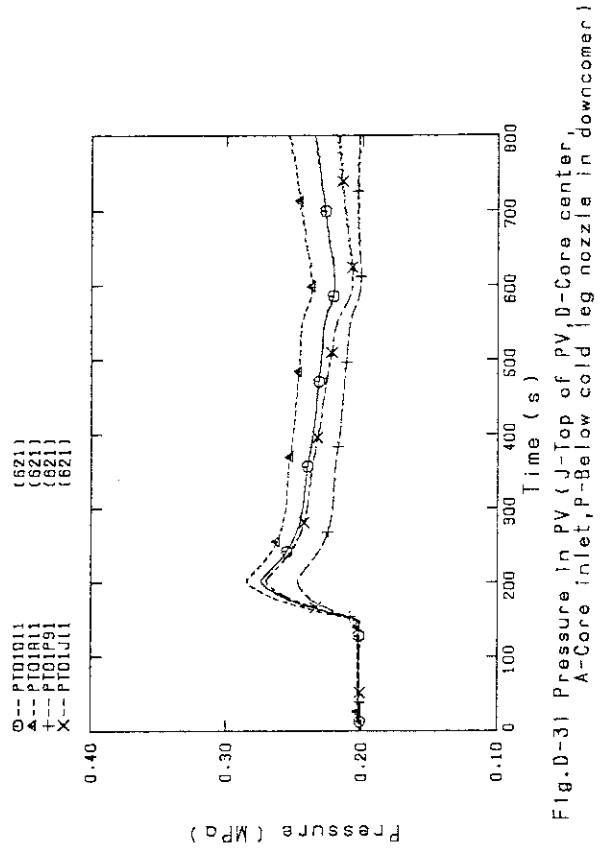

Fig.D-31 Pressure in PV (J-Top of PV, D-Core center, A-Core inlet, P-Below cold leg nozzle in downcomer)

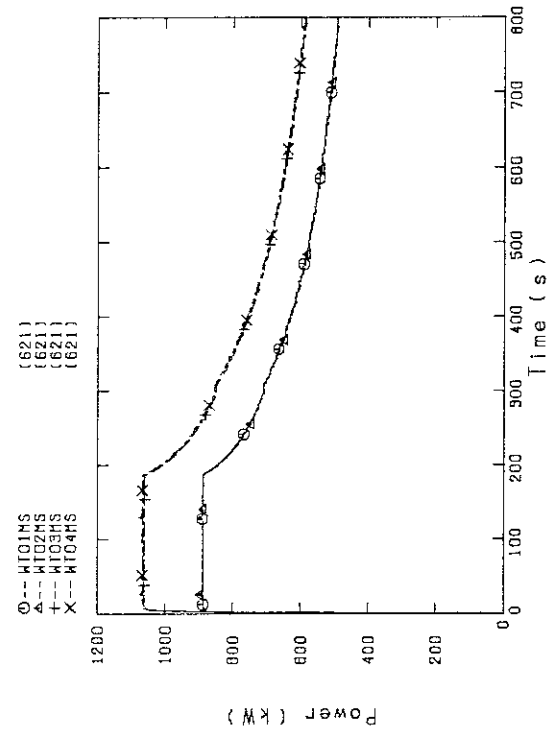

Fig.D-32 Bundle power (Bundle 1,2,3,4)

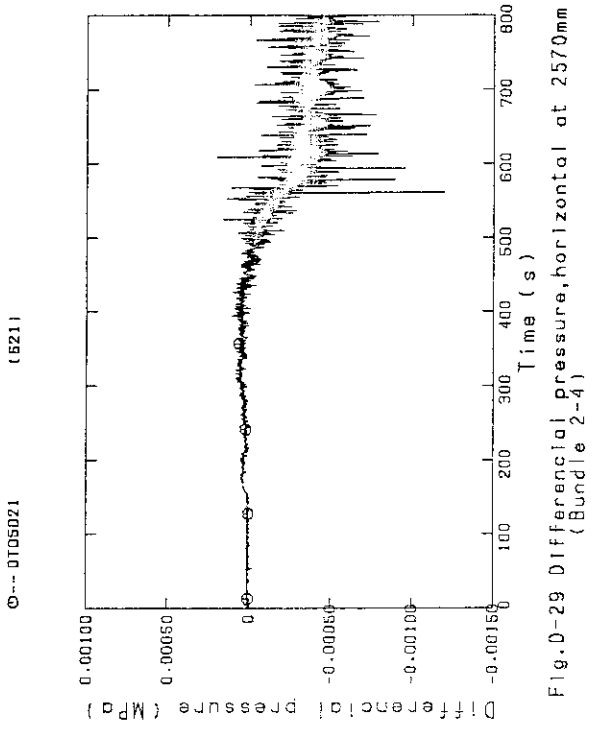

Fig.D-29 Differencial pressure, horizontal at 2570mm (Bundle 2-4)

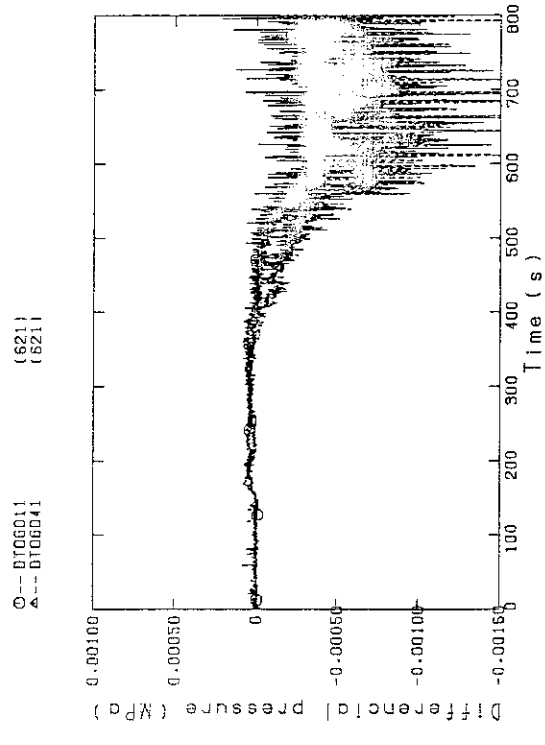

Fig.D-30 Differencial pressure, horizontal at 3235mm (11-Bundle 1-4, 41-Bundle 4-8)

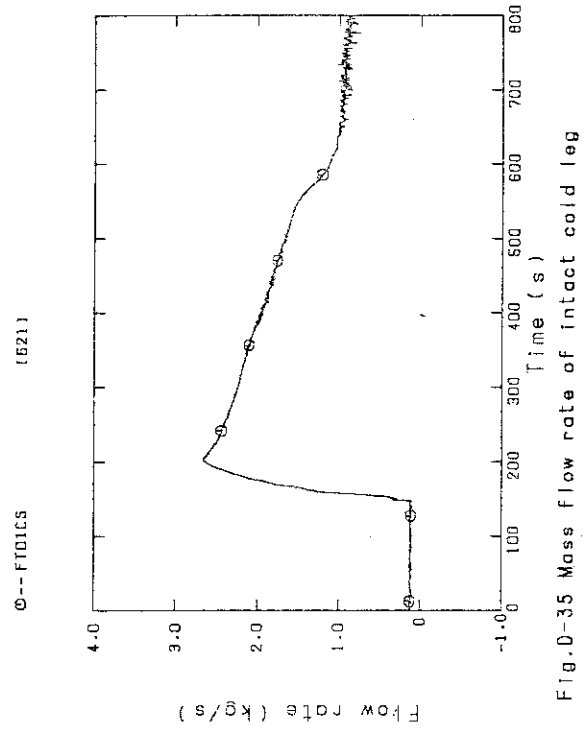

Fig.D-35 Mass flow rate of intact cold leg

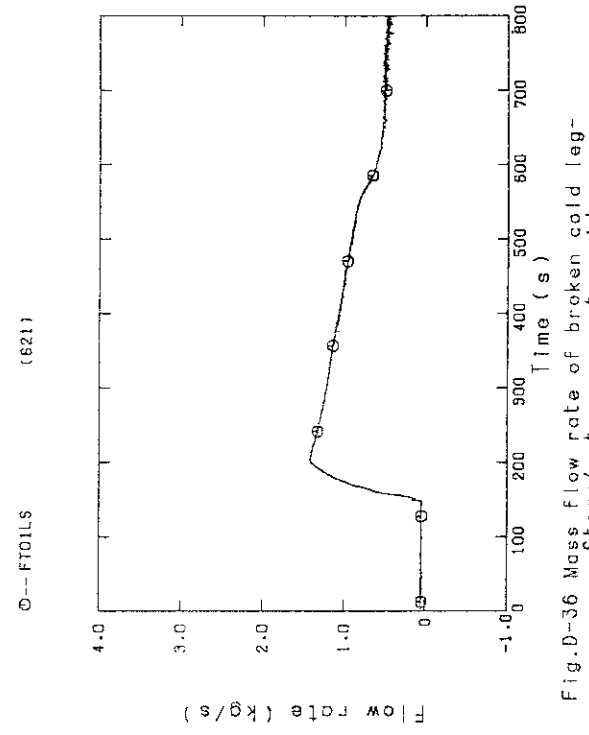

Fig.D-36 Mass flow rate of broken cold leg-Steam/water separator side

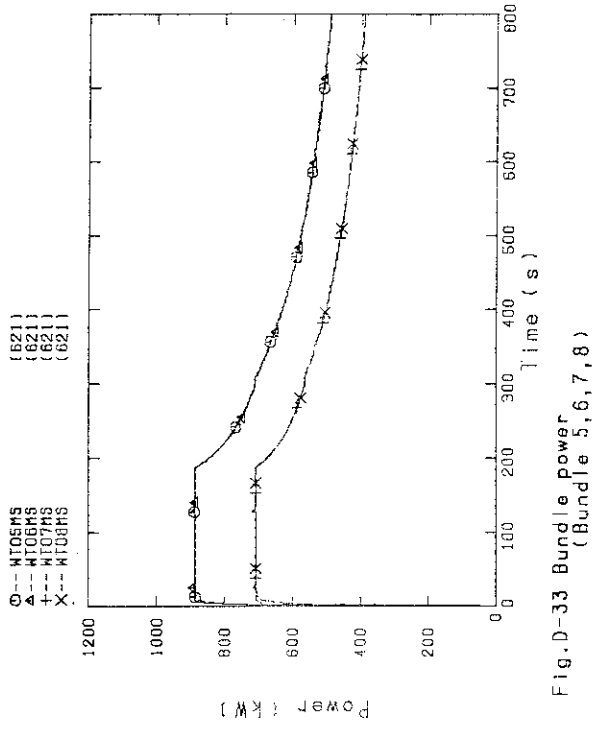

Fig.D-33 Bundle power (Bundle 5,6,7,8)

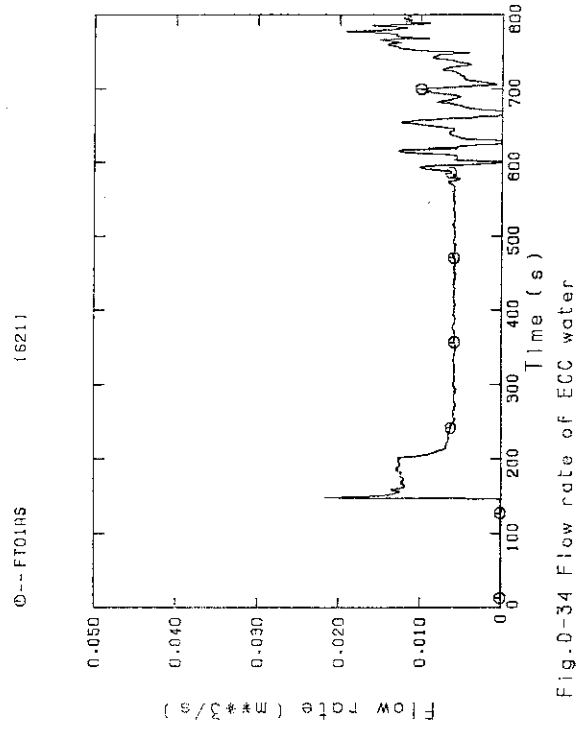

Fig.D-34 Flow rate of ECC water

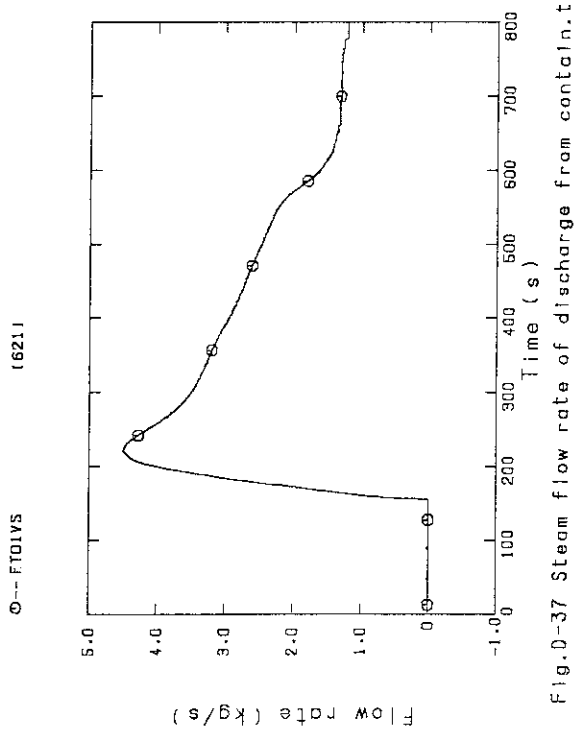

Fig.D-37 Steam flow rate of discharge from contain.tank-11

Appendix E Selected Data of Test S2-17

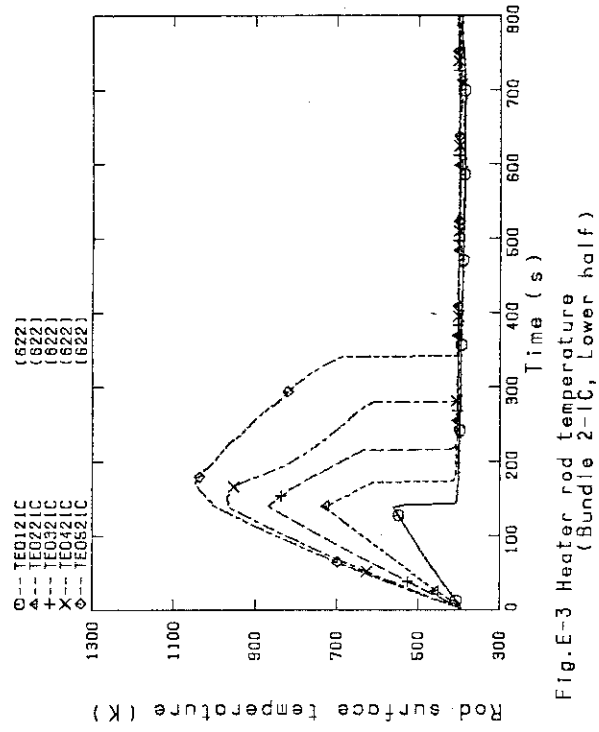

Fig.E-3 Heater rod temperature (Bundle 2-1C, Lower half)

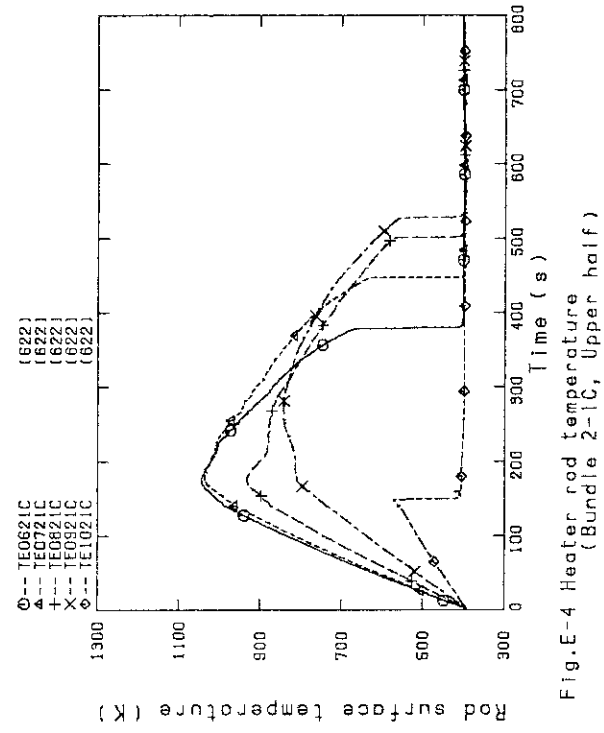

Fig.E-4 Heater rod temperature (Bundle 2-1C, Upper half)

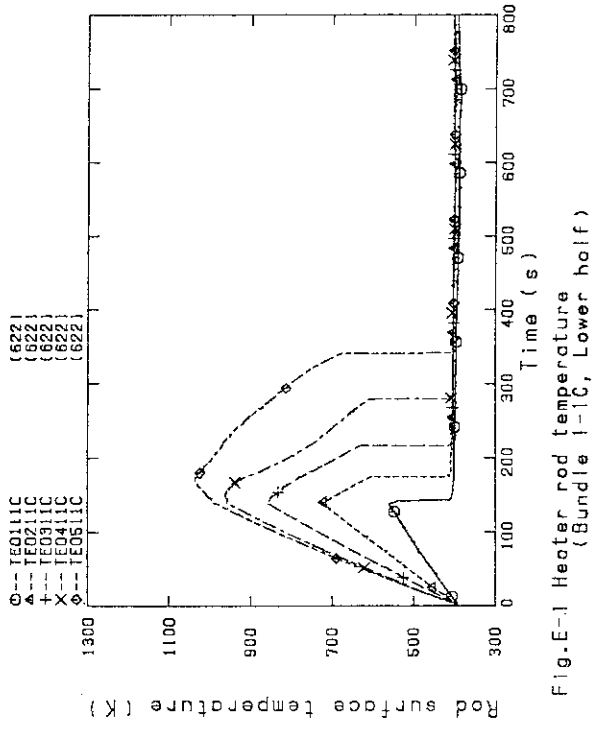

Fig.E-1 Heater rod temperature (Bundle 1-1C, Lower half)

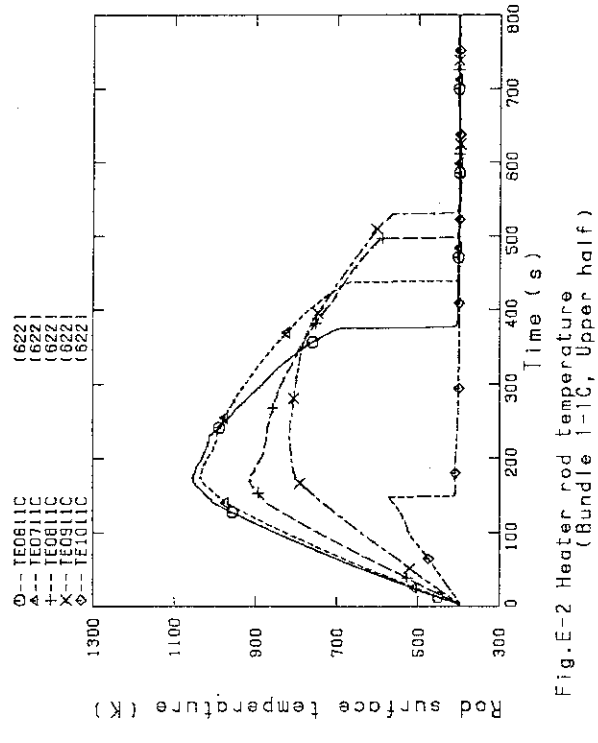

Fig.E-2 Heater rod temperature (Bundle 1-1C, Upper half)

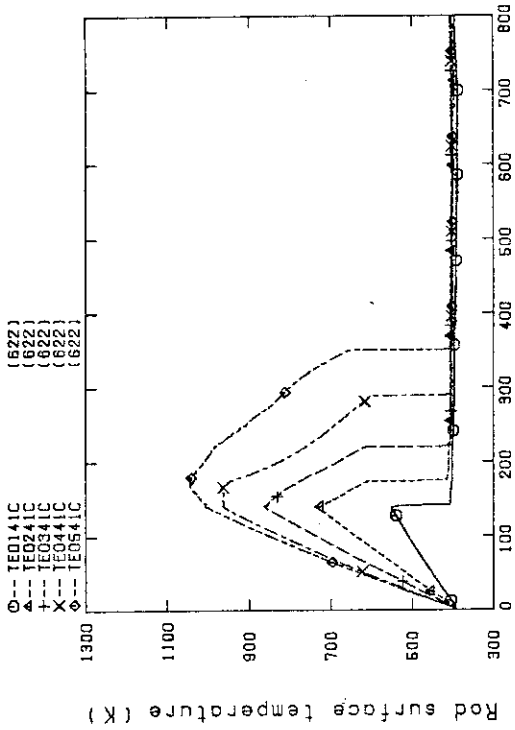

Fig.E-5 Heater rod temperature (Bundle 3-1C, Lower half)

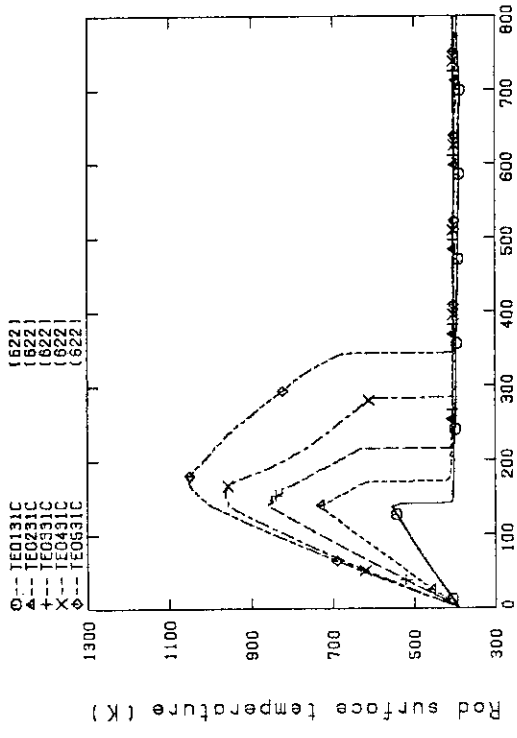

Fig.E-7 Heater rod temperature (Bundle 4-1C, Lower half)

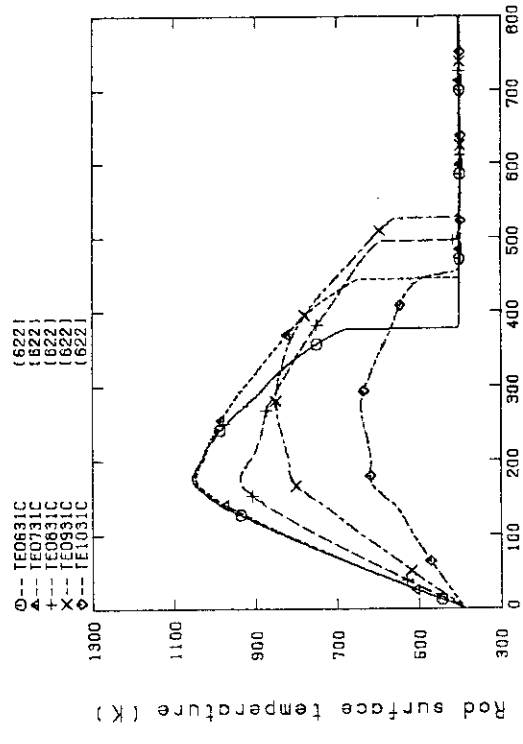

Fig.E-6 Heater rod temperature (Bundle 3-1C, Upper half)

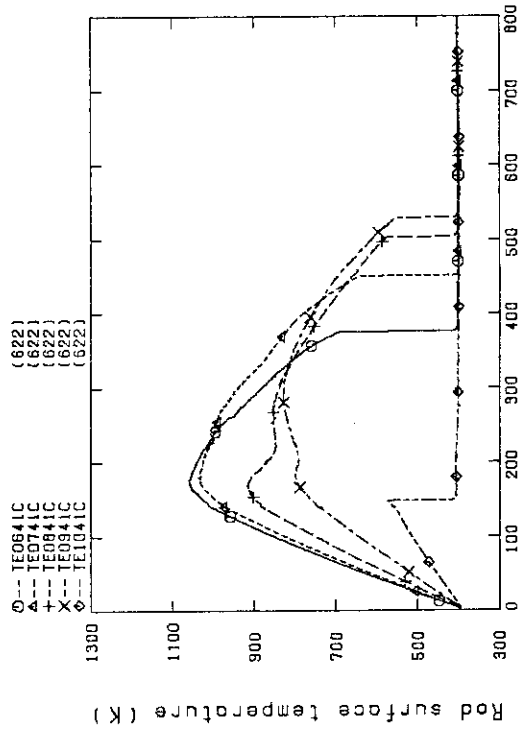

Fig.E-8 Heater rod temperature (Bundle 4-1C, Upper half)

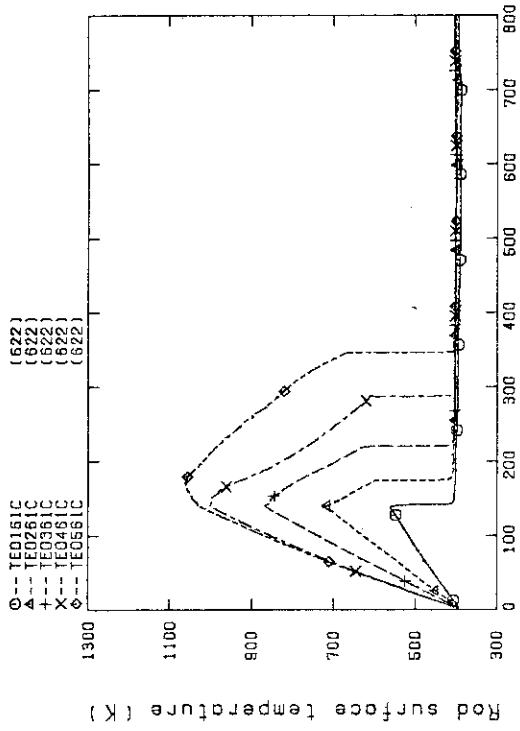

Fig.E-11 Heater rod temperature (Bundle 6-1C, Lower half)

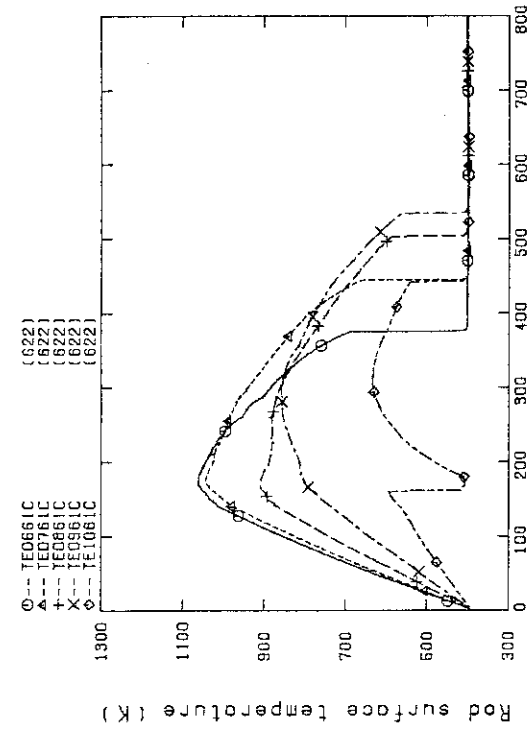

Fig.E-12 Heater rod temperature (Bundle 6-1C, Upper half)

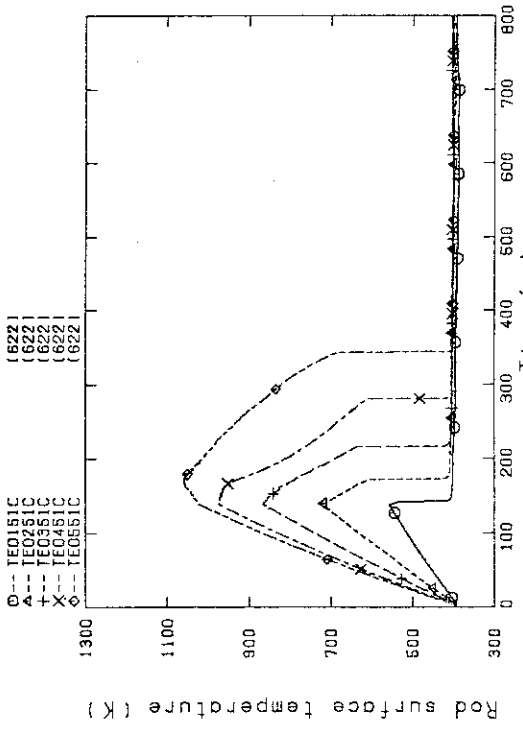

Fig.E-9 Heater rod temperature (Bundle 5-1C, Lower half)

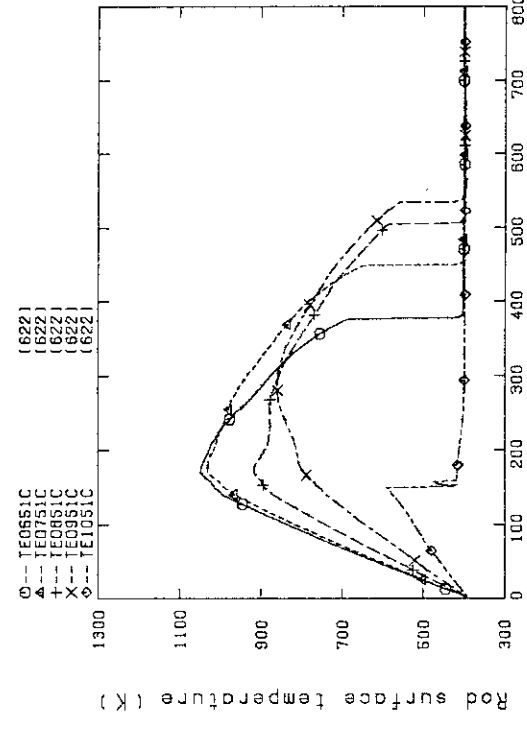

Fig.E-10 Heater rod temperature (Bundle 5-1C, Upper half)

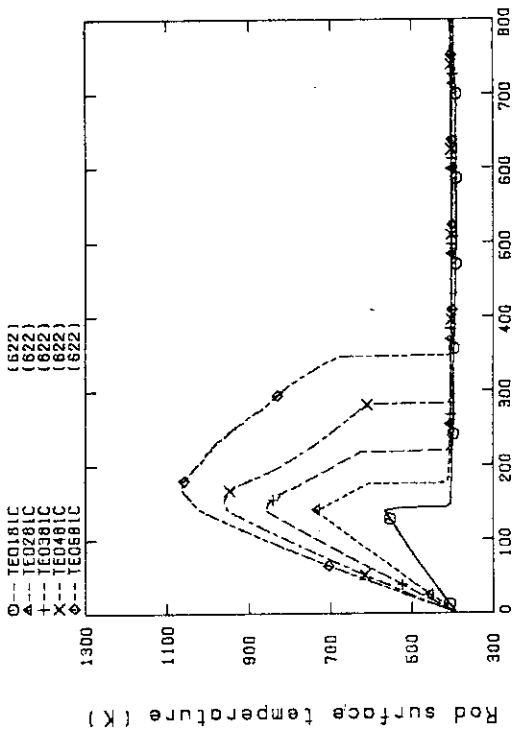

Fig.E-13 Heater rod temperature (Bundle 7-1C, Lower half)

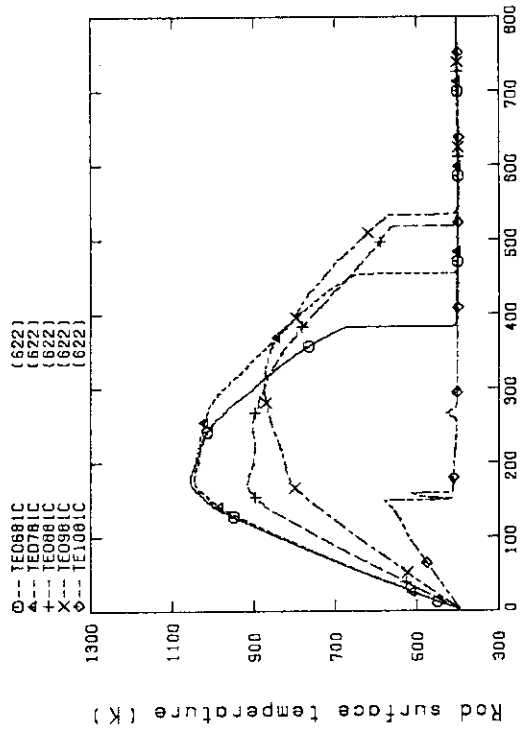

Fig.E-14 Heater rod temperature (Bundle 7-1C, Upper half)

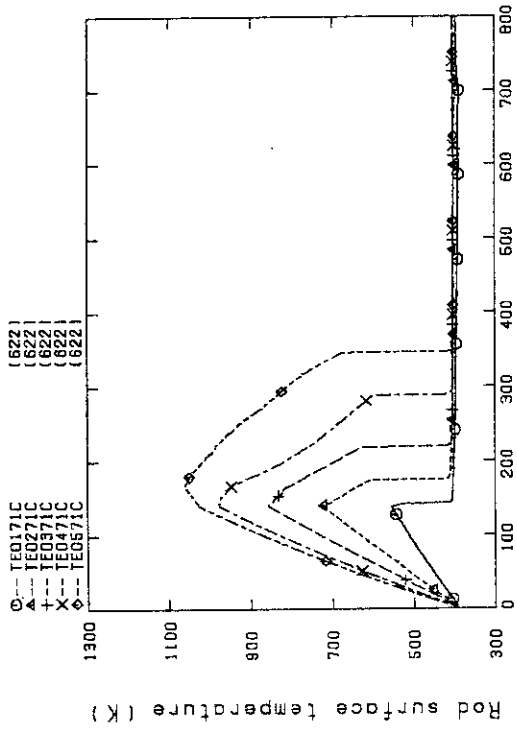

Fig.E-15 Heater rod temperature (Bundle 8-1C, Lower half)

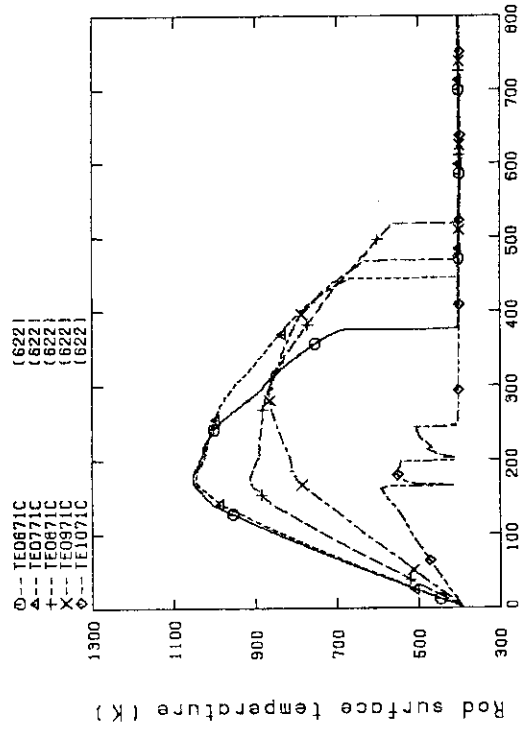

Fig.E-16 Heater rod temperature (Bundle 8-1C, Upper half)

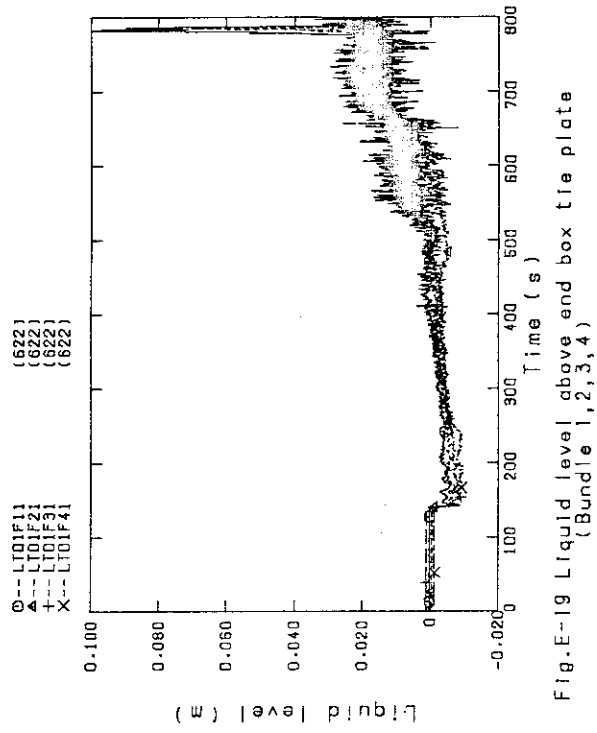

Fig.E-19 Liquid level above end box tie plate (Bundle 1,2,3,4)

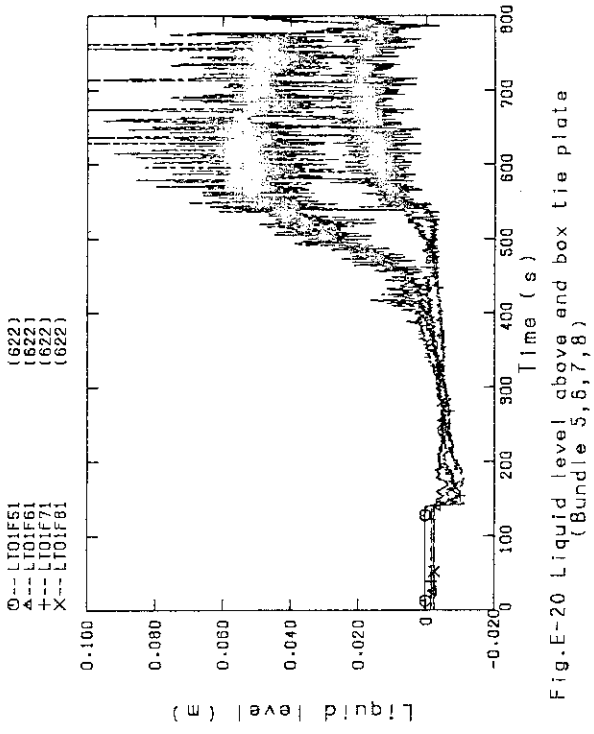

Fig.E-20 Liquid level above end box tie plate (Bundle 5,6,7,8)

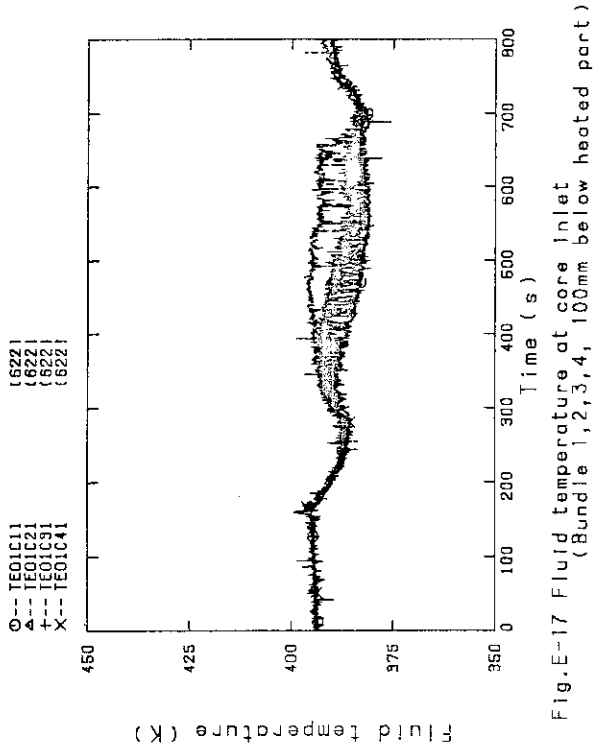

Fig.E-17 Fluid temperature at core inlet (Bundle 1,2,3,4, 100mm below heated part)

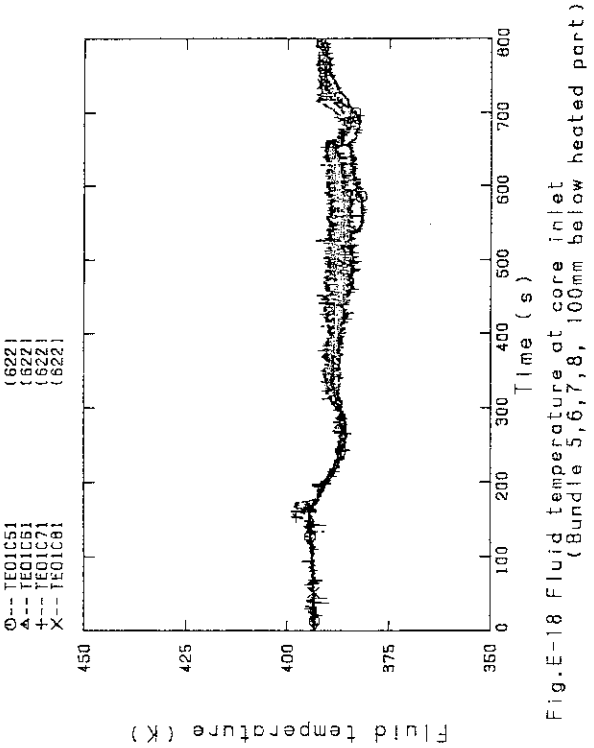

Fig.E-18 Fluid temperature at core inlet (Bundle 5,6,7,8, 100mm below heated part)

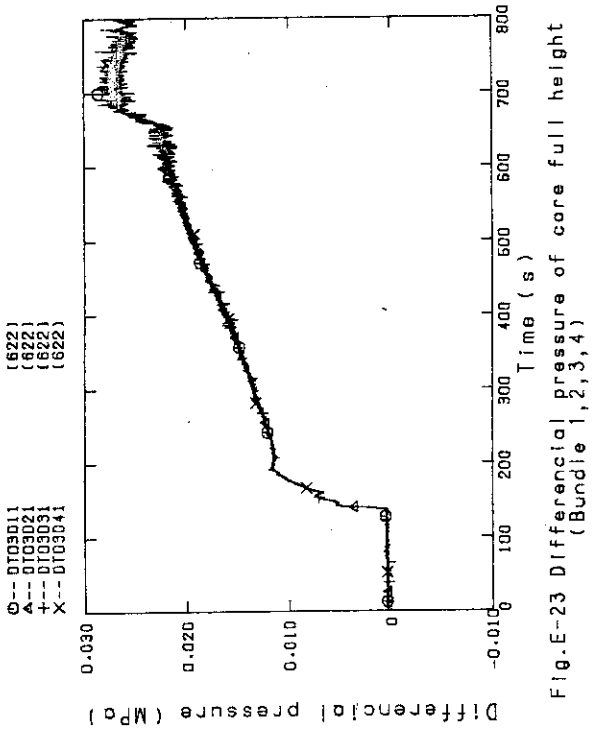

Fig.E-23 Differencial pressure of core full height (Bundle 1,2,3,4)

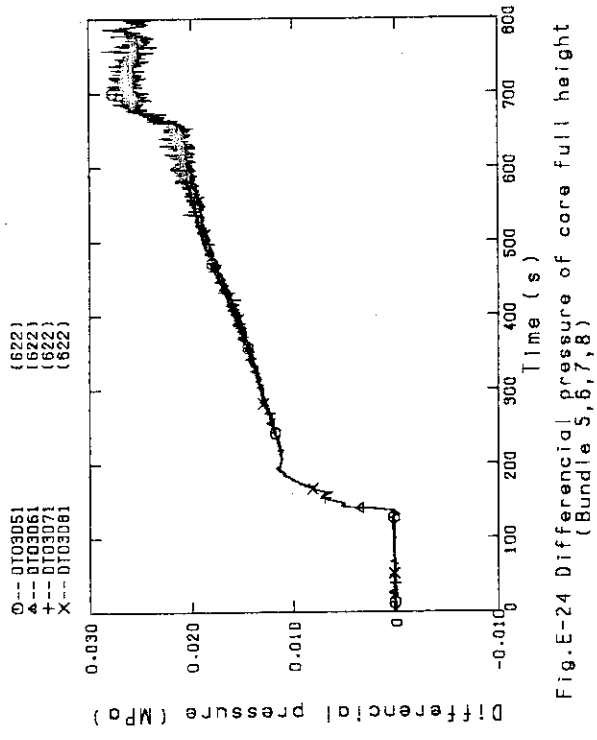

Fig.E-24 Differencial pressure of core full height (Bundle 5,6,7,8)

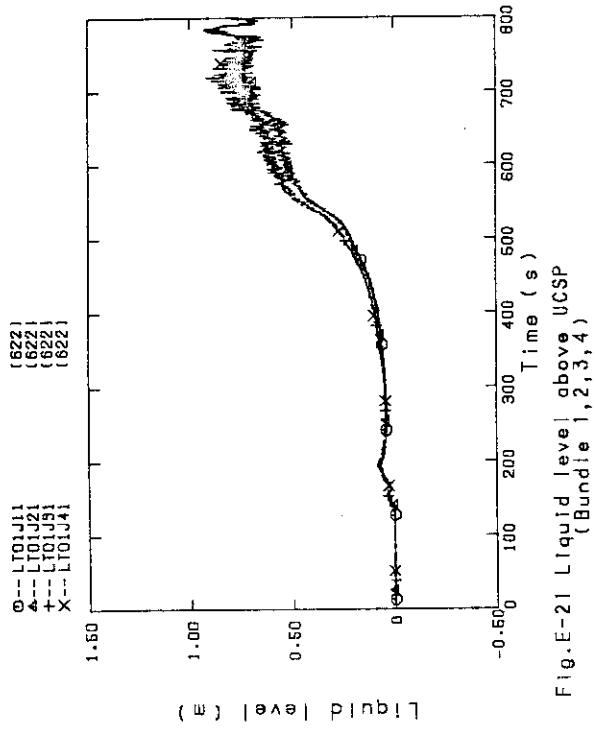

Fig.E-21 Liquid level above UCSP (Bundle 1,2,3,4)

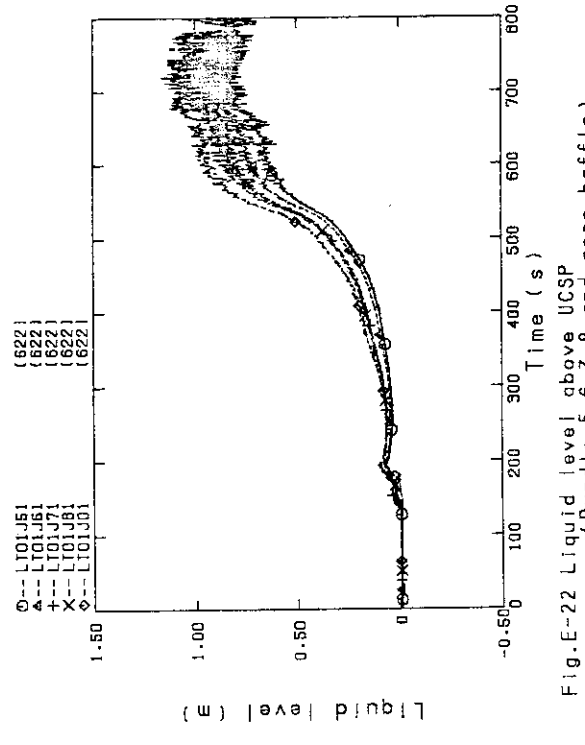

Fig.E-22 Liquid level above UCSP (Bundle 5,6,7,8 and core baffle)

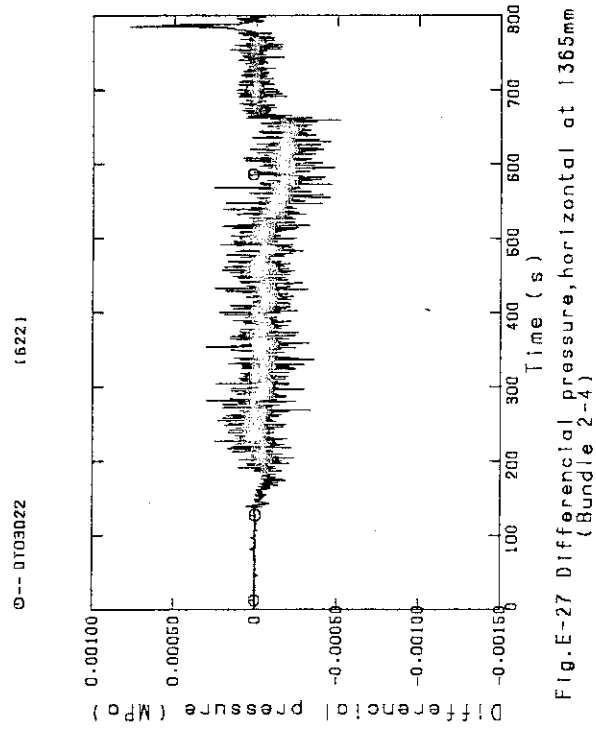

Fig.E-27 Differencial pressure,horizontal at 1365mm (Bundle 2-4)

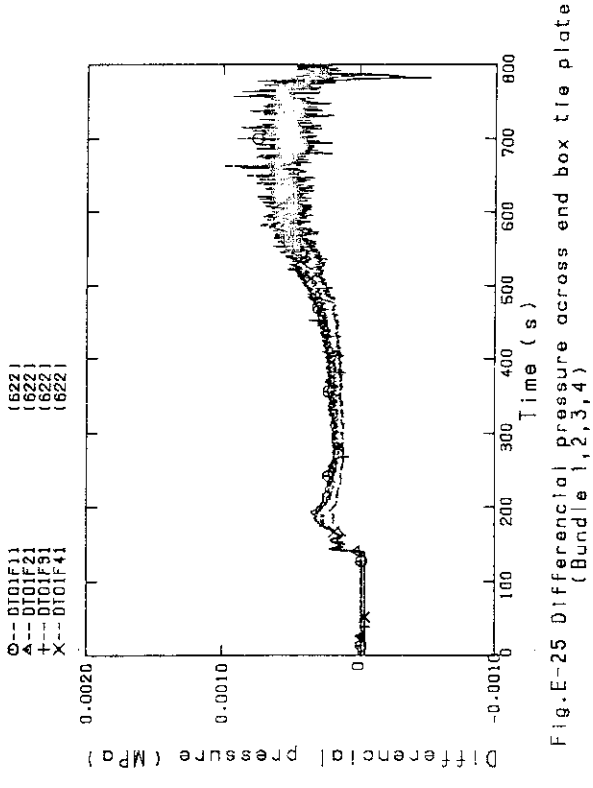

Fig.E-25 Differencial pressure across end box tie plate (Bundle 1,2,3,4)

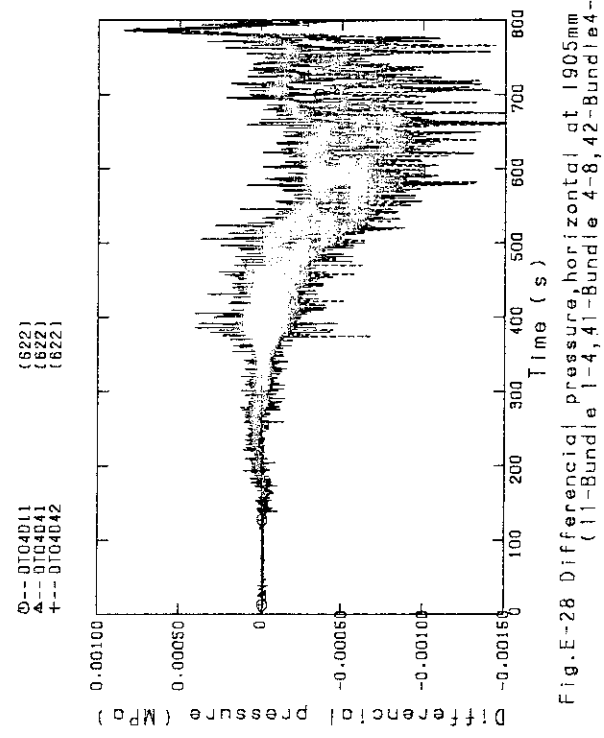

Fig.E-28 Differencial pressure,horizontal at 1905mm (11-Bundle 1-4,41-Bundle 4-8,42-Bundle4-6)

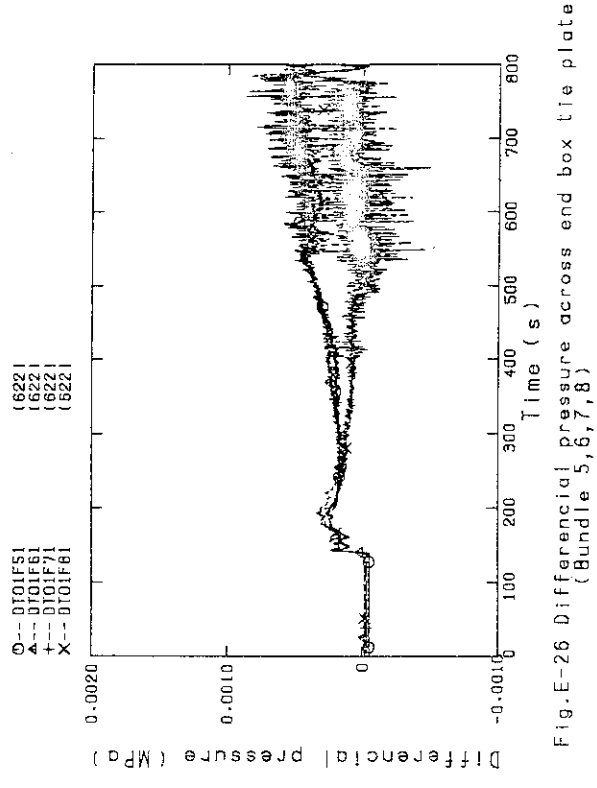

Fig.E-26 Differencial pressure across end box tie plate (Bundle 5,6,7,8)

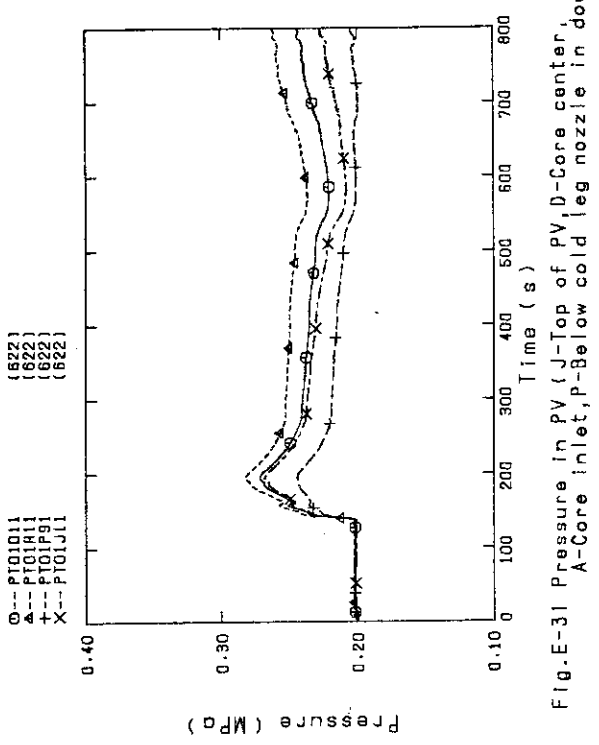

Fig.E-31 Pressure in PV (J-Top of PV, D-Core center, A-Core inlet, P-Below cold leg nozzle in downcomer)

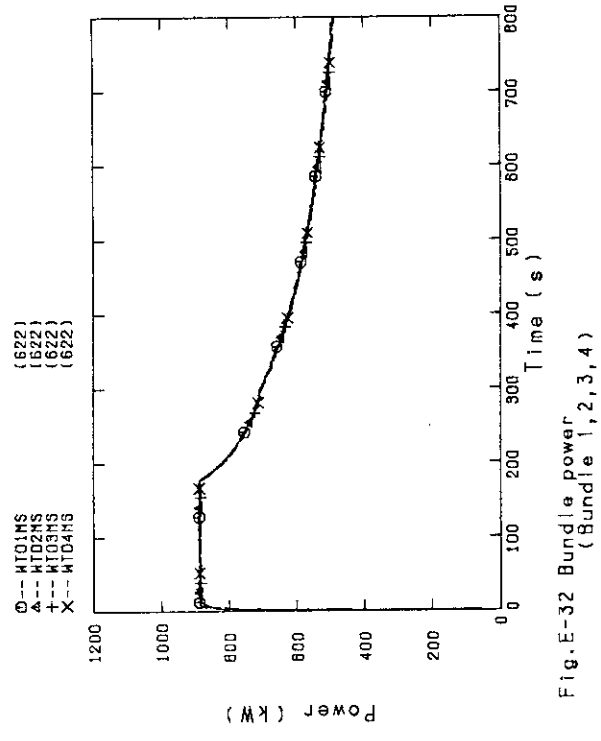

Fig.E-32 Bundle power (Bundle 1,2,3,4)

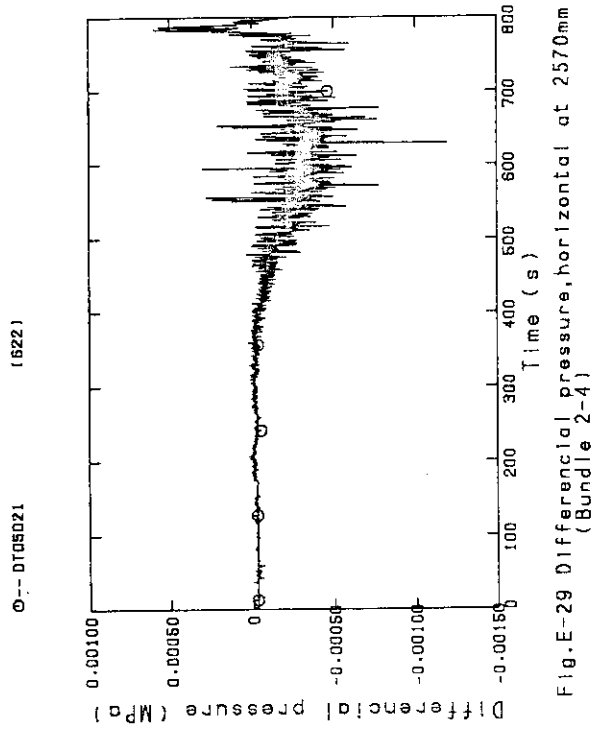

Fig.E-29 Differencial pressure,horizontal at 2570mm (Bundle 2-4)

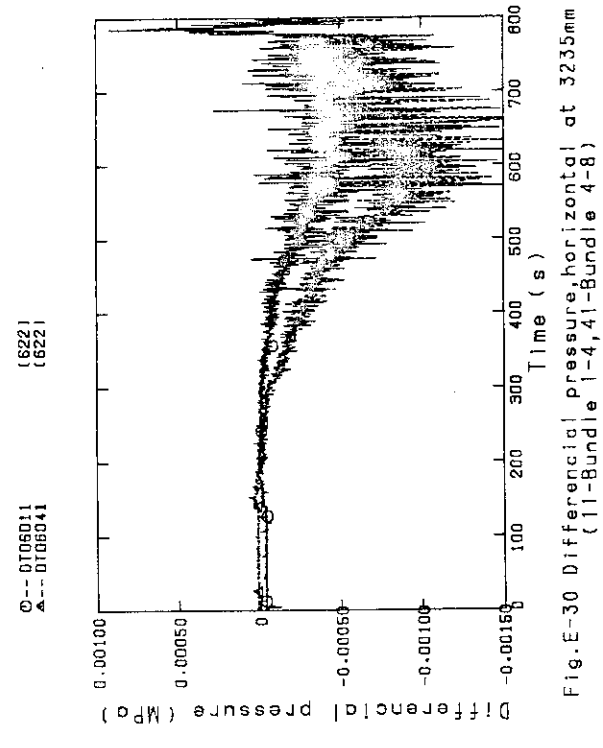

Fig.E-30 Differencial pressure,horizontal at 3235mm (11-Bundle 1-4,41-Bundle 4-8)

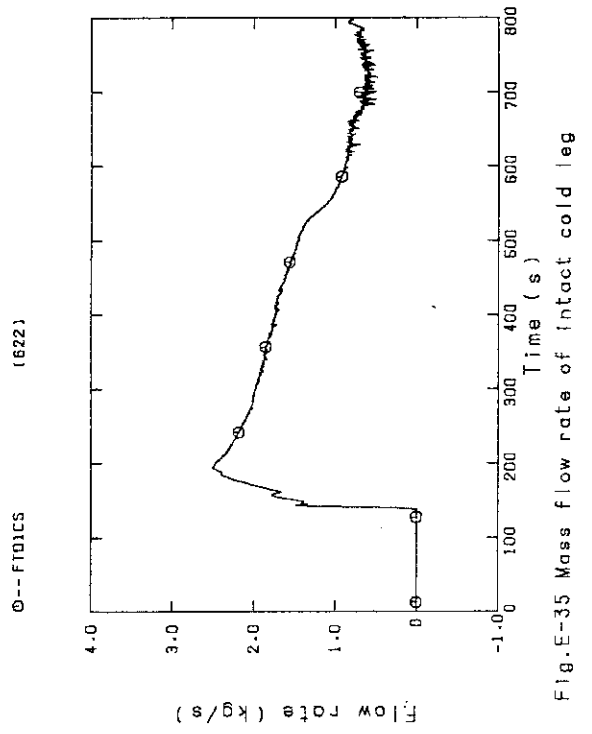

Fig.E-35 Mass flow rate of intact cold leg

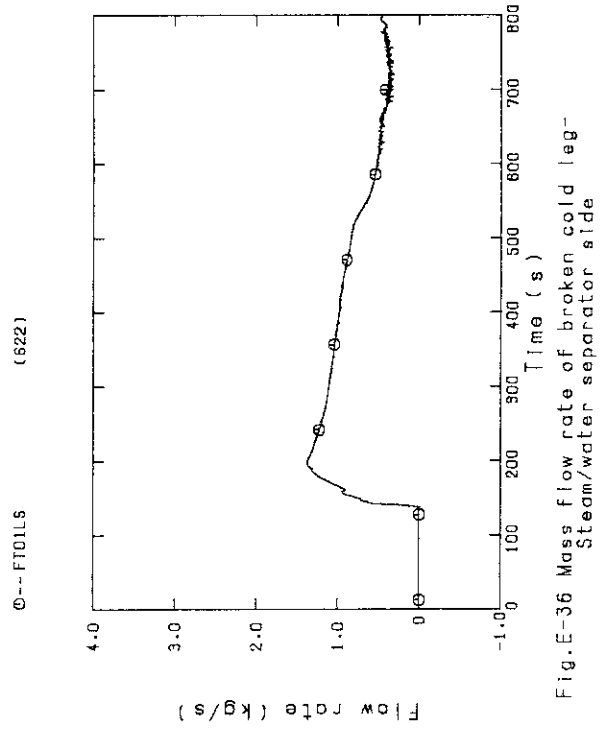

Fig.E-36 Mass flow rate of broken cold leg-Steam/water separator side

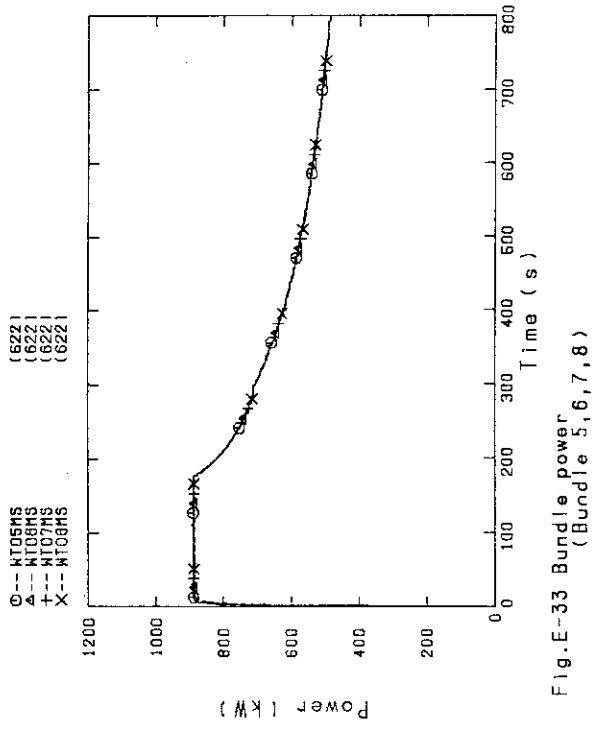

Fig.E-33 Bundle power (Bundle 5,6,7,8)

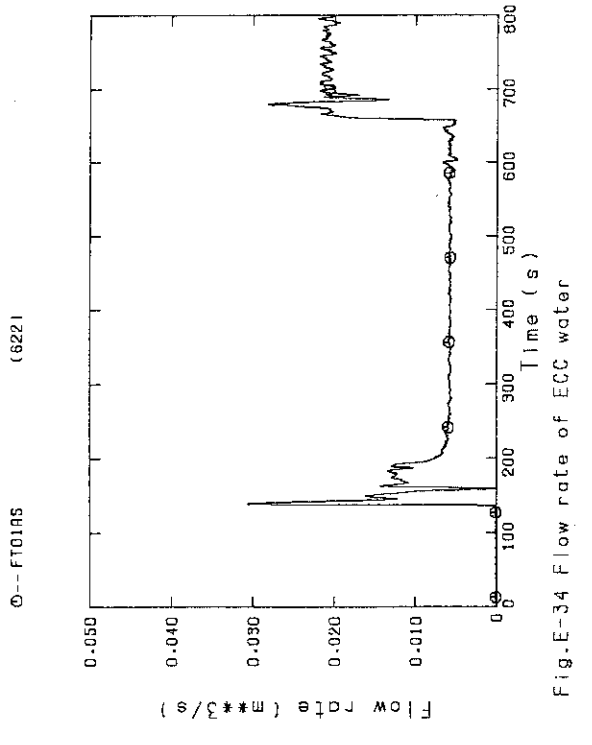

Fig.E-34 Flow rate of ECC water

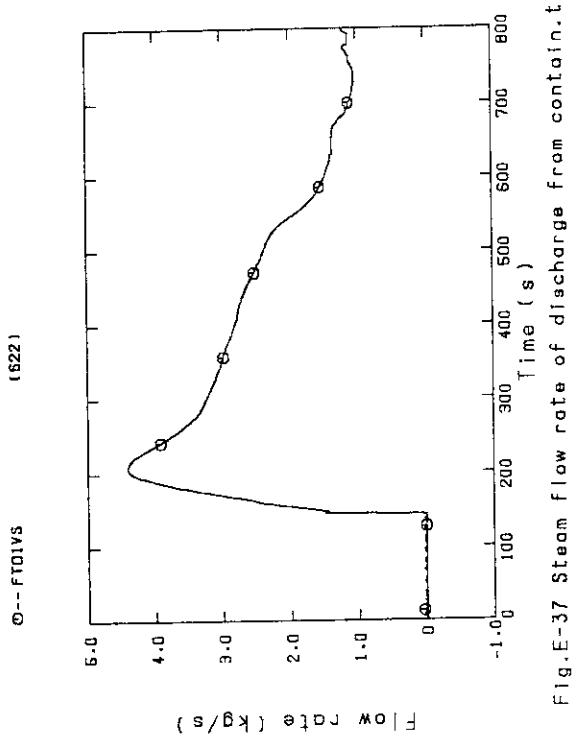

Fig.E-37 Steam flow rate of discharge from contain.tank-II